TECHNISCHE UNIVERSITÄT MÜNCHEN

Department Chemie

Lehrstuhl II für Organische Chemie

Measurement and Application of Anisotropic NMR Parameters in Stretched Polymer Gels: Structure Determination of Small Molecules

Grit Kummerlöwe

Vollständiger Abdruck der von der Fakultät für Chemie der Technischen Universität München zur Erlangung des akademischen Grades eines

Doktors der Naturwissenschaften

genehmigten Dissertation.

Vorsitzender:	Univ.-Prof. Dr. Steffen J. Glaser
Prüfer der Dissertation:	1. Priv.-Doz. Dr. Burkhard W. Luy
	2. Univ.-Prof. Dr. Klaus Köhler
	3. Priv.-Doz. Dr. Christina M. Thiele, Technische Universität Darmstadt

Die Dissertation wurde am 31.03.2010 bei der Technischen Universität München eingereicht und durch die Fakultät für Chemie am 04.05.2010 angenommen.

für mich.

I can resist everything but temptation.

(Oscar Wilde)

List of Publications

G. Kummerlöwe; S. Grage; C. Thiele; I. Kuprov; B. Luy:
'*Variable Angle NMR Spectroscopy and Its Application to the Measurement of Residual Chemical Shift Anisotropy*'
in preparation.

* G. Kummerlöwe; S. Kelch; M. Behl; A. Lendlein; B. Luy:
'*Artifact-Free Measurement of Residual Dipolar Couplings in DMSO by the Use of Cross-Linked Perdeuterated Poly(acrylonitrile) as Alignment Medium*'
submitted **2010**.

* G. Kummerlöwe; E. F. McCord; S. F. Cheatham; S. Niss; R. W. Schnell; B. Luy:
'*Tunable Alignment for All Polymer Gel/Solvent Combinations for the Measurement of Anisotropic NMR Parameters Using a Perfluorinated Elastomer Tube*'
Chemistry - A European Journal **2010**, in press, DOI: 10.1002/chem.201000108.

B. Laufer; A. O. Frank; J. Chatterjee; T. Neubauer; C. Más-Moruno; G. Kummerlöwe; H. Kessler:
'*The Impact of Amino Acid Side Chain Mutations in Conformational Design of Peptides and Proteins*'
Chemistry - A European Journal **2010**, *16*, 5385-5390.

* G. Kummerlöwe; S. Schmitt; B. Luy:
'*Cross-Fitting of Residual Dipolar Couplings*' in:
The Open Spectroscopy Journal **2010**, *4*, 16-27.

J. Geiger; M. K. Aneja; G. Hasenpusch; G. Yüksekdag; G. Kummerlöwe; B. Luy; T. Romer; U. Rothbauer; C. Rudolph:
'*Targeting of the Prostacyclin Specific IP1 Receptor in Lungs with Molecular Conjugates Comprising Prostaglandin I2 Analogues*' in:
Biomaterials **2010**, *31*, 2903-2911.

J. Geiger; M. K. Aneja; G. Hasenpusch; G. Yüksekdag; G. Kummerlöwe; B. Luy; T. Romer; U. Rothbauer; C. Rudolph:
'*Targeting of a G Protein-Coupled Receptor with Novel Molecular Conjugates Leads to Enhanced Pulmonary Gene Delivery*' in:
Human Gene Therapy **2009**, *20*, 1541-1541.

M. U. Kiran; A. Sudhakar; J. Klages; G. Kummerlöwe; B. Luy; B. Jagadeesh:
'*RDC Enhanced NMR Spectroscopy in Organic Solvent Media: The Importance for the Experimental Determination of Periodic Hydrogen Bonded Secondary Structures*' in:
Journal of the American Chemical Society **2009**, *131*, 15590-15591.

* D. Intelmann; G. Kummerlöwe; G. Haseleu; N. Desmer; K. Schulze; R. Fröhlich; O. Frank; B. Luy; T. Hofmann:
'*Structures of Storage-Induced Transformation Products of the Beer's Bitter Principle, Revealed by Sophisticated NMR and LC/MS Techniques*' in:
Chemistry - A European Journal **2009**, *15*, 13047-13058.

* G. Kummerlöwe; B. Luy:
'*Residual Dipolar Couplings for the Configurational and Conformational Analysis of Organic Molecules*' in:
Annual Reports on NMR Spectroscopy **2009**, *68*, 193-232.

* G. Kummerlöwe; M. U. Kiran; B. Luy:
'*Covalently Cross-Linked Gelatin Allows Chiral Distinction at Elevated Temperatures and in DMSO*' in:
Chemistry - A European Journal **2009**, *15*, 12192-12195.

* G. Kummerlöwe; B. Luy:
'*Residual Dipolar Couplings as a Tool in Determining the Structure of Organic Molecules*' in:
Trends in Analytical Chemistry **2009**, *28*, 483-493.

* G. Kummerlöwe; S. Knör; A. O. Frank; T. Paululat; H. Kessler; B. Luy:
'*Deuterated Polymer Gels for Measuring Anisotropic NMR Parameters with Strongly Reduced Artefacts*' in:
Chemical Communications **2008**, 5722-5724.

N. Cramer; S. Helbig; A. Baro; S. Laschat; R. Diestel; F. Sasse; D. Mathieu; C. Richter; G. Kummerlöwe; B. Luy; H. Schwalbe:
'*Synthesis and Biological Properties of Cylindramide Derivatives: Evidence for Calcium-Dependent Cytotoxicity of Tetramic Acid Lactams*' in:
ChemBioChem **2008**, *9*, 2474-2486.

* G. Kummerlöwe; F. Halbach; B. Laufer; B. Luy:
'*Precise Measurement of RDCs in Water and DMSO Based Gels Using a Silicone Rubber Tube for Tunable Stretching*' in:
The Open Spectroscopy Journal **2008**, *2*, 29-33.

* G. Kummerlöwe; J. Auernheimer; A. Lendlein; B. Luy:
'*Stretched Poly(acrylonitrile) as a Scalable Alignment Medium for DMSO*' in:
Journal of the American Chemical Society **2007**, *129*, 6080-6081.

G. Kummerlöwe; I. Balteanu; Z. Sun; O. P. Balaj; V. E. Bondybey; M. K. Beyer:
'*Activation of Methane and Methane-d_4 by Ionic Platinum Clusters*' in:
International Journal of Mass Spectrometry **2006**, *254*, 183-188.

G. Kummerlöwe; M. K. Beyer:
'*Rate Estimates for Collisions of Ionic Clusters with Neutral Reactant Molecules*' in:
International Journal of Mass Spectrometry **2005**, *244*, 84-90.

* Topics covered in these publications are part of following PhD-thesis.

Table of Contents

1 Introduction 5

2 Theory 7

2.1 Anisotropic Parameters 7

2.1.1 Dipolar Couplings 7

2.1.2 Other Anisotropic Effects 9

2.2 From Anisotropic to Residual Anisotropic Parameters 10

2.2.1 Concept of the Alignment Tensor 11

2.2.2 Flexible Molecules 15

2.3 Alignment Media 17

2.3.1 General Types of Alignment 17

2.3.2 Overview over Existing Alignment Media 18

2.3.3 Considerations for Choosing the Right Alignment Medium 21

2.4 Scaling of the Alignment Strength 27

2.4.1 Adjusting the Alignment Medium 28

2.4.2 Variable Angle NMR 31

2.4.3 Gel Stretching Apparatus 33

2.5 Measurement of Residual Anisotropic Effects 35

2.5.1 Measurement of RCSA 35

2.5.2 Measurement of RQCs 36

2.5.3 Measurement of RDCs 37

2.6 Analysis of Anisotropic Parameters 44

2.6.1 General Considerations 44

2.6.2 Using RDCs for Verification of a Structural Model 45

2.6.3 Using RDCs for Structure Refinement 51

2.6.4 Discrimination of Enantiomers and Absolute Configuration 52

2.6.5 Analysis under Presumption of the Molecule's Orientation 53

3 Development of new Alignment Media 55

3.1 Poly(acrylonitrile) 55

3.1.1 Introduction and Motivation 55

3.1.2 Cross-Linking of PAN 55

3.1.3 Swelling and Equilibration of PAN/DMSO Gels 58

3.1.4 NMR-Signals and Impurities of PAN/DMSO Gels 60

3.1.5 Tuning the Alignment Strength 62
3.1.6 Orientational Properties 63
3.1.7 Conclusion 65
3.2 Deuterated Polystyrene 66
3.2.1 Introduction and Motivation 66
3.2.2 Preparation of dPS Gels 66
3.2.3 Spectral Quality of 1D Proton Spectra 67
3.2.4 Deuterium Spectrum of a dPS Gel 68
3.2.5 Spectral Quality of 2D Heteronuclear Proton-Carbon Spectra 69
3.2.6 Spectral Quality of 2D Homonuclear Proton Spectra 70
3.2.7 Conclusion 73
3.3 Deuterated Poly(acrylonitrile) 74
3.3.1 Introduction and Motivation 74
3.3.2 Preparation of dPAN Gels 74
3.3.3 Spectral Quality of 1D Proton Spectra 75
3.3.4 Spectral Quality of 2D Heteronuclear Proton-Carbon Spectra 75
3.3.5 Conclusion 76
3.4 Covalently Cross-Linked Gelatin 78
3.4.1 Introduction and Motivation 78
3.4.2 Preparation of Covalently Cross-Linked Gelatin 79
3.4.3 Swelling Behavior of Covalently Cross-Linked Gelatin 80
3.4.4 Stability of e^--Gelatin/Water Gels Towards Temperature 81
3.4.5 Enantiomeric Discrimination in e^--Gelatin/Water Gels 83
3.4.6 Influence of Cross-Linking on the Alignment Properties of Gelatin 86
3.4.7 Prochiral Discrimination in e^--Gelatin/DMSO Gels 87
3.4.8 Conclusion 88
3.5 Poly(ethylene oxide) 89
3.5.1 Introduction and Motivation 89
3.5.2 Cross-Linking of PEO by Irradiation 89
3.5.3 Solvent-Range of Cross-Linked PEO 93
3.5.4 Spectral Properties of PEO Gels 94
3.5.5 Conclusion 97

4 New Ways of Scaling the Alignment 98
4.1 Stretching Device for Polar Solvents 98
4.1.1 Introduction and Motivation 98
4.1.2 Design of the Stretching Apparatus 99
4.1.3 Principle of Gel-Stretching within the Stretching Apparatus 100
4.1.4 Applicability and Limitations of the Stretching Apparatus 102
4.1.5 Linear Scaling of Anisotropic Parameters 104
4.1.6 Improving the Precision of RDC-Measurements 106
4.1.7 Conclusion 107
4.2 Stretching Device for all Solvents 109
4.2.1 Introduction and Motivation 109
4.2.2 Design of the Stretching Apparatus 109
4.2.3 Spectral Quality 111
4.2.4 Applicable Solvent Range 112
4.2.5 Conclusion 117
5 Structure Determination of Small Molecules 118
5.1 Configurational Analysis of a Degradation Product of Beer 118
5.1.1 Introduction and Motivation 118
5.1.2 Possible Structural Models of Tricyclocohumol 121
5.1.3 RDCs and J-couplings Measured on Tricyclocohumol 122
5.1.4 Configurational Analysis of Tricyclocohumol 123
5.1.5 Fitting Results 124
5.1.6 Conclusion 128
5.2 Configurational and Conformational Analysis of Staurosporine 129
5.2.1 Introduction and Motivation 129
5.2.2 Possible Conformations and Configurations of Staurosporine 130
5.2.3 RDCs Measured on Staurosporine 130
5.2.4 Fitting Results 131
5.2.5 Conclusion 133
5.3 Solving the Constitution of an Unknown Reaction Product 134
5.3.1 Introduction and Motivation 134
5.3.2 Analyzing the Unknown Compound by Classical Methods 134
5.3.3 New Approach for the Determination of a Molecule's Constitution 137

5.3.4 RDCs Measured for the Unknown Compound 138
5.3.5 Structural Models Used for RDC Analysis 138
5.3.6 Fitting Results 140
5.3.7 Discussion of Previous Data and Verification of the Constitution 141
5.3.8 Conclusion 143
5.4 Cross-Fitting of RDCs 144
5.4.1 Introduction and Motivation 144
5.4.2 The General Idea of Cross-Fitting RDCs 144
5.4.3 Two Steroids as Model Compounds 145
5.4.4 RDC Measurements 147
5.4.5 Calculation and Comparison of Alignment Tensors 148
5.4.6 Cross-Fitting RDCs via the Alignment Tensor 149
5.4.7 Differentiation of Diastereomers by Cross-Fitting RDCs 150
5.4.8 Differentiation of Diastereomers with Reduced RDC Data 152
5.4.9 Comparison with Other Methods 155
5.4.10 Direct Cross-Fitting of RDCs in Flexible Parts 156
5.4.11 Limitations and Potentials 157
5.4.12 Conclusion 158
6 Summary 159
7 Appendix 164
7.1 List of Abbreviations and Symbols 164
7.2 Supplemental Material for Chapter 3.1 168
7.3 Supplemental Material for Chapter 3.2 174
7.4 Supplemental Material for Chapter 3.3 175
7.5 Supplemental Material for Chapter 3.4 178
7.6 Supplemental Material for Chapter 3.5 183
7.7 Supplemental Material for Chapter 4.1 184
7.8 Supplemental Material for Chapter 4.2 188
7.9 Supplemental Material for Chapter 5.1 194
7.10 Supplemental Material for Chapter 5.2 195
7.11 Supplemental Material for Chapter 5.3 198
7.12 Supplemental Material for Chapter 5.4 203
8 References 218
Danksagung 239

1 Introduction

Structural analysis is one of the most important tasks in organic chemistry and biochemistry. Whether it is the constitution of a molecule, for example a reaction product or a newly isolated natural product, whether it is the stereochemistry of its chiral centers, or whether it is the conformation, for example of a biological active drug or its corresponding receptor, the determination of structure is always the first step. Without the knowledge about the molecular arrangement, questions about mechanism, activity, function or application won't be answered. Therefore it is not surprising, that a variety of different techniques exist, which deal with structural analysis.

High-resolution nuclear magnetic resonance (NMR) spectroscopy is one of the most important techniques for determining the structures of organic molecules. Sophisticated methods based on classical NMR parameters like chemical shifts, J-couplings, and nuclear Overhauser enhancement (NOE) have been developed for deriving constitution, configuration, and conformation of a molecule. The approach has been successfully applied to a vast number of molecules including thousands of biomacromolecules and uncountable natural and synthetic products.[1, 2]

However, all standard NMR parameters are of short-ranged nature: chemical shifts are typically affected by the first and second sphere of atoms surrounding the nucleus and usually provide only qualitative measures; ^{3}J-couplings are limited to dihedral angles via three covalent bonds; and through space connectivities via NOE can only be found up to 5 Å in favorable cases. As soon as the chain of short-ranged information is interrupted by NMR-inactive nuclei, a flexible linker, or overlapping signals, distant parts of a molecule cannot be correlated and the structure determination is bound to fail.

A potential solution for many of these problems can be found by the use of so-called *anisotropic parameters*: the nature of these parameters allows the extraction of angular information relative to the static magnetic field as an external reference. Therefore they make it generally possible to correlate independent parts of a molecule, even when they are far apart.

This thesis deals with different aspects of these anisotropic parameters. In chapter 2 the theoretical background will be discussed: the origin of anisotropic

parameters, the necessity to partially align a molecule in order to measure them and how this is achieved by so-called alignment media. An overview will be given on state-of-the-art alignment media, how to use them and how the alignment they introduce can be scaled. Furthermore, methods to measure anisotropic parameters as well as methods for their interpretation will be given.

Chapter 3 deals with the development of new alignment media. In five subchapters different newly developed polymer gels for the alignment of organic molecules are introduced. Their preparation is described, special properties are characterized, and potential applications are discussed. As will be shown, all the developed alignment media close important gaps in the variety of already existing alignment media.

The precise measurement of anisotropic parameters does not only require an alignment medium but also a proper strength of the induced alignment, as will be discussed in chapter 4. Significant developments for the scaling of alignment strength will be described in this part of the thesis.

Finally, applications of anisotropic parameters in structural analysis of small to medium sized organic molecules will be given in chapter 5. The four subchapters deal with new approaches for analyzing those parameters and describe examples for configurational, conformational as well as constitutional analysis.

2 Theory

2.1 Anisotropic Parameters

So-called anisotropic NMR parameters depend on the orientation of the molecules relative to the external magnetic field and therefore contain valuable structural information. However, in solution the molecule's orientation is averaged due to the Brownian motion and therefore no anisotropic parameters can be observed in isotropically averaged samples as for example liquids.

Hence anisotropic parameters can only be measured in solid state or in samples were the molecule of interest is *partially aligned*, as will be described in chapter 2.2. In such anisotropic samples a number of parameters can be observed, as for example dipolar couplings, chemical shift anisotropy, quadrupolar couplings in spin-1 nuclei, and pseudo-contact shifts in paramagnetic samples.[3, 4]

2.1.1 Dipolar Couplings

Next to scalar couplings via covalent bonds, dipolar couplings through space are probably the most important interactions in NMR spectroscopy. The origin of this interaction can be understood in a simplistic, classical picture if one considers spins as magnets with an inherent rotation at the Larmor frequency. Although spins are not oriented directly along the static magnetic field B_0, the integration over time of the fast rotating magnets yields a secular magnetic moment parallel or antiparallel to B_0 (see Figure 2.1. A, B). The magnetic field produced by spin I now adds up to the

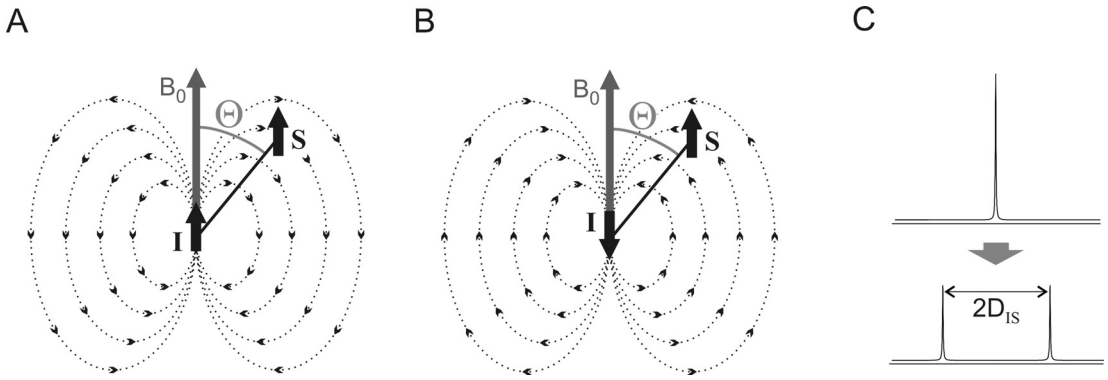

Figure 2.1.: Illustration of the dipolar interaction. The magnetic field induced by spin I adds up to the static magnetic field B_0 and leads to a shift of the resonance frequency of the close-by spin S. Since spins parallel (A) and antiparallel (B) to the magnetic field are about equally populated, a splitting with twice the dipolar coupling $2D_{IS}$ is observed (C).

static magnetic field felt by spin S and causes a shift of its resonance frequency, the so-called dipolar coupling. Since the spin I is almost equally populated parallel and antiparallel to B_0, a dipolar coupled signal shows a splitting as shown in Figure 2.1. C.

As one can experience by playing with permanent magnets, the interaction between two dipoles depends on the distance and on the angle between them. If a north pole gets close to a south pole, one feels an attractive force and, similarly, when two identical poles come together, one feels a repelling force. Furthermore, with the right angle between two magnets, one can also find an arrangement without interaction (Figure 2.2. A).

Similar to a classical magnet, the magnetic moment of spin I results in a magnetic field with the typical r^{-3}-dependence with respect to the distance r to the magnet and with the $(3 \cos^2 \Theta - 1)$-dependence with respect to the angle Θ relative to the axis of the magnetic moment (Figure 2.2. B). Since the magnetic moment of the spin is oriented along the static magnetic field B_0, this angle is identical to the angle with respect to B_0.

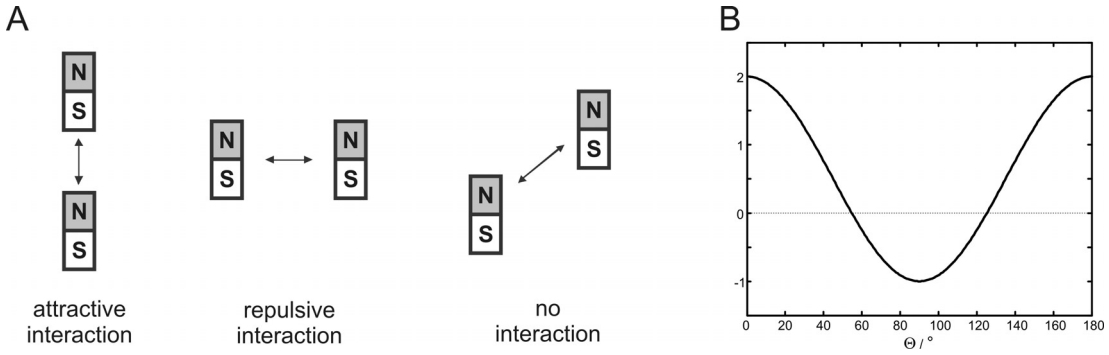

Figure 2.2.: Angular dependence of the dipolar interaction. Depending on the arrangement of two classical magnets the dipolar interaction between them might be attractive, repulsive or no interaction might be present (A). Similarly, the dipolar coupling between the two spins is directly proportional to the $(3 \cos^2 \Theta - 1)$-function (B) and can be used as angular information relative to the static magnetic field B_0.

Therefore strength and sign of this additional magnetic field vary, depending on the distance r between the two spins I and S and the angle Θ of their internuclear vector relative to B_0. The exact formula for the resulting dipolar coupling D_{IS} between two spins in a defined orientation is

$$D_{IS} = -\frac{\hbar \gamma_I \gamma_S \mu_0}{16\pi^2} \left\langle \frac{1}{r_{IS}^3} (3\cos^2 \Theta - 1) \right\rangle \qquad (2.1.)$$

with the gyromagnetic ratios γ_I and γ_S of the two spins, their distance r_{IS}, the angle Θ of the internuclear vector with B_0, the Planck constant $\hbar$, and the permeability of the vacuum μ_0. The brackets indicate an averaged over time.

2.1.2 Other Anisotropic Effects

Other anisotropic effects are chemical shift anisotropy (CSA), quadrupolar couplings, and pseudo contact shifts (PCS). As they play no or only a minor role within this thesis, they will be introduced only very briefly.

In solution only the isotropic component of the chemical shift tensor is measurable, but for oriented molecules the so-called zz-component of this tensor includes anisotropic components. Therefore the measurement of chemical shift anisotropy can in principal be used as structural information.

Quadrupolar couplings are only present in nuclei with spin ≥ 1 but due to the strong paramagnetic line broadening they are basically only relevant for deuterium nuclei. Quadrupolar couplings contain the same angular information as dipolar couplings, as the electronic field gradient tensor, which is responsible for the anisotropic interaction with the magnetic field, is usually aligned within 1° with the directly attached heteronucleus. Since the natural abundance of the deuterium isotope is only 0.015%, the measurement of quadrupolar interactions is limited to highly concentrated or isotopically enriched samples.

So-called pseudo contact shifts (PCS) are caused by the hyperfine coupling of a nuclei to an electron spin and can therefore only be observed in paramagnetic samples. The angular dependence and strength of the PCS is determined by the electron distribution of the paramagnetic center and can in general be used as a structural parameter.

As will be explained in the next chapter in detail for dipolar couplings, anisotropic effects reduce to *residual* anisotropic effects in partially aligned samples. As they play a minor role and as the underlying averaging is the same, this will not be explained in detail for the residual chemical shift anisotropy (RCSA) and the residual quadrupolar couplings (RQCs). However, specific aspects of RCSA and RQCs, their limitations and their measurement will be discussed in chapter 2.5.

2.2 From Anisotropic to Residual Anisotropic Parameters

Dipolar couplings are typically on the order of several thousand Hertz and lead to very broad lines in solid-state powder spectra. In liquid-state spectra, however, dipolar couplings are averaged to zero and sharp lines with high resolution are possible. Although dipolar couplings still contribute to relaxation processes like the NOE as a widely used structural parameter in NMR spectroscopy, a large amount of the potential structural information is lost by the averaging and valuable restraints would be obtained if dipolar couplings could be measured directly.

To be able to measure the desired additional structural information without significant loss in chemical shift resolution, an intermediate state between solid and liquid has to be reached: the molecule should be *partially aligned*. This can be achieved with the help of so-called alignment media (see chapter 2.3), which work as an orienting matrix as visualized in Figure 2.3. Within the alignment medium the molecule tumbles almost freely so that most of the anisotropic interactions are averaged out over time. However, the interaction with the oriented grid of the alignment medium prevents from complete averaging and a net orientation remains. One should point out, that this interaction between the molecule and the alignment medium might be of different character: steric, hydrophobic, dipolar, or even ionic interactions might be present.

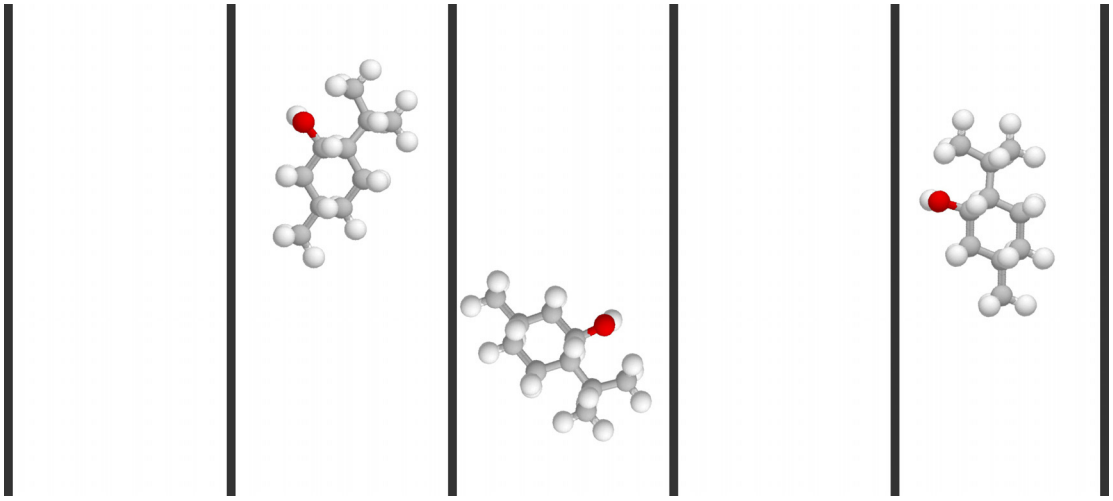

Figure 2.3.: Alignment media as a molecular grid. Solute molecules can tumble almost unhindered in the oriented matrix given by an alignment medium. Only a small fraction of time the molecule is oriented by the medium which leads to a time averaged net orientation. Despite the very intuitive picture, it should be mentioned that the situation is exaggerated here: in reality the molecular grid has a far larger mesh size compared to the aligned molecule.

In partially aligned samples, solute molecules are only oriented for a fractional amount of time. Typically would be the orientation for a time average of 0.05%. In this case a 23 kHz dipolar coupling between a carbon and its directly attached proton would reduce to a *residual* dipolar coupling (RDC) of only 11.5 Hz or a dipolar splitting of 23 Hz, which in many cases is also called RDC (see chapter 2.5.3 for the difference between those two nomenclatures). This way dipolar interactions can be measured with reasonable RDC-based line-broadening and therefore relatively high accuracy.

To use RDCs measured in partially aligned samples and obtain structural information, the partial averaging over time due to the tumbling of the molecule and its inherent flexibility has to be addressed by an adequate model. The description of the averaging in equation 2.1. is by no means trivial and the development of corresponding models for an effective inclusion of the flexibility of molecules is still an ongoing field of research. Therefore, the simplest case, the averaging of a completely rigid molecule, will be discussed firstly before effects of conformational averaging will be addressed.

2.2.1 Concept of the Alignment Tensor

If a rigid molecule with fixed distances and angles between all atoms is assumed, the averaging of equation 2.1. is only due to molecular tumbling of the molecule. The dipolar coupling in this case can be described by

$$D_{IS} = -\frac{\hbar\gamma_I\gamma_S\mu_0}{16\pi^2}\left(\frac{1}{r_{IS}^3}(3\left\langle\cos^2\Theta\right\rangle - 1)\right) \qquad (2.2.)$$

with averaging only over the angle Θ of the internuclear vector relative to the static magnetic field.

In an isotropic solution all orientations will be distributed equally, resulting in

$$\left\langle\cos^2\Theta\right\rangle = \frac{1}{3} \qquad (2.3.)$$

and the angular term will lead to a cancellation of all anisotropic interactions. In a partially oriented system, however, reduced dipolar couplings survive.

The description so far is based on the laboratory frame with the static magnetic field fixed along the z-axis and the molecule tumbling in space (Figure 2.4. A). For the description of orientational averaging it is useful to go into an arbitrary frame of reference which is fixed in the rigid molecule itself. In this reference frame the molecule is fixed in space while the magnetic field vector is changing its position (Figure 2.4. B).

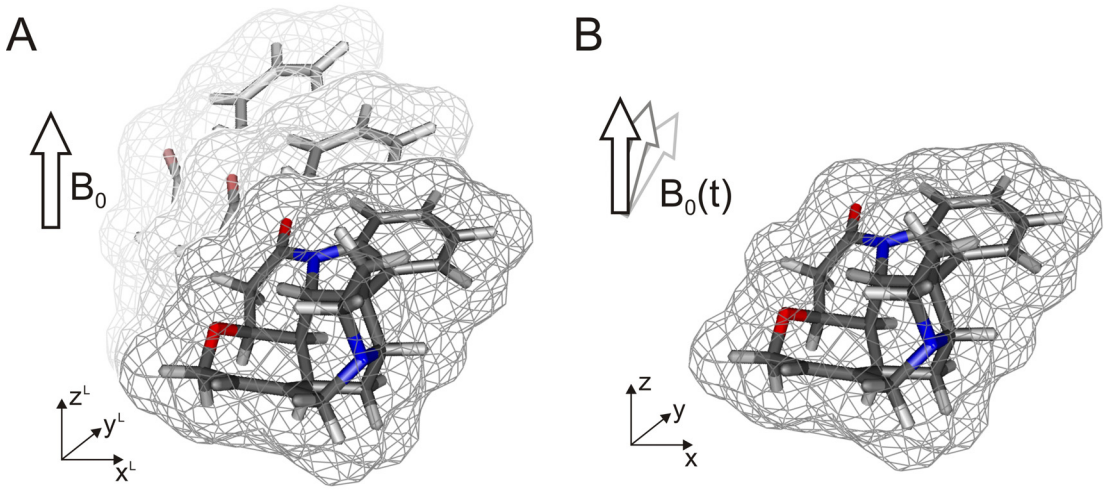

Figure 2.4.: In the laboratory frame (A) the molecule is tumbling with the static magnetic field fixed along the z-axis. In contrast, the reference frame of a rigid molecule (B) moves with the compound and leads to an effective variation of the magnetic field vector. *Reprinted from Reference [5] Copyright (2009), with permission from Elsevier.*

With the cylindrical symmetry of the magnetic field and the assumption of a cylindrically symmetric alignment medium with its director pointing into the same direction as the magnetic field, the distribution of the magnetic field can be described by the so-called probability tensor **P**. This tensor is a second order approximation of the orientational probability distribution of the magnetic field direction as seen in the molecular fixed frame of reference. It is represented by a 3 x 3 matrix with its elements $P_{\alpha\beta}$ describing the averaged probabilities to find the magnetic field at the angles ϑ_x, ϑ_y, ϑ_z relative to the axes of the reference frame of the molecule:

$$P_{\alpha\beta} = \left\langle \cos\vartheta_\alpha \cos\vartheta_\beta \right\rangle \;\; ; \;\; \alpha,\beta = (\mathrm{x,y,z}) \qquad (2.4.)$$

For a known probability matrix **P** the residual dipolar coupling constant for any spin pair I and S along the unit vector $\overrightarrow{r_{IS}}$ can be calculated as:

$$D_{IS} = -\frac{\hbar\gamma_I\gamma_S\mu_0}{16\pi^2}\left(\frac{1}{r_{IS}^3}(3\overrightarrow{r_{IS}}^T \mathrm{P}\overrightarrow{r_{IS}} - 1)\right) \qquad (2.5.).$$

Because of the condition for the probability distribution ($P_{xx} + P_{yy} + P_{zz} = 1$) and since **P** is symmetric along the diagonal, it is fully specified by only five independent parameters.

In a pictorial way the probability tensor can be imagined as an ellipsoid whose orientation is fixed to the molecular frame of reference. For example, when the molecule tumbles isotropically in solution there are equal probabilities to find the magnetic field vector along all the three principal axes of the probability tensor and as a consequence the ellipsoid reduces to a sphere (see Figure 2.5. C). The three principal axes $\hat{x}$, $\hat{y}$, and $\hat{z}$ of this ellipsoid are defined by the three eigenvectors of the matrix **P** and the lengths of the three half axes are defined by the eigenvalues $P_{\hat{x}}$, $P_{\hat{y}}$, and $P_{\hat{z}}$. In the special frame of reference defined by this principal axis system the matrix **P** is diagonal. In this case the eigenvalues (principal values) $P_{\hat{x}}$, $P_{\hat{y}}$, and $P_{\hat{z}}$ correspond to the probabilities to find the magnetic field along the principal axes $\hat{x}$, $\hat{y}$, and $\hat{z}$, respectively. Note, that the eigenvalues are usually ordered according to $P_{\hat{x}} \leq P_{\hat{y}} \leq P_{\hat{z}}$.

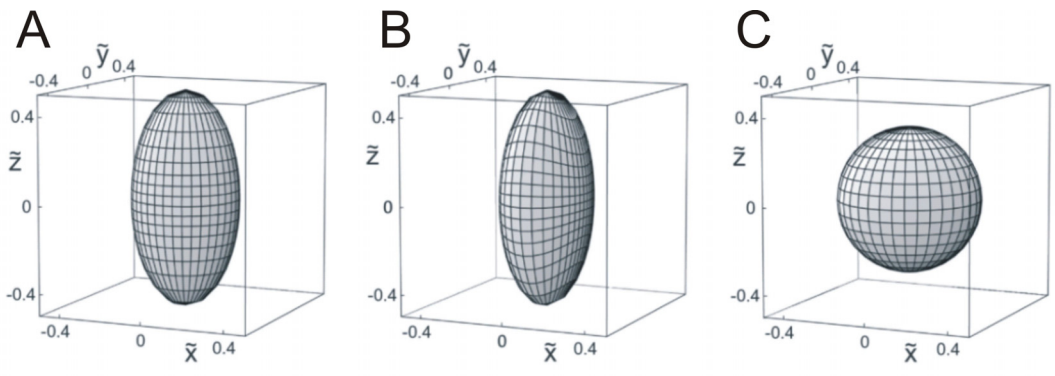

Figure 2.5.: Graphical representations of the probability tensor. Examples for three characteristic probability ellipsoids **P**, as seen from the principal axis system with axes $\hat{x}$, $\hat{y}$, and $\hat{z}$: An axially symmetric probability ellipsoid (A), a rhombic probability ellipsoid (B), and an isotropic probability ellipsoid (C). *Copyright Wiley-VCH Verlag GmbH & Co. KGaA. Reproduced with permission from Reference [6].*

Although the probability tensor **P** is very intuitive and sufficient to describe the resulting anisotropic parameters in a rigid molecule, it is more common to express the

partial alignment of the molecule in terms of the so-called alignment tensor **A**, which is given by

$$\mathbf{A} = \mathbf{P} - \frac{1}{3}\,\mathbf{1} \qquad (2.6.)$$

with **1** being the unit matrix. **A** has the same principal axes system as the probability tensor **P**. It describes how strongly the molecule deviates from isotropic tumbling, i.e. if it is less likely or more likely to find the molecule within a certain orientation compared to an isotropic distribution. It is important to note that by convention the principal values of the alignment tensor **A** are ordered with increasing magnitude ($|A_{\hat{x}}| \leq |A_{\hat{y}}| \leq |A_{\hat{z}}|$), which might lead to a reordering of the axis label.

With a given alignment tensor **A**, the residual dipolar coupling between spin I and S can now be calculated as:

$$D_{IS} = -\frac{\hbar\gamma_I\gamma_S\mu_0}{16\pi^2}\left(\frac{3}{r_{IS}^3}\vec{r}_{IS}^{\,T} A \vec{r}_{IS}\right) \qquad (2.7.).$$

Initial work on the interpretation of alignment was done by Saupe,[7, 8] who introduced the so-called Saupe matrix **S**, which is sometimes used for historical reasons instead of the alignment tensor **A**. They are simply related by a scaling factor:

$$\mathbf{S} = \frac{3}{2}\,\mathbf{A} \qquad (2.8.).$$

Furthermore the alignment is sometimes characterized by the axial (D_a) and rhombic components (D_r) of the alignment tensor:

$$D_a = \frac{3}{2}A_{\hat{z}} \;; \qquad D_r = A_{\hat{x}} - A_{\hat{y}} \qquad (2.9.).$$

It is worth to emphasize again, that the concept of the alignment tensor by its definition is only valid for rigid molecules or for rigid parts of a molecule. As most applications on medium-sized organic molecules reported today are based on an

interpretation of RDCs via the concept of the alignment tensor, it is no surprise to find that most molecules studied are relatively rigid.

However, as many interesting molecules can not be treated as rigid, there has been made a lot of effort to develop methods to treat flexible molecules in the last years. It turned out that the concept of the alignment tensor even allows the approximate description of conformationally averaged structures.

2.2.2 Flexible Molecules

For a flexible compound, r_{IS} and Θ in equation 2.1. are both depending on the conformation of the molecule and the interconversion of different structures is overlaid with the reorientation of the molecule as described in the previous section for a rigid molecule. The two processes can be separated in principle if their time scales are sufficiently different. Especially if the interconversion rate is fast compared to the reorientation rate, the molecule of interest can be described by an average structure with a single alignment tensor. For the case that conformational changes happen on a similar or slower time scale than the corresponding reorientation, each conformer has to be described by its own alignment tensor.[9, 10]

Concentrating on vibrational motions, it has first been shown by Lucas that RDCs for a molecule can be influenced if the motions are coupled to the reorientation processes.[11-13] The vibrational corrections to RDCs are generally small, estimated to be about 1-2% in the original publications[11, 12] and < 5% in later articles.[14] Since the experimental error of many RDCs is larger than this correction, it is usually safely neglected in corresponding configurational and conformational studies of larger molecules. However, it has been shown that vibrational corrections can account for RDCs and other anisotropic parameters measured in molecules with tetrahedral symmetry like methane or tetramethylsilane,[15-17] which should not show any anisotropic parameters at all in the rigid picture.

Models for the treatment of RDCs in flexible molecules can also be based on a mean-field approach. Instead of the alignment tensor which describes the anisotropic part of the orientational averaging of a rigid molecule, averaging over all orientations and conformations can also be achieved when describing the conformationally dependent probabilities to find a molecule in a certain orientation as a sum of an isotropic and anisotropic potential. The anisotropic potential can then be expanded into a series of functions with their coefficients as fitting parameters. As with the

alignment tensor approach, RDCs in addition to the ones used for the fitting process then provide highly useful structural information even for molecules with conformational flexibility. Several models like the Chord-model,[18] the additive potential (AP) model,[19] the maximum entropy (ME) approach[20] and their combination into the APME approach[21, 22] have been proposed.

Other ways of fitting RDCs to a number of conformations are based on theoretical calculations of potential conformers (e.g. by DFT calculations or by generating an ensemble of structures and sorting out lowest energy conformers in an QM/MM approach) and directly fitting RDCs to either a set of alignment tensors[23] or to a single alignment tensor as a crude approximation.[24, 25] Furthermore, RDC driven MD simulations have recently been used for the treatment of non-rigid molecules.[26] However, this is an ongoing field of research and the development of more approaches to analyze flexible molecules in conformational and configurational studies can be expected in the future.

2.3 Alignment Media

As described in chapter 2.2, an intermediate state between the total alignment in a solid and the isotropic averaging in solution must be achieved in order to measure residual dipolar couplings. This partial alignment is obtained by a so-called alignment medium, which works as an oriented molecular grid capable to constrain the tumbling of the molecule in a way, that a time averaged net orientation remains.

Over the last decades many different alignment media have been developed for various applications and usually one can divide them in two categories: those which cause very strong alignment and those which introduce only weak alignment. The first are designed to achieve maximum dipolar couplings in order to get a fundamental understanding of molecular arrangements and motions in very small molecules by a multitude of long-range couplings. However, this detailed and complex analysis is only applicable for very simple molecules. For small to medium-sized organic molecules, like natural or synthetic products and biologically active molecules, as well as for larger biomolecules fewer couplings should be present and hence the induced alignment should be relatively weak. As the focus of this thesis lies on medium-sized molecules, in the following the discussion of alignment media will be limited on very weakly aligning media.

2.3.1 General Types of Alignment

Three different ways of partially aligning a molecule are known today: alignment in a liquid crystalline phase, alignment in a stretched gel, and the orientation via paramagnetic ions.

Paramagnetic Alignment

As paramagnetic ions align in a magnetic field they can be used to align a molecule which either forms complexes with the ions itself or which can be equipped with a specifically designed tag complexing the ion. Paramagnetic alignment is frequently used in biomolecular NMR, where RDCs and pseudo contact shifts (PCS) provide valuable structural parameters. However their use for small molecules is quite limited since covalently attached paramagnetic centers usually broaden the lines of neighboring nuclei beyond detection and therefore no RDCs or other anisotropic parameter have been measured by paramagnetic alignment of small molecules so far.

Liquid Crystalline Phases

Liquid crystalline (LC) phases have been the first alignment media reported to partially align solute molecules for NMR measurements. Already in 1953 the proton resonance spectrum of *p*-azoxyanisole in its liquid crystalline phase has been reported by Spence et al.[27] The probably more famous first spectrum of a solute aligned in a liquid crystal was shown 1963 by Saupe and Englert, who acquired a spectrum of benzene dissolved in the thermotropic LC phase of a *p*-azoxyanisole derivate.[7] Many further examples for nematic, smectic and cholesteric liquid crystalline phases followed. Nowadays, mostly lyotropic mesophases instead of the thermotropic media are used. In both cases the alignment results from a spontaneous orientation of the liquid crystal in the strong external magnetic field. This provides the anisotropic grid which causes the solute to align.

Stretched Polymer Gels

Cross-linked polymers form gels upon swelling in a solvent and their network form a kind of molecular grid. If such a gel is mechanically stretched (or compressed) this grid gets an orientation and hence forms an anisotropic matrix. Therefore solute molecules diffused into such a stretched gel will be partially oriented by the interaction with the polymer network. Stretched polymer gels were introduced in 1981 by Deloche and Samulski,[28] who used this to study the polymer itself, but it took until 2000 that the first solute molecules diffused into stretched polymer gels were investigated.[29, 30] Since that, a variety of different polymer gels were developed for this approach of ‘strain induced alignment in a gel’ (SAG).

2.3.2 Overview over Existing Alignment Media

In the following an overview over liquid crystalline phases and polymer gels used as alignment media will be given. From the users point of view it makes sense to classify the existing alignment media with respect to their application into media for aqueous solutions, media for polar organic solutions, media for apolar organic solutions and media with the special feature of being chiral.

Alignment Media for Aqueous Solutions

A large number of alignment media for aqueous solutions has been found in the field of biomolecular NMR spectroscopy and many of them have been transferred to applications with small organic molecules. Initial aqueous alignment media focused on liquid crystalline phases. A large variety of so-called bicelles[31-34] has been adjusted to corresponding needs especially in protein NMR. Similarly, the liquid crystals known as Otting phases[35] are frequently used because of their relatively low cost and easy preparation. The preferred alignment media for nucleic acids are negatively charged filamentous Pf1 phage, which are also used for negatively-to-neutral charged proteins and sugars.[36-38] There is a large number of less frequently used liquid crystalline phases: for example cellulose crystallites,[39] the so-called Helfrich phases,[40-42] purple membranes,[43, 44] and mineral liquid crystals.[45, 46] Recently reported alignment based on DNA nanotubes[47] and nucleic acid G-tetrad structures[48] are probably too expensive to be of real use in small molecule NMR.

The use of gels as alignment media for aqueous solutions started with poly(acrylamide) (PAA) gels[29, 30, 49] which are commonly prepared in most biochemical laboratories. Based on this, a variety of copolymers of PAA with positively or negatively charged monomeric units have been introduced.[50, 51] Recent developments include also gelatin[52] as an inert, extremely low cost and widely applicable hydrogel as well as the closely related collagen.[53, 54] Alignment media with interesting features are so-called “composite alignment media”: liquid crystalline phases that are immobilized in a gel phase.[55-57]

Alignment Media for Apolar Organic Solvents

For typical apolar organic solvents like chloroform, dichloromethane, benzene, dioxane, or tetrahydrofurane a large variety of liquid crystalline alignment media exists, but typically with quite strong alignment.[3, 4]

Widely used alignment media for small organic molecules are poly(amino acids) like poly-γ-benzyl-L-glutamate (PBLG),[58-60] poly-γ-ethyl-L-glutamate (PELG),[61] or poly-ε-carbobenzyloxy-L-lysin (PCBLL).[62] A promising liquid crystalline phase with good alignment properties also for larger molecules appears to be 4-*n*-pentyl-4’-cyanobiphenyl (PCBP), which is a thermotropic liquid crystalline solvent.[63]

The first published gel-based alignment medium suitable for apolar solvents has been polystyrene (PS), which is compatible with all the above mentioned

solvents.[64, 65] Poly(vinyl acetate) (PVAc) is another robust polymer matrix with the solvent range extended to more polar solvents.[66] Poly(dimethylsiloxane) (PDMS), instead, extends the solvent range to more apolar solvents like hexane and is maybe the most widely used apolar gel at the moment.[67] Recently poly(methyl methacrylate) (PMMA) gels[68] and polyurethane (PU) gels[69] have been reported as alignment media for apolar organic solvents.

Alignment Media for Polar Organic Solvents

In contrast to aqueous and apolar solvents, weakly aligning media for polar organic solvents are sparse. Very few liquid crystalline phases are known, one of them being PBLG with DMF as the polar solvent.[70] Furthermore, poly(ethylene glycol) based phases with DMSO/water mixtures, like e.g. pentaethylene glycol monododecyl ether (called $C_{12}E_5$) exist.[71, 72]

As gel-based alignment media for polar organic solvents two polymers have been known so far: the already mentioned PVAc is a good alignment medium for most polar organic solvents including e.g. methanol, acetone and acetonitrile and works reasonably well with DMSO and DMF;[66] the so-called PH-poly(dimethyl acrylamide) (PH-PDMAA) can be produced with varying charged groups and also covers different solvents.[73]

However, especially for the very commonly used NMR solvent DMSO a robust alignment medium was missing so far, as no liquid crystalline phase works with pure DMSO and both mentioned gels have major disadvantages. This gap could be closed within this thesis by the development of cross-linked poly(acrylonitrile) (PAN) optimized as a gel-based alignment medium for DMSO. A full characterization of this already very important new alignment medium will be given in chapter 3.1.

Furthermore cross-linked poly(ethylene oxide) (PEO) was developed as alignment medium which covers a very broad range of solvents, reaching from water over polar organic solvents (including DMSO, methanol, acetonitrile) to apolar organic solvents (including dioxane, THF, dichloromethane, chloroform, benzene) and will be described in chapter 3.5.

Chiral Alignment Media

Many of the alignment media presented so far possess stereogenic centers, but only media with a large chiral super structure are referred to as chiral alignment media since only those are capable of distinguishing enantiomers.

A variety of chiral alignment media for organic solvents is known with the most widely used and best characterized being the poly(amino acids) PBLG and PCBLL.[58-60, 62] Both polymers form lyotropic mesophases and possess α-helical structures for which many examples of enantiomeric differentiation have been shown. In addition to chiral poly(amino acids) it was demonstrated that achiral media with chiral cages like cyclodextrines serve as alignment media with the potential of chiral discrimination.[74]

For water soluble compounds an alignment medium based on a glucopon/buffered water/*n*-hexanol lyotropic liquid crystal[75] was introduced and also the triple helical gelatin forms a chiral hydrogel and is especially interesting because of its unbeatable low price.[52] Besides water, conventional gelatin can also be used for water/DMSO mixtures with up to 80% DMSO.[76] Recently hydrogels of the commercially available polysaccharides ι- and κ-carrageenan have been reported as chiral alignment media for water as the solvent.[77]

A chiral alignment medium suitable for pure DMSO could be developed within the scope of this thesis: a covalently cross-linked derivate of gelatin the so-called e^--gelatin. Compared to conventional gelatin not only the suitable range of solvents but also the applicable temperature range could be improved, as will be described in chapter 3.4.

2.3.3 Considerations for Choosing the Right Alignment Medium

In the last section an overview over existing and newly developed alignment media was given and all alignment media for small to medium-sized molecule applications are summarized in Table 2.1. To choose the best alignment medium for a given problem, several things should be considered.

Solubility

In most of the cases the solvent which should be used for an analysis is given by the solubility of the solute to investigate, by a specific question, e.g. the conformation

in a particular solvent, or by preliminary studies, which were already done in a certain solvent. Very obvious, the alignment medium should be compatible with the desired solvent. However, this might not be sufficient. Furthermore also the solute should be compatible with the alignment medium, as it works as a kind of co-solvent. If not all three, solute, solvent and alignment medium, fit together different scenarios might happen: the solute might precipitate, the solid component of a liquid crystalline phase might precipitate, the necessary order in a liquid crystalline phase might break down, a polymer gel might not swell or shrink again, or the solute might simply not diffuse in a gel.

It is evident, that charged alignment media like phage or copolymers of PAA might exclude charged solutes, but not only charges also polarity might be crucial: the polycyclic aziridine studied in this thesis (see chapter 5.3) was apolar enough to dissolve sufficiently in chloroform but apparently too polar to diffuse in a PDMS/chloroform gel, although this polymer is swelling very good in halogenated solvents. As another example PVAc should be mentioned: several cyclic peptides tested did not diffuse into PVAc gels, neither in DMSO nor in methanol and it seems like this polymer excludes peptides in general.

These effects are often not predictable and one will simply need to try whether a solute fits to a desired alignment medium. However the examples show that the development of new alignment media is always desirable, although in the meanwhile the whole range of solvents is covered one might need an alternative medium for a particular problem.

Stability

If one deals with an unstable solute, one might need to consider special characteristics of certain alignment media, e.g. if moisture would be a problem. Using cross-linked polymers as orienting media, one might get problems with residual radicals (due to chemical cross-linking or due to the irradiation used for cross-linking), which are still present in the gel. For most samples this is not a problem, but a sensitive molecule might degrade.

Furthermore also the stability of the alignment medium itself might be an issue, if specific conditions are desired. Especially with liquid crystalline phases, but also with conventional gelatin, one is usually limited to certain ranges of temperature or pH.

Table 2.1.: Alignment media for small to medium-sized molecules.

Description	Compatible solvents	Remarks	Ref.
Liquid Crystals			
Pf1 phage	D_2O	charged	[36-38]
Bicelles, micelles	D_2O		[31-34]
Purple membranes	D_2O		[43,44]
Cellulose crystals	D_2O		[39]
V_2O_5	D_2O		[45]
$H_3Sb_3P_2O_{14}$	D_2O		[46]
C_mE_n / n-alkyl alcohol (Otting phases)	D_2O		[35]
cetylpyridinium halogenides / hexanol (Helfrig phases)	D_2O		[40-42]
$C_{12}E_5$	DMSO/D_2O		[71,72]
4-*n*-pentyl-4'-cyanobiphenyl (PCBP)	n.a.	orienting solvent	[63]
Poly-γ-benzyl-L-glutamate (PBLG)	$CDCl_3$, CD_2Cl_2, DMF, THF, Dioxane	chiral	[58-60,70]
Poly-γ-benzyl-L-glutamate (PBLG) (high MW)	$CDCl_3$, CD_2Cl_2, DMF, THF, Dioxane	chiral, weaker alignment	[81]
Poly-γ-ethyl-L-glutamate (PELG)	$CDCl_3$, CD_2Cl_2	chiral	[61]
Poly-ε-carbobenzyloxy-L-lysin (PCBLL)	$CDCl_3$, CD_2Cl_2	chiral	[62]
immobilized media	D_2O	LC in gel	[55-57]
DNA nanotubes	D_2O		[47]
G-tetrad structures	D_2O		[48]
Stretched Gels			
Gelatin	D_2O	chiral, cheap	[52]
Collagen	D_2O	chiral	[53,54]
e^--gelatin	D_2O, DMSO	chiral	chapter 3.4
Poly (acrylamide) (PAA)	D_2O		[29,30,49]
Acrylamide copolymers	D_2O	charged	[50,51]
Dimethylacrylamide co-polymers (PH-PDMAA)	D_2O, DMSO, DMF	charged	[73]
Poly (acrylonitrile) (PAN), deuterated PAN (dPAN)	DMSO, DMF		chapters 3.1, 3.3
Poly (vinyl acetate) (PVAc)	$CDCl_3$, CD_2Cl_2, CD_3OD, CD_3CN, DMSO, DMF, C_6D_6, acetone, THF, EtOAc, dioxane		[66]
Poly (ethylene oxide) (PEO)	$CDCl_3$, CD_2Cl_2, CD_3OD, CD_3CN, DMSO, DMF, C_6D_6, acetone, benzene, THF, TFE, EtOAc, dioxane, D_2O, mixtures	single NMR signal	chapter 3.5
Poly (methyl methacrylate) (PMMA)	$CDCl_3$, CD_2Cl_2, CD_3CN, acetone, C_6D_6, EtOAc		[68]
Polyurethan (PU)	$CDCl_3$, CD_2Cl_2, CD_3CN, acetone, C_6D_6		[69]
Polystyrene (PS), deuterated PS (dPS)	$CDCl_3$, CD_2Cl_2, THF, C_6D_6, dioxane		[64,65], chapter 3.2
Poly (dimethylsiloxane) (PDMS)	$CDCl_3$, CD_2Cl_2, C_6D_6, n-hexane	single NMR signal	[67]

Signal Overlap

An important aspect of very weakly aligning media is the overlap with undesired signals from the alignment medium itself. Liquid crystals like the poly(amino acids) usually provide relatively strong alignment and the proton signals of the alignment medium are strongly broadened due to the multitude of large homonuclear dipolar couplings. The resulting effect on spectra is just a slight increase of the baseline. The situation is different for weakly aligning polymer gels where broad polymer signals and signals from residual monomers and radical starters might be present. In highly concentrated samples it is usually easy to distinguish such signals from solute peaks and especially in 2D or 3D spectra the probability of overlap is quite low. However, at low solute concentrations large signals from the polymer with their broad feet might impose serious problems for RDC detection. One way to circumvent this problem is to pick an alignment medium with NMR signals in regions that do not overlap with the NMR spectrum of the molecule of interest. PMMA, for example, does not contain any aromatic signals[68] and might be used instead of PS[65] if signals in this region show overlap. An even better gel in this respect is PDMS, which shows a single signal at 0.1 ppm that can be suppressed by water suppression methods.[67]

The best choice, of course, would be an alignment medium free of any signals. So far, only the liquid crystalline phase PCBP has been reported as a perdeuterated medium to align small molecules, but no gel-based alignment medium has been modified in that way.

Within this thesis two polymers have been produced in its perdeuterated form to get basically signal-free alignment media for small molecules: the deuterated form of polystyrene (dPS) will be characterized in chapter 3.2 and the deuterated form of poly(acrylonitrile) (dPAN) will be discussed in chapter 3.3.

Sample Preparation

Samples of liquid crystalline phases are usually prepared by dissolving the solid component (e.g. the polyaminoacid PBLG or PCBLL) together with the molecule of interest in the desired solvent (e.g. $CDCl_3$) within an NMR-tube (see Figure 2.6. A). As these solutions are typically very viscous, special care has to be taken in homogenizing them. This is usually done by centrifuging it back and forth in the NMR-tube, which is quite time-consuming. However, after this procedure the sample is ready to be measured.

In contrast, the preparation of gel-based alignment media requires some more time. There are different ways of achieving the necessary mechanical stretching of the polymer gel, the most common one is the following: A dry stick of the cross-linked polymer is placed into an NMR tube and swollen by the addition of a solvent. The swelling gel reaches the glass walls of the tube and further swelling is limited in these directions, hence automatically results in a stretching (see Figure 2.6. B). Depending on the polymer it takes several days or even weeks until the gel is fully swollen and equilibrated. As a certain percentage of gels is breaking during the swelling and equilibration process, one usually allows the gels first to swell without the compound and later adds the solute molecule to the equilibrated gel after checking its quality. Therefore, in addition to the equilibration time, some days for diffusion of the compound in the pre-swollen gel matrix are necessary, especially when dealing with valuable samples.

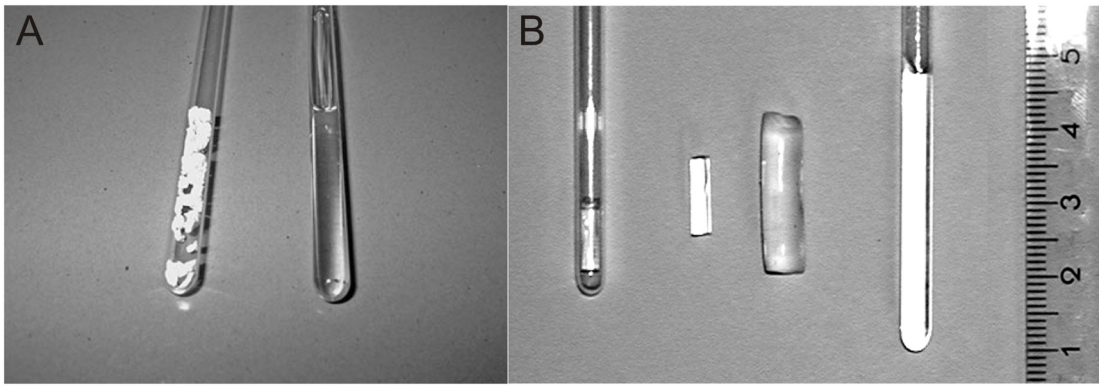

Figure 2.6.: Preparation of a liquid crystalline and a gel-based alignment medium. An example for a liquid crystalline sample is shown in (A): dry PBLG in an NMR-tube (left) and a readily prepared sample of the lyotropic mesophase (right). An example for a stretched gel at various stages of the preparation is shown in (B): dry cross-linked PS as an unswollen polymer stick in a standard NMR tube (left), polymer stick directly after polymerization and fully swollen (middle), and polymer stick swollen in an NMR-tube with an effective stretching along the tube axis (right). *Copyright Wiley-VCH Verlag GmbH & Co. KGaA. Reproduced with permission from References [78] and [64].*

Other preparation schemes for stretching of polymer gels, like drying and re-swelling on a glass capillary,[50] using a funnel to squeeze pre-swollen gels into the NMR-tube,[79] or compressing a pre-swollen gel with a Shigemi-plunger[29, 49] are rarely used for small molecule applications, as the induced alignment is usually too weak.

This introduces another crucial point for choosing the right alignment medium: for each application the proper degree of alignment must be introduced into the sample. Apparently this is very important and there are several ways to achieve this, which will be discussed in detail in the following chapter.

2.4 Scaling of the Alignment Strength

To get spectra with the best possible resolution while being able to precisely measure RDCs, it is necessary to carefully adjust the alignment strength. In Figure 2.7. the amide region of efrapeptin C, a 15 amino acid peptide, is shown in PDMS/$CDCl_3$-gels with two different alignment strengths as monitored by the residual quadrupolar coupling of the solvent $CDCl_3$. While the spectrum with the lower alignment (see Figure 2.7. A) will certainly allow the straight-forward extraction of RDCs, the stronger alignment (see Figure 2.7. B) leads to linewidths of approximately 60 Hz, mainly due to unresolved $^1H,^1H$-RDCs. Clearly in the latter case extraction of coupling constants becomes much more difficult, hence the alignment of a molecule should not be too strong. On the other hand, too weak alignment might average the RDCs to an extent, where the couplings are in the order of the experimental error. Therefore the alignment strength should be adjusted to an adequate size. As a rule of thumb, the largest RDC between a proton and a directly attached carbon should be in the range of $\pm$ 30 Hz, as it can be derived from equation 2.1. considering the different gyromagnetic ratios and bond lengths.[80]

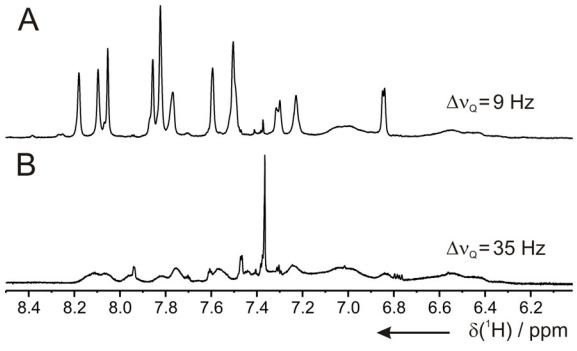

Figure 2.7.: Importance of the right alignment strength. The amide region of the ^1H-1D spectrum of the 15 amino acid peptide efrapeptin C is shown for the alignment in two different PDMS/$CDCl_3$ gels with deuterium quadrupolar splittings $\Delta\nu_Q$ of the solvent of 9 Hz (A) and 35 Hz (B). The increased alignment strength leads to line widths of $\approx$ 60 Hz of the amide signals which usually prohibits accurate extraction of RDCs. *Reprinted from Reference [5] Copyright (2009), with permission from Elsevier.*

To monitor the alignment strength of a particular alignment medium, it is common to measure the quadrupolar splitting $\Delta\nu_Q$ (see chapter 2.5.2) of the deuterated solvent by acquiring a simple ^2H-1D spectrum. Often, out of this value a rough estimate of the partial alignment a solute molecule will experience in this alignment medium is

made. However, this should be done with caution, as comparing quadrupolar splittings of the solvent with RDCs of the solute is a comparison of the alignment an alignment medium introduces in the solvent molecules with that introduced in the solute molecules. It is obvious, that quadrupolar splittings of different solvents used for a LC-phase or a gel should not be compared. Furthermore it makes no sense to compare quadrupolar splittings of the same solvent in different LC-phases or gels in order to draw conclusions about the RDCs to expect for a solute in this different media. The particular interactions between the alignment media and the observed molecule (solvent or solute) leading to the measureable partial alignment, might be of different nature and therefore not comparable. However, because of its good accessibility the quadrupolar splitting is widely used to classify the alignment strength of a particular alignment medium and when comparing different samples of the same combination of alignment medium, solvent and solute, the observed quadrupolar splittings and RDCs behave linear to a very good approximation. Moreover, maximum RDCs observed for one solute in an alignment medium/solvent combination might give a hint for the range of RDCs to expect for a second solute in the same alignment medium and solvent, provided that the interactions leading to the partial alignment are similar for both solutes.

In general, the strength of alignment induced by an alignment medium can be varied in various ways which will be summarized in the following sections. The direct way is the variation of the alignment medium itself, which, however, usually involves the preparation of a new sample. More sophisticated methods like variable angle NMR or the stretching of gels in a specialized stretching device allow the scaling of alignment in a single sample.

2.4.1 Adjusting the Alignment Medium

In partially aligned samples, the solute molecules typically experience a time averaged interaction with the alignment medium with only very short contact times. An increase of the alignment strength in this case can simply be achieved by increasing the number of oriented (polymer) chains and therefore the number of contacts per time with the solute. Depending on the type of medium, different possibilities exist for achieving this.

Adjustment of Liquid Crystalline Phases

A characteristic feature of liquid crystalline phases is their limitation to certain concentration and temperature ranges. Especially the lower concentration limit for a first order phase transition leads to a minimum alignment strength. Above this first order phase transition of lyotropic mesophases, their alignment strength can typically be increased by a higher concentration of the liquid crystal. A certain percentage of this solid part is automatically oriented by the static magnetic field and the time averaged alignment is approximately linear with the concentration of the polymer chains, phage, bicelles, or other oriented structures. In Figure 2.8. A the concentration dependence of the alignment strength is shown for filamentous Pf1 phage with a very small lower limit of alignment. In this way, by adding phage or by diluting the liquid crystalline phase one can easily adjust the alignment strength.

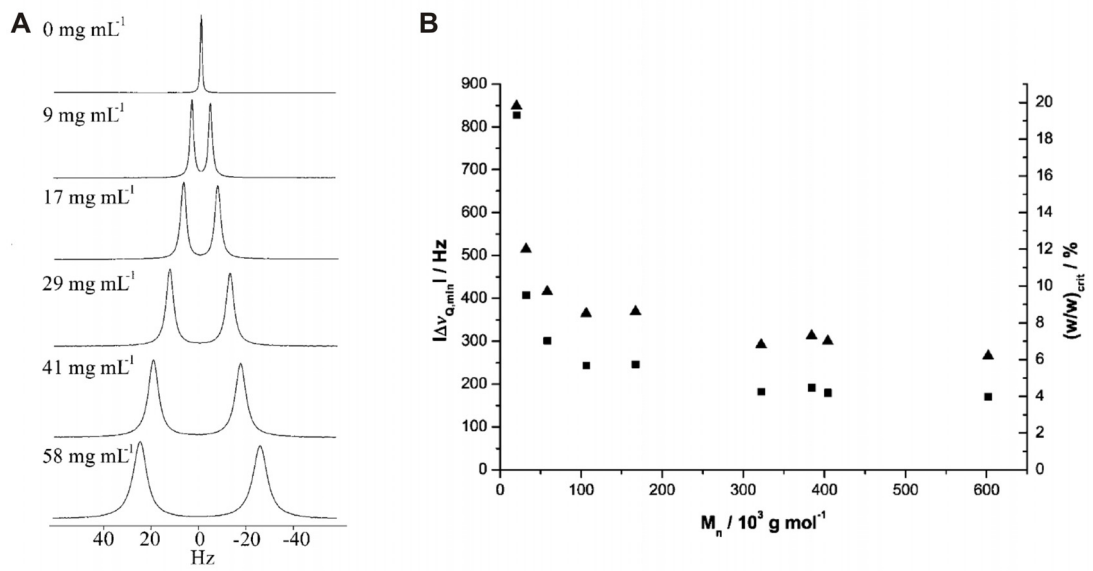

Figure 2.8.: Scaling of alignment in lyotropic liquid crystals. The alignment is roughly proportional to the concentration of the solid part of the crystalline phase as shown with deuterium spectra for different concentrations of Pf1 phage in D_2O (A). The critical concentration for the first order phase transition (▲) of PBLG/$CDCl_3$ liquid crystalline phases and therefore the minimal alignment strength, monitored by the quadrupolar splitting of the solvent (■), decrease with increasing molecular weight of PBLG (B). *(A) Reprinted by permission from Macmillan Publishers Ltd: Nature Structural Biology [37], copyright (1998). (B) Copyright Wiley-VCH Verlag GmbH & Co. KGaA. Reproduced with permission from Reference [81].*

In liquid crystals for apolar organic solvents the same rules apply, however, due to the relatively large lower limit of alignment, the variation in alignment strength can only be achieved down to the concentration of the first order phase transition of the

mesophase. Unfortunately, for most of the liquid crystalline phases known this lower limit of alignment is already quite large for medium-sized organic molecules. Interestingly, the concentration for the first order phase transition and therefore also the minimum achievable alignment strength of such liquid crystals decreases with an increased persistent length of the polymer. Recently it was shown for PBLG with very high molecular weight that in this way the minimum alignment strength can be reduced significantly (see Figure 2.8. B), making it possible to reliably extract RDCs for medium-sized organic molecules.[81] However, commercially available liquid crystalline phases for organic solvents typically posses a minimum alignment strength, which is too large and scaling it down requires more sophisticated techniques, like variable angle sample spinning (see chapter 2.4.2).

Adjustment of Polymer Gels

In an unstretched gel, polymer chains are randomly distributed in all three dimensions and solute molecules, although interacting constantly with the gel matrix, are not aligned. As soon as the gel is stretched, however, more polymer chains are oriented in the stretching direction than perpendicular to it and a net alignment results.

It is clear, that the alignment strength increases with the degree of stretching of the gel. This can be varied in different ways depending on the method used for stretching (see previous section). When using the stretching-by-restricted-swelling approach shown in Figure 2.6. B, simply the diameter of the dry stick relative to the inner diameter of the NMR-tube can be varied. For a given stick, the usage of 4 mm or even 3 mm tubes instead of the standard 5 mm tubes can be of interest and smaller variations might be achieved by the use of thick-wall or thin-wall tubes. When synthesizing the polymer sticks, the diameter of the stick can be varied to basically any size and fine-tuning of the alignment is possible. Since the swelling strength of a polymer stick in different solvents can vary dramatically, the stretching of course also depends on the solvent used.[65]

Another possibility of scaling the alignment lies in the variation of the polymer itself. In chemical synthesis, the amount of radical starter defines the average length of polymer chains and the amount of cross-linker added to the reaction influences the stiffness of the polymer network. The longer the average chain length of the polymer and the more cross-linked the gel is, the stronger the alignment gets.[65, 66] In

Figure 2.9. the dependence of the alignment strength, monitored by the quadrupolar splitting of the deuterated solvent, on the amount of cross-linker (A) and on the amount of radical starter (B) is shown for PS/$CDCl_3$ gels as an example. The same rule applies for polymer gels cross-linked via accelerated electrons, where in turn the irradiation dose defines the amount of cross-linking in the gel.[67]

Finally, within the limits of the melting and boiling point of the solvent used, the alignment can also be varied by a change of temperature. For a PS/$CDCl_3$ gel, for example, a factor of 2.4 in alignment strength can be achieved over the accessible temperature range (see Figure 2.9. C).

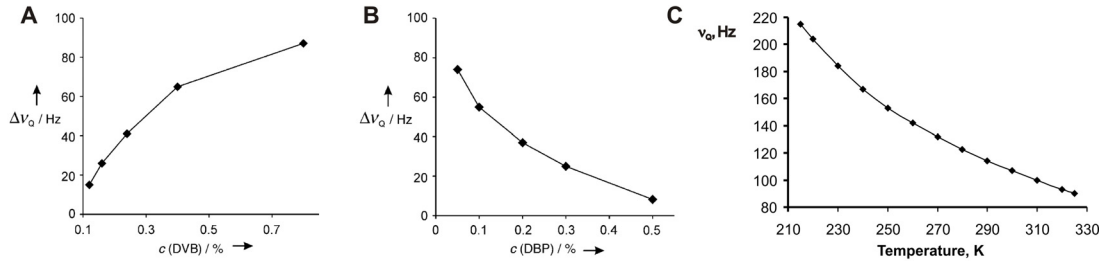

Figure 2.9.: Scaling of alignment in gel-based alignment media. The alignment strength, monitored by the quadrupolar splitting of the solvent $CDCl_3$, increases with the amount of cross-linking (concentration of cross-linker DVB) (A) and the length of the polymer chains (and therefore decreases with the concentration of radical starter DBP) (B). Furthermore the alignment is reduced by higher temperatures due to the enhanced motional averaging (C). *(A, B) Copyright Wiley-VCH Verlag GmbH & Co. KGaA. Reproduced with permission from Reference [64]. (C) Reproduced in part with permission from Reference [65] Copyright 2005 American Chemical Society.*

The methods described so far, like varying chain length, concentration, or amount of cross-linking, give the possibility to prepare samples of different alignment strengths and especially with the gel-based alignment media the range of achievable alignment strengths is not limited. Nevertheless, each alignment strength requires a new sample to be prepared, which is not only time-consuming, but might also cost valuable sample. Methods to vary the alignment in a single sample, as discussed in the next sections, are therefore highly desirable.

2.4.2 Variable Angle NMR

In chapter 2.1.1 dipolar couplings were introduced with the averaging over all possible orientations (see equation 2.1.). Later on, in chapter 2.2.1 the averaging was included in the alignment tensor, assuming that the average director of the alignment

medium is parallel to the magnetic field. Considering a possible deviation of the average director relative to the magnetic field by the angle Θ_{dB} leads to the expression

$$D_{IS} = -\frac{\hbar\gamma_I\gamma_S\mu_0}{16\pi^2}\left(\frac{3}{2}\cos^2\Theta_{dB} - \frac{1}{2}\right)\left\langle\frac{1}{r_{IS}^3}(3\cos^2\Theta_{md} - 1)\right\rangle \qquad (2.10.)$$

with Θ_{md} being the angle between the internuclear vector within the molecule and the average director of the alignment medium.

The equation implies that RDCs can generally be scaled if the director can be varied independently of the static magnetic field, which has already been derived by Saupe in his original theory of NMR in liquid crystalline phases.[8] For liquid crystalline phases and for gel-based alignment media, this variation of the director is achieved in different ways, as will be described in the following.

Variable Angle Sample Spinning

For liquid crystalline phases the sample has to be spun around its axis, as it is done by magic angle sample spinning (MAS) in solid state NMR. In high resolution MAS experiments this spinning leads to a fast change of the orientation of the crystal relative to the magnetic field, which in principal leads to a director parallel to the spinning axis. Regarding equation 2.10. this would correspond to Θ_{dB} being 54.7° (the magic angle) and thus to a cancelation of the whole term, as the first bracket would become zero.

In liquid crystalline phases the average director will always orient parallel or perpendicular to the magnetic field, depending on the sign of the anisotropy of the magnetic susceptibility of the particular liquid crystal.[14] However, the orientation along the magnetic field takes place with a certain time constant which depends on the rotational viscosity and the magnetic field strength.[82] In samples spun around an axis not parallel to the magnetic field this leads to a continuous reorientation of the liquid crystals and therefore spinning is a way to vary the director of alignment for liquid crystalline phases.

The average director of a nematic phase with positive magnetic susceptibility anisotropy will be aligned along the rotational axis as long as the angle of the rotational axis relative to the static magnetic field is < 54.7°. For angles larger than the magic angle, the average director aligns perpendicular to the magnetic field which

leads to strongly modulated spectra. At the magic angle itself, the orientation of the director is not defined. For nematic phases with negative magnetic susceptibility anisotropy a stable rotation axis is only obtained for angles > 54.7°.[83] Generally, spinning above a certain threshold frequency is needed, which depends on the viscosity and the magnetic field.[84, 85] Since most liquid crystalline phases used today are lyotropic mesophases with relatively small magnetic susceptibility anisotropy, it should be noted that the orientation of the director is also influenced by the inertial torque when spinning fast.[86] The effect leads to an upper limit for the sample spinning frequency under which stable conditions for director alignment are obtained. It is generally the case that the window of rotational frequencies is the smaller the lower the magnetic susceptibility anisotropy is.[86]

With the according probe head, variable angle sample spinning (VASS)[86] allows the scaling of alignment and therefore the scaling of all anisotropic interaction close to zero, as demonstrated e.g. for RDCs measured on strychnine in PBLG/$CDCl_3$.[87] Many applications[86-95] have been reported using the approach of VASS and many more can be expected in the future. However, the method is of course limited by the necessary hardware.

Variable Angle NMR with Gels

As has been shown previously, the change of the average director of the alignment medium can also be applied to gel-based alignment media.[96-98] In this case, the director is given by the mechanical stretching along the tube axis, which might simply be varied in the magnetic field with an appropriate probe head. For this variable angle (VA) NMR sample spinning is not necessary.

In contrast to VASS NMR for liquid crystalline phases, VA NMR with stretched gels can be used for the whole range of angles Θ_{dB} from 0° to 90°.[98] At the magic angle a complete removal of all anisotropic interactions can be used for simulating an isotropic state in the aligned sample.[96, 98]

2.4.3 Gel Stretching Apparatus

Several devices have been developed to stretch gels. One of the first stretching devices is the one introduced by Chou et al. which squeezes a poly(acrylamide) gel into an open-cut NMR-tube via a funnel.[79] However, the device just helps to prepare the sample but is not able to adjust the alignment strength. The method introduced by

Ishii and Tycko uses a Shigemi plunger to compress the gel in an NMR-tube and, depending on the pressure put on the plunger, different alignment strengths can be obtained.[29, 49] A similar approach based on the strong swelling capacity of charged hydrogels uses the Shigemi plunger simply as a restriction for gel swelling.[51] The alignment strength in this case can be increased by slightly loosening the plunger and letting the hydrogel swell stronger with an increased effective stretching. However, this approach is a one-way-street since a swollen gel can hardly be pushed back to a smaller size without destruction of the sample.

A totally different stretching apparatus was introduced by the group of Kuchel:[99] a flexible silicone rubber tube, which contains the gel, is placed inside an open-cut NMR-tube and fixed at the bottom by a rubber plug. After stretching the gel to the desired strength by pulling the rubber tube, the position of the latter one is fixed by a corresponding screwing device at the top of the NMR-tube. With gelatin/D_2O as the gel-based alignment medium, Kuchel et al. were able to show that rapid, arbitrary and reversible scaling of the alignment strength is possible with this kind of apparatus.[99, 100]

Within this thesis, a slightly modified version of this stretching apparatus, applicable for standard 5 mm liquid-state NMR equipment, was designed and it was shown that the containing silicone tube can not only stretch gelatin/D_2O but also other polymer gels based on polar solvents like D_2O and DMSO. This will be discussed in detail in chapter 4.1.

Furthermore this approach could be extended to the whole range of gel-based alignment media by the use of a perfluorinated rubber tube instead of the silicone tube, as will be discussed in chapter 4.2.

2.5 Measurement of Residual Anisotropic Effects

To measure anisotropic parameters one usually has to acquire appropriate spectra for the measurement of shifts or couplings in an isotropic state and in an anisotropic state. This is because the anisotropic shift or coupling simply adds up to the isotropic one. Therefore in the anisotropic state the sum of isotropic and anisotropic contribution will be measured, while in the isotropic state only the isotropic shift or coupling is present. The differences of those shift or coupling values then give the desired anisotropic parameters.

Usually this requires two samples, the substance in isotropic solution and the substance in the anisotropic alignment medium. Alternatively, methods for scaling the alignment strength (see chapter 2.4) like variable angle methods or the gel stretching apparatus can be used to achieve no alignment and therefore isotropic conditions within the same sample. However, it is always necessary to acquire at least two spectra.

The only exception among the anisotropic effects is the quadrupolar interaction, as there is no isotropic quadrupolar coupling. Therefore the coupling measured in the anisotropic state is directly the desired RQC.

2.5.1 Measurement of RCSA

Changes in chemical shifts due to the partial alignment of a molecule in an alignment medium are easy to measure. However, as discussed in detail before,[96] a considerable part of this changes is due to the co-solvent effect of the alignment medium. Therefore the isotropic and the anisotropic measurements should be done in the *same* sample, as it could be realized with variable angle sample spinning (VASS)[86, 87] or variable angle NMR in stretched gels (VA-NMR)[96] (see also chapter 2.4.2). In this approaches isotropic chemical shifts are measured at the magic angle, while the anisotropic measurements are carried out at an angle different to the magic angle.

One more problem for the accurate measurement of RCSA is the fact, that chemical shifts are values relative to a reference, usually the solvent signal or standards like e.g. tetramethylsilane (TMS). As this reference molecule might also partially align in the alignment medium, it might have its own RCSA value, which should be taken into account. As has been shown, even molecules with tetrahedral

symmetry as TMS, methane, CCl_4 or NH_4^+ are partially aligned[15] and show chemical shift changes[96] depending on the strength of alignment. Because of the small RCSA values observed for the reference molecules it is usually neglected but represents a systematic error for RCSA measurements.

Also the interpretation of RCSA values is much more difficult than for RDCs and good estimates for the chemical shift tensors of the molecule have to be made e.g. by ab initio methods.

Due to the difficulties in measuring RCSA, it has been used only in a few applications so far, like for example the relative orientation of α-helices in proteins from so-called PISEMA-wheels[101] or the backbone orientation of nucleic acids from ^{31}P-RCSA data.[102] For small molecules first attempts to measure RCSA have been made.[96]

2.5.2 Measurement of RQCs

The splitting, which results from residual quadrupolar couplings, is frequently measured in deuterium 1D spectra of the deuterated solvent of a sample, as was mentioned already in chapter 2.4. In this case one only measures the splitting, usually called $\Delta\nu_Q$, but not the residual quadrupolar coupling, which in addition is characterized by a sign. However, out of 1D spectra one can not extract the sign, which would be necessary to use it as structural information. For this purpose more sophisticated spectra, like a P.E.-COSY type heteronuclear correlation experiment,[97] would be necessary.

For the use of an estimate of the alignment strength (see chapter 2.4), however, the splitting is absolutely sufficient. If not mentioned otherwise, throughout this thesis all quadrupolar splittings measured from 1D spectra are given as positive values, regardless of the (unknown) sign of the RQC causing that splitting.

Considering the difficulties in determining the sign of RQCs and the necessity of a highly concentrated or isotopically enriched sample, it is not surprising that RQCs are barely used for structure determination of small molecules. Almost exclusively the group around J. Courtieu uses deuterium NMR on small organic molecules in anisotropic samples, mainly for the distinction of enantiomers in chiral alignment media (see references [103-106] and references therein).

2.5.3 Measurement of RDCs

In partially aligned samples residual dipolar splittings, D, simply add to the splitting of scalar couplings, J (see Figure 2.10.). The splitting observed in the anisotropic state, T, is therefore the sum of J and D:

$$T = J + D \qquad (2.11.)$$

(Note, that other publications consider the residual dipolar coupling, D_{IS}, given by $T = J + 2D_{IS}$. This coupling D_{IS} is in consistence with the equations given in chapters 2.1 and 2.2. However, throughout this thesis all RDC values are named with D and describe the anisotropic contribution to the observed splitting as given in equation 2.11. The factor 2 between coupling and splitting is simply a scaling and does not affect the analysis of RDCs as long as all values are used in the same manner.)

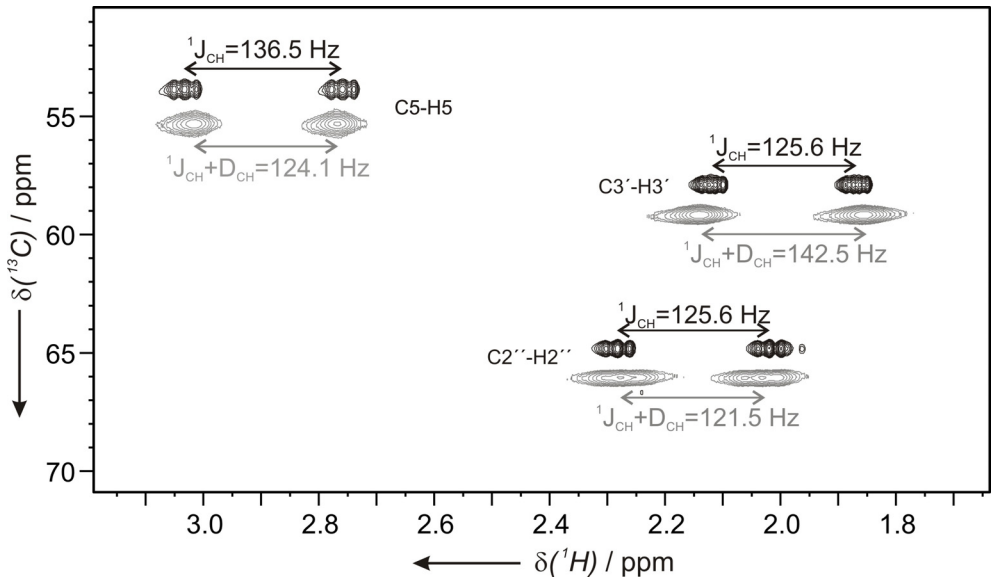

Figure 2.10.: So-called CLIP-HSQC spectra[107] for the measurement of RDCs. The region of CH signals of the tricyclic hydrocarbon discussed in chapter 5.1 is shown for the isotropic sample (black) and the anisotropic sample (gray, shifted for clarity). Residual dipolar couplings, D, only present in the anisotropic sample add to the scalar couplings, J, observed in the isotropic sample.

To measure RDCs, in principle most experiments for measuring scalar couplings can be used the same way to extract dipolar couplings. In practice, however, the required precision for measuring RDCs is usually higher than for scalar couplings and the sign information of the measured couplings is needed. As a result, existing

methods have been strongly revised and extended during the last decade and further techniques can be expected in the future.

Since the focus of this thesis is on small organic molecules which are usually only available at natural isotope abundance, none of the experiments specifically designed for labeled macromolecules will be described here, but only those pulse sequences used within this work will be mentioned in the following sections. After this short description of the used experiments, the method for extraction of couplings out of the resulting spectra will be explained.

Experiments to Measure One-Bond RDCs

The most easily measured RDCs are along one-bond heteronuclear couplings. In organic molecules, this are typically $^1D_{CH}$ or $^1D_{NH}$ couplings as obtained from the difference of $^1T_{CH} = {}^1J_{CH} + {}^1D_{CH}$ and $^1T_{NH} = {}^1J_{NH} + {}^1D_{NH}$ measured in the partially aligned sample and the corresponding scalar couplings $^1J_{CH}$ or $^1J_{NH}$ of the isotropic sample. If the alignment strength is adjusted correctly, RDCs are significantly smaller than corresponding scalar couplings of known sign and sign-sensitive measurement of RDCs is most easily achieved. Since the distance between directly bound nuclei is usually well-known and fixed, RDCs can also directly be translated into relative angular information, which makes one-bond RDCs the most frequently used anisotropic information.

Regarding the actual pulse sequences used for coupling measurements, conventional heteronuclear multiple-quantum correlation (HMQC) or heteronuclear single-quantum correlation (HSQC) experiments can be recorded without heteronuclear decoupling during acquisition. However, if transfer delays are not well-matched with the $^1T_{CH}$ ($^1T_{NH}$) couplings, dispersive antiphase contributions to the signals are obtained, for which the individual multiplet components have to be phased separately to obtain correct coupling constants.[108] An elegant way to circumvent individual phasing of the multiplet components is achieved by the CLIP-HSQC (see Figure 2.11. A) which removes dispersive antiphase components prior to detection.[107] The experiment leads to spectra with outstanding overall quality, which is even improved when using recently optimized BEBOP excitation[109-111] and BIBOP inversion[111] pulses and corresponding universal rotation pulses using the construction scheme by Luy et al.[112] For overlap of α and β components of

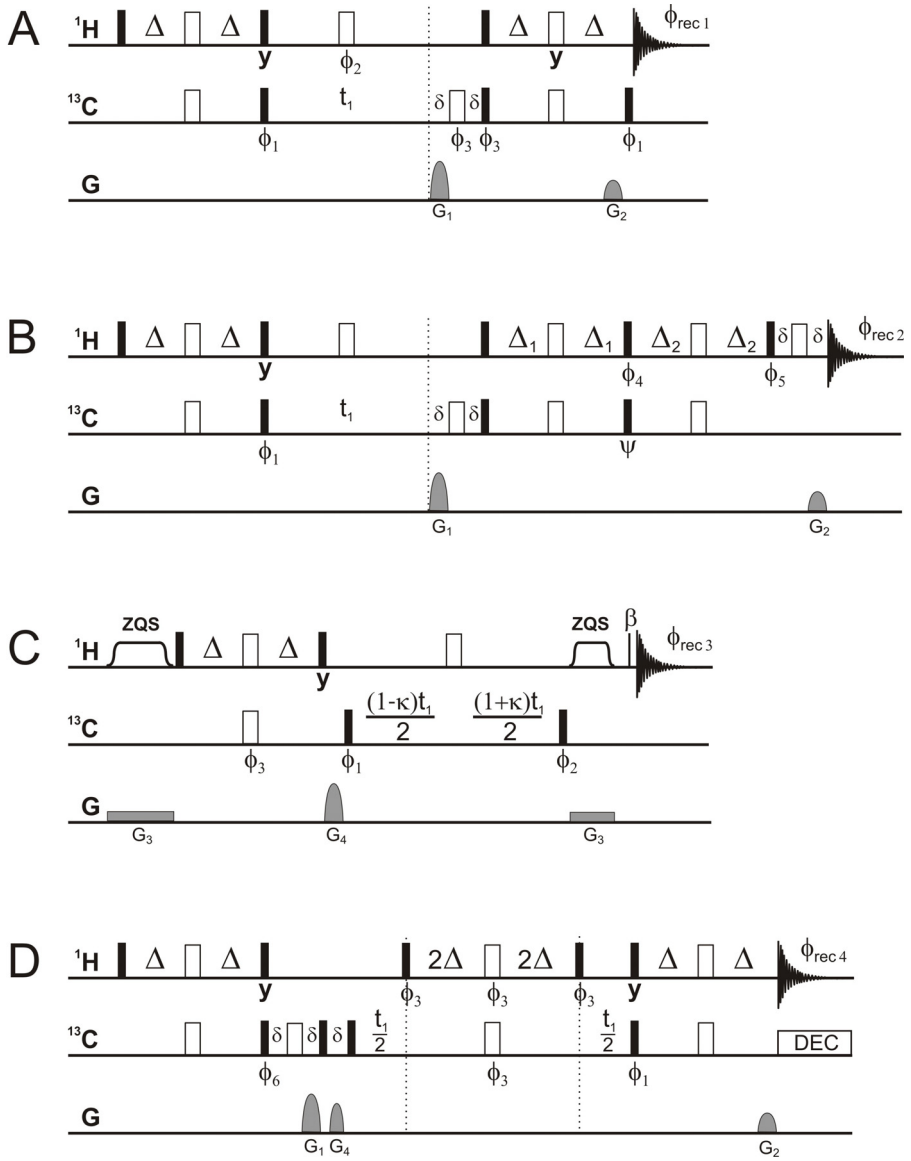

Figure 2.11.: Pulse sequences used for RDC measurements. (A) The CLIP-HSQC for the measurement of $^1T_{CH}$ couplings with pure absorptive multiplets.[107] (B) HSQC-IP/AP for measurement of $^1T_{CH}$ couplings with samples at low concentrations. By acquiring spectra with the phase $\Psi = x$ and $\Psi = -x$, the corresponding added/subtracted spectra can also be used to extract $^2T_{HH}$ couplings of CH_2 groups.[113] (C) The P.E.-HSQC to extract $^2T_{HH}$ and $^1T_{CH}$ couplings in a single experiment.[114] It results in an E.COSY-type pattern with the two couplings in the direct dimension and κ times $^1T_{CH}$ in the indirect dimension (see Figure 2.12.). (D) The J-BIRD^{d,X}-HSQC with heteronuclear J-evolution in the indirect dimension is designed for maximum resolution.[52]
Filled and open bars indicate 90° and 180° pulses unless indicated otherwise. The delays δ are determined by the duration of applied gradients, $\Delta = 1/(4\ ^1T_{CH})$ and the corresponding delays Δ_1 and Δ_2 have to be adjusted to the expected spin systems according to reference.[113] The β-pulse refers to a short pulse with a flip angle of typically 30°-40°.[114] Phases are $\varphi_1 = \varphi_{rec2} = x,-x$; $\varphi_2 = 4(x),4(-x)$; $\varphi_3 = 2(x),2(-x)$; $\varphi_6 = (y),4(-y)$; $\varphi_{rec1} = -x,x,x,-x$; $\varphi_{rec2} = \varphi_{rec4} = x,-x,x,-x,-x,x,-x,x$; HSQC-IP and HSQC-AP experiments are obtained for $\varphi_6 = y$, $\varphi_7 = x$ or $\varphi_6 = x$, $\varphi_7 = y$, respectively. Gradients must fulfill the ratios $G_1:G_2 = 40.1:10$ for carbon as the heteronucleus and G_4 as purge gradient should not be a multiple of G_1 or G_2. Gradient G_3 together with adiabatic inversion pulses indicated by ZQS have to be adjusted for the Keeler z-filter scheme.[115] *Reprinted from Reference [5] Copyright (2009), with permission from Elsevier.*

multiplets, the CLAP-HSQC in a kind of IPAP approach provides additional resolution.[107]

A second set of experiments for samples at low concentrations, where the most sensitive approach for coupling measurement at good resolution is needed, is given by the HSQC-IP/AP sequences[113] shown in Figure 2.11. B. Phases have to be corrected individually in this case and obtained couplings might not be as accurate as for the CLIP-HSQC,[107] but for low signal-to-noise ratios the pulse sequences represent a very good compromise.

In the experiments mentioned so far, signal widths are generally broadened by either heteronuclear long-range couplings or passive homonuclear couplings. The situation can significantly be improved by selective decoupling using BIRD filter elements.[116, 117] The approach has been applied in several versions for measuring RDCs using (J+D)-evolution periods with a central $BIRD^{d,X}$-filter.[52, 118-120] In Figure 2.11. D an experiment with (J+D)-evolution in the indirect dimension optimized for best resolution in the coupling-dimension is shown.[52]

Experiments to Measure RDCs Between Geminal Protons

A second class of easily measured RDCs with fixed geometry are along homonuclear $^2J_{HH}$ scalar couplings found in methylene and methyl groups. A number of sophisticated experiments have been developed for the sign-sensitive measurement of these couplings: The most easily applied experiment is probably the P.E.HSQC[114] described in Figure 2.11. C which is best in cases where overlap is not a problem. The experiment results in an E.COSY-type pattern with the $^2T_{HH}$ and $^1T_{CH}$ couplings in the direct dimension and $\kappa \cdot {}^1T_{CH}$ in the indirect dimension. The tilt of the resulting multiplet is given by the sign of the $^2T_{HH}$ coupling relative to the (known) sign of the $^1T_{CH}$ coupling (see Figure 2.12.).

Other techniques resulting in further reduced multiplet structures require a couple or more spectra to be acquired and combined, but potentially lead to spectra with better resolved signals.[113, 121, 122] The extension of the HSQC-IP/AP approach shown in Figure 2.11. B to the closely related HSQC-IP(x)/IP(-x) and HSQC-AP(x)/AP(-x) allows the sign-sensitive measurement of $^2T_{HH}$ couplings in separated sub-spectra.[113] A general problem with the extraction of homonuclear two-bond couplings are frequently observed second-order artifacts which often prohibit a simple extraction of coupling constants in all of the available experiments.

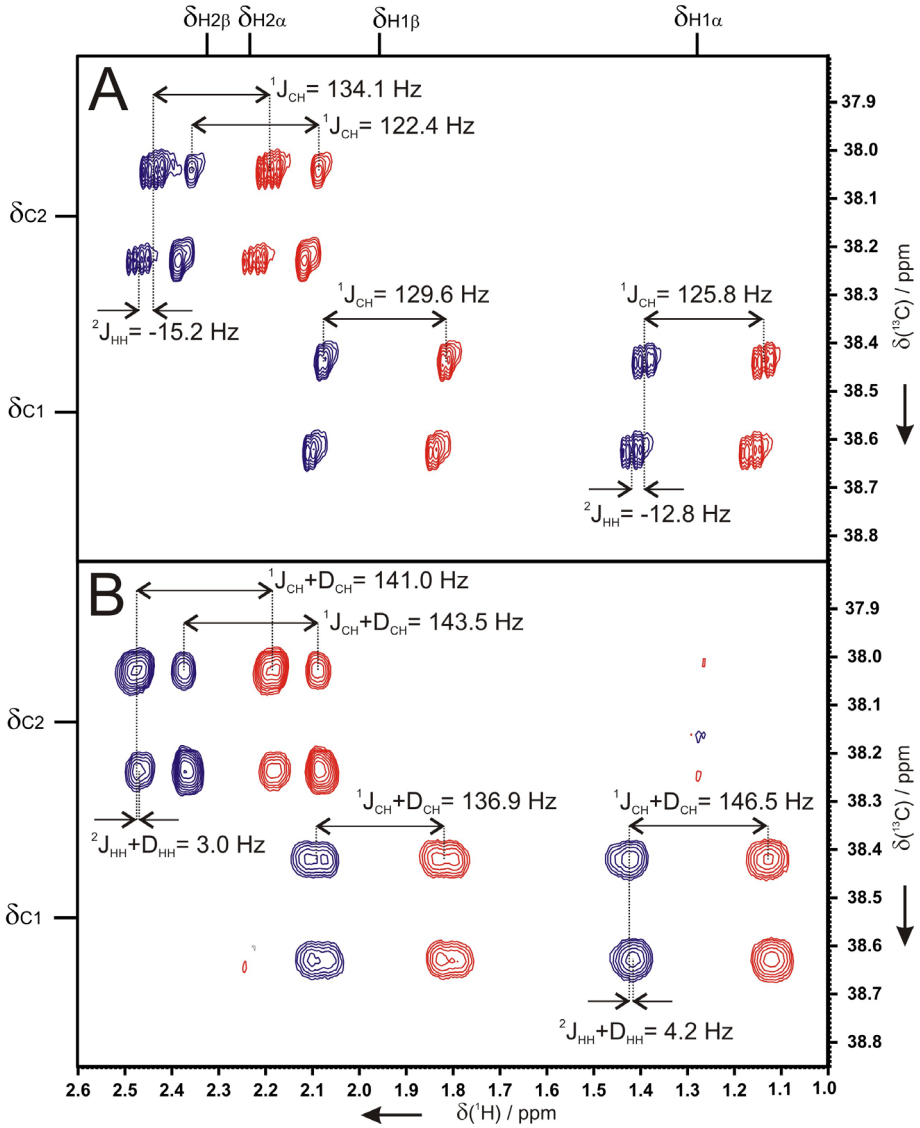

Figure 2.12.: The P.E.HSQC[114] for simultaneous extraction of $^2T_{HH}$ and $^1T_{CH}$ couplings. Details of P.E.HSQC spectra acquired on 5-α-cholestan-3-one in a chloroform solution (A) and in a stretched PDMS/$CDCl_3$ gel (B), showing the multiplets of the methylene groups at C1 and C2 (for details on the substance see chapter 5.4). One-bond $^1H,^{13}C$-couplings and geminal $^1H,^1H$-couplings are assigned in the spectra. Note that the sign-information of the homonuclear couplings is given by the tilt of the multiplet and that in this case the tilt changes upon alignment in the gel as the negative $^2J_{HH}$-couplings (A) are compensated by the larger positive D_{HH}-couplings of both methylene groups in the aligned spectrum (B). Blue indicates positive, red negative contour levels.

Other RDCs

Especially in small molecules with few protons available, the additional measurement of other RDCs than the above mentioned are important for obtaining sufficient structural information.

It has been shown that long range $^{1}H,^{13}C$ RDCs[123, 124] and RDCs along $^{1}J_{CC}$ couplings[125] and even $^{2}J_{CC}$ couplings[126] can be used. Such carbon-carbon RDCs are one order of magnitude smaller than the corresponding proton-carbon or proton-proton RDCs, which should be taken into account. The same is the case for long-range proton-carbon RDCs, which are therefore very difficult to measure with the necessary accuracy.

The sign sensitive extraction of homonuclear proton-proton RDCs is difficult because of the multitude of long-range RDCs contributing to the proton multiplet and they are potentially difficult to interpret since the interproton distance is usually not known and might be strongly modulated by the inherent flexibility of the molecule. Therefore their measurement won't be discussed here, nor will the measurement of RDCs to other heteronuclei like ^{31}P or ^{19}F be discussed, as their analysis is not part of this thesis.

Extraction of Couplings from a Spectrum

The measurement of RDCs requires high accuracy and a realistic determination of experimental errors. Therefore a scheme for the extraction of couplings out of the acquired spectra was used, which will be described in the following for the example of one-bond heteronuclear couplings out of CLIP-HSQC spectra.

$^{1}T_{CH}$ coupling constants are extracted by selecting a slice along the direct dimension of the CLIP-HSQC at the appropriate carbon frequency and manually shifting a copy of the slice until the corresponding multiplet components were centered with respect to each other (see Figure 2.13.). In doing so, special care has to be taken regarding the determination of experimental errors as line-broadening and strong coupling artifacts can have confound impact on the accuracy of determined coupling constants. This is done by the procedure visualized in Figure 2.13.: After extraction of corresponding 1D-slices, α- and β-components of the multiplets were shifted relative to each other and the shift in Hz is taken as the coupling constant. For an error estimate, not the center of the signals was overlapped, but the left- and rightmost positions of overlap of the two multiplet components with special consideration of the flanks and feet of the signal of interest. This left- and rightmost shifts are used for the estimation of the individual maximum error of a coupling.

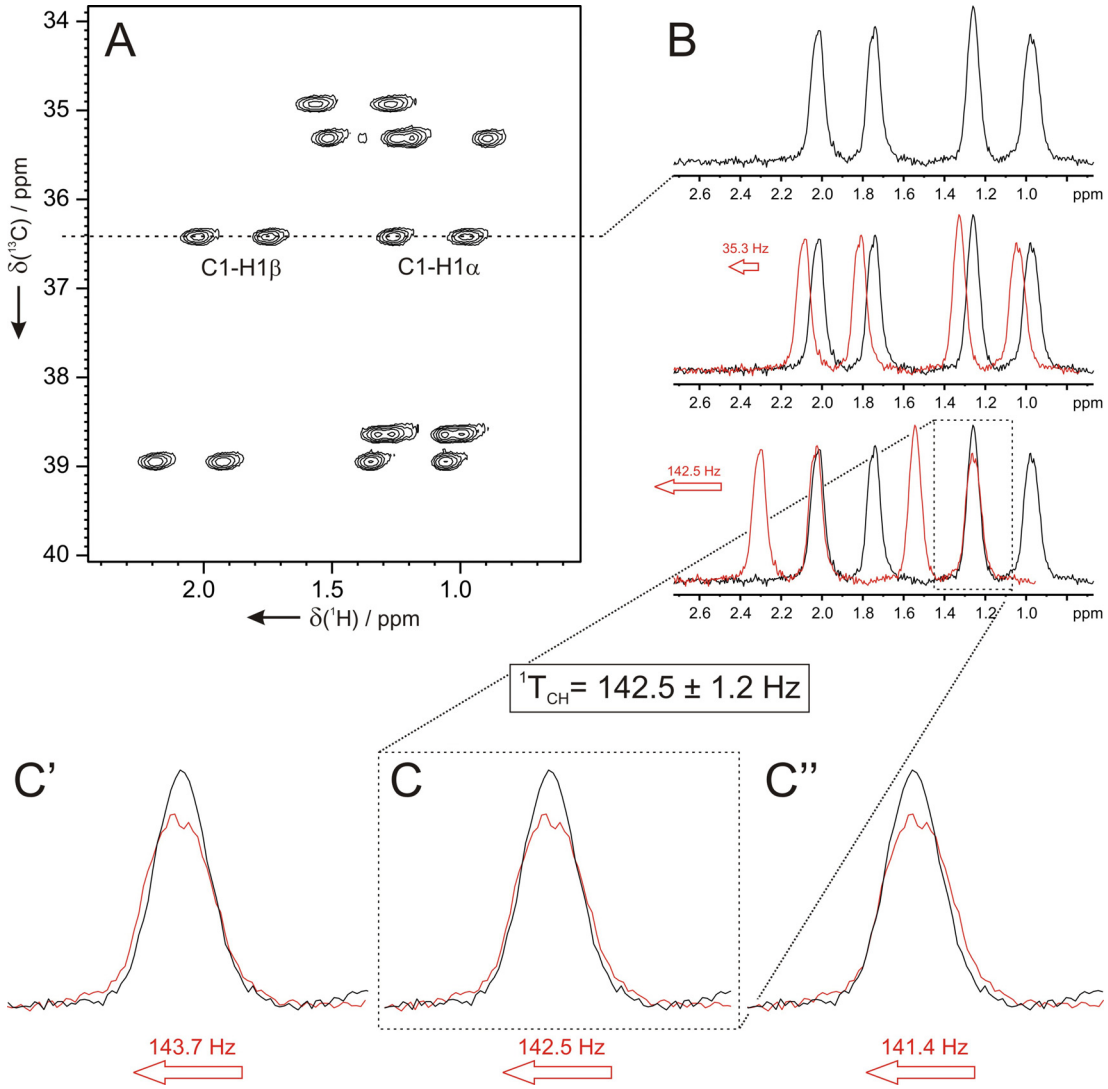

Figure 2.13.: Extraction of $^{1}T_{CH}$ couplings and estimation of the individual maximum error of a specific coupling. A detail of the CLIP-HSQC spectrum of cholesterol in a stretched PDMS/$CDCl_3$ gel (A) shows the two doublets of both protons attached to C1 (for details on the substance see chapter 5.4). A slice at the C1 carbon frequency was taken (B) and a copy of the slice (shown in red) is shifted relative to it to achieve maximum overlap of the two multiplet components as shown for the C1-H1α signal. While the overlap of the center of the multiplet components (C) reflects the coupling constant, the overlaps at the right (C') and left flank (C'') allow the estimation of the maximum individual error. For the example shown (C1-H1α) a coupling constant of $^{1}T_{CH} = 142.5 \pm 1.2$ Hz was determined. (The coupling constant for C1-H1β was determined in analogy to be 137.4 ± 1.0 Hz.)

2.6 Analysis of Anisotropic Parameters

The wealth of information included in anisotropic NMR parameters and the diverse field of application arising from this lead to a variety of different approaches to analyze them. Which approach to use, mainly depends on the problem to be solved. However, one aspect always has to be considered: anisotropic parameters depend on the molecule's orientation which is usually not known before but part of the analysis.

In this chapter some principle aspects for analyzing RDCs will be given, along with some methods used for different tasks. Out of the multitude of different approaches only those used in the following chapters of this thesis will be discussed in detail.

2.6.1 General Considerations

A molecules orientation can be described by the alignment tensor, as introduced in chapter 2.2.1, as long as the molecule can be considered as rigid. The five independent components of the alignment tensor can be derived by mathematical methods like the singular value decomposition (SVD)[127] if a minimum set of five independent RDCs is available. Independent in this context means, that out of the five internuclear vectors for the RDCs no two are oriented parallel to each other and no more than three lie in a plane. Any additional RDC can be used as structural information. Less then five RDCs are only useful if the orientation of the molecule is known from elsewhere.

It is worth to emphasize again, that the concept of the alignment tensor is only applicable if the molecule (or at least those parts of the molecule which are analyzed) can be considered as rigid. For flexible molecules or the analysis of dynamics other approaches have to be used (see chapter 2.2.2), which are not discussed in detail here, as all systems studied within this thesis were rigid enough to be treated by a static approach.

Using a static approach also excludes the use of $^{1}H,^{13}C$-RDCs measured within a methyl group, as this is usually rotating fast. However, as the rotation is around a well known axis, the chemical bond connecting the methyl group with its adjacent neighbor, the averaging due to that rotation can be transformed to a coupling along this bond, as Verdier et al. showed.[125] According to this, the $^{1}H,^{13}C$-RDC measured

for a methyl group can be converted in a $^{13}C,^{13}C$-RDC or $^{15}N,^{13}C$-RDC for methyl groups attached to a carbon or a nitrogen, respectively.

2.6.2 Using RDCs for Verification of a Structural Model

RDCs are commonly used to verify a proposed structural model. As mentioned before, an alignment tensor for a given structure can be calculated by singular value decomposition (SVD)[127] as implemented in programs like PALES.[128, 129] With this alignment tensor all RDCs can be back-calculated according to equation 2.7. and compared with measured RDCs. If measured and back-calculated couplings are equal, the structural model used for the SVD-fit is consistent with the experimental data.

This method has been applied to thousands of protein structures (see also chapter 2.6.3) and many small to medium sized molecules (see below). In most cases the program PALES[128, 129] is used, as this is not only performing the SVD-fit and the back-calculation of RDCs but also validating the fitting results. For SVD-fitting the "-bestFit" option of PALES[128, 129] is used, which needs the structural model in the form of a pdb-file and a list of all measured RDCs as inputs. As results of the fitting one gets the parameters of the alignment tensor **A** and the corresponding Saupe matrix **S**, the back-calculated RDCs, and a comparison of measured and back-calculated values, which is also validated in terms of different quality factors (see below).

It is important to keep in mind, that a good correlation between measured and back-calculated RDCs only means that the experimental values are compatible with the proposed structural model. Therefore it is only verification but never a proof for a correct structure. It is always possible that another (not considered) structure might as well fit with the experimental data. On the other hand, wrong structures are clearly falsified if experimental and back-calculated data are inconsistent.

It is obvious, that the verification of a structural model becomes the more reliable the more independent RDCs are used for fitting. This is especially important under the condition that five independent RDCs are necessary for the calculation of the alignment tensor and only those RDCs more then five are used for the validation. To put it the other way around: with five or less independent RDCs every structural model gives a perfect match between measured and back-calculated values in the SVD-fitting. For any reliable analysis significantly more then five RDCs are necessary.

Structural Analysis by Verification/Falsification of Proposed Structures

Many questions concerning the conformation[130-146] or the configuration[23-25, 67, 68, 136, 145, 147-151] of a molecule have been treated as verification or falsification of given structural models. Therefore different conformers or different diastereomers of a molecule have been fitted to the experimental RDCs leading to an exclusion of wrong structures and support of only one "correct" structure. As an example, the configurational analysis of the spirocyclic spriroindene by Freudenberger et al.[67] is shown in Figure 2.14.: only one of the two possible diastereomers shown in Figure 2.14. A leads to back-calculated RDCs consistent with the experimental data as the plot of back-calculated vs. measured RDCs shows (see Figure 2.14. B). The other diastereomeric structure can be excluded because back-calculated RDCs do not correlate with the measured couplings.

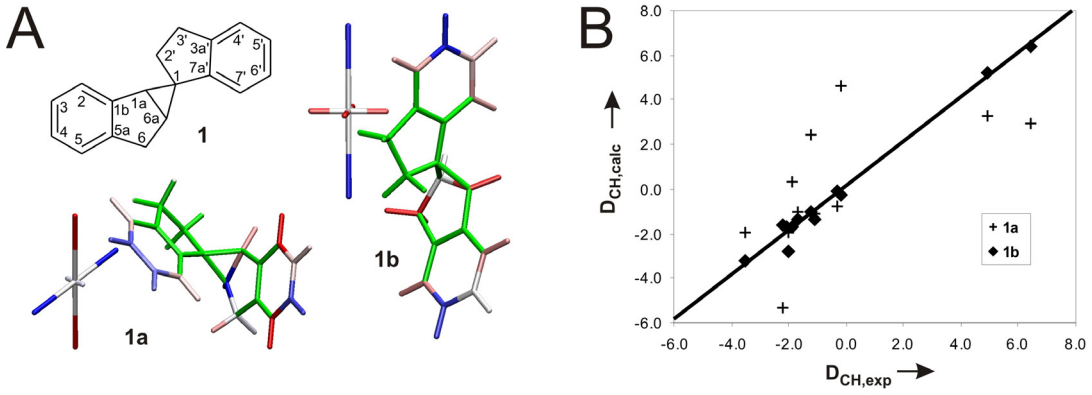

Figure 2.14.: Example for the determination of relative configuration by verification and falsification of proposed structures. The spiroindene **1** in principle can adopt two configurations **1a** and **1b** (A). By plotting experimental vs. back-calculated RDCs (B), clearly **1a** can be excluded as the correct structure while **1b** is consistent with the experimental data and therefore regarded as the actual configuration of **1**. The two structures are shown with color-coding of measured RDCs (red, negative RDCs; blue, positive RDCs; green, no RDCs measured or RDCs not used in analysis) along with the principle axes of the fitted alignment tensors (A). *Reproduced with permission from Reference [67] Copyright 2004 American Chemical Society.*

Plots like in Figure 2.14. B are frequently shown to illustrate how good or bad the correlation between measured and back-calculated values is. Another common way to illustrate the fitting results is shown in Figure 2.14. A: the alignment tensor is represented by its principal axes in the same coordinate system as the molecule and color-coding shows measured RDCs along the corresponding vectors (in Figure 2.14. A the CH-bonds as only one-bond CH-RDCs have been used). The color of the

alignment tensor representation shows the sign of RDCs to expect along the individual axes.

The approach of verifying a structural model by SVD-fits of measured RDCs has been intensively used within this thesis. By fitting different possible structures against a set of experimental RDCs, the configurational analysis of a degradation product of beer has been performed, as will be described in chapter 5.1 and the configurational and conformational analysis of a natural product has been determined, as described in chapter 5.2. For another natural product the conformation found in the crystal has been verified to be the same in solution (see chapter 4.2.4).

Furthermore the approach of verifying and falsifying structures has been performed for the first time to determine the *constitution* of a molecule, as will be shown in chapter 5.3.

Resonance Assignment by Verification/Falsification

Like different proposed structures can be validated by the SVD-fit of measured RDCs, this is also possible with different proposed assignments for a molecule. In this case the different input-"structures" have the same molecular assembly but ambiguously assigned atoms are renamed. This is especially useful for the prochiral assignment of the two protons in a methylene group which is often an open question in the assignment of a molecule,[61, 64, 66, 152] but can also be used for the prochiral assignment of two methyl groups (as used in chapter 5.1). As will be shown in chapter 5.3 it even can be used for the assignment of two completely independent groups or atoms, if for example classical methods for the assignment failed.

Quality Factors for Validation of Fits

The comparison between measured and back-calculated RDCs for a proposed structure is usually done by plotting calculated vs. experimental data, as done in the example by Freudenberger et al. shown in Figure 2.14. B. However, if fits for many different structures are to be compared a good measure for the quality of the fit is necessary, as plotting all results would become too time-consuming.

For this purpose the program PALES[128, 129] gives several quality factors for the comparison of back-calculated and measured RDCs. They all have their advantages and disadvantages.

Commonly used is the correlation coefficient R (or its square R^2), which is calculated according to equation 2.12. with $x_{meas.}$ and $x_{calc.}$ being the measured and back-calculated values, respectively, and n being the total number of RDCs. It indicates the strength of a linear correlation in this case between measured and back-calculated RDCs (the value for R should be close to ± 1 for a good linearity). However it makes no statement about the characteristics of this linear correlation and clearly for the necessary comparison only the linear correlation with the slope 1 and an intercept of 0 is reasonable.

$$R = \frac{\frac{1}{n}\sum^{n}\left[(x_{meas.} - \overline{x_{meas.}}) \cdot (x_{calc.} - \overline{x_{calc.}})\right]}{\sqrt{\frac{1}{n}\sum^{n}(x_{meas.} - \overline{x_{meas.}})^2} \cdot \sqrt{\frac{1}{n}\sum^{n}(x_{calc.} - \overline{x_{calc.}})^2}} \quad ; \quad \bar{x} = \frac{1}{n}\sum^{n} x \qquad (2.12.)$$

Better suited in this respect, is the RMSD value (in the PALES output wrongly named "RMS"), the root mean square deviation:

$$RMSD = \sqrt{\frac{1}{n}\sum^{n}(x_{meas.} - x_{calc.})^2} \quad [Hz] \qquad (2.13.).$$

It gives a kind of averaged difference between measured and calculated values in the unit of the values, so in case of RDCs in Hz. It should be as small as possible and significantly smaller than the experimental values used for fitting. As the RMSD as a quality factor is always to be seen relative to the size of the measured values (e.g. the RMSD value of 1 Hz is worse if the experimental couplings are in the range of ± 10 Hz compared to an RMSD of 1 Hz if the couplings are in the range of ± 100 Hz), Cornilescu et al.[153] introduced the quality factor Q as defined by equation 2.14.

$$Q = \frac{RMSD}{RMS} = \frac{\sqrt{\frac{1}{n}\sum^{n}(x_{meas.} - x_{calc.})^2}}{\sqrt{\frac{1}{n}\sum^{n}(x_{meas.})^2}} \qquad (2.14.)$$

In this equation RMS is the root means square of the measured values and therefore the quality factor Q is the quality factor RMSD weighted by the average size of measured values. Q should be as small as possible, significantly smaller than 1 and as the correlation factor R it has no unit.

The quality factors R, RMSD and Q all describe in on way or the other, how strong measured and back-calculated values differ, or how far the value is away from the diagonal in the plot of back-calculated vs. measured RDCs (as e.g. shown in Figure 2.14. B).

For the two plots shown in Figure 2.15. A and B the mentioned quality factors would indicate two about identically good (or bad) fits, as both the outlying points marked in red are equally far away from the diagonal. If, however, the experimental errors of measured RDCs are plotted along the values, as shown in Figure 2.15. C and D, it is obviously that the fit in C, where the values are along the diagonal within their error range, is far better than the one in D, were one of the outlying points has an experimental error far smaller than the deviation from the diagonal.

Consequently, a good quality factor should consider how strong measured and back-calculated values differ *and* it should take into account the experimental error of the measured values. This is described by χ^2 as defined by equation 2.15.

$$\chi^2 = \sum^{n} \left(\frac{x_{meas.} - x_{calc.}}{\Delta x_{meas.}} \right)^2 \qquad (2.15.)$$

with $\Delta x_{meas.}$ being the experimental errors of x_{meas}. As χ^2 increases with an increasing number n of measured RDCs, it should be normalized. Therefore a better quality factor would be

$$n / \chi^2 \qquad (2.16.)$$

which should be as high as possible, preferably larger then 1.

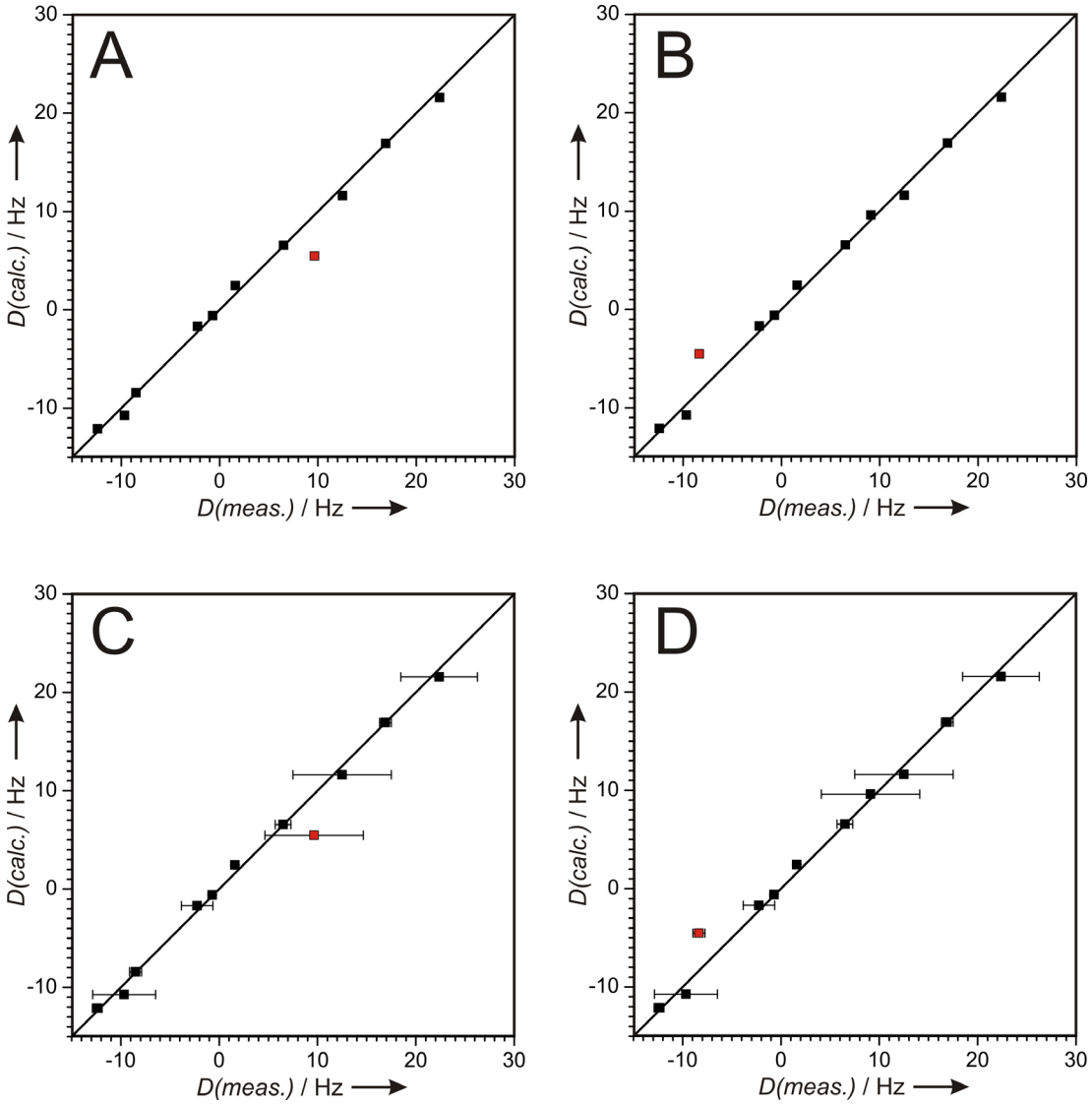

Figure 2.15.: Illustration of the importance to consider differing experimental errors for the validation of fit quality. The two outlying points in plot (A) and plot (B) (marked in red) are equally far away from the diagonal as the difference in measured and back-calculated value is equal. This results in equal values for the quality factors R, RMSD and Q, hence the two fitting results are evaluated as equally good. If one considers the experimental errors of the measured RDCs as shown in the plots (C) and (D), it is obvious that the fit shown in (C), which is equal to the fit shown in (A), is better than the fit shown in (D) which is equal to the fit shown in (B). However, the experimental error is not taken into account in the quality factors R, RMSD and Q, but only in n/χ^2.

The quality factor n/χ^2 is optimized for the comparison of different fits to a single set of experimental RDCs, including the important individual maximum error estimates for the measured values. However it is of limited use to compare the quality of fits for completely different systems.

Throughout this thesis in most cases the quality factor n/χ^2 is used to validate the fits of different structural models against the same set of measured RDCs. However,

for comparison also the correlation coefficient R and the quality factor Q by Cornilescu et al.[153] is given in the tables of the Appendix.

The program PALES,[128, 129] which was exclusively used within this thesis for all RDC fits, gives the quality factors R, RMSD, Q, and χ^2 as output for its fits. Obviously for the calculation of χ^2 it is necessary to give the experimental errors of measured RDCs as an input. For a reasonable quality factor n/χ^2 it is indispensable to do a realistic estimation of the individual experimental error for each measured coupling. Probably the best way to do this, is described in chapter 2.5.3 (Figure 2.13.). However, even if not n/χ^2 is used as the quality factor, a reasonable error estimation should be done, as the experimental error given as input in PALES[128, 129] is not only used for the calculation of χ^2 but also influences the alignment calculated. Within the fitting procedure PALES[128, 129] allows values with larger error to deviate stronger from the given values, than those with smaller error. This stronger deviation within the given error, which makes absolutely sense, is on the other hand punished with the quality factors R, RMSD and Q, as they do not consider this larger experimental error of the individual coupling. This is one more argument for the use of n/χ^2 as the quality factor for RDC-fits with PALES.

2.6.3 Using RDCs for Structure Refinement

The verification of structures by PALES,[128, 129] as described in the previous chapter, uses given structural models in the form of pdb-files, which are not going to be changed. With other programs, however, it is possible to modify structures in order to fit to the experimental RDCs. This is frequently done in biomolecular NMR for structures of proteins or nucleic acids[154] but also examples for linear or cyclic peptides,[135, 137, 140, 141, 146] sugars[130-132, 155] or natural products[24, 25, 145] have been reported.

For this purpose, a number of different structure calculation packages can use one-bond RDCs as structural restraints in addition to angular restraints from $^3J_{HH}$ couplings and distance restraints from NOE-signals. In this programs (for example CNS,[156] XPLOR-NIH,[157] DYANA,[158] AMBER[159, 160]), the RDC constraints are incorporated as an explicit target potential in addition to the classical potential energy function of the particular force field. As RDCs are treated as angular restraints, the orientation of the molecule has to be given as an input for the structure refinement. As the orientation is normally unknown a priori, often an iterative

procedure is used, calculating the alignment with SVD-based programs, using the obtained orientation for structure refinement and recalculating the orientation again for the refined structure to use this for the next step of refinement.[135, 154]

2.6.4 Discrimination of Enantiomers and Absolute Configuration

To discriminate enantiomers by anisotropic parameters, a chiral alignment medium as described in chapter 2.3.1 is needed. Due to the chiral super-structure of these alignment media, e.g. a helix, two enantiomers are aligned in a different manner. This leads to different sets of anisotropic parameters for both enantiomers which therefore might be discriminated, as shown in both examples of Figure 2.16.

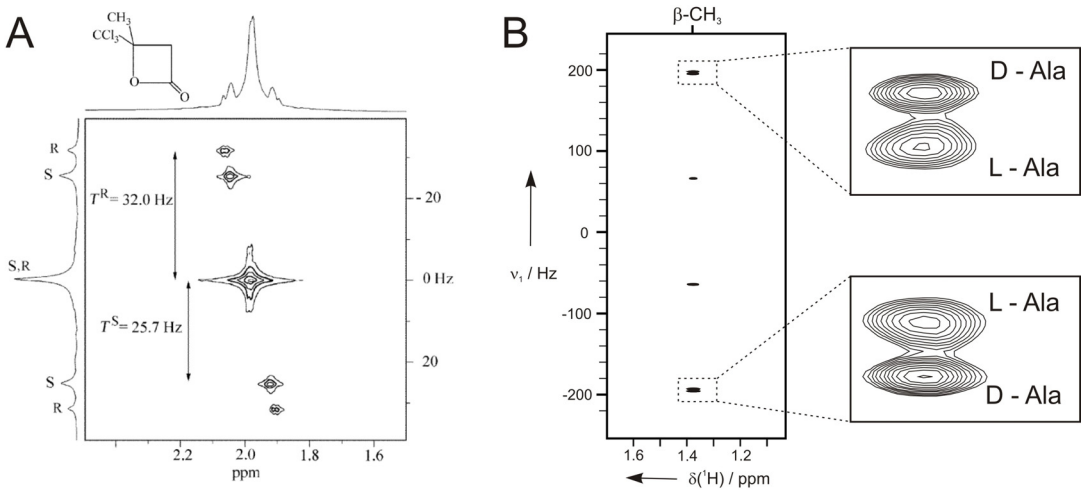

Figure 2.16.: Examples for the distinction of enantiomers. (A) The distinction of enantiomers in a sample of 3-methyl-4,4,4-trichlorobutyric-β-lactone 21.5% enriched with the S enantiomer and dissolved in PBLG/$CDCl_3$ is done by ^{1}H-^{1}H-RDCs between the methyl protons using a SERF 2D experiment.[161] (B) Separation of enantiomers using a two-dimensional J-^{1}H,^{13}C-BIRD^{d,X}-HSQC[52] (see also Figure 2.11. D) recorded for a mixture of L-Ala/D-Ala (1.2:1) in gelatin/D_2O. The determination of enantiomeric excess is possible by integration. *(A) Reprinted from Reference [161] Copyright (2002), with permission from Elsevier. (B) Copyright Wiley-VCH Verlag GmbH & Co. KGaA. Reproduced with permission from Reference [52].*

As shown in the two examples, the different size of RDCs for both enantiomers leads to a separation of the signals, which even allows the determination of enantiomeric excess by integration. This distinction can be achieved not only by different RDCs, but also by differences in chemical shift anisotropy and by different residual quadrupolar couplings.[105] However, in the spectra it is not possible to distinguish which set of signals belongs to which enantiomer. In the examples shown,

this was only possible by comparison with an enantiomerically pure sample or an enantiomerically enriched sample of one known enantiomer.

For the differentiation of enantiomers by anisotropic parameters in a chiral alignment medium it would be necessary to know the different orientations of the enantiomers in the chiral medium. With an SVD-fit of two mirror-imaged structures against a set of measured RDCs one would obtain two equally good fits for both enantiomers and consequently one could not differentiate them. Marathias et al.[162] claim to differentiate between the enantiomers of ibuprofen with RDCs measured in PBLG/$CDCl_3$. According to their results of searching for lowest energy conformers in a PBLG/$CDCl_3$ simulated environment, the two enantiomers shall possess different conformations in the chiral alignment media (hence, they are no mirror images any more!) which in each case fit only to one of the two measured sets of RDCs.[162] However, this is the only reported example of this kind and it is doubtful whether the used approach might be a general procedure for the determination of absolute configuration. On the other hand, if once it will be possible to reliably predict the orientation of a molecule in a chiral alignment medium this would bring the determination of absolute configuration by RDCs in reach.

In analogy to the distinction of enantiomers, it is possible to distinct prochiral (or enantiotopic) groups in a chiral alignment medium. While those groups would show the same size and sign of anisotropic parameters in an achiral environment, they are differently aligned in the chiral environment and hence possess different anisotropic parameters. This has been shown for several molecules in the chiral alignment media PBLG and PCBLL, gelatin,[76] and polysaccharides.[77]

The discrimination of enantiomers and prochiral groups as described here, will be used to characterize the newly developed alignment medium introduced in chapter 3.4.

2.6.5 Analysis under Presumption of the Molecule's Orientation

To calculate a molecule's orientation by SVD-fitting of experimental anisotropic parameters, a minimum of five independent values is necessary and only every additional value gives structural information. Therefore a significantly large set of experimental data is needed for a structural analysis. It would be desirable if the set of necessary parameters could be reduced, and indeed this would be possible if the molecule's orientation would be known without using the experimental data to

determine it. This would circumvent the SVD-fitting and expected RDCs could be directly calculated from the known alignment according to equation 2.7. The program PALES[128, 129] provides this calculation in its "-saupe" option which needs, next to the pdb-file and the RDC list, the parameters of the Saupe matrix as input.

However, the alignment of a molecule is usually not known a priori. An elegant and effective solution would be the prediction of alignment from first principles. Many attempts have been made to predict the alignment of a molecule by considering steric[128] and electrostatic[163] interactions between the solute and the alignment medium, as it is for example done in PALES ("-stPales" option).[129] Other approaches use inherent properties of the solute molecule like its tensor of gyration.[164, 165] The prediction of alignment works well for large biomacromolecules, but for small molecules the effects of the fine-structure of the alignment medium and corresponding dynamics play a much more important role and therefore often lead to wrong results (see also chapter 5.4).

A different approach, based on the idea that molecules with very similar structure should orient in the same manner if aligned by the same alignment media under identical conditions, has been used by Ziani et al.[166] By comparison of residual quadrupolar couplings measured for similar structures of known chirality, they were able to determine the absolute configuration of a small chiral molecule.[166]

In chapter 5.4 it will be shown that this approach of cross-fitting anisotropic parameters between structurally similar molecules works also for RDCs.

3 Development of new Alignment Media

3.1 Poly(acrylonitrile)

3.1.1 Introduction and Motivation

While a multitude of adequate alignment media exists for aqueous solutions and apolar organic solvents (see chapter 2.3.2), only few orienting media with limited applicability are reported for the standard solvent in pharmaceutical NMR, DMSO. Mixtures of pentaethylene glycol monododecyl ether ($C_{12}E_5$) with D_2O and DMSO as a lyotropic nematic phase have a narrow range of alignment and are not suitable for pure DMSO.[72] Stretched gels based on cross-linked poly(vinyl acetate) are freely scalable in their alignment for a large number of small molecules, but cyclic peptides as an important class of molecules do not diffuse into them.[66] Finally, poly(dimethylacryl amide)-based copolymer gels[73] worked well with a number of peptides,[140] but exclude many molecules due to their negative charge. Therefore the aim of this project was the development of a freely scalable, uncharged alignment medium applicable to a wide range of molecules.

Besides the applicability for DMSO, it was of great importance to find an alignment medium, which possesses as less NMR-signals as possible. Therefore poly(acrylonitrile) (PAN) was chosen and the aim was to cross-link PAN by irradiation with accelerated electrons, as it was successfully done for poly(dimethylsiloxane) (PDMS),[67] in order to avoid undesired NMR-signals originating from chemical cross-linking.

3.1.2 Cross-Linking of PAN

It is crucial for the cross-linking by irradiation[167] that on the one hand, the polymer has an amorphous state and on the other hand, the shape which is desired for the gel (in this case a cylindrical form). As has been shown for several examples, cross-linking upon irradiation will not occur within crystal regions of the polymer.[168-170] However, commercially available pure PAN is a white powder and it is necessary to get it in the right form in order to cross-link it by irradiation. Because of its high crystallinity and its degradation upon heating,[171] this is a rather challenging task.

Step by step different procedures were developed to obtain stretched gels of cross-linked PAN which can be used as an alignment medium for the measurement of anisotropic NMR parameter.

Cross-linked PAN of the first Generation[96]

Sticks of poly(acrylonitrile) were obtained by precipitation out of a DMSO solution: A highly viscous solution of PAN (≈ 300 g/L) was filled in paper rolls with inner diameters of 3.5-4.5 mm. The filled paper rolls were then placed in solutions with stepwise increased content of methanol: DMSO/MeOH 2:1 (20 min, 80°C); DMSO/MeOH 1:1 (20 min, 65°C); pure MeOH (60 min, 50°C). Finally, the paper was removed and precipitated PAN-sticks were dried at 70°C for 24 hours. By this procedure dry PAN-sticks of 2.5-3.5 mm were obtained (see Figure 3.1. A). The polymer sticks were then cross-linked by irradiation with accelerated electrons (for details see Appendix). The cross-linked sticks have been placed in 5 mm NMR-tubes and DMSO-d_6 was added. The restricted swelling in the tube leads to the necessary stretching of the gel (see Figure 3.1. B).

The obtained stretched gels of PAN could be used as alignment media for the measurement of anisotropic parameters, however, the gels showed poor homogeneity and long-term stability[96] and therefore alternative preparation schemes were developed.

Cross-linked PAN of the second Generation[96]

PAN/DMSO-d_6-solutions of different concentrations (ranging from 100 g/L to 280 g/L) were filled in standard 5 mm-NMR-tubes and in silylated NMR-tubes and irradiated by accelerated electrons directly in the NMR-tubes (for details see Appendix). Upon addition of DMSO on top of the in-tube cross-linked polymer, the gels swell further and get automatically stretched (see Figure 3.1. C).

The stretched gels obtained by this method have excellent alignment properties, are very homogeneous and robust. Furthermore the preparation is very easy compared to the cross-linked PAN of the first generation and production in larger quantities is possible. Hence, cross-linked PAN of the second generation is preferred and all studies described in chapters 3.1.3 - 3.1.6 were carried out with samples prepared by this procedure. Nevertheless, a problem arises when irradiated tubes with the cross-linked PAN/DMSO gel get too cold, as it might be the case while shipping

samples during winter times: the DMSO in the gel freezes out and emerging crystals disrupt the gel. Depending on the concentration this happens between 0-10°C and it is therefore desirable to produce dry PAN-sticks which can be transported safely and which are of better homogeneity than the sticks of the first generation.

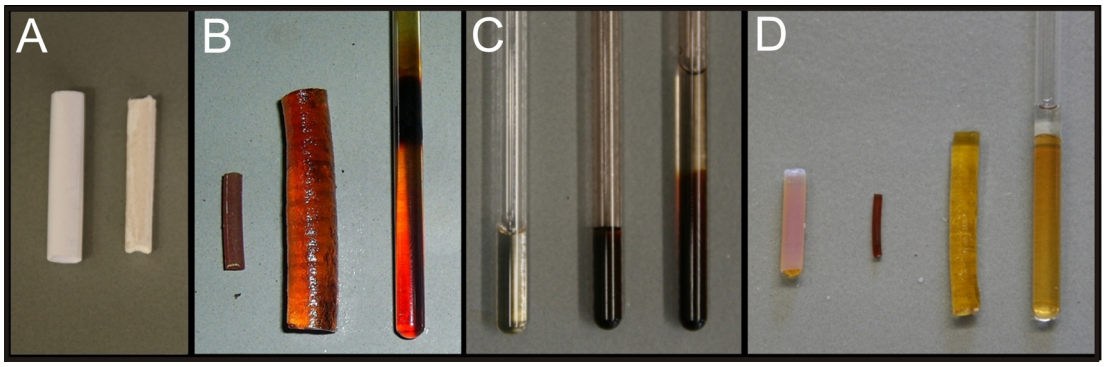

Figure 3.1.: Preparation of cross-linked poly(acrylonitrile). PAN of the first generation is produced as shown in (A, B): highly viscous solutions of linear PAN are filled in paper rolls (A, left) and precipitated to obtain sticks (A, right). After drying and irradiation with accelerated electrons the sticks of cross-linked PAN (B, left) can be swollen to gels in DMSO (B, middle). If this is done in an NMR tube, the gel gets automatically stretched by the restriction of the tube walls (B, right). (C) shows different steps for the preparation of PAN of the second generation: solutions of linear PAN in DMSO-d_6 are filled in NMR tubes (C, left) and irradiated (C, middle). After that, the addition of DMSO leads to swelling and stretching of the PAN/DMSO gels within the NMR tubes (C, right). The preparation of PAN of the third generation is shown in (D): DMSO-solutions of PAN are irradiated in Teflon® tubes (D, left) and dried to obtain sticks of cross-linked PAN (D, middle) which can be re-swollen in DMSO and get automatically stretched when re-swelling inside an NMR tube (D, right).

Cross-linked PAN of the third Generation

Combining the strategies for the preparation of PAN gels of the first and the second generation, PAN/DMSO solutions have been filled in glass or Teflon® tubes, cross-linked by irradiation with accelerated electrons (for details see Appendix) and then precipitated. For the last step the tubes were peeled off and the cross-linked gels obtained by the irradiation were placed in solutions with stepwise increased content of water: DMSO/H_2O 5:1; 1:1; 1:3 and pure H_2O (each for several days at room temperature). Precipitated sticks of cross-linked PAN were then dried at 50°C for 3 days. By this procedure PAN-sticks of 1.0-4.0 mm were obtained (see Figure 3.1. D), which can be re-swollen and stretched in NMR-tubes or in the stretching devices described in chapters 4.1 and 4.2.

The sticks of the third generation can be stored and transported easily in the dry form, and the gels obtained by swelling of this sticks are as homogeneous as the gels of the second generation.

3.1.3 Swelling and Equilibration of PAN/DMSO Gels

Depending on the preparation scheme and the amount of irradiation, the cross-linked PAN sticks are swelling to approximately 15 times their original volume in DMSO and 20 times their volume in DMF. Swelling in water or less polar organic solvents like methanol or chloroform is not observed (see Figure 3.2.).[96]

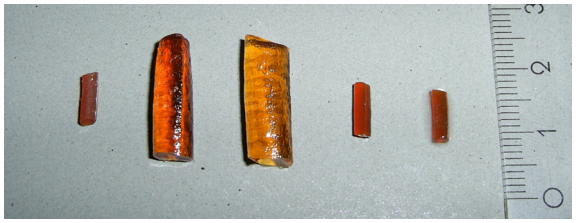

Figure 3.2.: Swelling of cross-linked PAN sticks in various solvents. From left to right: dry PAN-polymer stick of the first generation with 2.4 mm diameter and identical sticks after 5 days in DMSO, DMF, methanol and chloroform.[96]

As alignment media, only PAN/DMSO gels have been investigated, gels of PAN and DMF were not tested so far. Most of the characterizations of PAN gels have been done with gels of the second generation and as long as not stated otherwise the following studies have all been done with these gels of irradiated PAN/DMSO-d_6 solutions. However, it is most likely that the results obtained for the second generation of PAN could be transferred to gels of the first and third generation as well.

A general problem of DMSO based gels is the slow swelling and therefore also slow equilibration of the stretched gels due to the high viscosity of the solvent. For PAN/DMSO gels it takes typically several weeks at room temperature to obtain a well equilibrated gel with homogeneous alignment and narrow lines in the deuterium spectrum (see Figure 3.3.). Higher temperatures and silylated NMR-tubes help in speeding up this process (see Figure 3.4.).

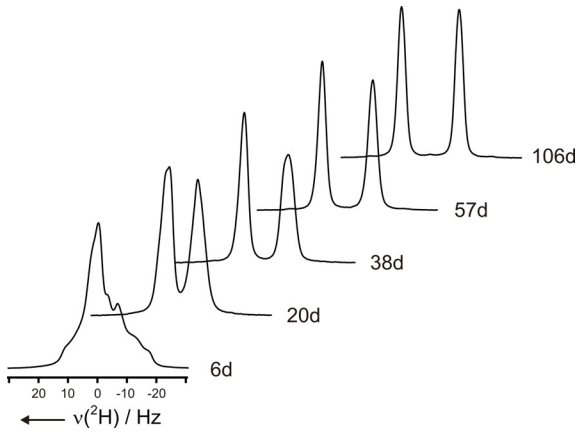

Figure 3.3.: Equilibration of a PAN/DMSO-d_6 gel. A PAN gel in a silylated NMR-tube was allowed to swell at room temperature and ^{2}H-1D spectra of DMSO-d_6 have been recorded after different time intervals to monitor the equilibration process.

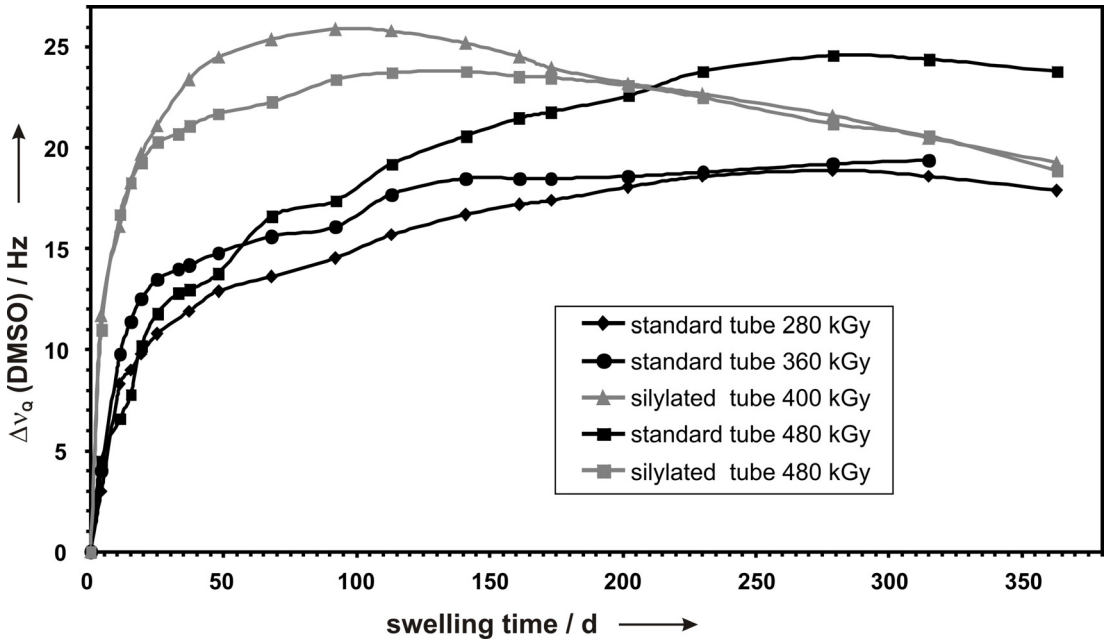

Figure 3.4.: Equilibration and aging of PAN gels. Quadrupolar splitting $\Delta\nu_Q$ of DMSO-d_6 taken from ^{2}H-1D spectra of five individual samples irradiated with 280 kGy, 360 kGy, and 480 kGy accelerated electrons in a conventional NMR-tube, and 400 kGy and 480 kGy in NMR-tubes which were silylated prior to irradiation. The swelling at room temperature is enhanced for silylated NMR-tubes. Narrow lines in the deuterium spectra have been recorded for all samples after at least 50 days. However quadrupolar splittings are further growing slowly before declining again. Samples can be used as alignment media for several months before the alignment breaks down completely (e.g. the sample with 360 kGy was broken after about one year).

3.1.4 NMR-Signals and Impurities of PAN/DMSO Gels

Spectral Quality of PAN Gels

The ^{1}H-NMR-spectrum of a PAN/DMSO-gel is shown in Figure 3.5. A. The cross-linked PAN results in two broad signals at 2.0 ppm (CH_2-groups) and 3.2 ppm (CHCN-groups). In addition, a triplet from $^{14}NH_4^+$ (7.0 ppm) and signals of unknown impurities (3.8, 6.0, 6.3 ppm) are observed. These impurities are already visible in non-cross-linked PAN, but their intensities seem to increase slightly upon irradiation.[96] As DMSO is quite hygroscopic, small amounts of water diffused into the gel, however, this is more a problem of DMSO as a solvent and not of the PAN gels. The intensity of the water signal can be reduced by adding molecular sieve to the DMSO on top of the gel.

Figures 3.5. B and C show the ^{1}H amide region and a ^{1}H,^{13}C-CLIP-HSQC spectrum[107] of 8 mg *cyclo*(-D-Ala-Ala-Ala-(*N*Me)Ala-Ala-)[172] diffused into a PAN/DMSO-gel with a final concentration of the two observed conformers of ≈ 16 mM (see chapter 3.1.6 and Appendix for details on the peptide). Although peptide signals overlap with the intensive polymer signals in the ^{1}H-1D-NMR-spectrum, the additional resolution of the ^{13}C-chemical shifts in the 2D experiment prevent signal overlap in this case and the full set of one-bond D_{CH}-RDCs can be obtained.

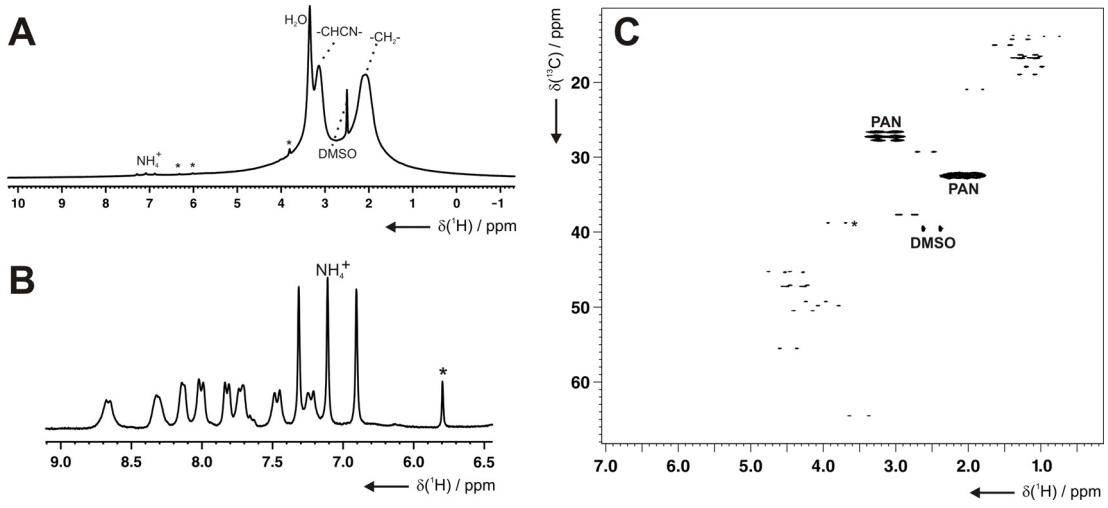

Figure 3.5.: Various spectra of a PAN/DMSO-gel used for measuring RDCs on *cyclo*(-D-Ala-Ala-Ala-(*N*Me)Ala-Ala-). (A) ^{1}H-1D of the gel without peptide added. Asterisks indicate small impurities, other signals are annotated correspondingly. (B) Amide region of the peptide diffused into the gel. The two conformations of about equal intensities and a final concentration of ≈ 16 mM are visible. (C) The CLIP-HSQC spectrum[107] for the extraction of one-bond ^{1}H-^{13}C coupling constants shows no overlap between signals of the alignment medium and the solute.

Suppression of NMR Signals

Since other solute molecules might well have overlapping cross peaks in a 2D-spectrum, several possibilities of reducing the backbone polymer signals have been investigated. Presaturation of one or both of the backbone signals leads to a significant decrease of peak intensities[96] but might also infer efficient saturation of

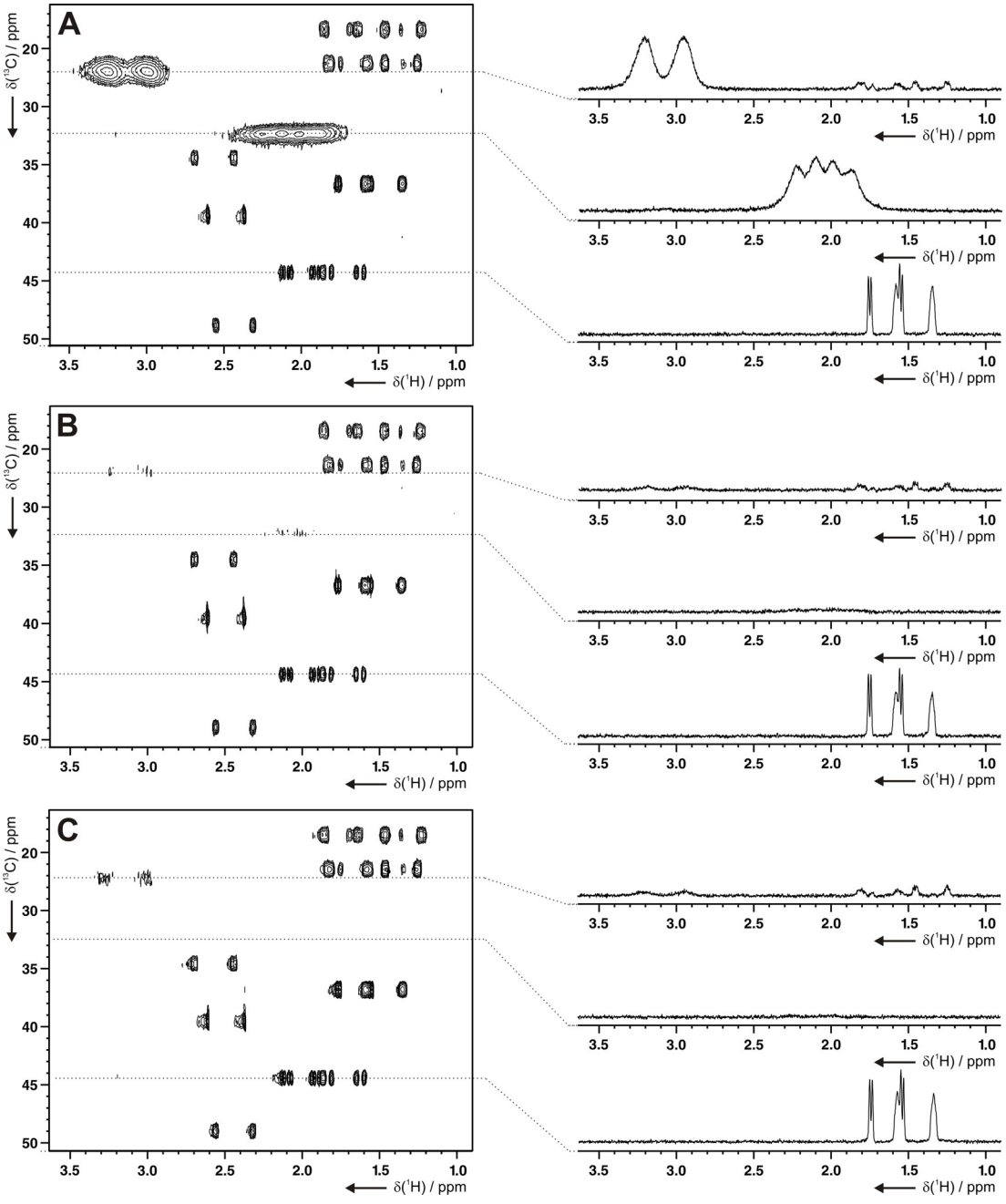

Figure 3.6.: Suppression of polymer signals using CPMG and z-relaxation filters. (A) $^{1}H,^{13}C$-CLIP-HSQC without relaxation filter, (B) the same experiment with identical parameters and an additional 175 ms CPMG period[173] applied directly after the initial excitation pulse, (C) the experiment with a z-relaxation filter of 500 ms incorporated as described by Luy et al.[65] Traces show for comparison the –CHCN– and $–CH_2–$ groups of the polymer, and the methylene group C3-H3a/b cross peaks of ≈ 100 mM norcamphor diffused into the gel. All traces and contours are scaled identical.

the solute molecule. Best signal suppression was obtained by applying a CPMG-based relaxation filter[173] or a less power consuming z-relaxation filter[65] as can be seen in Figure 3.6. This suppression methods work very well for small solute molecules, however, with increasing size of the solute its signals get suppressed as well. In this case an alternative alignment medium might be necessary, as for example the one described in chapter 3.3.

3.1.5 Tuning the Alignment Strength

As with all gel-based alignment media, the degree of alignment in PAN/DMSO-gels can easily be varied with different parameters.

The strength of orientation induced by the gel increases with an increasing amount of cross-linking, i.e. an increasing irradiation dose (see Figures 3.7. A and B), as previously also shown for irradiation cross-linked PDMS gels[67] and chemically cross-linked PS[64] and PVAc[66] gels. Furthermore an increasing chain length of the polymer leads to stronger alignment (see Figure 3.7. A), as also found for the mentioned polymers.[64-67]

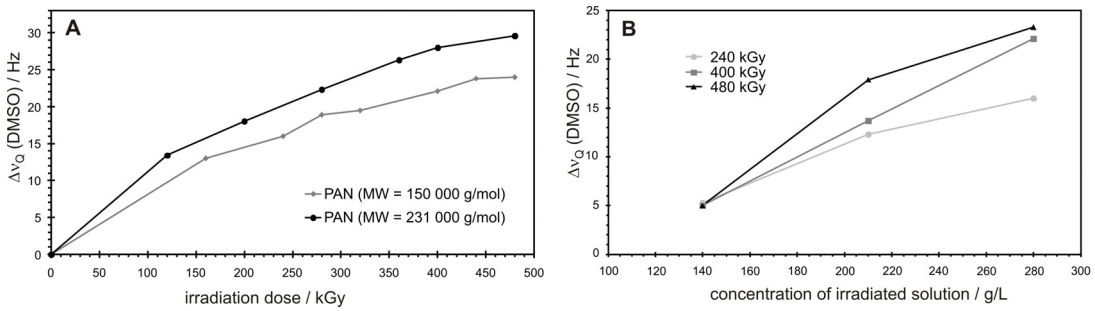

Figure 3.7.: Tuning of the alignment strength of PAN/DMSO gels. (A) Quadrupolar splitting $\Delta\nu_Q$ of PAN/DMSO gels with respect to the irradiation dose applied for cross-linking. All gels were cross-linked inside the NMR-tube as a 280 g/L PAN/DMSO-d_6 solution. Linear polymers of two different molecular weights have been used. The induced alignment increases with the chain length of the polymer and the irradiation dose applied for cross-linking. (B) Quadrupolar splitting $\Delta\nu_Q$ of various gels with respect to the initial concentration of the PAN (MW=150000 g/mol)/DMSO-d_6 solution used for irradiation with accelerated electrons. Increasing the polymer concentration leads to larger alignment strength. All samples were measured after 57 days of equilibration in silylated NMR-tubes.

In contrast to PS, PDMS, PVAc and other polymers, the preparation of the cross-linked PAN of the second generation does not allow the tuning of the alignment strength by varying the ratio of stick and tube diameter. However, an additional

tuning is possible by varying the initial concentration of the PAN/DMSO solution which is irradiated (see Figure 3.7. B).

PAN/DMSO gels of the second generation with quadrupolar splittings between 3 Hz and 40 Hz could be obtained by varying concentration, irradiation dose and chain length.

3.1.6 Orientational Properties

To explore the range of solutes compatible with PAN/DMSO-gels, different compounds have been tested. Norcamphor as a small organic compound, the standard sugars glucose and sucrose and the peptides *cyclo*(-*a*AA(*N*Me)AA-), *cyclo*(-R(Pbf)GD(O*t*Bu)fK-) and *cyclo*(-RNalAGyR-) readily diffused in the pre-swollen gels and $^{1}H,^{13}C$ one-bond as well as $^{1}H,^{15}N$ one-bond RDCs have been measured (see Appendix).

For norcamphor as a test molecule which has been studied intensively in different PS[65] and PVAc[66] based gels, properties of the alignment tensor in a PAN/DMSO gel obtained with a SVD-fit by PALES[128, 129] are given in Figure 3.8. A comparison with results for a PVAc/DMSO gel[66] reveals a rather similar alignment in both gels.

$D_a = 1.893447 \cdot 10^{-04}$
$D_r = 3.054770 \cdot 10^{-05}$
$A_{xx} = -1.4352 \cdot 10^{-04}$ (0.41650, -0.18779, 0.88953)
$A_{yy} = -2.3517 \cdot 10^{-04}$ (0.64699, 0.74860, -0.14489)
$A_{zz} = 3.7869 \cdot 10^{-04}$ (0.63869, -0.63587, -0.43329)
$R^2 = 0.998$

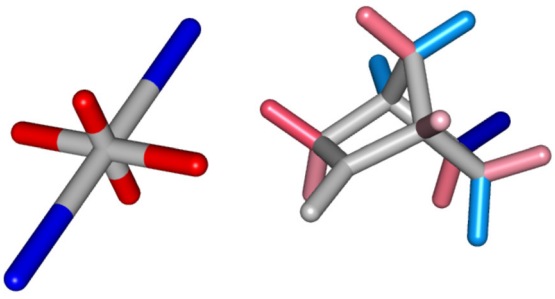

Figure 3.8.: Alignment tensor properties of norcamphor in a PAN/DMSO gel. Alignment tensor parameters as calculated with PALES[128, 129] using the RDCs measured in a gel of the second generation (see Appendix): axial and rhombic components (D_a, D_r) and principal axes of the alignment tensor (A_{xx}, A_{yy}, A_{zz}) with their corresponding eigenvectors are given. The accuracy of the fits is described by R^2. The structure of norcamphor is shown with color-coded bonds representing negative (red) and positive (blue) $^{1}H,^{13}C$-RDCs and the axes of the corresponding alignment tensor drawn next to it.

Besides the above mentioned compounds, other groups have studied some more molecules in PAN/DMSO gels prepared within this thesis, including cyclic peptides,

complex organic molecules und natural compounds.[24, 25, 146, 174] None of the compounds tested so far, did not diffuse into a pre-swollen PAN/DMSO gel, which indicates a wide range of compatible solutes in contrast to the narrow range of solvents tolerated by PAN.

Table 3.1. gives an overview over compounds measured in PAN/DMSO gels and their strength of alignment, monitored by the range of RDCs measured in comparison with the quadrupolar splitting of the solvent. It could be used as a rough estimation for the range of RDCs to expect for a molecule to be measured in a PAN gel.

Table 3.1.: Overview over compounds measured in PAN/DMSO gels. Listed is their size and range of measured RDCs in comparison with the quadrupolar splitting $\Delta\nu_Q$ of the solvent measured in the used gel.

Compound		**Size**[a]	**$\Delta\nu_Q$ [Hz]**	**Range of RDCs**[b] **[Hz]**	**Ref.**
norcamphor	small bicycle	$C_7H_{10}O$ 110.1	21.1	-8.2 to 13.3	[96]
sucrose	di-sugar	$C_{12}H_{22}O_{11}$ 342.3	40.4	-18.7 to 15.3	A[c]
cyclo(-*a*AA(*N*Me)AA-)	cyclic peptide (5 amino acids)	$C_{16}H_{27}N_5O_5$ 369.4	21.2	-7.5 to 36.4	A[c]
cyclo(-RNalAGyR-)	cyclic peptide (6 amino acids)	$C_{45}H_{64}N_{16}O_8$ 957.1	15.8	-23.7 to 20.0	chapter 4.1.
hymenistatin	cyclic peptide (8 amino acids)	$C_{46}H_{68}N_8O_{12}$ 924.5	≈ 12	-25.2 to 42.5	[174]
((-)-menthyl)-(5-oxo-5,6-dihydro-2H-pyran-2-yl)-diphtalate	flexible organic molecule	$C_{23}H_{28}O_6$ 400.5	≈ 20	-14 to 16	[174]
saggittamide A	flexible long-chain hydrocarbon	$C_{48}H_{81}N_3O_{18}$ 988.2	14.9	8.1 to 16.9	[24]
sucro-neolambertellin	glycoside	$C_{26}H_{29}O_{15}$ 581.1	15.6	-11.2 to 21.2	[25]
cylindramide	macrocyclic lactam	$C_{27}H_{34}N_2O_5$ 466.2	13.9	-20 to 25	[146]
tricyclocohumol[d]	tricyclic hydrocarbon	$C_{20}H_{30}O_6$ 365.2	21.0	-12.4 to 17.4	chapter 5.1.
GIPFFPVHLKR[d]	linear peptide (11 amino acids)	$C_{65}H_{99}N_{17}O_{12}$ 1309.8	8.6	-14.1 to 17.6	chapter 3.3 A[c]
parthenolide	chair-like bicycle	$C_{14}H_{18}O_3$ 234.3	4.5	-6.4 to 7.4	chapter 4.2 A[c]

[a] size in terms of molecular formula and molecular weight in g/mol
[b] $^1H,^{13}C$ one-bond RDCs
[c] data is given in the Appendix
[d] has been measured in deuterated PAN (see chapter 3.3.)

3.1.7 Conclusion

In summary, it has been shown that stretched poly(acrylonitrile)/DMSO gels are very useful alignment media for the measurement of anisotropic NMR-parameters. The few broad NMR-signals resulting from the polymer backbone can be reduced by relaxation filters and small detected impurities can be neglected. The strength of alignment is freely scalable by the chain-length of the polymer, the irradiation dose used for cross-linking and other parameters. As the presented alignment medium is uncharged and compatible with peptides, natural products and other molecules, it is widely applicable and closes a gap in the variety of existing alignment media.

In the meanwhile, the developed PAN/DMSO gels are a favored alignment medium for small to medium-sized molecules soluble in DMSO as many requests, several already published projects[24, 25, 146, 174] and a number of yet unpublished projects of other research groups show.

This project was already started during the Master's Thesis and first results (preparation of cross-linked PAN of the first and second generation, swelling behavior and RDCs of norcamphor in a PAN/DMSO gel) have already been published there.[96] Poly(acrylonitrile) of high molecular weight (MW=231000 g/mol) was synthesized in the group of Prof. Dr. Andreas Lendlein from the *Center for Biomaterial Development at the Institute of Polymer Research, GKSS Research Center* (Teltow, Germany). The cyclic peptides were synthesized by Dr. Jörg Auernheimer, Dr. Burkhardt Laufer and Dr. Jayanta Chatterjee (TUM, Munich). Irradiation of the polymer samples was done at *BetaGammaSystems* (Saal a.d. Donau, Germany).

Results presented in this chapter have been published:

Grit Kummerlöwe; Jörg Auernheimer; Andreas Lendlein; Burkhard Luy: '*Stretched Poly(acrylonitrile) as a Scalable Alignment Medium for DMSO*' in *Journal of the American Chemical Society* **2007**, *129*, 6080-6081.

3.2 Deuterated Polystyrene

3.2.1 Introduction and Motivation

In the last years a multitude of new alignment media for the alignment of small molecules have been developed, closing gaps in the range of applicable solvents and achieving a better scalability of the alignment strength. With the help of this media molecules can be partially aligned and anisotropic parameters can be measured. However, alignment media generally introduce undesired NMR-signals which might severely overlap with signals of the molecule of interest and become especially annoying in polymer gels at low alignment strengths.

One solution to the problem is the use of an alignment medium with few NMR signals, like PDMS with only one ^{1}H NMR signal at 0.1 ppm.[67] This is of course a strong limitation in the choice of alignment medium, and sometimes it might be not possible due to solubility or other considerations. Another solution might be the use of relaxation filter methods[65] (see also chapter 3.1.4), but for some polymers this does not work. As has been shown in great detail, NMR signals originating from polystyrene (PS) can hardly be removed using relaxation filter experiments.[65] Especially the apparently dynamic side chains of PS lead to aromatic proton signals with T_2 times similar to small organic molecules. A more generally applicable approach might be the perdeuteration of the alignment medium which has been previously applied to the liquid crystalline phase 4-*n*-pentyl-4'-cyanobiphenyl-d_{19}.[63]

The aim of this project was therefore to produce fully deuterated polystyrene gels, bearing all advantages of scalability, solubility and easy handling of PS gels but with practically no ^{1}H NMR signals originating from the alignment medium. The preparation and characterization of the new alignment medium made of stretched gels of cross-linked deuterated polystyrene, called dPS gels, is the topic of this chapter. A first application of dPS gels for the configurational and conformational analysis of a natural product, will be presented in chapter 5.2.

3.2.2 Preparation of dPS Gels

Deuterated polystyrene/chloroform gels have been prepared in a similar way as described previously for non-deuterated polystyrene.[64]

Polymerization of Cross-Linked dPS

Perdeuterated and cross-linked polystyrene (dPS) was made out of commercially available styrene-d_8, divinylbenzene (DVB) as cross-linker and azobisisobutyronitrile (AIBN) as radical starter. The latter two were used in their non-deuterated form, as they are only needed in very small amounts and as they are not commercially available or very expensive.

Glass tubes with inner diameters of 2.4 mm, 3.4 mm and 4.0 mm were sealed on one end by melting and dried carefully, followed by a treatment with a 1:1 mixture of chlorotrimethylsilane and dichloromethylsilane for 18 h to ensure hydrophobic glass surfaces. After washing with dichloromethane, tubes were dried at 50°C.

Styrene-d_8 (98%, Sigma) and divinylbenzene (80%, Fluka) were filtered through basic aluminium oxide (pH 10) and further purified by cryogenic condensation and vacuum distillation, respectively. The monomers then were degassed for 15 minutes under vacuum in an ultrasonic bath and ventilated with argon.[175]

The purified styrene-d_8 was mixed with different amounts of DVB (0.2%; 0.5%; 1.0% (w/w)) and AIBN (0.1% (w/w)) and filled into the glass tubes. Open ends of the tubes were sealed by melting and polymerization was performed for 5 days at 45°C and another two days at 60°C.[175] Glass tubes were destroyed mechanically to obtain the sticks of cross-linked dPS.

Preparation of Gels

Stretched gels of deuterated polystyrene and chloroform were prepared with the approach of restricted swelling in a glass tube: sticks of cross-linked dPS were placed in NMR-tubes and $CDCl_3$ was added for swelling. The gels were allowed to swell and equilibrate for at least 3 weeks before NMR experiments were carried out. Different alignment strengths were achieved by the different amount of cross-linking (different DVB concentration) and by varying the ratio of stick-diameter and tube-diameter. For comparison analog gels of non-deuterated polystyrene and $CDCl_3$ were prepared (for details see Appendix).

3.2.3 Spectral Quality of 1D Proton Spectra

For a first comparison, ^{1}H-1D-spectra of stretched polystyrene/chloroform and deuterated polystyrene/chloroform gels have been recorded (see figure 3.9. A). The

reduction of NMR signals originating from the polymer is enormous. For the dPS gel only small remaining signals originating from residual protons of styrene-d_7 and the non-deuterated DVB and AIBN are present. The most intense signal in the spectrum of the dPS gel is the residual solvent peak of $CDCl_3$ at 7.26 ppm.

The dramatic improvement of spectral quality can easily be seen as soon as approximately 25 mM strychnine is diffused into the gel and corresponding 1D-spectra are recorded (Figure 3.9. B): While signals from the polymer PS dominate the spectrum in the non-deuterated case, they are hardly visible in the dPS sample.

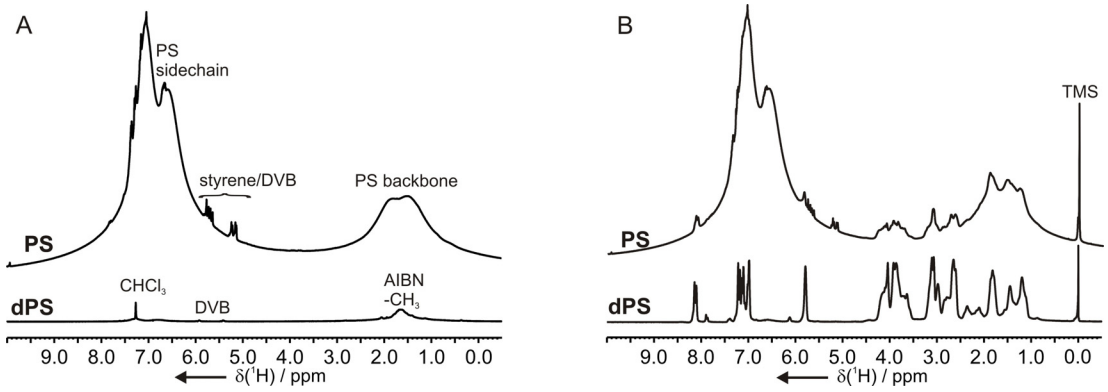

Figure 3.9.: Comparison of ^1H 1D-spectra acquired on various stretched PS/$CDCl_3$ and correspondingly deuterated and stretched dPS/$CDCl_3$ gels. (A) Comparison of proton 1D-spectra of the polymer gels without additional solute. Selected signals of the alignment media have been assigned. (B) Corresponding 1D-spectra of the stretched gels with ≈ 25 mM strychnine diffused into them show the dramatic improvement of spectral quality upon deuteration of the alignment medium.

3.2.4 Deuterium Spectrum of a dPS Gel

To estimate the alignment strength of a stretched gel deuterium 1D-spectra are recorded in order to measure the quadrupolar splitting of the solvent. In this respect it is interesting in how far the perdeuteration of the polymer affects the deuterium spectrum. Apparently, almost no signals of the dPS remain because of the fast relaxation of the quadrupolar nucleus in the stretched and therefore anisotropic polymer matrix: they can hardly be seen as broad humps in the aliphatic and aromatic region (see Figure 3.10.). The deuterium spectrum shows basically only the solvent peak $CDCl_3$ with its quadrupolar splitting. Very weak and sharp signals originate from remaining monomers (styrene-d_8) and impurities of unknown origin.

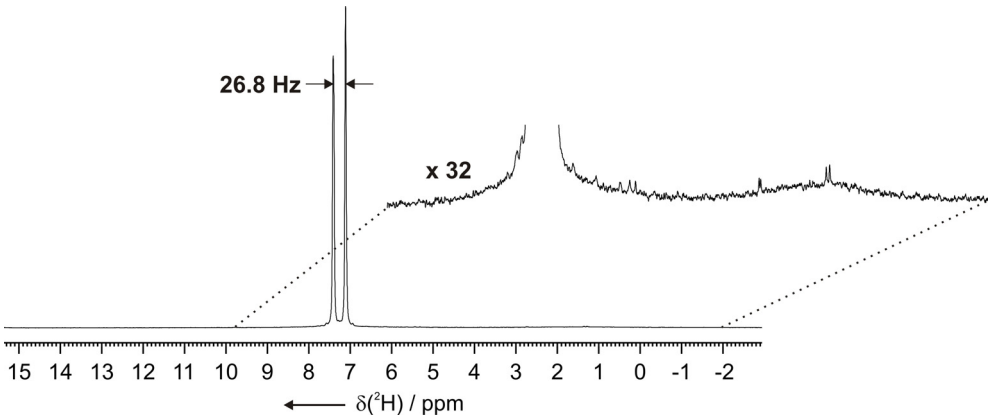

Figure 3.10.: ^{2}H 1D-spectrum of a stretched dPS/$CDCl_3$ gel. The spectrum basically contains the solvent signal with its 26.8 Hz quadrupolar splitting. Polymer signals can be seen only as very broad humps and weak, sharp signals originate from monomers and unknown impurities.

3.2.5 Spectral Quality of 2D Heteronuclear Proton-Carbon Spectra

As seen in Figure 3.8. B signals from the non-deuterated polymer can make it impossible to identify solute signals in a ^{1}H-1D-spectrum. On the other hand, in two-dimensional heteronuclear experiments as used for the extraction of one-bond $^{1}H,^{13}C$-RDCs, signal overlap is usually reduced due to the additional spectral dimension. However, as the CLIP-HSQC[107] of approximately 4 mM staurosporine diffused in a PS/$CDCl_3$ gel clearly demonstrates, overlap in the aromatic region is still a significant problem at low solute concentrations (Figure 3.11. A). The corresponding spectrum in a dPS/$CDCl_3$ gel shows no overlap with the very small residual polymer signals and allows the extraction of all aromatic RDCs (Figure 3.11. B). With all of the RDCs in hand, the configurational and conformational analysis of the natural product staurosporine is possible, as will be shown in chapter 5.2.

It is worth to mention, that the quality of spectra is not only improved in terms of less signal overlap, but also by an increasing signal-to-noise-ration of solute signals: without the intense signals originating from the polymer, the *receiver gain* of the spectrometer can be adjusted. Therefore solute signals get more intense, leading to better spectra and/or less measurement time, especially for low solute concentrations (see also chapter 3.2.6).

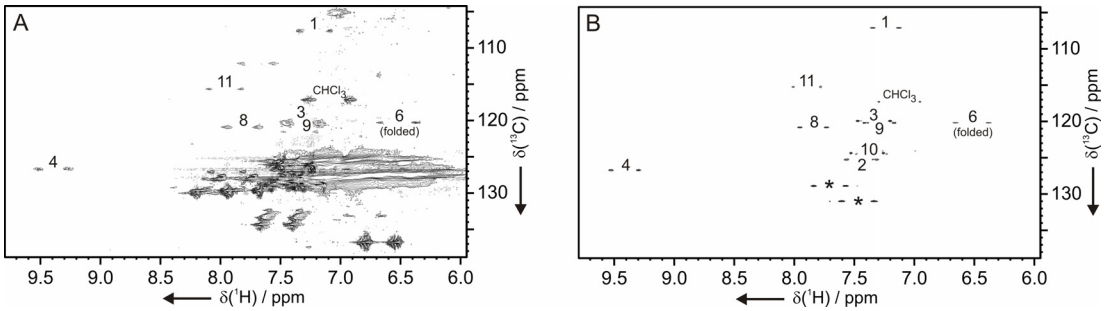

Figure 3.11.: Aromatic region of CLIP-HSQC spectra[107] acquired on the corresponding gels of non-deuterated PS (A) and deuterated dPS (B) containing ≈ 4 mM staurosporine. Contour levels were adjusted to allow for the identification of staurosporine signals as far as possible. Cross peaks are assigned wherever possible (for the structure of staurosporine see chapter 5.2). Residual unidentified signals originating from the alignment medium are marked with an asterisk.

3.2.6 Spectral Quality of 2D Homonuclear Proton Spectra

In addition to the improvements in heteronuclear experiments the perdeuteration of the alignment medium also allows the acquisition of clean homonuclear correlation experiments. Figure 3.12. shows a comparison of J-ONLY-TOCSY spectra[176] acquired on samples of strychnine in a PS/$CDCl_3$ (Figure 3.12. A) and a dPS/$CDCl_3$ gel (Figure 3.12. B). Although all experimental parameters are in favor of the non-deuterated gel (600 MHz vs. 500 MHz spectrum, approximately twice the concentration of strychnine, lower alignment strength resulting in much smaller multiplet patterns and sharper lines), the significantly higher quality of the dPS/$CDCl_3$ spectrum is clearly visible. Because of intense polymer signals in the PS/$CDCl_3$ sample the receiver gain had to be set to 32 compared to 2048 in the dPS/$CDCl_3$ case, leading to significantly lower noise and spectral artifacts for the latter one.

Moreover, potential overlap is reduced: in the non-deuterated case broad peaks are visible at 1-2 ppm and 6-7.5 ppm that are absent in the deuterated case and a multitude of relatively narrow TOCSY and ROE cross peaks affects the aromatic region very seriously since they cannot be distinguished from cross peaks of the solute. In contrast, the spectrum recorded in the deuterated gel is of excellent quality.

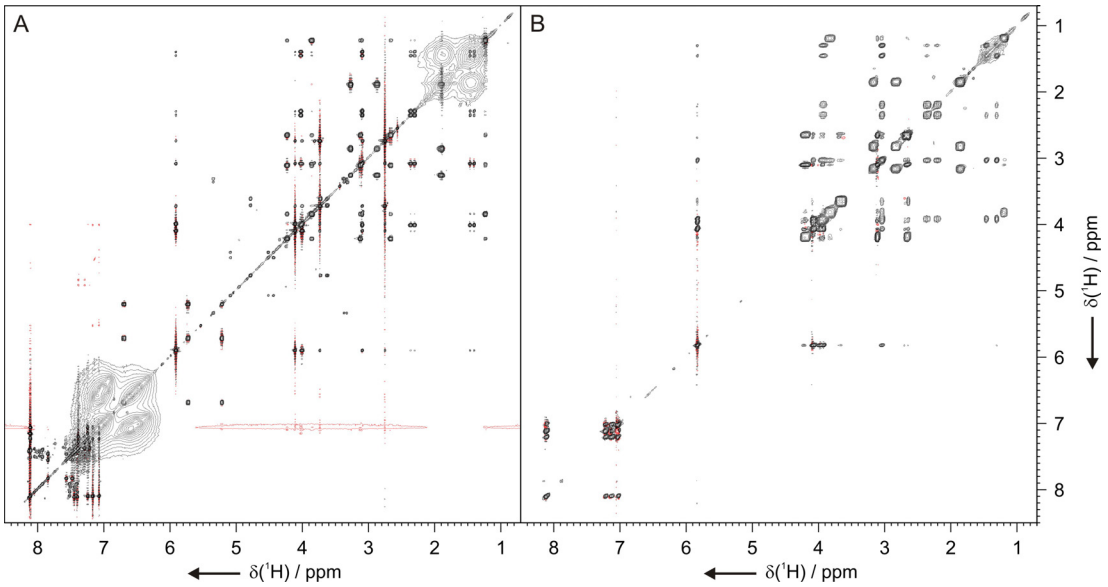

Figure 3.12.: Comparison of J-ONLY-TOCSY spectra[176] of strychnine acquired in a PS/$CDCl_3$ (A) and a dPS/$CDCl_3$ gel (B). Although the concentration of strychnine is higher and the alignment strength of the gel lower in the case of the PS gel (A), the spectrum recorded in the dPS gel (B) is clearly of higher quality.

In Figure 3.13. the aliphatic region of three TOCSY spectra recorded on strychnine in a dPS/$CDCl_3$ gel is shown. While in a PS/$CDCl_3$ gel the reduced dynamic range and overlap with the polymer backbone signals (see Figure 2.12. A) make the interpretation of the spectra almost impossible, spectra recorded in a dPS gel are clean enough to reliably extract all cross peaks.

The TOCSY experiments shown differ in the multiple pulse sequence used in the mixing period: While the so-called J-ONLY-TOCSY (Figure 3.13. A) with its JESTER-1 sequence shows only correlations via scalar couplings,[176] the DIPSI-2 sequence (Figure 3.13. B) leads to positive scalar and negative dipolar polarization transfer and combinations of them.[177, 178] While the J-ONLY-TOCSY can be used in partially aligned samples to reassign scalar coupled spin systems with shifted chemical shifts,[176] the additional cross peaks present in the DIPSI-2 experiment can be used to identify neighboring spin systems that are now coupled through space via $^1H,^1H$-RDCs[179] (see color-coded assignments in Figure 3.13.). The MOCCA-XY16 TOCSY experiment, optimized for maximum combined scalar and dipolar transfer,[180] is shown in Figure 3.13. C.

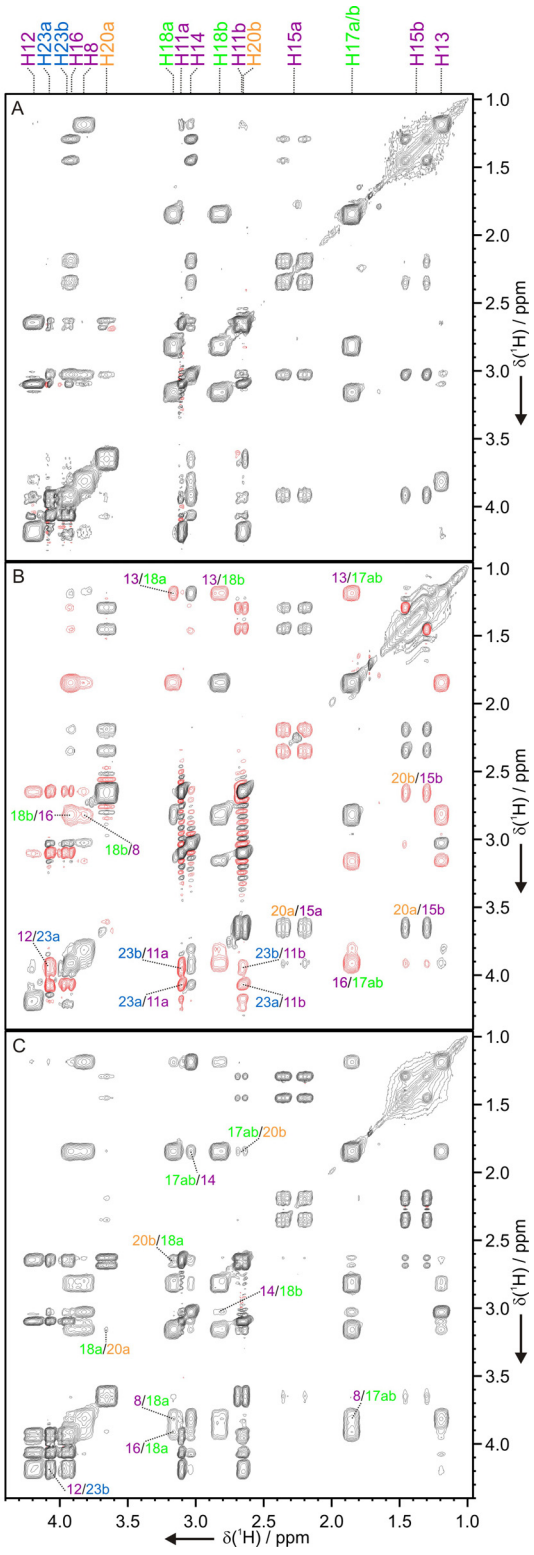

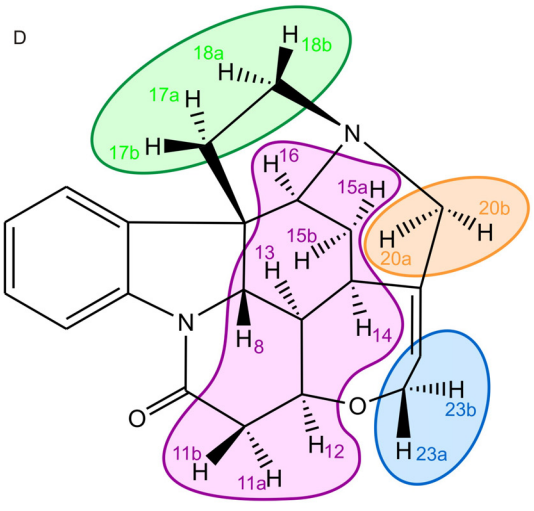

Figure 3.13.: The absence of polymer signals in dPS/$CDCl_3$ gels allows the measurement of homonuclear correlation experiments. For example, TOCSY-type spectra with varying mixing sequences and dipolar transfer behavior can be recorded: (A) J-ONLY-TOCSY,[176] in which RDCs are not active and only classical J-coupled spin systems are correlated; (B) the DIPSI-2 mixing sequence which results in mostly negative cross peaks from RDCs while conventional positive cross peaks originate from J-dominated correlations;[177] (C) The MOCCA-XY16 mixing sequence, optimized for maximum efficient transfer via RDCs with always positive cross peaks.[180]
Positive and negative cross peaks are drawn in black and red contour lines, respectively. Resonance assignment is color coded according to the spin systems of strychnine as shown in (D).

3.2.7 Conclusion

In summary, it has been shown for the example of cross-linked polystyrene, that perdeuterated polymer gels significantly improve the quality of spectra measured on samples partially aligned in the stretched gel.

The almost signal free and scalable alignment medium enables the measurement of RDCs without overlapping signals and at very low concentrations of the solute. Furthermore it allows the acquisition of any kind of homonuclear correlation experiments, as has been shown for various TOCSY-type experiments. Small residual polymer signals of the dPS presented here originate from the non-deuterated cross-linker DVB and radical starter AIBN, which could be further reduced by using the corresponding deuterated substances or by substituting the radical starter with a proton-less one.

The example of deuterated poly(styrene) suitable for apolar solvents, shows the wealth of the approach to perdeuterate the alignment medium. In principle this method can be extended to other polymer gels suitable for polar solvents, enabling the acquisition of high quality spectra with scalable alignment for the most common NMR solvents. In the next chapter a second example for a perdeuterated polymer gel will be shown: deuterated poly(acrylonitrile).

This project was done in cooperation with Dr. Sebastian Knör (TUM Munich), who did the synthesis of cross-linked polystyrene and cross-linked deuterated polystyrene.

Results presented in this chapter have been published:

Grit Kummerlöwe; Sebastian Knör; Andreas O. Frank; Thomas Paululat; Horst Kessler; Burkhard Luy: *'Deuterated Polymer Gels for Measuring Anisotropic NMR Parameters with Strongly Reduced Artefacts.'* in *Chemical Communications* **2008**, 5722-5724.

3.3 Deuterated Poly(acrylonitrile)

3.3.1 Introduction and Motivation

As shown for the example of deuterated polystyrene gels (see chapter 3.2), the approach of perdeuteration of the alignment medium can significantly improve spectral quality of samples in anisotropic environment. Since dPS gels, like the non-deuterated PS gels, are only applicable for apolar organic solvents,[65] it would be desirable to extent this approach to polymers used as alignment medium for solutes in polar solvents.

The aim of this project was therefore to produce fully deuterated poly(acrylonitrile) gels, with all the advantages of PAN, as they were described in chapter 3.1, but without ^{1}H-NMR signals originating from the alignment medium. First results for the cross-linked deuterated poly(acrylonitrile), called dPAN, and its DMSO gels are topic of this chapter.

3.3.2 Preparation of dPAN Gels

With the experiences of cross-linking the linear polymer PAN by irradiation with accelerated electrons, this method was to be applied also for deuterated PAN. As the polymer is not commercially available in its deuterated form, it was necessary to polymerize it out of the deuterated monomer.

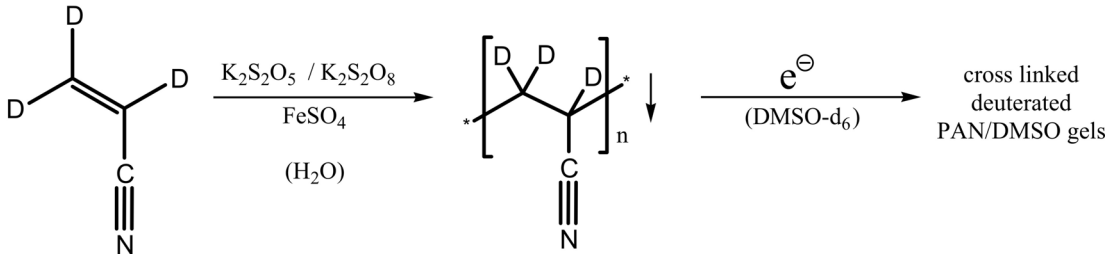

Figure 3.14.: Preparation of deuterated poly(acrylonitrile) gels: The polymerization of acrylonitrile-d_3 was carried out in water using a proton less redox-system as radical initiator. The precipitated polymer was washed and dried before dissolving it in DMSO-d_6. The polymer solution was then filled in glass or Teflon® tubes and irradiated with accelerated electrons to obtain gels of cross-linked dPAN analog to the production of the corresponding non deuterated gels.

The polymerization was done in water, using the proton-less redox-system $K_2S_2O_5$ / $K_2S_2O_8$ as radical starter (for details see Appendix). During polymerization

the building polymer precipitates and after filtering, washing and drying, it was dissolved in DMSO and irradiated as solution in cylindrical glass or Teflon® tubes. Cross-linked dPAN gel cylinders were precipitated in an analogous way as the non-deuterated PAN of the third generation (see chapter 3.1.2) to obtain dry sticks of the cross-linked polymer.

3.3.3 Spectral Quality of 1D Proton Spectra

For a first comparison ^{1}H 1D-spectra of stretched poly(acrylonitrile)/DMSO and deuterated poly(acrylonitrile)/DMSO gels have been recorded (see Figure 3.15.). As for polystyrene and its deuterated form, the reduction of NMR signals originating from the polymer is enormous. For the dPAN gel only small remaining signals originating from residual protons of acrylonitrile-d_2 are present, except for the solvent signals, which built the most intense signals in the spectrum. The improvement of spectral quality is already obvious from these 1D-spectra.

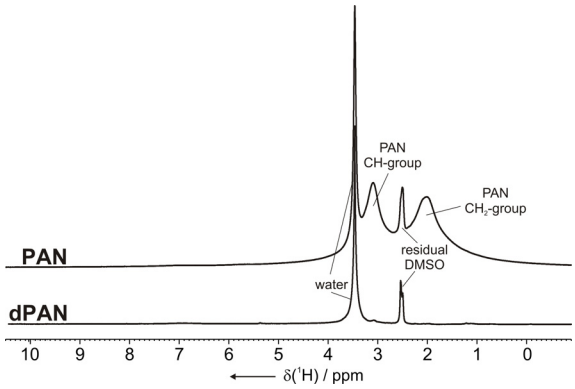

Figure 3.15.: Comparison of proton 1D-spectra of stretched poly(acrylonitrile) gels. In the case of the non deuterated PAN/DMSO gel (top) broad peaks of the polymer backbone dominate the spectrum, while for the deuterated dPAN/DMSO gel (bottom) besides the solvent signals only very small peaks originating from residual protons of acrylonitrile-d_2 are visible.

3.3.4 Spectral Quality of 2D Heteronuclear Proton-Carbon Spectra

As already discussed, overlap of solute signals decreases in heteronuclear 2D-spectra due to the additional spectral dimension and for all examples shown for PAN/DMSO gels so far (see chapter 3.1) signal overlap was not an issue. An counter-example is shown in Figure 3.16. The histidin Cβ-group of the linear peptide Gly-Ile-Pro-Phe-Phe-Pro-Leu-His-Val-Lys-Arg dissolved in a PAN/DMSO gel

severely overlaps with the CH-group of the polymer. Although the concentration of the peptide is relatively high, a coupling extraction out of the CLIP-HSQC spectrum[107] is not possible in this case (see Figure 3.16. C). The corresponding CLIP-HSQC spectrum of the peptide in the deuterated alignment medium dPAN/DMSO is clearly of higher spectral quality and an extraction of the couplings of the histidin Cβ-group is possible (see 3.16. A and B).

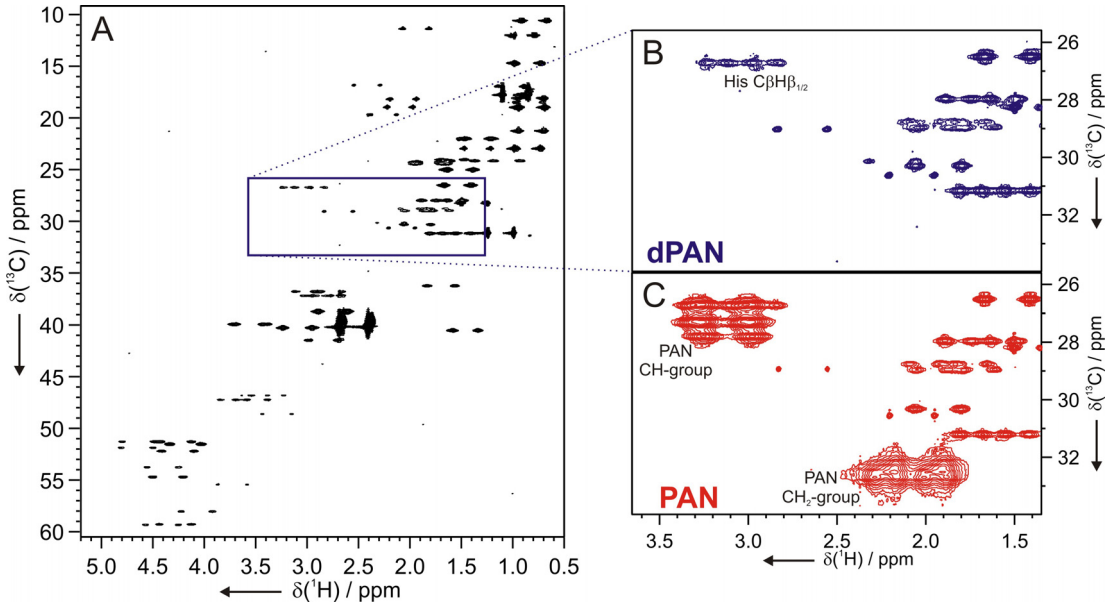

Figure 3.16.: CLIP-HSQC spectrum[107] of the linear peptide Gly-Ile-Pro-Phe-Phe-Pro-Leu-His-Val-Lys-Arg dissolved in a stretched dPAN/DMSO gel (A). The region where the polymer signals would appear is enlarged (B) to allow the comparison with the corresponding spectrum of the peptide in a non deuterated PAN/DMSO gel (C). Although peptide concentration is relatively high the couplings of the Histidin Cβ-group can not be extracted in the case of the non deuterated gel because of signal overlap.

3.3.5 Conclusion

By the deuteration of cross-linked poly(acrylonitrile) an almost signal free and easily scalable alignment medium for DMSO as the solvent was produced. It has been shown that it significantly improves spectral quality and enables the measurement of RDCs without overlapping signals origination from the polymer.

In summary, it has been shown for a second example that perdeuterated polymer gels significantly improve the quality of spectra on partially aligned samples. With the deuterated poly(acrylonitrile) for polar organic samples as presented here and the deuterated polystyrene for apolar organic samples as presented in chapter 3.2 a broad

range of solvents is covered with basically signal free alignment media. For the future it might be worth to consider the perdeuteration of poly(acrylamide) as an important medium for water soluble compounds.

This project was done in cooperation with Dr. Aleksandra Volkmann, Dr. Steffen Kelch, and Dr. Marc Behl, of the group of Prof. Dr. Andreas Lendlein from the *Center for Biomaterial Development at the Institute of Polymer Research, GKSS Research Center* (Teltow, Germany). They gave useful advices for the polymerization of deuterated PAN and produced a second batch of dPAN. Irradiation of the polymer samples was done at *BetaGammaSystems* (Saal a.d. Donau, Germany).

Results presented in this chapter will be published soon:

Grit Kummerlöwe; Steffen Kelch; Marc Behl; Andreas Lendlein; Burkhard Luy: '*Artifact-Free Measurement of Residual Dipolar Couplings in DMSO by the Use of Cross-Linked Perdeuterated Poly(acrylonitrile) as Alignment Medium*' **2010**, submitted.

3.4 Covalently Cross-Linked Gelatin

3.4.1 Introduction and Motivation

The distinction of enantiomers by NMR spectroscopy using chiral orienting media is a very powerful and well-established method.[103, 105, 181, 182] The discrimination in this case is based on the differential alignment of molecules in anisotropic media which possess a chiral super structure. The approach allows the separation of compounds without polar groups, such as saturated chiral hydrocarbons[183] or monofluorinated compounds[184] and prochiral elements in symmetrical molecules,[185] which are hard to get by with conventional analytical methods like e.g. chromatography.

A large number of suitable chiral alignment media are known for apolar solvents, typically liquid crystalline phases of homo-poly-peptides[60-62, 186, 187] (see also chapter 2.3.2). In contrast only collagen-based gelatin[52, 76, 100] and collagen[53] itself have been shown to discriminate enantiomers in aqueous solution. In this case, the chiral distinction ability as well as the cross-linking of the hydrogels is induced by the triple-helical structure of collagen which is formed via hydrogen bonds between the three individual peptide chains. The necessary anisotropy of the corresponding samples is obtained either by stretching a suitable polymer stick by swelling it directly in an NMR tube[52, 53] or by using an appropriate stretching device (see chapter 2.4.3).[76, 99, 100]

Since the cross-linking in gelatin and collagen is based on hydrogen bond formation, gels soften significantly at temperatures above 35°C and enantiomeric distinction is no longer possible.[76] Therefore attempts have been made to covalently cross-link gelatin, by the use of glutaraldehyde,[76] but this did not lead to the desired distinction of enantiomers at higher temperatures.

The aim of this project was, to covalently cross-link gelatin, in order to discriminate enantiomers at higher temperatures. With the good experiences of cross-linking gel-based alignment media by irradiation with accelerated electrons (see chapter 3.1 or reference [67]) it was intended to use this method also for a covalent cross-linking of gelatin. In the following chapters, the preparation of covalently cross-linked gelatin and the characterization of this new alignment medium is described.

3.4.2 Preparation of Covalently Cross-Linked Gelatin

As has been mentioned before (see also chapters 3.1.2), a polymer has to be in an amorphous state in order to be cross-linked by irradiation.[168, 169] Furthermore, to use it as an alignment medium, the resulting cross-linked polymer should be in a cylindrical shape of an appropriate size. As commercially available gelatin is a powder, different approaches have been tried to produce cylindrical sticks of gelatin.

Two different protocols were developed to produce sticks of covalently cross-linked gelatin: preparation scheme A includes irradiation of preformed, dry gelatin sticks and preparation scheme B involves the drying of previously irradiated gelatin hydrogels (see Figure 3.17. for an overview).

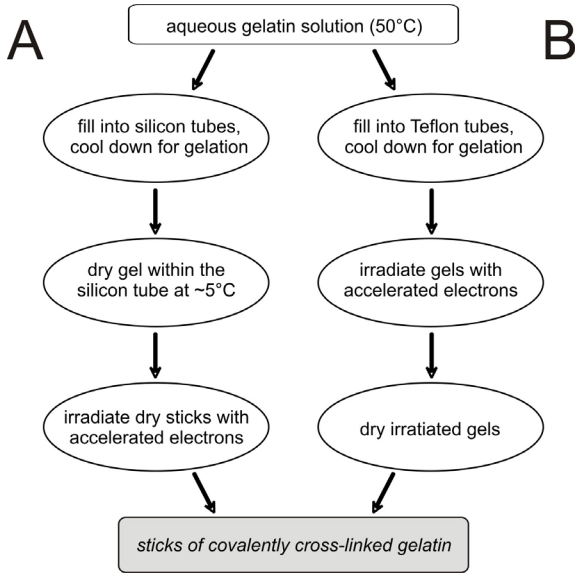

Figure 3.17.: Preparation schemes for covalently cross-linked gelatin. It is possible to either preform sticks of gelatin to be irradiated (preparation scheme A, left) or to dry irradiated gelatin hydrogels (preparation scheme B, right) to obtain sticks of covalently cross-linked gelatin.

A: Sticks of gelatin were obtained by drying cylindrical hydrogels of gelatin: 40% (w/v) gelatin was dissolved in water at 50°C and the solution was filled in silicone tubes with an inner diameter of 3.0 mm. After cooling the solution to 5°C, the obtained gelatin hydrogel within the silicone tubing was cut into pieces of about 25 mm length. Those were stored at 5°C for about one week and the dried sticks obtained by this procedure could easily be separated from the silicone tubes. The so-produced dry gelatin sticks are cylindrical and of about 18 mm length and 2.0 mm

diameter. Sticks of gelatin have then been irradiated with accelerated electrons to obtain covalently cross-linked gelatin (see Appendix for details).

B: Cylindrical hydrogels of various diameters and concentrations were prepared: gelatin was dissolved in water at 50°C with concentrations of 20%, 30% and 40% (w/v). The warm solutions were then filled into Teflon® tubes with inner diameters of 2.4 mm, 3.0 mm and 4.0 mm and lengths of 20-30 cm and stored at 5°C to form hydrogels. Then gels were irradiated within the Teflon® tubes by accelerated electrons keeping them cool in an ice/water bath (see Appendix for details). The irradiated hydrogels were peeled out of the Teflon® tubes (which are decomposed by irradiation) and cut into pieces of about 20 mm length. At room temperature the gels dried in about 3 days and cylindrical sticks of about 15 mm length and diameters of 1.5 - 2.5 mm were obtained.

The sticks obtained with both preparation schemes could be used as an alignment medium, as will be described in the following chapters. Due to the cross-linking by electron-irradiation it will be called e^--gelatin. In principle the necessary stretching of e^--gelatin gels can be achieved by the classical restricted swelling approach in an NMR-tube. However, for all NMR-studies done within this project the newly developed stretching device for arbitrary stretching of gels, which will be described in chapter 4.1, was used.

3.4.3 Swelling Behavior of Covalently Cross-Linked Gelatin

To investigate the solubility and swelling properties of e^--gelatin, corresponding sticks prepared according to preparation scheme A and irradiated with a total irradiation dose of 80 kGy were placed in various solvents and stored at room temperature for about one week. Strong swelling was observed for water and no swelling was observed for methanol, ethanol, acetonitrile, tetrafluorethanol, acetone and dimethylformamide. Surprisingly, a reasonable swelling was observed in DMSO, which is not a solvent of conventional gelatin (see Figure 3.18.).

Furthermore, the swollen e^--gelatin gels turned out to preserve their cylindrical shape even for higher temperatures (up to 90°C), which is in contrast to conventional, not irradiated gelatin (see Figure 3.18.).

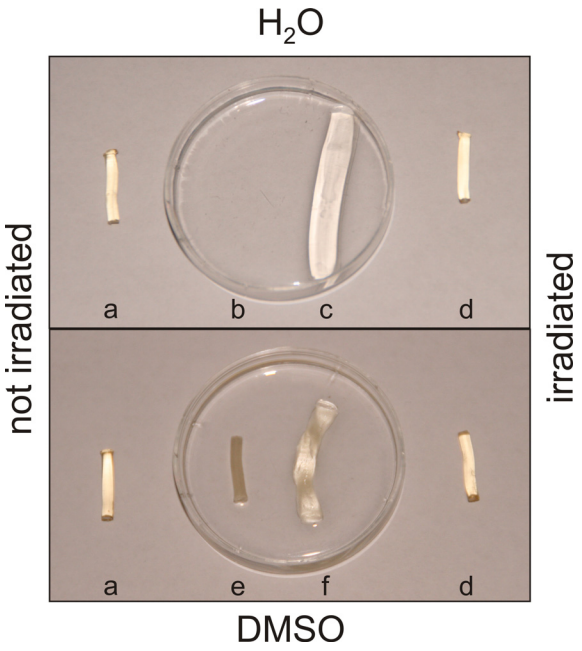

Figure 3.18.: Photograph of differently treated gelatin and e^--gelatin sticks: dry gelatin stick (a) and e^--gelatin stick (d) and similar sticks after being kept in water for 3 days at 50°C (b, c) or after being kept for 3 days in DMSO at room temperature (e, f). The covalently cross-linked e^--gelatin is forming gels in water (c) and DMSO (f), while conventional gelatin dissolves completely in water at higher temperatures (b) and is not swelling or dissolving in DMSO (e). *Copyright Wiley-VCH Verlag GmbH & Co. KGaA. Reproduced with permission from Reference [188].*

3.4.4 Stability of e^--Gelatin/Water Gels Towards Temperature

As a first check whether the e^--gelatin gels are applicable as alignment media for the measurement of anisotropic parameters, several e^--gelatin/D_2O gels have been mechanically stretched within the stretching apparatus (see chapter 4.1) and deuterium 1D experiments have been acquired. Not surprisingly, it was possible to measure a quadrupolar splitting of the solvent in the stretched gels and therefore it can be concluded, that e^--gelatin can be used as an alignment medium. However this is also possible with conventional gelatin, so the interesting point was to compare the behavior of the e^--gelatin gels upon heating. Therefore different stretched e^--gelatin gels have been slowly heated within the spectrometer and the development of their quadrupolar splitting has been monitored.

In Figure 3.19. A the quadrupolar splitting of D_2O as a measure of the alignment strength is shown with ascending temperature for stretched gelatin/D_2O samples with different irradiation doses. While the alignment for conventional gelatin breaks down completely at ≈ 35°C, quadrupolar splittings can be measured up to 70°C for e^--gelatin, but the splittings decrease with temperature also for the e^--gelatin samples. The overall reduction of alignment at higher temperatures can be attributed to two different processes: firstly the breakage of hydrogen bonds and secondly the

increased dynamics within the gel which leads to a general reduction of the anisotropic interaction between polymer and solvent molecules, which also has been observed in previous studies[65, 67] (see also Figure 2.9. C).

For higher irradiation doses and therefore higher covalent cross-linking, the decrease of the quadrupolar splitting due to temperature rise is less pronounced (see Figure 3.19. A).

The amount of alignment due to covalently vs. hydrogen bond cross-linked polymer networks can also be estimated by the temperature curves shown in Figure 3.19. B. Apparently, conventionally hydrogen bonded networks and covalently cross-linked polymer co-exist to a large extent when the gel is heated initially, but after heating the particular gel to 55°C only the covalent network component survives. As a consequence, repeated heating/cooling cycles do not result in a further noticeable reduction of alignment.

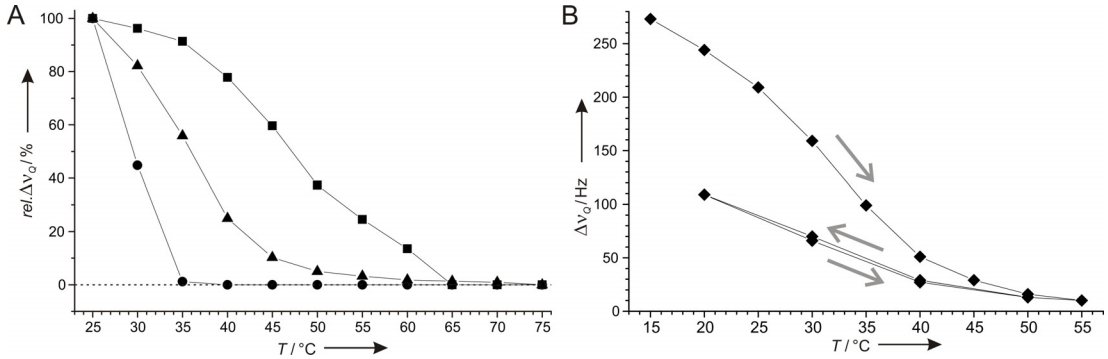

Figure 3.19.: Temperature dependence of the quadrupolar splitting $\Delta\nu_Q$ of different gelatin gels. (A) The relative quadrupolar splitting rel.$\Delta\nu_Q$ of D_2O (normalized to $\Delta\nu_Q$ at 25°C) drops with ascending temperatures. While for 30% conventional gelatin (●) no alignment above 35°C is observed, e^--gelatin with 80 kGy (▲), and e^--gelatin with 320 kGy (■) irradiation of accelerated electrons show quadrupolar splittings even for higher temperatures. (B) The initial decrease of the quadrupolar splitting of a 40% / 60 kGy e^--gelatin gel upon heating is stronger than the increase upon cooling the gel again as only the anisotropy of the covalent network survives. Consequently reheating/cooling does not lead to a further reduction in alignment due to the melting of hydrogen bonds. *Copyright Wiley-VCH Verlag GmbH & Co. KGaA. Reproduced with permission from Reference [188].*

The change in alignment upon heating and cooling is partly due to the melting and reforming of hydrogen bonds. As this is a slow process, waiting times of approximately one hour are necessary for stable alignment conditions, as can be seen in Figure 3.20. The quadrupolar splittings shown in Figure 3.19. B are those acquired after 6 h of equilibration.

Notably, changes in the quadrupolar splitting and therefore in the alignment strength are strongest in the region of 30-40°C, the melting point of gelatin (see Figures 3.19. and 3.20.).

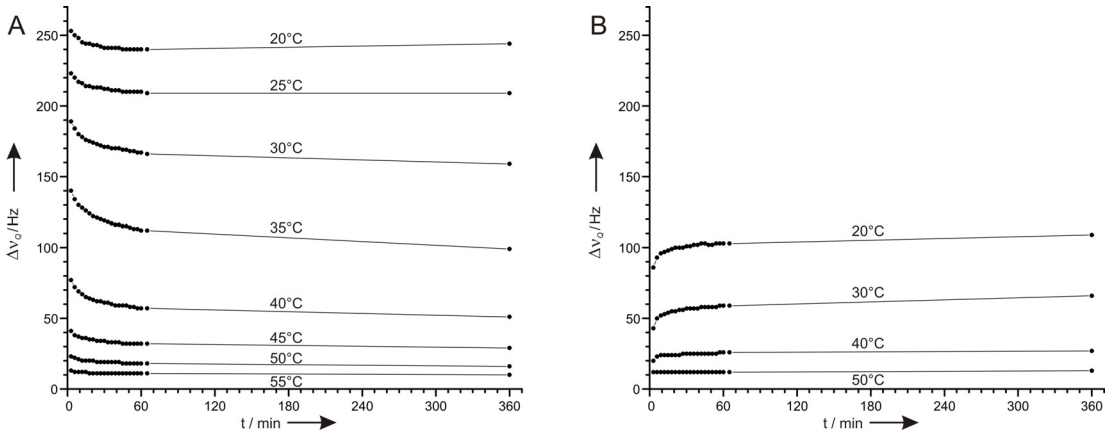

Figure 3.20.: Change of alignment upon heating and cooling of an e^--gelatin/D_2O gel. Quadrupolar splittings $\Delta\nu_Q$ of the solvent D_2O are shown as a function of time after a certain temperature change. Heating was performed in 5°C steps starting at 15°C and the quadrupolar splitting was monitored over 6 hours before the temperature was further increased (A). Cooling of the same sample was performed and monitored in an analog way but in steps of 10°C (B).

3.4.5 Enantiomeric Discrimination in e^--Gelatin/Water Gels

Since covalently cross-linked e^--gelatin might have a different molecular arrangement compared to conventional gelatin and as this might change upon heating, a crucial question is, whether the chiral, triple helical super structure is still present in e^--gelatin and whether this chirality is sufficient to distinguish enantiomers. Furthermore, it has to be investigated how the potential to distinguish enantiomers develops upon heating, as this causes a melting of hydrogen bonds.

For this reason a sample was prepared with a 2:1 mixture of L-Ala and D-Ala, for which was shown previously that the two enantiomers can be distinguished with stretched gelatin[52, 100] and collagen.[53] The e^--gelatin/D_2O gel was stretched and by using the J-BIRD^{d,X}-HSQC experiment[52] it was possible to distinguish both enantiomers of alanine due to their different alignment in the chiral alignment medium (see Figure 3.21.). Therefore it can be concluded, that the potential of gelatin to distinguish enantiomers is not destroyed upon irradiation with accelerated electrons.

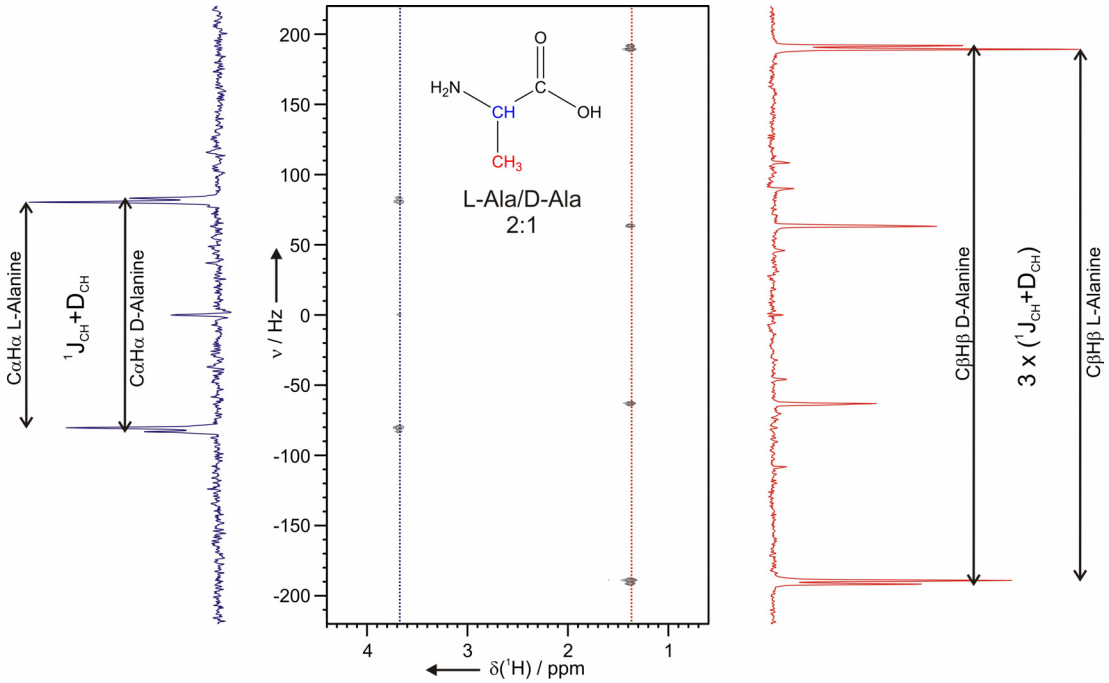

Figure 3.21.: Discrimination of alanine enantiomers in an e^--gelatin/D_2O gel with a 2:1 mixture of L-Ala and D-Ala. The expansion from the two-dimensional $^1H,^{13}C$-J-BIRD^{d,X}-HSQC experiment[52] at 310 K (37°C) is shown with traces along the J-dimension at Hα (blue) and Hβ proton (red) chemical shifts of alanine. From the 1D slices ($^1J_{CH}+D_{CH}$) and 3*($^1J_{CH}+D_{CH}$) coupling constants can be measured for CαHα and CβHβ groups, respectively.

The stretched e^--gelatin/D_2O gel was then heated to test for the enantiomeric discrimination at elevated temperatures. As the slices along the J-dimension of the $^1H,^{13}C$-J-BIRD^{d,X}-HSQC experiment[52] (see Figure 3.22.) show, chiral discrimination can be achieved in this case up to approximately 55°C.

One-bond CH-RDCs of the CαHα and CβHβ groups of D-Ala and L-Ala in an e^--gelatin/D_2O gel have been extracted out of the 1D traces at various temperatures while stepwise heating, cooling and reheating of the gel. To investigate the dependence of RDCs on the temperature without the influence of the overall alignment strength, normalized RDCs (RDCs normalized by the corresponding quadrupolar splitting of the solvent) have been calculated and plotted against the temperature (see Figure 3.23. and Appendix). Obviously normalized RDCs at a given temperature do not depend on previous heating or cooling of the gel.

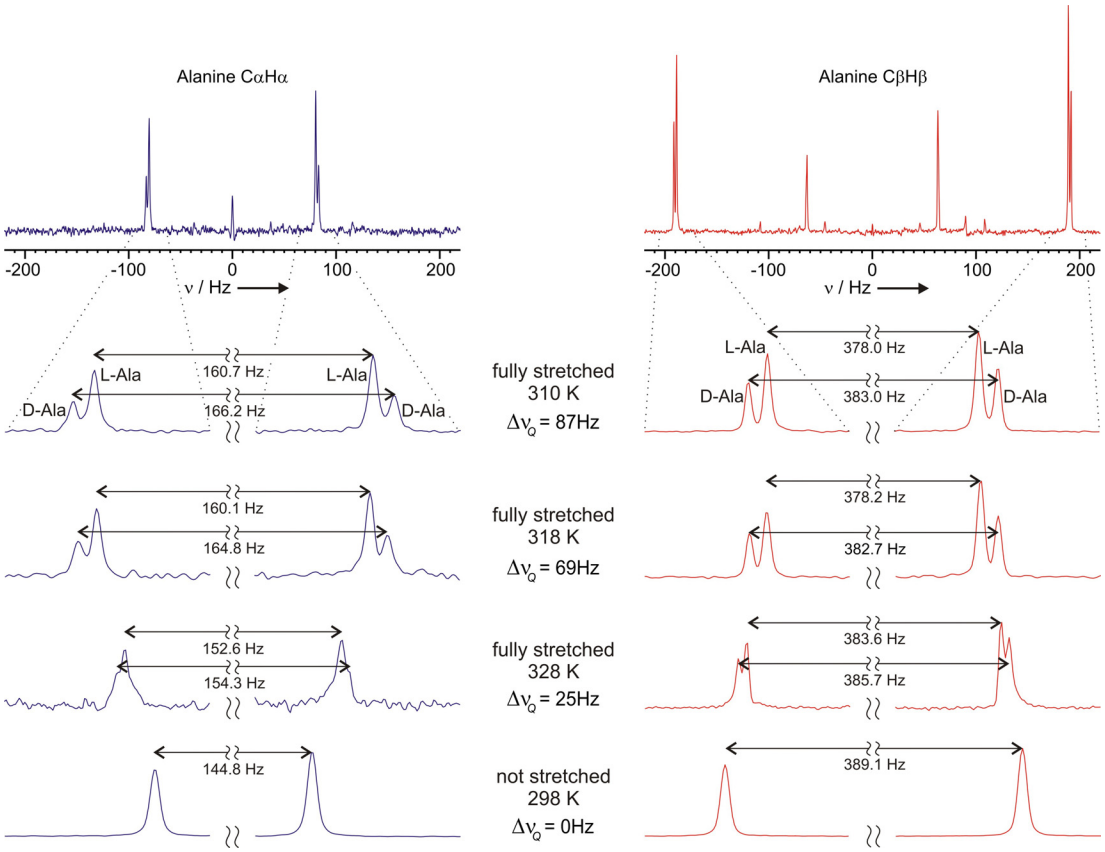

Figure 3.22.: Discrimination of alanine enantiomers in an e^--gelatin/D_2O gel at various temperatures. Enlargements of the 1D column traces from the $^{1}H,^{13}C$-J-BIRD^{d,X}-HSQC[52] shown in Figure 3.21. for CαHα (blue) and CβHβ (red) at various temperatures and for the unstretched gelatin sample. In this case, distinction of enantiomers at both chemical shifts is possible up to 328 K (55°C).

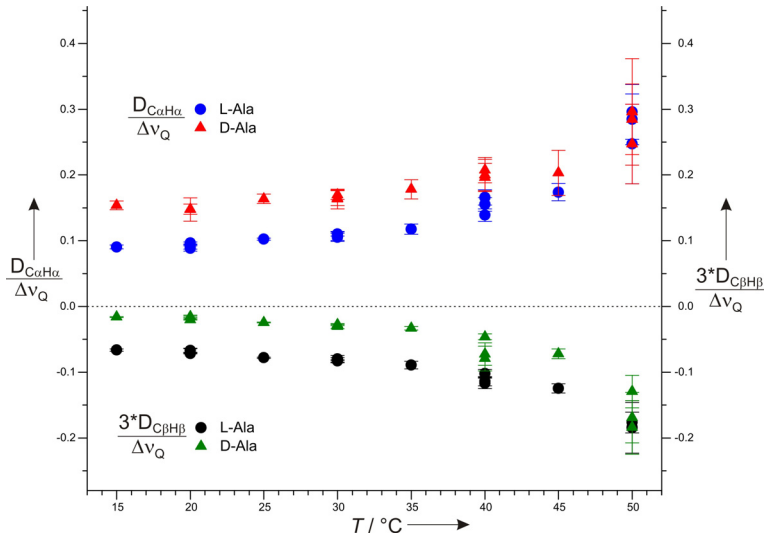

Figure 3.23.: Normalized one-bond RDCs do not show changes of alignment properties due to the temperature history of the gel since all normalized RDCs at a given temperature are practically identical within the experimental error. Around 35°C, the melting point of conventional gelatin, changes of normalized RDCs with temperature get stronger, most likely because of the breakage of triple-helix-stabilizing hydrogen bonds. At 50°C enantiomers cannot be distinguished any more.

3.4.6 Influence of Cross-Linking on the Alignment Properties of Gelatin

To investigate whether the alignment tensors of a solute in conventional gelatin gels and e^--gelatin gels differ, sucrose was chosen as a test molecule. For a sample of sucrose in conventional gelatin (for data of conventional gelatin see chapter 4.1) and a sample of sucrose in e^--gelatin $^1T_{CH}$ couplings for different degrees of stretching of the gels have been measured using the CLIP-HSQC pulse sequence.[107]

A plot of measured $^1T_{CH}$ couplings against the quadrupolar splitting of the solvent D_2O at the same degree of stretching (see Figure 3.24.), reveals that RDCs and therefore the alignment tensors are practically the same in both alignment media. This is an additional evidence for the more or less conserved structural properties of gelatin after irradiation with accelerated electrons. (Measured couplings and fitted slopes of $^1T_{CH}$ couplings are given in the Appendix).

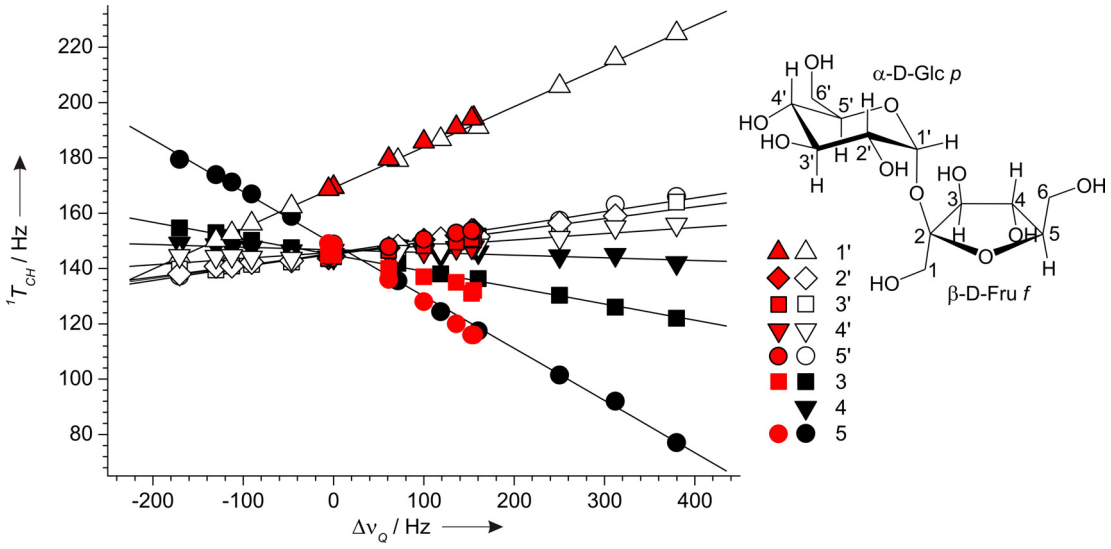

Figure 2.24.: Comparison of $^1T_{CH}$ couplings for sucrose in conventional and covalently cross-linked gelatin. Couplings of sucrose are shown as a function of the quadrupolar splitting ($\Delta\nu_Q$) of D_2O observed at different degrees of stretching. Gels have been stretched within the stretching apparatus, which will be described in chapter 4.1. The slopes of individual CH-groups of sucrose are almost identical for the measurement in conventional gelatin/D_2O (black), compared to those in e^--gelatin/D_2O (red), indicating only very minor differences in the alignment properties between the two gels.

3.4.7 Prochiral Discrimination in e⁻-Gelatin/DMSO Gels

While conventional gelatin tolerates DMSO only in DMSO/D_2O mixtures,[76] e⁻-gelatin swells in DMSO/D_2O mixtures with high DMSO concentrations and even in pure DMSO (see Figure 3.18.), suggesting its use as an alignment medium for DMSO.

As the chiral distinction of enantiomers in gelatin is believed to originate from the triple helical fold stabilized by hydrogen bonds and as DMSO is a well-known hydrogen-bond-breaker, the main concern was, whether e⁻-gelatin/DMSO gels possess a chiral superstructure which would be able to distinguish enantiomers.

As a first test, deuterium spectra of stretched e⁻-gelatin/DMSO-d_6 gels were acquired. Astonishingly, four lines of two quadrupolar doublets can be observed (see Figure 3.25. A). This finding can only be explained by a chiral superstructure, leading to different residual quadrupolar couplings for the two prochiral methyl groups of DMSO. Furthermore this is a clear indication that chiral discrimination in general could be possible with DMSO as the sole solvent, as it generally indicates the non-equivalence of the solute molecules upon inversion.

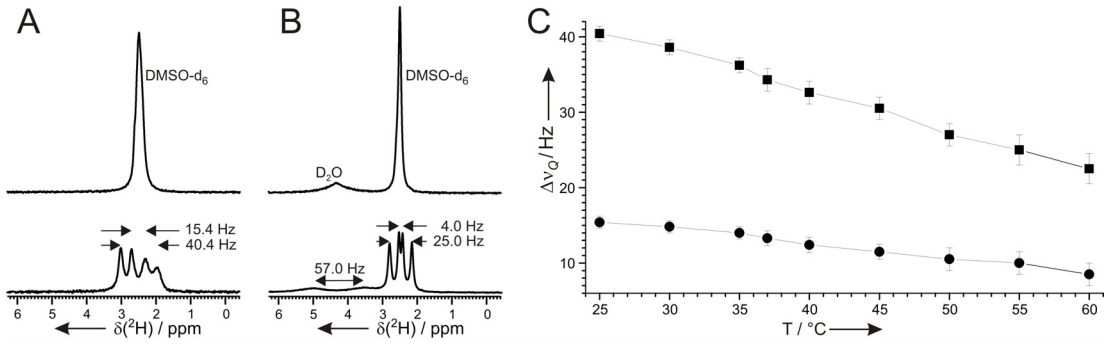

Figure 3.25.: Quadrupolar splittings of DMSO-d_6 in stretched e⁻-gelatin gels. Deuterium 1D spectra of e⁻-gelatin swollen in pure DMSO-d_6 (A) and e⁻-gelatin swollen in DMSO-d_6/D_2O (4:1) (B) without stretching and stretched within the stretching apparatus described in chapter 4.1. The prochiral methyl groups of DMSO can easily be distinguished by differences in their residual quadrupolar splittings. The temperature dependence of the quadrupolar splittings $\Delta\nu_Q$ of the methyl groups of DMSO-d_6 in the stretched e⁻-gelatin/DMSO-d_6 gel (C) shows that prochiral discrimination is also possible at elevated temperatures.

The two prochiral methyl groups of DMSO exhibit strikingly different residual quadrupolar splittings of 15.4 Hz and 40.4 Hz in a stretched e⁻-gelatin swollen in pure DMSO-d_6 (see Figure 3.25. A) and 4.0 and 25.0 Hz in stretched e⁻-gelatin swollen in

80% DMSO-d_6 / 20% D_2O (see Figure 3.25. B), indicating that the alignment tensor depends on the content of water in the gel.

Heating the e^--gelatin/DMSO-d_6 gel reveals that the distinction of prochiral methyl groups of DMSO-d_6 can also be observed at temperatures well above 60°C (see Figure 3.25. C), and therefore behaves similar to e^--gelatin swollen in D_2O.

3.4.8 Conclusion

In summary, it has been shown that gelatin irradiated with accelerated electrons allows the distinction of enantiomers using anisotropic NMR parameters like RDCs or RQCs. The so-called e^--gelatin is not only cross-linked via hydrogen bonds, as conventional gelatin, but also covalently cross-linked, as the temperature stability of the derived gels proves. By the discrimination of the enantiomers of alanine it has been shown, that the chiral superstructure of gelatin is preserved in e^--gelatin/water gels and can be used for chiral discrimination even at elevated temperatures.

Furthermore the irradiation cross-linked e^--gelatin can be used as an alignment medium for DMSO as the sole solvent. By the discrimination of the prochiral methyl groups of DMSO-d_6 in stretched e^--gelatin/DMSO gels it has been shown, that chiral discrimination in general could be possible with this new alignment medium.

The results are of special interest since to the knowledge of the author chirality dependent alignment was neither reported for pure DMSO as the solvent, nor for water and DMSO at elevated temperatures and therefore e^--gelatin potentially opens the field to a variety of polar chiral molecules. Future research will need to show to which extent more complex enantiomers can be differentiated in stretched gels of e^--gelatin.

This project was done in cooperation with M.Sc. Marelli Udaya Kiran (Indian Institute of Chemical Technology, Hyderabad), who helped in preparing several samples and who acquired spectra used for Figures 3.19. A and 3.25. Irradiation of gelatin samples was done at *BetaGammaSystems* (Saal a.d. Donau, Germany).

Results presented in this chapter have been published:

Grit Kummerlöwe; Marelli Udaya Kiran; Burkhard Luy: '*Covalently Cross-Linked Gelatin Allows Chiral Distinction at Elevated Temperatures and in DMSO*' in *Chemistry - A European Journal* **2009**, *15*, 12192-12195.

3.5 Poly(ethylene oxide)

3.5.1 Introduction and Motivation

Although a multitude of alignment media exists which cover a broad range of solvents, the development of new alignment media probably won't stop. Frequently it happens, that a substance which is soluble in a particular solvent does not diffuse into a polymer gel swollen in that particular solvent, thus an alternative medium is necessary. Furthermore, it has been shown that signal overlap with signals originating from the alignment medium might be a problem, but not all alignment media can easily be deuterated. So it might be of help to have an alternative alignment medium in which signals do not overlap. Moreover, for some less frequently used solvents there is still no alignment medium available, but might be desired for special applications. Therefore, the development of new alignment media with different properties seems to be highly useful.

A very good candidate for a polymer to be used as alignment medium is poly(ethylene oxide) (PEO). Promising characteristics of PEO are the fact, that it shows only one single NMR signal, its good solubility in water, chloroform and acetonitrile, and that it is a relatively cheap polymer, available in many different chain lengths.

The aim of this project was therefore, to cross-link PEO, preferably by irradiation as this does not introduce additional signals, and to prepare gels of cross-linked PEO which can be used as an alignment medium. Solvent range, applicability to different solutes and general properties of PEO gels should be investigated.

3.5.2 Cross-Linking of PEO by Irradiation

The advantages of cross-linking a polymer by irradiation, like the homogeneous distribution of cross-links, the easy and arbitrary dosage of the amount of cross-linking and the fact that no additional signals of any chemical cross-linker will be present, make this approach the favorite way to modify a polymer in order to use it as an alignment medium. The cross-linking of polymers by irradiation is long

known,[167] and recently good experiences with irradiation by accelerated electrons for the production of alignment media have been made (see chapters 3.1, 3.3, and 3.4 and reference [67]).

However, for cross-linking by irradiation the polymer has to be in an amorphous state, as no cross-linking between crystallites will occur.[168-170] Thus, in a solid polymer with high crystallinity irradiation won't form a homogeneous network which can swell to a stable gel. For PDMS cross-linked by irradiation[67] this is no problem, as the pure linear polymer is an amorphous paste. For PAN and gelatin, best results with cross-linking by irradiation have been achieved, when the polymers were either dissolved, thus irradiated in solution or gel form, or when the polymer was precipitated or dried out of its solution, thus probably containing some residual solvent molecules (see chapters 3.1.2 and 3.4.2). Obviously in the latter form the content of crystallites is small enough to allow the desired cross-linking.

PEO, in contrast, turned out to be a problematic polymer, because it has a very high crystallinity when the chain length exceeds a certain size. PEO with low molecular weight (e.g. 400 g/mol) is a liquid or paste, but for PEO with higher molecular weight (larger than 1000 g/mol) the crystals dominate its characteristics. Therefore different more or less successful attempts have been made to cross-link PEO with accelerated electrons, as summarized in the following.

Irradiation with Accelerated Electrons

As the cross-linking of PEO in aqueous solutions upon irradiation with an electron beam has been reported already,[189] and as cross-linking in solution was successfully applied also for PAN (chapter 3.1) and gelatin (chapter 3.4), this was tried first.

Different solutions of PEO have been irradiated with accelerated electrons using irradiation doses from 10 to 480 kGy. Therefore, PEO of 35000 g/mol has been dissolved in water, chloroform, dichloromethane, acetonitrile, TFE, dioxane, DMF, DMSO and methanol up to the limit of solubility (see Appendix for maximum concentrations estimated in the different solvents) and with different concentrations beneath this maximum concentration.

None of the solutions could be successfully cross-linked to an homogeneous gel. Either large amounts of bubbles of the released hydrogen formed, transforming the

solutions in foam but not in gels, or the solutions were not cross-linked but degraded. The latter was the case for DMF, DMSO, methanol and the halogenated solvents, probably as very reactive radicals are formed which cause extensive chain scission. The former was the case for water, TFE, dioxane and acetonitrile as the solvents.

The formation of large amounts of hydrogen upon irradiation is not surprising, if one regards, that for every formed cross-link one hydrogen molecule is released.[167] Some solvents, like e.g. water, might even form additional gas upon irradiation, however, this cannot be prevented. Upon cross-linking of the PEO, which for sure happened in these irradiated solutions, this gas could not escape from the building network and thus formed bubbles. This foam-building was observed for total irradiation doses of 120 to 200 kGy or more, as this seems to be the point were the network becomes stable enough. With less irradiation bubbles could escape, however, the polymer was not sufficiently cross-linked to be used as an alignment medium. This is probably the difference to literature reported hydrogels of PEO (with total irradiation doses of maximal 150 kGy)[189] which were used for other purposes and therefore did not need to be as form-stable as it is necessary to resist the strain induced upon stretching (which is elementary for an alignment medium, as only with stretching the gel matrix becomes anisotropic). Obviously, with increasing stability of the gel, the formation of bubbles increases as the gas can not escape any more.

This formation of bubbles is no problem in a solid polymer. Therefore attempts have been made to form sticks of PEO, with as few as possible crystallites in it. Additives like softener or other auxiliaries as they are used in plastics engineering, were not used, in order not to contaminate the polymer with substances causing additional signals in the NMR spectrum.

It was tried to break crystallization of PEO by mixing polymers with different chain length. Therefore mixtures of PEO with 400, 1000, 4000, 8000 and 35000 g/mol in different ratios and combinations have been made by melting the polymers and mixing them at about 70°C, before filling the mixtures in Teflon® tubes for irradiation. None of the tested mixtures formed homogeneous sticks which could be swollen to gels after irradiation.

Furthermore it was tried to irradiate melts of PEO and also melted mixtures of PEO with different chain lengths. The idea behind this approach was, that in the melt there are no crystallites and no solvent can cause additional gas formation upon

irradiation. However, hydrogen formation upon cross-linking was sufficient to produce a high amount of bubbles in those samples.

Probably the most successful way to cross-link PEO by irradiation with accelerated electrons, was found by combining the previous ideas: irradiate a solid, as there gas can escape without the formation of bubbles and break the crystallinity by dissolving the polymer.

Therefore PEO was dissolved in water at a concentration where the solution does not change its volume upon freezing (this concentration was estimated to be 0.65 g/mL). The solution has been filled in Teflon® tubes and was then quick-frozen with liquid nitrogen. During irradiation these samples were kept cool on dry ice. However, when unfreezing the irradiated samples, bubbles produced a foam instantaneously, as obviously a lot of gas was trapped but could not escape. Therefore those frozen and irradiated PEO/water mixtures were kept at -20°C to give the gas time to escape out of the solid. And indeed, after about 1 year storage the samples could be defrosted without bubble formation.

By drying the obtained gels at room temperature, first sticks of cross-linked PEO could be obtained, which can be used as alignment medium after re-swelling in an appropriate solvent (see chapter 3.5.3).

However, producing cross-linked sticks of PEO with a procedure lasting one year is not very handy. Therefore the search for alternative production ways continued.

γ-Irradiation

Besides the formation of hydrogels upon irradiation with electrons,[189] it is also described in literature to produce such gels out of aqueous PEO solutions by irradiation with γ-rays.[190] However, also in this case, total irradiation doses do not exceed 100 kGy, which is obviously not a problem for their use as drug-delivering biocompatible membranes.[190]

It was nevertheless tried to use γ-rays to cross-link PEO sufficiently enough to use it as an alignment medium. An advantage compared to the irradiation with electrons, is the fact, that with the γ-ray source used (a ^{60}Co source of the radiochemistry

department) the irradiation rate could be significantly reduced. The idea was, that with a smaller rate but therefore longer irradiation times, the forming hydrogen would have more time to escape before the network starts to get too stable. Samples of PEO in water were therefore irradiated with small rates of γ-rays for 5 days, which resulted in total irradiation doses of 100 to 300 kGy. This was done for different concentrations of PEO (30 to 50% (w/v)), different chain lengths (4000, 8000, 35000, 1 Mio g/mol) and in different tubes (glass, Teflon®, PE tubes).

As a result, hydrogels of PEO with different mesh-sizes were obtained which could be used as aligning media after drying and re-swelling. However, more then 50% of all irradiated samples were not usable because of intense bubble-formation. No significant correlation of bubble-formation with the concentration or the irradiation rate could be observed. Although it seemed that treatment of PEO solutions with ultrasound prior to irradiation improved the situation, the formation of bubbles seemed to be somewhat randomly.

In summary, it was successful to obtain cross-linked PEO sticks by irradiation either with electrons (using frozen water solutions) or γ-rays (using low irradiation rates compensated by very long irradiation times). As will be described in the following, those sticks can be used as alignment media for a variety of different molecules. However, the reliable and reproducible way to obtain PEO sticks on a larger scale, with reasonable yields and worthwhile efforts is still not found.

Therefore a broad characterization of this new alignment medium was not possible so far and only preliminary results will be presented in the following.

3.5.3 Solvent-Range of Cross-Linked PEO

Dry sticks of cross-linked PEO have been placed in a variety of different solvents and solvent mixtures. Although linear PEO is very well soluble in water, TFE, chloroform, dichloromethane and acetonitrile, its solubility in solvents like DMSO, DMF, methanol, dioxane and THF is rather poor (for estimated solubility of linear PEO see Appendix). Therefore it was surprising how strong cross-linked PEO is swelling on almost every tested solvent (see Figure 3.26.).

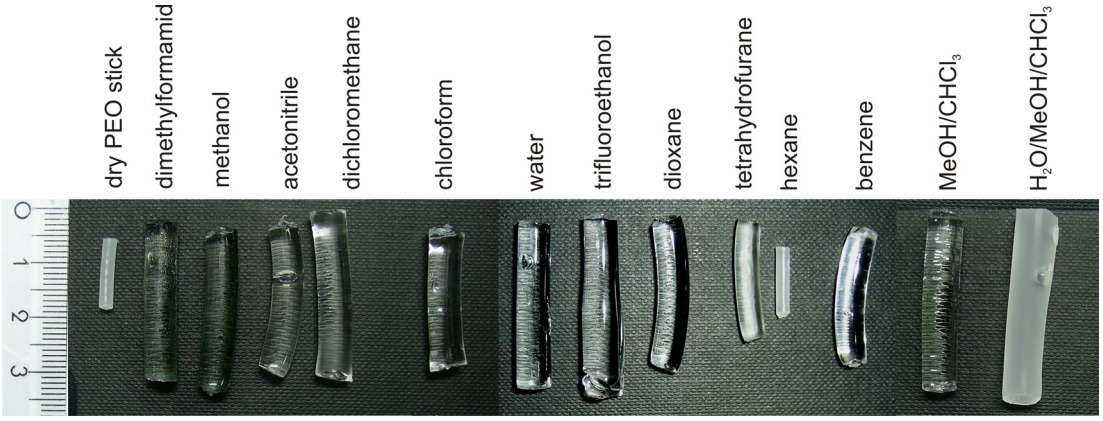

Figure 3.26.: Solvent applicability of cross-linked PEO. A dry stick of cross-linked PEO (left) is shown in comparison with identical sticks after being kept for 48 h in the solvent stated above. Accept for hexane, PEO swells in all tested solvents (also in DMSO, although not shown here) to gels with at least twice its original size.

The only solvent tested, which seems to be not compatible with cross-linked PEO is hexane. Beside that, the solvent range of PEO gels is as wide as for no other known alignment medium, ranging from apolar solvents like benzene or chloroform to polar solvents like methanol or DMSO and water. Among the solvents compatible with cross-linked PEO are also rarely used solvents like e.g. trifluoroethanol (TFE) for which no alignment media existed so far. Due to its wide solvent range, also mixtures of different solvents might be used for gels of cross-linked PEO.

3.5.4 Spectral Properties of PEO Gels

One advantage of poly(ethylene oxide) over other polymers, like e.g. PAN, is the fact that it possesses only one proton and carbon NMR signal originating from both methylene groups of each monomeric repeating unit. Therefore spectral overlap with solute signals is less probable. As can be seen from spectra shown in Figure 3.27., this signal appears at ≈ 3.8 ppm in the ^{1}H and ≈ 70 ppm in the ^{13}C dimension, respectively.

As can be seen in the ^{1}H-1D spectrum (see Figure 3.27. A), this signal is relatively sharp, which on the one hand reduces overlap, on the other hand it suggests that it might be hard to suppress this signal with relaxation methods.

In Figure 3.27. B and C the CLIP-HSQC spectra[107] for sucrose in a PEO/D_2O gel and for norcamphor in a PEO/$CDCl_3$ gel are shown, demonstrating that sugars and small organic compounds are compatible with the polymer. However, in Figure 3.27. B one can see, that PEO might be not the best choice for sugars, as its signal overlaps with one signal of the glucose ring of sucrose.

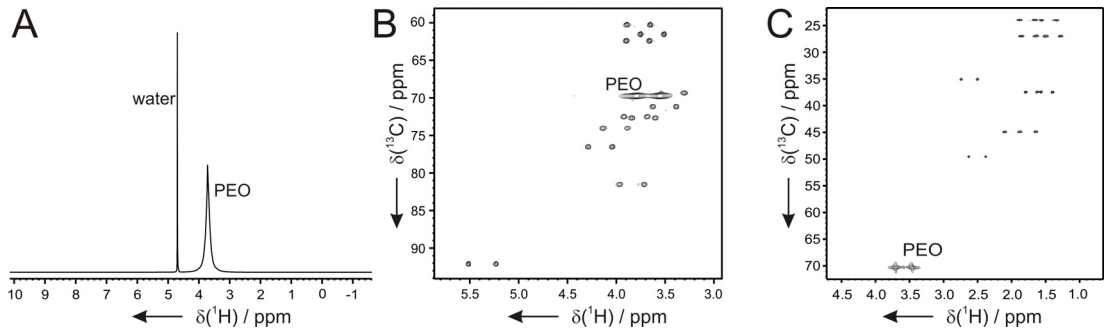

Figure 3.27.: Spectral properties of PEO gels. In (A) the 1D-^{1}H-spectrum of a PEO/D_2O gel is shown, demonstrating the relative sharp line of the polymer signal. The CLIP-HSQC spectrum[107] of sucrose in a PEO/D_2O gel is shown in (B) and the CLIP-HSQC spectrum[107] of norcamphor in a PEO/$CDCl_3$ gel in (C).

Not only test substances like sucrose, norcamphor, hydroquinidine or menthol with a rather high concentration have been aligned in PEO gels. A "real live example" is shown in Figure 3.28. For the structural investigation of the cyclic peptide Cilengitide[191, 192] RDCs have been measured in PEO/water, PEO/methanol and PEO/DMSO gels. The 1D proton and deuterium spectra of the latter one are shown in Figure 3.28. A. Clearly, the huge polymer signal dominates the spectrum acquired on a sample of ≈ 10 mg Cilengitide in a PEO/DMSO gel. However, in the CLIP-HSQCs spectrum acquired on that sample no overlap of peptide signals with the PEO signal affected RDC extraction.

Besides the cyclic peptide Cilengitide, which was aligned in different PEO gels, also linear peptides are compatible with PEO, like e.g. the transmembrane helix dimer c65, which has been aligned in a PEO/D_2O/TFE gel.[193]

Figure 3.29. shows an application of PEO for the solvent acetonitrile. For RDC analysis a substituted [2.2]-paracyclophane has been aligned in a PEO/MeCN gel.

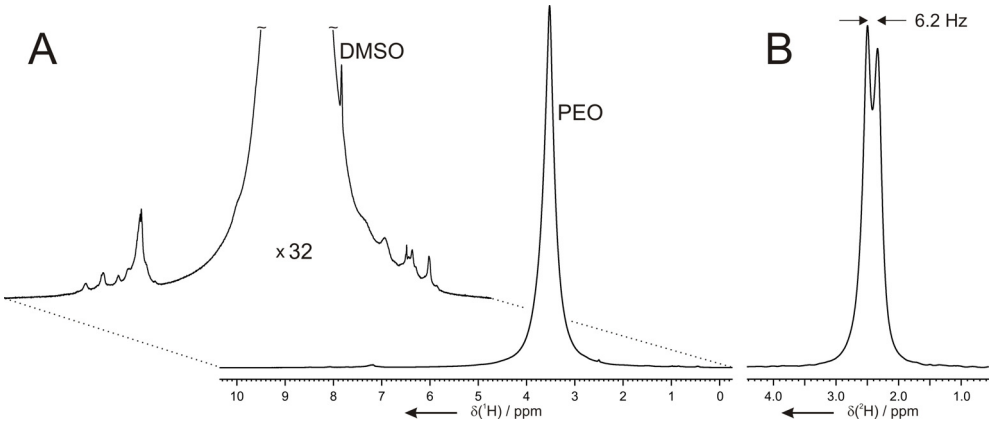

Figure 3.28.: 1D spectra acquired on a stretched PEO/DMSO gel with ≈ 10 mg Cilengitide. The proton spectrum (A) is dominated by the polymer signal and only in the enlargement the weak signals of the low concentrated peptide are visible. However, RDC extraction out of 2D spectra was not affected by signal overlap with the polymer. In the deuterium spectrum (B) the quadrupolar splitting of the solvent DMSO is shown.

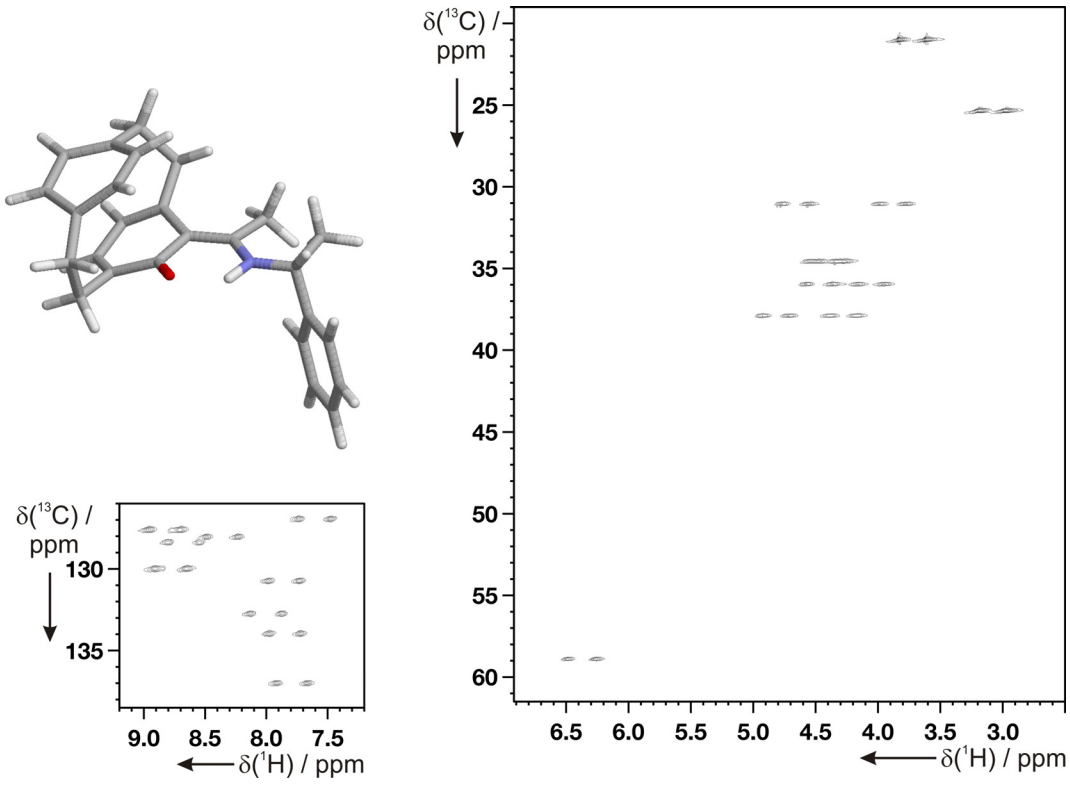

Figure 3.29.: Application for a PEO/MeCN gel. The substituted [2.2]-paracyclophane depicted to the left, was aligned in a PEO/MeCN gel to measure RDCs. Shown are CLIP-HSQC spectra[107] of the aliphatic (right) and aromatic region (left).

3.5.5 Conclusion

It has been shown, that cross-linked poly(ethylene oxide) is suitable as an alignment medium for a very broad range of solvents, including water, polar organic solvents like DMSO, DMF and methanol, and apolar organic solvents like chloroform, dichloromethane and benzene. For TFE, a helix stabilizing solvent which is often used for structural investigations of helices, the cross-linked PEO is the first suitable alignment medium. Furthermore it seems to be applicable for mixtures of different solvents, which is desirable for special applications, but not reported for any alignment medium so far. Also the range of solutes compatible with PEO seems to be very wide: sugars, small organic molecules, linear and cyclic peptides, proteins and even DNA diffused into the gels of PEO.

However, the preparation of cross-linked PEO sticks is not trivial. So far, no easy and effective method for a reproducible cross-linking of PEO by irradiation has been found. Many attempts have been made, but further improvements will be necessary for the preparation on a larger scale.

Furthermore, the gels will have to be characterized in more detail. Mesh sizes and the degree of induced anisotropy in dependence on concentrations, chain lengths and irradiation doses need to be investigated before PEO can be widely used.

This project was done in cooperation with M.Sc. Felix Halbach (TUM, Munich), who helped in preparing PEO samples for γ-irradiation and made experiments concerning swelling properties in different solvents. γ-irradiation was done in cooperation with Wolfgang Stöwer and Dr. Christoph Lierse von Gostomski from *Chair for Radiochemistry* (TUM, Munich). Irradiation of the polymer samples with accelerated electrons was done at *BetaGammaSystems* (Saal a.d. Donau, Germany).

Results presented in this chapter have not yet been published.

4 New Ways of Scaling the Alignment

As has been discussed in chapter 2.4, it is of high importance to adjust the degree of alignment to the right strength in order to measure anisotropic parameters with high accuracy. Besides the preparation of a new sample which possesses a different alignment strength due to e.g. a different chain-length or a different amount of cross-linking, more sophisticated ways are desirable, which can change the degree of alignment in a single sample. This is not only less time and sample consuming than preparing a new sample. Furthermore, it also allows the measurement of anisotropic parameters under different alignment strengths but with otherwise similar conditions, which for some applications might be very useful.

In the next chapters the development of two different stretching devices, which allow the scaling of alignment in a single sample, will be discussed. Furthermore it will be outlined in how far this can be applied for a more precise measurement of RDCs.

4.1 Stretching Device for Polar Solvents

4.1.1 Introduction and Motivation

As has been shown recently by the group of Kuchel, a stretching device based on a flexible silicone rubber tube provides an easy, rapid, and reversible variation of alignment strength. Within this stretching apparatus conventional gelatin was arbitrarily stretched and thereby the degree of alignment varied.[99]

The goal of this project was to redesign the apparatus introduced by Kuchel et al. for the use in standard 5 mm NMR probe heads, as the initial device by Kuchel was limited to 10 mm NMR equipment.[99] Furthermore the applicability of the approach for other gel-based alignment media, besides the conventional gelatin as Kuchel et al. used in their apparatus, should be tested. Therefore different polymer-based alignment media with water and DMSO as solvents have been studied.

4.1.2 Design of the Stretching Apparatus

Following the fundamental principles of Kuchel et al., the stretching apparatus was redesigned to fit into a standard 5 mm high resolution probe head as shown in Figure 4.1. Silicone tubing placed inside an open-cut 5 mm NMR-tube and fixed with a T-shaped Teflon® plug at the bottom, is used as an expandable container for the swollen gel with the solute molecule inside. When stretching the silicone tubing, the polymer gel is stretched as well, which in turn leads to partial alignment and measurable anisotropic NMR-parameters.

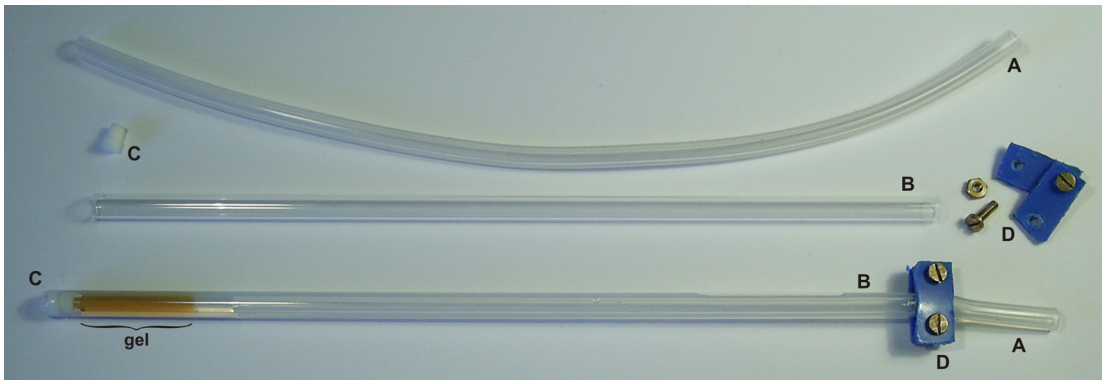

Figure 4.1.: Stretching apparatus redesigned for 5 mm standard high resolution NMR probe heads. The flexible silicone tube (A) is placed inside an open-cut 5 mm NMR tube (B) and fixed with a specially designed T-shaped Teflon® plug (C) at the bottom. Plastic clamp and brass screws (D) are used to fixate the stretched silicone tube at the top of the device. Inside the assembled apparatus a reddish-brown poly(acrylonitrile)/DMSO gel is ready to be stretched.

When setting up the apparatus, one has to take care in choosing the right silicone rubber tubing (see chapter 4.1.4). The experiments presented in this thesis, have been made with two different kinds of high quality silicone tubing: tubes of 4.0 mm outer and 3.0 mm inner diameter (purchased from J. Lindemann GmbH, Helmstedt, Germany) and tubes of 4.2 mm outer and 2.4 mm inner diameter (purchased from VWR International GmbH, Darmstadt, Germany). Depending on the tube diameters, the diameters of the Teflon® plug used for fixation at the bottom of the device have to be adjusted to ensure a reliable mounting of the silicone.

4.1.3 Principle of Gel-Stretching within the Stretching Apparatus

Upon stretching of the silicone tube by pulling on its upper end, a gel inside the silicone tube will be mechanically stretched and anisotropic NMR parameters can be observed. As the alignment strength of a molecule depends on the degree of anisotropy of the aligning matrix, the size of measurable anisotropic parameters can be varied by the amount of mechanical stretching of the polymer gel. Within the stretching device this amount of mechanical stretching can very easily be varied by the degree of pulling the silicone tube. As this is only limited by the force applied for pulling (until the point the tube breaks) this scaling is arbitrarily and as the pulling force can be reduced again, resulting in less stretching of the tube and the gel inside, it is also reversible.

As the degree of stretching the gel in the apparatus is crucial for the alignment strength, Kuchel et al. defined the so-called "extension factor",[100] which will be named Ξ in the following. It is calculated from the length of the stretched and the unstretched gel according to equation 4.1.:

$$\Xi = \frac{length\ of\ stretched\ gel}{length\ of\ unstretched\ gel} - 1 \qquad (4.1.).$$

Therefore the extension factor Ξ will be zero for the unstretched state and e.g. 1 for stretching the gel to double its original length. As an example of stretching gels with the stretching apparatus, a PAN/DMSO gel at various extensions is shown in Figure 4.2.

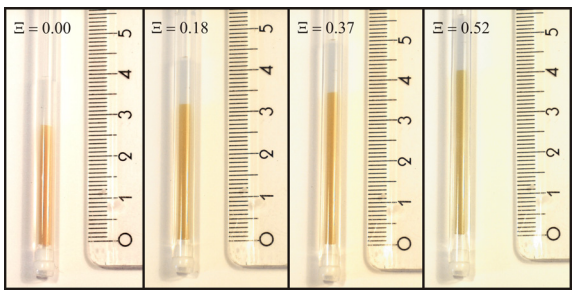

Figure 4.2.: Bottom part of a stretching apparatus with a PAN/DMSO gel at various extensions.

In the original publications by Kuchel et al. a linear relationship between the extension factor and anisotropic parameters in the gel is proposed.[99] Although it

sounds intuitive, that half the stretching will result in half the measurable quadrupolar or dipolar couplings, there is no conclusive theory explaining a linearity. However, for the range of extension factors which can be achieved with the stretching device, the quadrupolar splittings measured for the solvents of gels stretched within the device, are linear to the extension factor with a very good approximation. As an example, the quadrupolar splittings of two e^--gelatin gels at various stages of stretching within the stretching apparatus are plotted against the corresponding extension factors of the gels (see Figure 4.3.). The observed behavior is about linear as also observed for all other gels measured in the stretching device (data not shown).

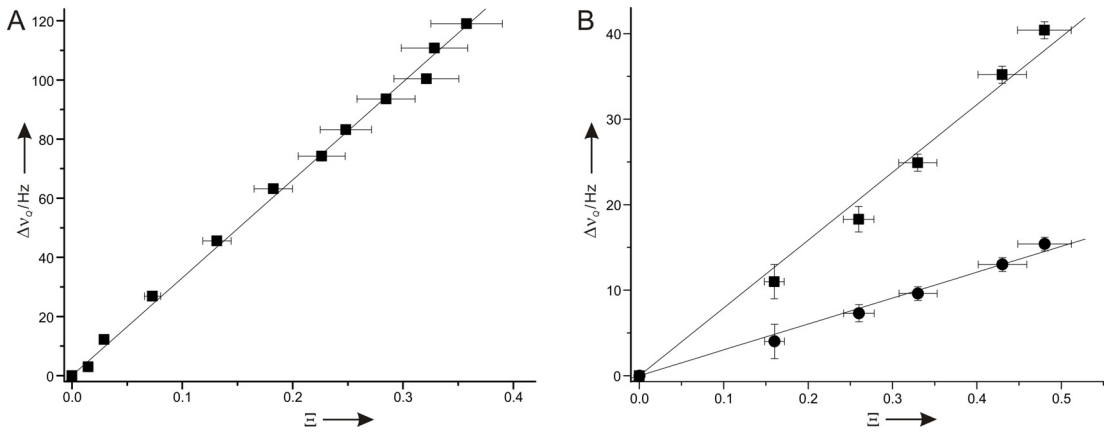

Figure 4.3.: Scaling of the alignment strength with the stretching apparatus. Quadrupolar splittings $\Delta\nu_Q$ of the solvent at 298 K as a function of the extension factor of the gel for an e^--gelatin/D_2O gel (A) and an e^--gelatin/DMSO-d_6 gel (B). As observed for other gels, the splitting varies approximately linearly in the monitored range of extension.

With the introduced stretching device it is generally only possible to stretch gels but not to compress them, which would also lead to an anisotropy of the gel matrix and therefore to measurable anisotropic NMR parameters. An exception of this is conventional gelatin as it is only cross-linked via hydrogen bonds and can therefore be recasted inside the rubber tube by a simple heating and recooling cycle. For this purpose a gelatin gel is stretched to full extension and heated to about 50°C so that all hydrogen bonds melt. Then the gel is cooled down so that the hot gelatin solution forms a gel again, which is fully isotropic and hence no anisotropic parameters can be observed. By releasing the stretching of the silicone tube the gelatin gets compressed and therefore anisotropic parameters can be observed (see Figure 4.5. in chapter 4.1.5). The extension factor for gelatin gels compressed in this way gets negative according to equation 4.1.

4.1.4 Applicability and Limitations of the Stretching Apparatus

Solvents

In order to test how far the apparatus is applicable to conventional polymer gels, several samples were prepared containing different polymers with gel diameters adjusted to accommodate for the dimensions of the silicone tube within the stretching device. Next to the conventional gelatin as used by Kuchel et al.,[76, 99, 100] the stretching apparatus is also applicable to other water-based gels like PAA/D_2O, PEO/D_2O and e^--gelatin/D_2O and to DMSO based gels like PAN/DMSO and e^--gelatin/DMSO. Some examples of polymer gels within the stretching device are shown in Figure 4.4.

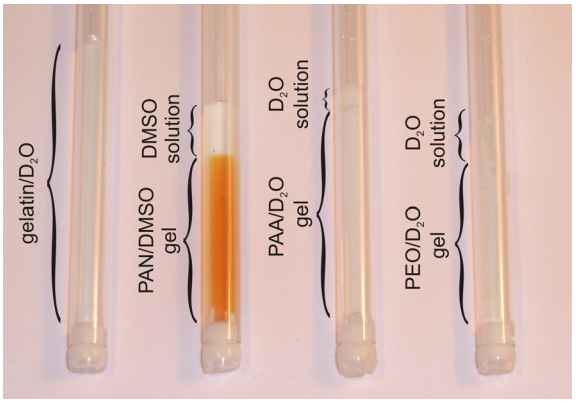

Figure 4.4.: Various gels used to measure anisotropic parameters with the stretching apparatus. From left to right: gelatin/D_2O, PAN/DMSO, PAA/D_2O, and PEO/D_2O.

All prepared samples could easily be stretched by the silicone-based stretching device with very good long-term stability of the hydrogels. The PAN/DMSO samples were stable for several weeks and measurements of desired couplings could easily be achieved. However, after about one month the gels suddenly started to shrink to their original, dry size. As it is known that water leads to a precipitation of PAN/DMSO gels (see chapter 3.1.2), it was tested in how far the humidity of air would be sufficient to let a PAN/DMSO gel shrink. Therefore a PAN/DMSO gel covered with dry DMSO was kept in an open vial with access to air. Within a few weeks the gel started to shrink as the critical amount of water was reached because of the humidity of the air and the well-known hygroscopic character of DMSO. This experiment leads to the interpretation that the stretching device allows water in the form of humidity to diffuse slowly via the silicone rubber tubing into the gel and causes the observed gel shrinking.

Since silicone rubber swells in most apolar organic solvents (silicone, also named PDMS, is used for gel preparation with those solvents[67]), it cannot be used inside the stretching apparatus for solvents like chloroform, benzene, or dichloromethane. Tubing made out of fluorinated elastomer materials as e.g. Viton® or Kalrez® solve this issue of solvent compatibility, as will be described in chapter 4.2. However, silicone rubber tubing appears to be compatible with practically all aqueous gels and also allows measurements using highly polar organic solvent-based gels like PAN/DMSO, although the silicone tubing, especially in the stretched state, seems to allow water to diffuse inside the sample. This implies limitations when a sample has to be free of water.

Shimming

For high quality spectra a good homogeneity of the magnetic field within the sample must be achieved as inhomogeneity results in broad lines. Concerning the complex assembly of the stretching device with glass tube, silicone tube and gel, the shimming of such samples might be problematic. In this respect, special care must be taken for the silicone tube used, as some silicone tubing has non-concentric holes and very rough surfaces which significantly reduce shimming capabilities. Furthermore tubing was found with paramagnetic filling material that resulted in spectra with line widths of 40 Hz and broader, which of cause should be avoided.

With the high quality silicone tubing used in the experiments shown here, it is generally possible to obtain line widths of about 2 Hz which improve even further for stronger extension of the tubes, as the active volume decreases and the sample in the center of the B_0-field is more easily shimmed.

Sample volume

The downside of the stretching apparatus designed for 5 mm NMR-tubes is, of course, decreased sample volume. Since the silicone rubber tube is placed inside the conventional glass tube, the active sample volume is considerably reduced. This is even more the case when the rubber tube is stretched in order to be able to measure anisotropic parameters like RDCs. Compared to a conventional gel sample made of a polymer stick swollen inside a standard 5 mm NMR tube, the sensitivity decreases approximately by a factor of 2 to 5, depending on the used silicone tube and the degree of stretching. For samples limited on the amount of available substance this is

usually not a big problem as one can simply increase the concentration in the smaller volume, however, for samples limited by the solubility of substance the decreased sample volume might be a considerable disadvantage of the method.

4.1.5 Linear Scaling of Anisotropic Parameters

As discussed in chapter 4.1.3, quadrupolar splittings measured within gels stretched with the stretching apparatus increase about linear with the extension of the stretched gels. To investigate how other anisotropic parameters behave, samples of sucrose as a test molecule dissolved in different gels have been prepared: 1.) conventional gelatin in D_2O, 2.) PAA/D_2O and 3.) PAN/DMSO (for details see Appendix). On sucrose heteronuclear $^{1}H,^{13}C$ one-bond couplings that contain the most easily accessible RDCs have been measured using the so-called CLIP-HSQC[107] pulse sequence. For each gel CLIP-HSQC and deuterium 1D spectra at different degrees of stretching (and in the case of gelatin also different degrees of compression) have been measured.

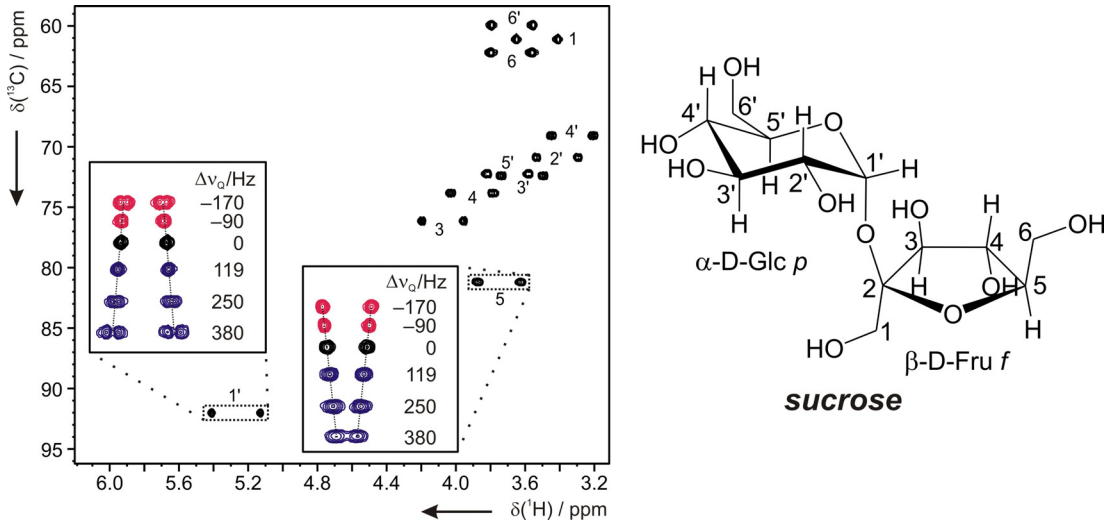

Figure 4.5.: CLIP-HSQC[107] of sucrose in 40% gelatin. The black spectrum corresponds to the isotropic stage (non-stretched). Peaks 1 to 6 belong to the fructose ring, while 1' to 6' belong to the glucose ring of sucrose as named within the structure shown to the right. Insets show two signals (C1'-H1' and C5-H5) of various stages of stretching (blue) and compression (red). Peaks are separated in the vertical direction according to the corresponding quadrupolar splitting $\Delta\nu_Q$ of the solvent D_2O. The linear dependence between observed $^{1}T_{CH}$-couplings and the quadrupolar splittings is evident.

The resulting CLIP-HSQC[107] of sucrose in unstretched gelatin at 293 K is shown in Figure 4.5. as an example. While the methylene moieties show identical proton chemical shifts and do not allow reliable coupling extraction, all methine

heteronuclear one-bond couplings can be measured from non-overlapping signals. For two signals corresponding to H1'-C1' of the glucose ring and H5-C5 of the fructose ring, the cross peaks are also shown in the insets of Figure 4.5. at various stages of stretching of the silicone tubing. Cross peaks drawn in blue indicate stretched gelatin, while red cross peaks mark spectra measured in compressed gelatin. Gel compression was achieved by heating the fully stretched gelatin sample to 50°C and subsequently releasing the recooled silicone tubing. As expected, the compressed gel shows anisotropic parameters with opposite sign compared to the stretched gel. Note that the sign of quadrupolar splittings can not be extracted from conventional deuterium 1D spectra (see chapter 2.1.2) and were set arbitrarily to positive for stretched gelatin and negative for compressed gelatin.

The extracted one-bond heteronuclear couplings $^1T_{CH} = {}^1J_{CH} + D_{CH}$ are shown in Figure 4.6. A. Clearly, the linear relations of the measured D_{CH} couplings with respect to the extension factor Ξ and the quadrupolar splitting of the solvent $\Delta\nu_Q$ are evident.

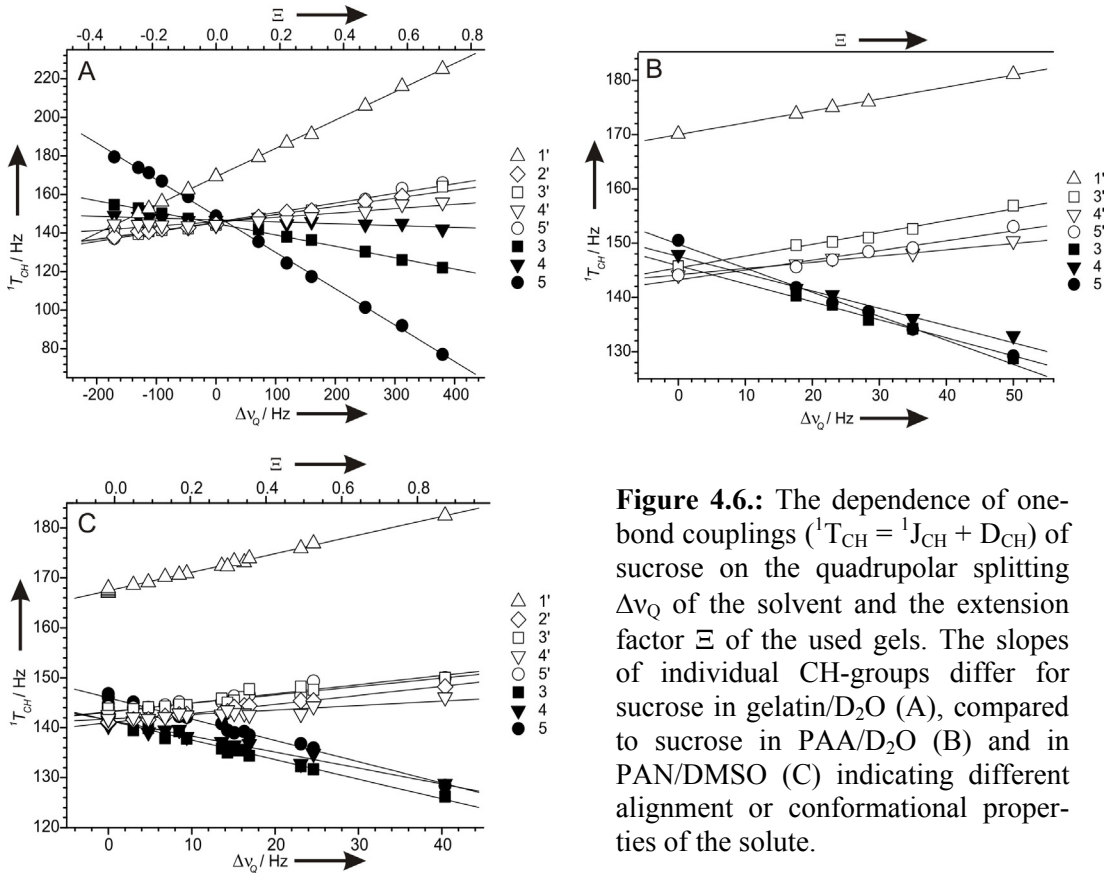

Figure 4.6.: The dependence of one-bond couplings ($^1T_{CH} = {}^1J_{CH} + D_{CH}$) of sucrose on the quadrupolar splitting $\Delta\nu_Q$ of the solvent and the extension factor Ξ of the used gels. The slopes of individual CH-groups differ for sucrose in gelatin/D_2O (A), compared to sucrose in PAA/D_2O (B) and in PAN/DMSO (C) indicating different alignment or conformational properties of the solute.

Analog plots of the measured heteronuclear couplings of sucrose in PAA/D_2O and PAN/DMSO are shown in Figures 4.6. B and C, respectively. Since those gels are

covalently cross-linked, heating up the gel will not change its shape and only measurements of the stretched gel are possible. Interestingly, the slopes of individual methine groups are different for PAA and PAN as compared to gelatin, indicating different resulting alignment tensors for the different alignment media.

4.1.6 Improving the Precision of RDC-Measurements

The $^{1}T_{CH}$ coupling constants as shown in Figure 4.6. were extracted by selecting a slice of the CLIP-HSQC at the appropriate carbon frequency and manually shifting a copy of the slice until the corresponding multiplet components were centered with respect to each other (see chapter 2.5.3; Figure 2.13.). Although the signal to noise ratio of the sucrose spectra seems to be sufficient for a highly accurate coupling measurement, extracted couplings deviate up to 2.6 Hz from the linear fit. For most deviations, the choice of ^{13}C-frequency for the slice and the variation of line shapes within the multiplets (due to spectral artifacts or second order contributions) seem to be responsible for the differences in individual coupling extractions.

However, due to the linear relationship of RDCs with the quadrupolar splitting of the solvent, a linear fit through couplings measured at different degrees of stretching leads to a slope that can be extracted with a significantly higher precision than it would be possible from individual experiments (for details see Appendix). This slope is directly proportional to the RDCs and represents a parameter that is independent of a specific alignment strength. In this way the stretching device can be used to extract residual dipolar couplings or other anisotropic parameters with much higher accuracy.

As a second test molecule for the linear scaling of anisotropic parameters and the resulting improvement of RDC measurements, a small cyclic peptide *cyclo*(Arg–Nal–Ala–Gly–D-Tyr–Arg) (Nal = 2-Naphthylalanine) was used. The peptide is soluble in DMSO and was therefore measured in a sample with a PAN/DMSO-d_6 gel (for details see Appendix). Like for sucrose, several CLIP-HSQC spectra[107] at different stages of stretching were acquired and corresponding $^{1}T_{CH}$ coupling constants for all methine and methyl groups were measured (see Figure 4.7.). Also in this case the linear relationship between the heteronuclear one-bond couplings of the peptide and the quadrupolar splitting of the solvent DMSO is

obvious and a corresponding linear fit can be used for a precise measurement of RDCs (for details and assignment of the peptide see Appendix).

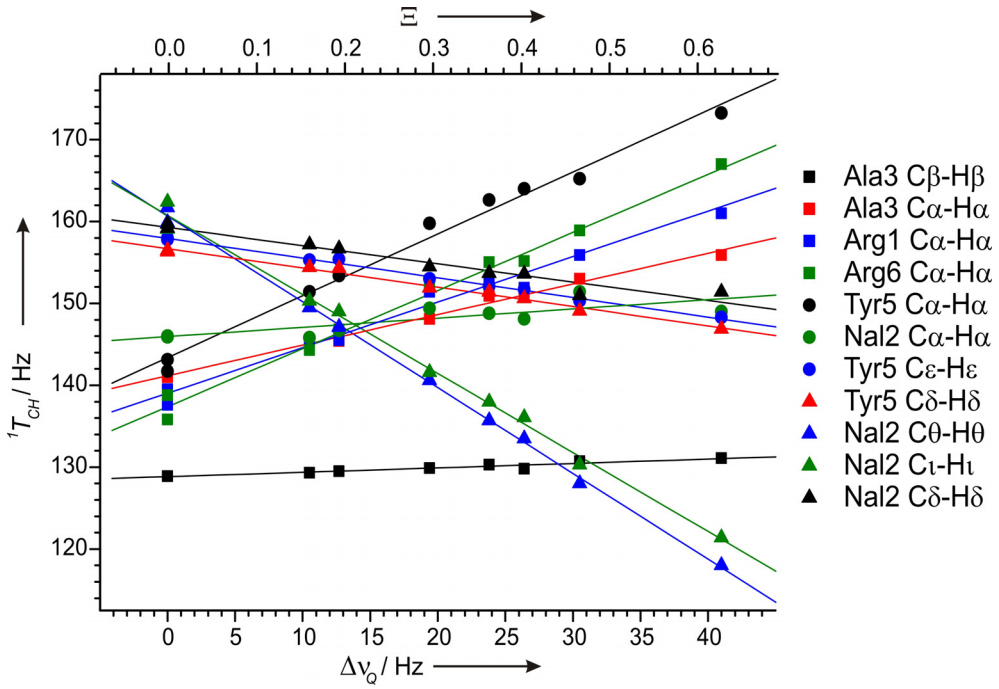

Figure 4.7.: One-bond $^1T_{CH}$-couplings of methine and methyl groups of *cyclo*(Arg–Nal–Ala–Gly–D-Tyr–Arg) with respect to the quadrupolar splitting $\Delta\nu_Q$ of DMSO-d_6 (bottom axis) and the extension factor Ξ of the PAN gel (top axis).

4.1.7 Conclusion

Using the principle setup provided by Kuchel et al.,[99] it was demonstrated that a rubber-based stretching apparatus can be used to induce tunable alignment for a number of hydrogels and gels based on DMSO. $^1T_{CH}$ splittings can be measured for a number of different alignment strengths, allowing RDC-measurements of high precision from the slope of $^1T_{CH}$ couplings vs. the quadrupolar coupling $\Delta\nu_Q$ of the deuterated solvent.

The ease of scaling the alignment, the relatively good shimming properties of the apparatus and the full compatibility with standard 5 mm high resolution NMR equipment make the method widely applicable to the structure determination of all kinds of polar molecules, including e.g. most compounds of pharmaceutical interest and biomacromolecules. The extension of the approach to apolar solvents is desirable and will be discussed in the following chapter.

Some more advantages of using the stretching device have not yet been addressed here, but might be used in the future: RDCs and in particular the scaling of alignment might be used to vary overlap among signals of interest, which gives another tool to enhance the accuracy of the desired dipolar couplings. Furthermore the stretching device with its rapid and reversible scaling of alignment significantly improves the flexibility and accuracy of RDC measurements. For example, long-range $^{1}H,^{13}C$ and one-bond $^{13}C,^{13}C$ RDCs are approximately one order of magnitude smaller than corresponding heteronuclear $^{1}H,^{13}C$ one-bond couplings and their accurate measurement with conventional methods is a problem due to their small values. With the stretching apparatus it should be possible to tune the size of RDCs in such a way that optimal conditions for their measurement are obtained. In contrast to other procedures, like the scaling using variable angle sample spinning,[86, 87] standard liquid state NMR equipment with its superior B_0-homogeneity can be used.

Another often neglected issue is the fact that any kind of alignment medium, if based on liquid crystalline phases or stretched polymer gels, might influence the average conformation of a given solute molecule. When measuring couplings in isotropic solution and inside the alignment medium, conformational changes in the two different environments can potentially lead to erroneous RDCs. A tremendous advantage of the stretching apparatus is that couplings with varying alignments can be measured in the same sample using the presented approach. In this way errors resulting from separate preparations of isotropic and aligned samples can be excluded.

This project was done in cooperation with M.Sc. Felix Halbach (TUM, Munich), who prepared the PAA sample and acquired all spectra recorded on this sample. The cyclic peptide was synthesized by Dr. Burkhardt Laufer (TUM, Munich).

Results presented in this chapter have been published:

Grit Kummerlöwe; Felix Halbach; Burkhardt Laufer; Burkhard Luy: '*Precise Measurement of RDCs in Water and DMSO Based Gels Using a Silicone Rubber Tube for Tunable Stretching*' in *The Open Spectroscopy Journal* **2008**, *2*, 29-33.

4.2 Stretching Device for all Solvents

4.2.1 Introduction and Motivation

As has been discussed in the previous chapter, there are several advantages of a stretching device to arbitrarily stretch gel-based alignment media. Therefore it is desirable to widely apply this method. However, the stretching apparatus equipped with a silicone tube, as described so far, is limited to polar solvents like water and DMSO because it is incompatible with more apolar organic solvents like chloroform, dichloromethane, or tetrahydrofuran.

The aim of this project was to overcome this major limitation by the use of a tube material which is resistant enough to all common solvents but flexible enough to be used as an expandable tube. Furthermore, the tube material should not allow water and humidity to penetrate into the gel sample, as the silicone tube does, and it would be desirable that the tube material would have no additional NMR signals. As will be described in the following chapters, the perfluoroelastomer Kalrez® 8002 by DuPont Performance Elastomers is an ideal material for this purpose. The design of the stretching apparatus with this new tube material and its properties and applicability will be discussed.

4.2.2 Design of the Stretching Apparatus

Following the design of the stretching device equipped with a silicone tube (see chapter 4.1), the flexible perfluorinated elastomer tube is placed inside a cut-open 5 mm NMR-tube and fixed at the bottom (see Figure 4.8.). As with the original

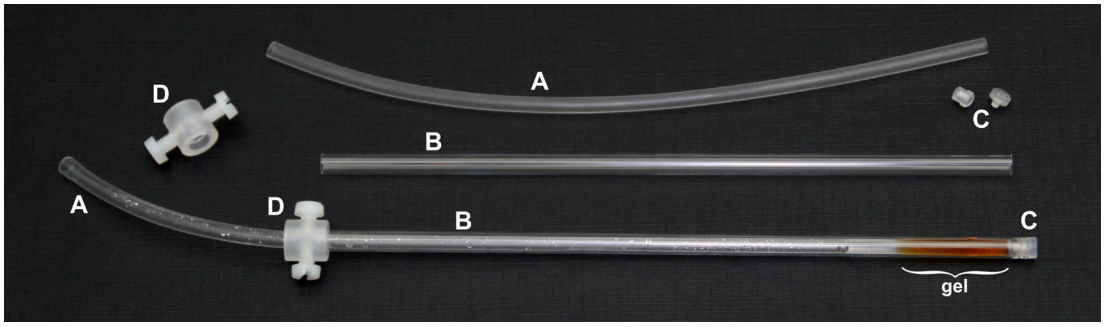

Figure 4.8.: The new stretching apparatus for 5 mm standard high resolution NMR probe heads. The flexible Kalrez® 8002UP tube (A) is placed inside a cut-open 5 mm NMR tube (B) and fixed with a specially designed PCTFE screw (C) at the bottom. A PCTFE device with nylon screws (D) is used to fix the stretched tube at the top. Inside the assembled apparatus a reddish-brown PAN/DMSO gel is ready to be stretched.

apparatus, the rubber tube works as an expandable container for the swollen gel with the solute molecule inside. Upon stretching of the flexible tube the polymer gel is stretched as well, which in turn leads to partial alignment of the solute and measurable anisotropic NMR-parameters.

Tubing

After testing a variety of different materials, the perfluoroelastomer Kalrez® 8002 was found to be the ideal material for the given task. It has a superior resistance against most chemicals (see technical information given by DuPont in the Appendix) and a high purity. For example, no detectable paramagnetic impurities are present as this is the case for most other similar materials like e.g. Viton®.

Kalrez® 8002UP perfluoroelastomer parts tubes with inner/outer diameters of 3.2/4.2 mm were specifically produced at DuPont Performance Elastomers for this project.

Fixation of the Rubber Tube at the Bottom

The simple T-shaped Teflon® plug, as used to fixate the silicone tubing at the bottom of the stretching device (see chapter 4.1.2) is not sufficient to fixate the perfluoroelastomer tube, because its smoother surface is not sticking at all to the glass walls of the cut-open NMR tube. Therefore, a variety of different plugs (e.g with barbed hooks) were tested, but the only reliable method for fixation was found in a specially designed screw clamp, which tightly holds the Kalrez® 8002UP tube. It is important to consider, that this bottom part of the apparatus must fit within the probe head of the spectrometer and therefore should not exceed 5 mm in diameter. The

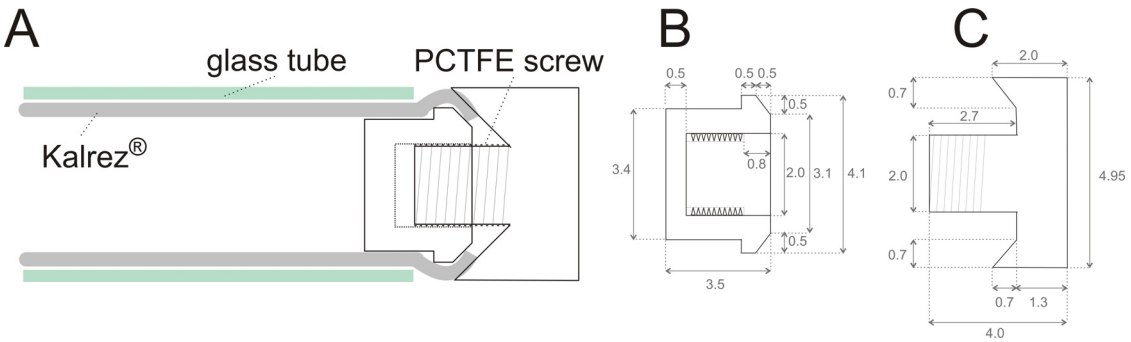

Figure 4.9.: Screw clamp for fixation of the flexible Kalrez® 8002UP tube at the bottom of the stretching device. The principle of holding the rubber tube tightly is shown in (A) and dimensions (in mm) of the two parts of the specially designed PCTFE screw are given in (B) and (C).

working principle and all dimensions of the designed screw are shown in Figure 4.9. Poly(chloro tetrafluoro ethylene) (PCTFE) was chosen as material for the screw because of its mechanical properties (hard enough and easy to process) and its chemical resistance.

Clamp for Holding the Stretched Tube

Although the very simple clamps initially used for fixating the stretched silicone tubes at the upper part of the stretching device (see chapter 4.1.2) would be also sufficient for the fixation of the Kalrez® 8002UP tube, a more sophisticated clamp made out of PCTFE and nylon screws, was designed. This new clamp is not only easier to handle (e.g. no screwdriver is necessary) but it is also more easy to fixate the upper part of the rubber tube in the middle of the cut-open NMR tube, which is essential for good shimming.

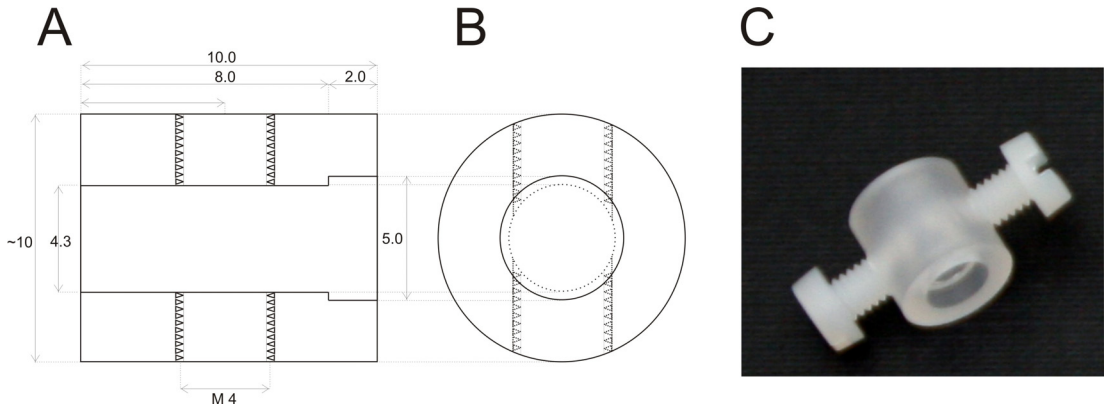

Figure 4.10.: Clamp with screws to fix the stretched Kalrez® 8002UP tube at the top of the stretching device. Blueprints of the clamp with dimensions (in mm) as seen from the side (A) and from top (B) and a photograph of the clamp together with the nylon screws (C) are shown.

4.2.3 Spectral Quality

As the new rubber tube material is a perfluorinated elastomer, no signals of the stretching device appear in proton-based spectra. Hence, the quality of NMR-spectra is substantially improved using the Kalrez® 8002UP tubing compared to identical spectra recorded with the silicone tubing. In Figure 4.11. the ^{1}H-1D-spectra of two identical gel samples with alanine in gelatin/D_2O stretched within a silicone tube and within a Kalrez® 8002UP tube are compared. While the silicone tubing shows an

intense, broad signal around 0.1 ppm, there is no additional signal from the Kalrez® 8002UP tubing, which not only leads to cleaner spectra, but also to an improved sensitivity as the receiver gain of the spectrometer can be increased.

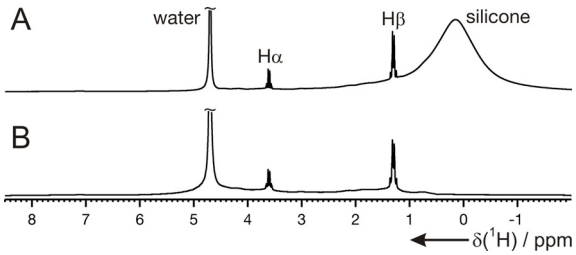

Figure 4.11.: Comparison of ^{1}H-1D spectra acquired in a stretching device equipped with silicone tubing (A) and Kalrez® 8002UP tubing (B) containing identical samples of 1M alanine (L-Ala/D-Ala in 2:1 ratio) in 50% gelatin in D_2O (w/v). In the case of the silicone tube a broad signal around 0.1 ppm dominates (A), while the Kalrez® 8002UP tube does not contribute to the spectrum (B). Additional low-intensity background contributions originate from the alignment medium gelatin.

4.2.4 Applicable Solvent Range

Although the material is not fully inert against halogenated hydrocarbons (according to information given by DuPont), the tubing can be used with all common NMR solvents, including chloroform and dichloromethane. This is in contrast to the originally used silicone tubing (see chapter 4.1) as can nicely be seen in Figure 4.12.

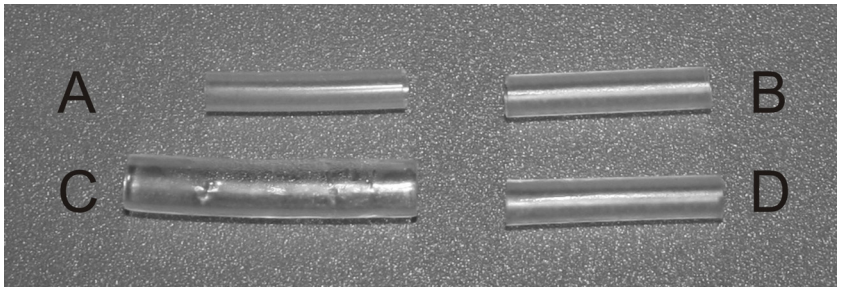

Figure 4.12.: Compatibility of different tubes for halogenated solvents. Short pieces of silicone tubing (A) and Kalrez® 8002UP tubing (B) and identical pieces kept in chloroform for 2 days (C, D) are shown for comparison. The silicone tube is swelling in chloroform to ≈ 1.5 times its length and ≈ 1.2 times its diameter (C) and hence not applicable as tubing for the stretching apparatus with chloroform-based gels. In contrast, the Kalrez® 8002UP tube is not affected by chloroform (D).

The Kalrez® 8002UP tube was tested with gels containing water, DMSO, chloroform, dichloromethane, acetonitrile, methanol and trifluoroethanol and with none of the tested solvents a problem arose. In the following some applications of the

the Kalrez® 8002UP tube will be discussed, reflecting the broad solvent range applicable with this new material.

Example for a Chloroform-Based Gel - Linear Scaling of Alignment

The new material can also be used with halogenated solvents, like chloroform and dichloromethane. As an example, the stepwise stretching of a PDMS/$CDCl_3$ gel[67] containing hydroquinidine as a test molecule was monitored. Therefore, a number of CLIP-HSQC spectra[107] at different extensions have been acquired (see Figure 4.13. A).

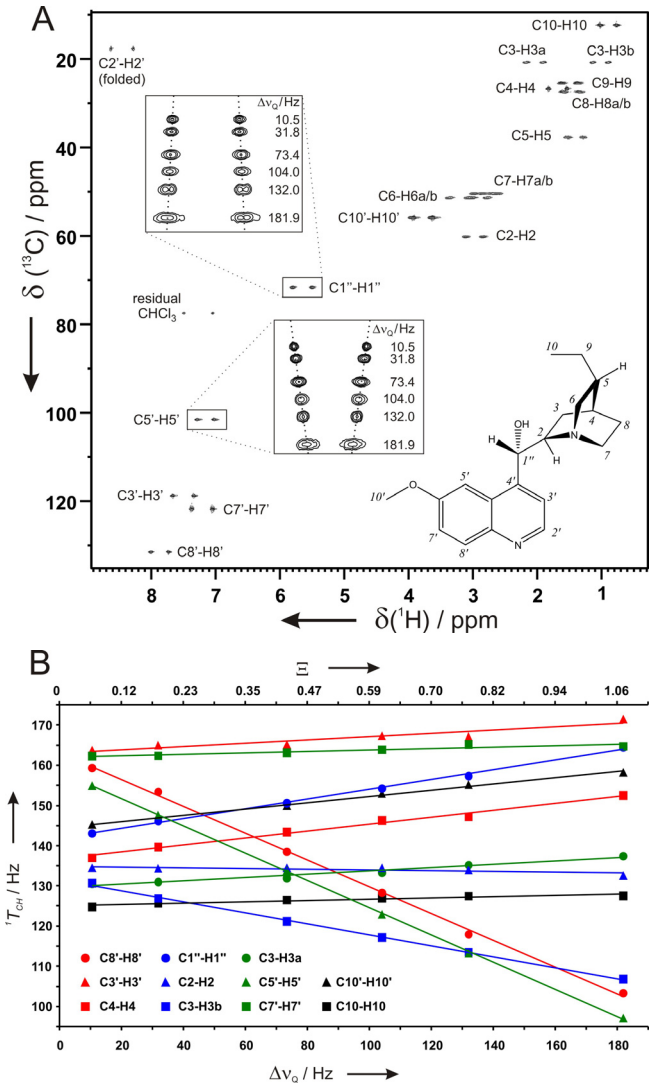

Figure 4.13.: (A) CLIP-HSQC spectrum[107] of hydroquinidine in a PDMS/$CDCl_3$ gel. Insets show two signals (C1"-H1" and C5'-H5') at various stages of stretching with peaks separated in the vertical direction according to the corresponding quadrupolar splitting $\Delta\nu_Q$ of the solvent $CDCl_3$. The linear dependence between observed $^1T_{CH}$ couplings and quadrupolar splittings is evident. (B) One-bond CH-couplings ($^1T_{CH} = {}^1J_{CH} + D_{CH}$) of hydroquinidine with respect to the quadrupolar splitting $\Delta\nu_Q$ of the solvent $CDCl_3$ and the extension factor Ξ of the used PDMS gel. Due to the linear relationship of RDCs with the quadrupolar splitting a linear fit of couplings measured at different degrees of stretching leads to a slope that can be extracted with a higher precision than it would be possible from individual experiments.

As shown for the stretching apparatus equipped with silicone, the alignment strength and therefore anisotropic NMR parameters are approximately proportional to the so-called extension factor Ξ and the plot of $^1T_{CH}$ couplings against Ξ or the

quadrupolar splitting $\Delta\nu_Q$ reveals highly precise RDCs as the slopes of corresponding linear fits (see chapter 4.1.6). This scaling of one-bond couplings for the stepwise stretching of the hydroquinidine sample is shown in Figure 4.13. B.

Example for a Water-Based Gel - Discrimination of Alanine Enantiomers in Gelatin

As has been shown previously,[52, 53, 100] stretched gelatin provides the possibility of distinguishing enantiomers (see also chapter 3.4). The distinction is even more facile with the Kalrez® 8002UP tubing, as demonstrated by repeating a set of ^{1}H-1D-spectra of different samples of L- and D-alanine (see Figure 4.14.). The advantage of no additional ^{1}H signals of the Kalrez® 8002UP tube increases the sensitivity of the experiments (by adjusting the receiver gain accordingly) and therefore it is even possible to determine the enantiomeric excess of the alanine enantiomers in simple 1D spectra.

Figure 4.14. (next page): Differentiation of enantiomers and estimation of enantiomeric excess of an alanine mixture. ^{1}H-1D spectra of alanine samples in 50% gelatin stretched with a Kalrez® 8002UP tube to the same extension (for all spectra $\Delta\nu_Q(D_2O) \approx 400$ Hz): pure D-Ala (A), pure L-Ala (B) and 2:1 mixture of D-Ala and L-Ala (D). Expansions for the Hα (left) and Hβ (right) signals are shown in (C). Addition of the spectra for D-Ala (red) and L-Ala (blue) in the ratio 2:1 results in the spectrum one would expect for a 2:1 mixture of D-Ala and L-Ala (purple). The actual measured spectrum of a 2:1 mixture at similar alignment strength is shown in black for comparison (C, D).

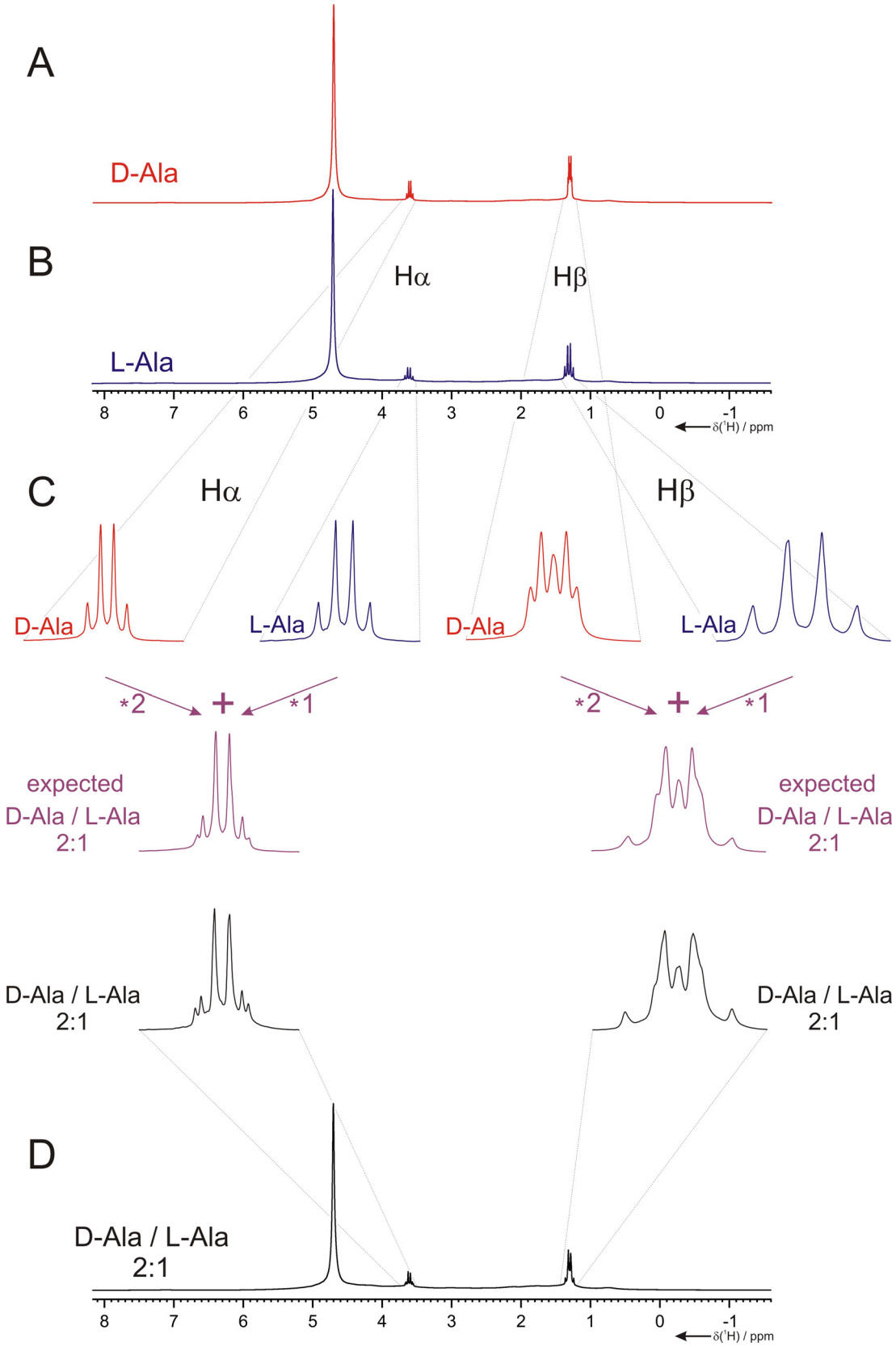
A
D-Ala
B
Hα
Hβ
L-Ala
8 7 6 5 4 3 2 1 0 -1
δ(¹H) / ppm
C
Hα
Hβ
D-Ala
L-Ala
D-Ala
L-Ala
*2
+
*1
*2
+
*1
expected
D-Ala / L-Ala
2:1
expected
D-Ala / L-Ala
2:1
D-Ala / L-Ala
2:1
D-Ala / L-Ala
2:1
D
D-Ala / L-Ala
2:1
8 7 6 5 4 3 2 1 0 -1
δ(¹H) / ppm

Example for a DMSO-Based Gel - Conformational Analysis of a Natural Product

As another test molecule the natural product parthenolide, a sesquiterpenic lactone isolated from *Chrysanthemum parthenium*,[194] was investigated. A set of 16 one-bond RDCs could be obtained for the compound in a PAN/DMSO gel stretched within the stretching apparatus equipped with a Kalrez® 8002UP tube. RDCs fitted with the program PALES[128, 129] confirm the presence of a chair-like conformation of the compound in DMSO solution, as previously measured by x-ray crystallography[195] and as proposed by MM-calculations.[196]

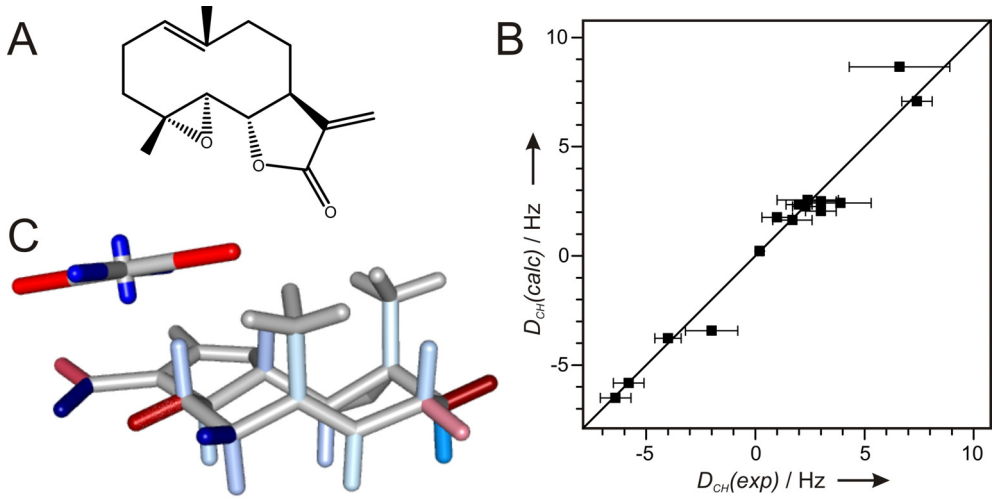

Figure 4.15.: Conformational analysis of the natural product parthenolide (A) by RDCs measured in a PAN/DMSO gel stretched with the stretching device equipped with a Kalrez® 8002UP tube. The plot of back-calculated vs. measured RDCs (B) for the chair-like conformation confirms this structural model in solution. The molecule in its chair-like conformation is shown with color-coded bonds (red: negative; blue: positive RDCs) and the axes of the corresponding alignment tensor next to it (C).

In contrast to corresponding gels in the silicone-based device, where penetrating humidity leads to shrinking gels within a couple of weeks (see chapter 4.1.4), the used PAN/DMSO gel is stable for at least one year. Therefore the Kalrez® 8002UP tube is of special advantage for samples which are sensitive to water, as humidity can not diffuse through the gas-tight walls of the perfluorinated tube.

4.2.5 Conclusion

In summary, the stretching apparatus equipped with the perfluorinated Kalrez® 8002UP tube is an ideal tool to partially align molecules for measuring anisotropic NMR parameters. It allows an easy, arbitrary and reversible adjustment of alignment strength in practically all polymer gel matrices, with all the advantages discussed already in chapter 4.1.7 for the silicone-based apparatus. It has been shown that the Kalrez® 8002UP tube is applicable to all gel-based alignment media, including those with apolar solvents. In contrast to the previously reported stretching device based on silicone tubes, the perfluorinated elastomer tube does not contribute to ^{1}H-NMR-spectra and is generally gas-tight, which, for example, prevents the diffusion of humidity into the sample. Especially in combination with perdeuterated polymer gels (see chapters 3.2 and 3.3), the presented stretching apparatus is of high interest for samples at low concentration as it provides proton spectra void of signals originating from the alignment medium.

An important issue for the applicability of the stretching apparatus beyond this project is of course the accessibility of the tube material. In the meanwhile attempts have been made to sell the elastomer tube itself as well as the whole stretching device, hence one can expect that it will be intensively used by other groups in the near future. Because of the expensive elastomer part, the stretching device equipped with a Kalrez® 8002UP tube will be of a significantly higher price compared to the silicone-tube based apparatus, however for many applications the silicone tube is no alternative.

This project was done in cooperation with Dr. Elizabeth F. McCord, Dr. Steve F. Cheatham, Steve Niss and Russell W. Schnell from DuPont, who contributed with fruitful discussions to the right choice of elastomer material and who specially produced the tubes for this project. Otto Strasser and his team (TUM, Munich) manufactured all clamps and screwing devices.

Results presented in this chapter will be published soon:

Grit Kummerlöwe; Elisabeth F. McCord; Steve F. Cheatham; Steve Niss; Russell W. Schnell; Burkhard Luy: '*Tunable Alignment for All Polymer Gel/Solvent Combinations for the Measurement of Anisotropic NMR Parameters Using a Perfluorinated Elastomer Tube*' in *Chemistry - A European Journal* **2010**, in press, DOI: 10.1002/chem.201000108.

5 Structure Determination of Small Molecules

5.1 Configurational Analysis of a Degradation Product of Beer

5.1.1 Introduction and Motivation

The analysis of residual dipolar couplings is a powerful tool for the determination of the relative configuration of small to medium-sized molecules, and especially necessary if classical NMR methods fail. The aim of this project was to analyze the stereochemistry of a tricyclic hydrocarbon, which was isolated as a degradation product of a bitter compound in beer. Standard NMR analysis via ROESY and J_{HH}-couplings were not conclusive enough to unambiguously solve the structure.

The Beer's Bitter Principle

Undesirable changes in the attractive aroma, in particular, a significant decrease of bitter intensity as well as a change of the bitter taste quality towards a lingering, harsh bitterness has long been known as a shelf-life limiting factor of beer. Multiple studies demonstrated that aging of beer induces a decrease of the total amount of *cis*- and *trans*-iso-α-acids, the well-known bitter principles of beer, which are formed upon adding hop (*Humulus lupulus* L.) during wort boiling[197] (see Figure 5.1.).

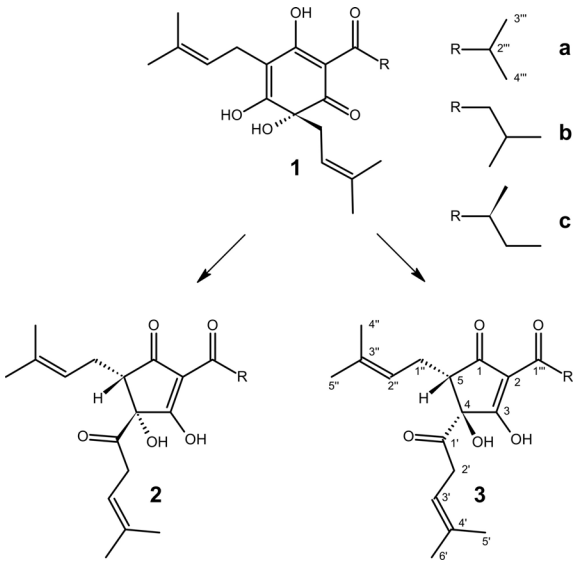

Figure 5.1.: Formation of the beer's bitter principle. The α-acids (1), a major hop compound class, are transformed to *cis*- (2) and *trans*-iso-α-acids (3) by a thermally driven isomerization reaction. *Copyright Wiley-VCH Verlag GmbH & Co. KGaA. Reproduced with permission from Reference* [197].

Whereas microbiological spoilage and haze formation determined the quality of beer in the past, the deterioration of the attractive aroma as well as the bitterness gives nowadays the limitation for the shelf live of beer products. Although aging of beer is long known to induce a significant decrease of bitter intensity as well as a change of the bitter taste quality, the molecular basis of this deterioration of bitterness was not known.

Aging of Beer and Degradation of the Bitterness

Although exclusively the *trans*-iso-α-acids, but not the *cis*-iso-α-acids, were found to be degraded upon storage of beer,[198-200] the key transformation products formed exclusively from the *trans*-isomers were not known. Therefore, Daniel Intelmann from the group of Prof. Thomas Hofmann at the "Chair of Food Chemistry and Molecular Sensory Science" at the Technische Universität München investigated the aging of beer by suitable model experiments.[201] Purified *trans*-isocohumulone (3a in Figure 5.1.) was treated for 6 h at 60°C in a methanol-water mixture and the transformation products were isolated by preparative RP-HPLC as a series of previously unkown *trans*-specific iso-α-acid transformation products, named tricyclocohumol, tricyclocohumene, isotricyclocohumene, tetracyclocohumol, and epitetracyclocohumol, respectively. Their chemical structures were determined by means of HRMS and NMR spectroscopy (see below).[201]

Furthermore, HPLC-MS/MS analysis of these compounds, which exhibit a lingering harsh bitter taste, confirmed their generation during aging of beer.[201] The determination of bitter taste recognition threshold concentrations of these substances explained the storage-induced changes of the beer's bitter taste on a molecular level for the first time.[201, 202]

Structural Investigations of the Degradation Products

Hofmann and coworkers determined the chemical structures of the transformation products by HRMS and classical NMR techniques like COSY, HMQC, HMBC and INADEQUATE, as they are shown in Figure 5.2. A. For the tetracycles tetracyclocohumol (7a) and epitetracyclocohumol (8a), they were able to determine the relative stereochemistry by ROESY and $^{3}J_{HH}$-coupling analysis as depicted in Figure 5.2. B. The absolute stereochemistry was concluded from the configuration at

C4 and C5 of the precursor analog *trans*-isoadhumolone (3c in Figure 5.1.), which was determined by X-ray diffractometry.[201]

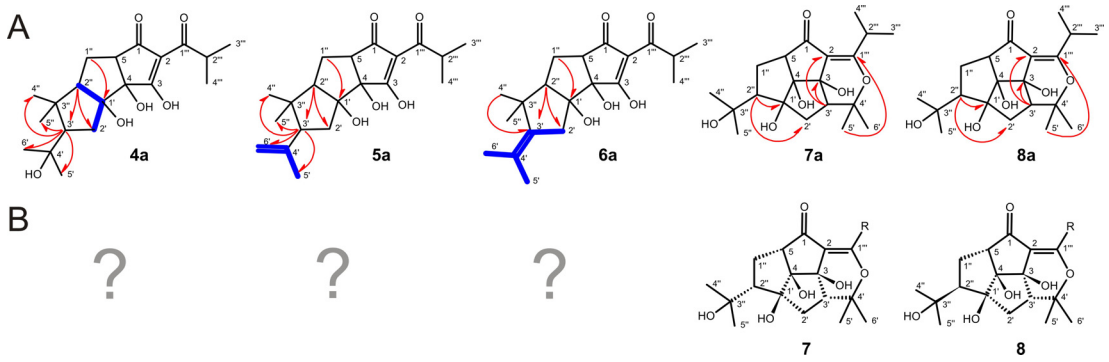

Figure 5.2.: Structures of the identified transformation products 4a-8a formed from trans-isocohomulone (3a). The tri- and tetracyclic compounds have been named tricyclocohumol (4a), tricyclocohumene (5a), isotricyclocohumene (6a), tetracyclocohumol (7a), and epitetracyclocohumol (8a), respectively. In (A) chemical structures of the five compounds are shown with selected ^{1}H-^{1}H-COSY (blue bold bonds) and ^{1}H-^{13}C-HMBC correlations (red curved arrows). The stereochemistry as determined by ROESY intensities and $^{3}J_{HH}$-coupling analysis is shown in (B).[201]

Open Questions for Tricyclocohumol

The stereochemical analysis of tricyclocohumol (4a) turned out to be rather challenging with classical methods. Major problems for this, are the quaternary carbons C1' and C3", which interrupt the chain of $^{3}J_{HH}$ couplings. While for the tetracycles this could be overcome with the analysis of ROESY intensities, corresponding ROESY spectra for tricyclocohumol were not conclusive. An additional problem for the analysis of J_{HH} couplings and ROESY cross peaks is the prochiral assignment of the CH_2-groups, which is not known a priori but usually determined by J_{HH} couplings and ROESY analysis. Consequently, there was too much uncertainty in assignment of resonances and stereochemistry left using classical methods only. Therefore, the aim of this project was to support the configurational analysis and the assignment of prochiral resonances of tricyclocohumol by the use of RDCs next to the classical J_{HH}-couplings.

For the tricycles tricyclocohumene (5a) and isotricyclocohumene (6a), which are only formed in very small amounts upon aging of beer, not enough substance was available for a detailed analysis. However, as they are formed in an analog mechanism from the same precursor as tricyclocohumol (4a),[203] their stereochemistry is considered to be the identical.

5.1.2 Possible Structural Models of Tricyclocohumol

The tricycle exhibits 5 stereogenic centers within the five-membered rings, which in principle could form 32 different stereoisomers (see Figure 5.3.). As the absolute configuration can anyway not be determined with the used methods the problem can be reduced to 16 diastereomers.

In order to assign the stereocenters of the structural models, a *systematical* numbering of the ring system was chosen to be in line with the name according to the IUPAC recommendations (see Figure 5.3. A). The short labels for the diastereomers (e.g. RSSRS) as they will be used in the following are obtained by the stereo-descriptors in the order of the IUPAC-numbering. However, this IUPAC numbering is *only* used for the order of the stereo-descriptors. In all Tables, Figures and descriptions throughout this chapter the numbering of the molecule will be as in Figure 5.3. B. This numbering was derived from the numbering of the precursor molecule (see Figure 5.1.).

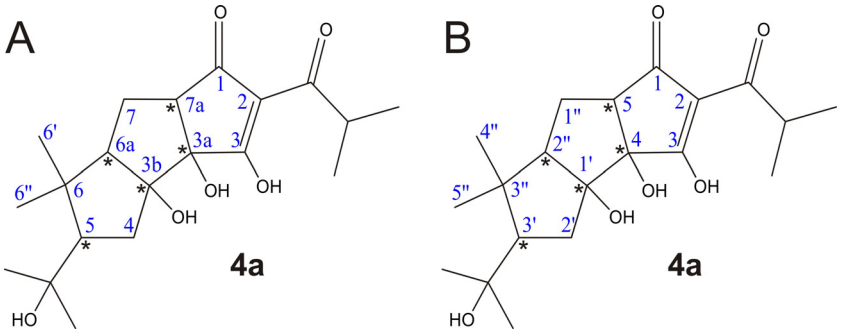

Figure 5.3.: Chemical structure of tricyclocohumol (4a) with different numbering systems. The systematic numbering of carbon atoms according to the IUPAC recommendations (A) is only used for the order of the stereo-descriptors in the short name of the diastereomers as e.g. RSRRS. The numbering of carbon atoms as derived from the precursor *trans*-iso-α-acid (3a) (see Figure 5.1.) and as shown in (B) is used in all other Figures, Tables and descriptions throughout this chapter.

The absolute configuration at C4 and C5 can be derived from the *trans*-isoadhomulone (3c) X-ray structure (see above), reducing the possible diastereomers to 8. However, the aim was to leave the relative stereochemistry between C4 and C5 open in the analysis and therefore confirm this presumption. For the J_{HH}-coupling and RDC analysis only the stereocenter at C5 was fixed and all other stereocenters were varied. Using the stereo-descriptors according to the IUPAC numbering, the S configuration at C5 and the R configuration at C4 (as derived from the precursor's

X-ray structure) would translate into possible diastereomers RxxxS. Nevertheless all 16 diastereomers xxxxS were analyzed.

In addition to the four stereocenters, the ambiguous prochiral assignment for the protons at C2' (H2'α and H2'β) and C1" (H1"α and H1"β) and for the methyl groups at C3" (C4" and C5") should be permutated. This leads to 8 possible prochiral assignments, named a-h, for all 16 diastereomers. For the RSSSS diastereomer this prochiral assignments are depicted in Figure 5.4.

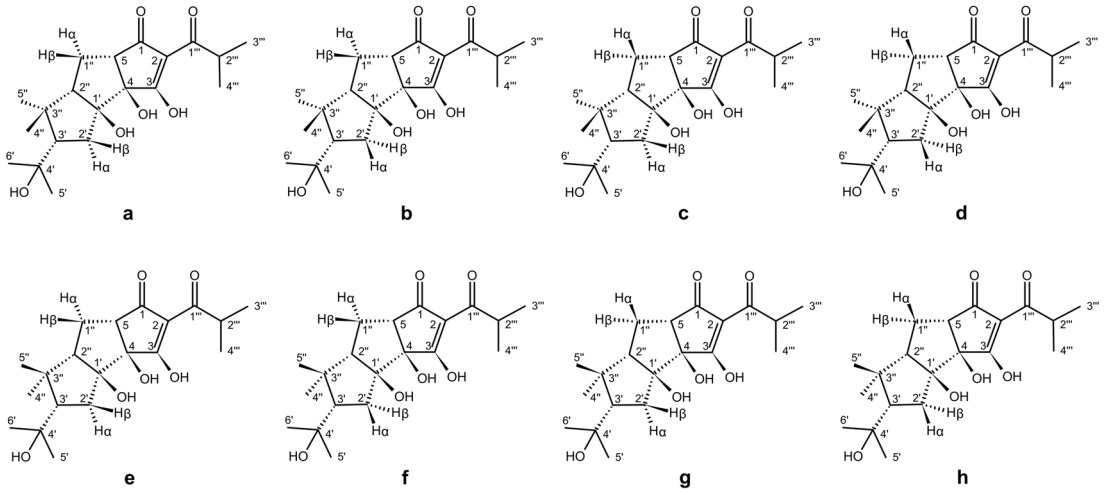

Figure 5.4.: Possible prochiral permutations for the RSSSS diastereomer of tricyclocohumol. The 8 different structural models with the assignments at C2', C1" and C3" permutated are named a-h.

With 16 possible diastereomers and 8 possible prochiral assignments for each of them, a total of 128 possible structural models has to be tested.

5.1.3 RDCs and J-couplings Measured on Tricyclocohumol

Initial spectra for tricyclocohumol were acquired in methanol-d_4 and $^{3,4}J_{HH}$ couplings have been extracted from a ^{1}H-1D spectrum. (For chemical shifts and extracted coupling values see Appendix.) Out of this, eight J_{HH} couplings can be used for the configurational analysis.

Later on, additional spectra were recorded in DMSO-d_6 with chemical shift values very similar to the corresponding methanol sample. On this sample CLIP-HSQC[107] and P.E.HSQC[114] spectra have been acquired for the determination of scalar one-bond ^{1}H,^{13}C-couplings and two-bond ^{1}H,^{1}H-couplings, respectively. For the

measurement of RDCs the compound was diffused into a deuterated polyacrylonitrile/DMSO-d_6 gel (see chapter 3.3) which was stretched within a stretching apparatus equipped with a Kalrez® 8002UP tube (see chapter 4.2) for partial alignment. Corresponding CLIP-HSQC[107] and P.E.HSQC[114] spectra have been acquired for the gel sample, which was estimated to have an approximate concentration of 0.4 mol/L. Neglecting couplings of the flexible side chains, and converting couplings of the methyl groups, altogether 11 D_{CH}, D_{CC} and D_{HH} RDCs within the tricyclic core can be used for the RDC analysis (see Table 5.1.).

Table 5.1.: Chemical shifts in DMSO and one-bond $^1H,^{13}C$-couplings as well as two-bond $^1H,^1H$-couplings for tricyclocohumol in DMSO and in the stretched dPAN/DMSO-gel.

Group[a]		$\delta(^{13}C)$ [ppm][b]	$\delta(^1H)$ [ppm][b]	$^1J_{CH}$ (DMSO) [Hz]	$^1J_{CH} + D_{CH}$ (PAN) [Hz]	D_{CH} [Hz]
C5	H5	53.8	2.89	136.5 ± 0.1	124.1 ± 0.5	-12.4 ± 0.5
C2'	H2' α	37.2	1.50	123.0 ± 2.2	135.0 ± 4.5	12.0 ± 5.0
C2'	H2' β		1.58	131.5 ± 2.2	144.0 ± 4.5	12.5 ± 5.0
C3'	H3'	57.9	1.98	125.6 ± 0.2	142.5 ± 0.6	16.9 ± 0.6
C5'	H5'	29.4	1.14	124.7 ± 0.1	127.8 ± 0.3	3.1 ± 0.3 [c]
C6'	H6'	30.8	0.98	124.8 ± 0.1	124.7 ± 0.3	-0.1 ± 0.3 [c]
C1"	H1" α	25.9	1.45	129.0 ± 0.5	129.5 ± 1.5	0.5 ± 1.6
C1"	H1" β		1.94	135.4 ± 0.5	141.9 ± 0.6	6.5 ± 0.8
C2"	H2"	64.8	2.15	130.0 ± 0.3	121.5 ± 0.5	-8.5 ± 0.6
C4"	H4"	22.8	1.06	125.9 ± 0.2	120.0 ± 1.0	-5.9 ± 1.0 [d]
C5"	H5"	35.3	1.17	124.1 ± 0.2	126.6 ± 0.3	2.5 ± 0.4 [d]
C2"'	H2"'	35.3	3.47	132.2 ± 0.2	149.6 ± 0.3	17.4 ± 0.4 [c]
C3"'	H3"'	17.1	1.03	127.9 ± 0.5	132.4 ± 0.6	4.5 ± 0.8 [c]
C4"'	H4"'	17.6	1.03	128.0 ± 0.5	132.2 ± 0.3	4.2 ± 0.6 [c]
Group[a]				$^2J_{HH}$ (DMSO) [Hz]	$^2J_{HH} + D_{HH}$ (PAN) [Hz]	D_{HH} [Hz]
H2'α	H2'β			-12.9 ± 2.5	12.9 ± 3.0	25.8 ± 3.9
H1"α	H1"β			-13.5 ± 2.0	-20.2 ± 2.5	-6.7 ± 3.2

[a] Numbering according to structure in Figure FF5.3.FF B. [b] Chemical shifts in DMSO taken from CLIP-HSQC- and ^1H-1D-spectrum and referenced to the solvent signal ($\delta(^{13}C)$ = 39.5 ppm; $\delta(^1H)$ = 2.50 ppm). [c] RDCs within the flexible side-chains have not been used for fitting. [d] D_{CH}-couplings of methyl-groups have been converted to the corresponding D_{CC}-couplings[125] (D_{CC}(C4"-C3" = 1.6 ± 0.3 Hz; D_{CC}(C5"-C3") = -0.7 ± 0.1 Hz).

5.1.4 Configurational Analysis of Tricyclocohumol

The aim was to determine the configuration and the prochiral assignment of all resonances of tricyclocohumol by the combination of J_{HH}-coupling and RDC analysis.

Therefore a total number of 16 diastereomeric structural models of tricyclocohumol was created and energy-minimized using the program Sybyl.[204] These models were subsequently the input for the program PALES[128, 129] for fitting experimental RDC data and for the J-prediction routine within the program MestreNova.[205]

Within the RDC-fitting procedure, prochiral protons at carbons C1" and prochiral methyl groups attached to C3" have been permutated since their assignment was ambiguous. The prochiral protons at C2' showed RDCs which were identical within the error of the experiment (see Table 5.1.) and therefore they were not subject to permutation during the RDC analysis. RDCs of flexible side chains were not included in the fitting procedure.

The prediction of J_{HH}-coupling constants for the 16 structural models was done with the program MestreNova.[205] In contradiction to the RDC-fitting procedure, the assignment of the prochiral protons at C2' and C1" were permutated for the fitting with the predicted values. The prochiral methyl groups attached to C3" have not been permutated since no J_{HH}-coupling constants could be measured for the protons at C4" and C5".

For the RDC analysis as well as for the J_{HH}-coupling analysis experimental data and back-calculated/predicted data were compared in terms of calculating the quality factor n/χ^2 for each fit.

5.1.5 Fitting Results

A Comparison of all quality factors n/χ^2 for the fits of measured RDCs and measured J_{HH}-coupling constants for the different possible diastereomers with the corresponding permutations of prochiral assignment is shown in Figure 5.5.

The fitting results demonstrate that only one configuration fulfills both RDC and J-coupling data, thus leading to the unambiguous stereochemical assignment of tricyclocohumol to be the RSSSS diastereomer. The prochiral assignment is determined by the fits of RDCs and J_{HH}-couplings to be the one as depicted in Figure 5.7. Also the plots of calculated vs. experimental data for selected diastereomers and permutations shown in Figure 5.6. clearly indicate that measured couplings are only consistent with the structural model RSSSS (e).

Figure 5.5. (next page): Comparison of quality factors n/χ^2 for the fits of measured RDCs (upper part) and measured HH-scalar couplings (bottom part) against the different possible diastereomers of tricyclocohumol. For each diastereomer altogether 8 different permutations (a-h) of diastereotopic groups have been fitted. Because of almost identical RDC values within the C2' methylene group, its permutation was not considered in the RDC-fits. Similarly, the permutation of the methyl groups C4" and C5" were not considered in the J-coupling fits. Clearly permutation (e) (for correct diastereotopic assignment see Figure 5.4.) of the RSSSS diastereomer gives best fits for RDCs as well as for J-couplings.

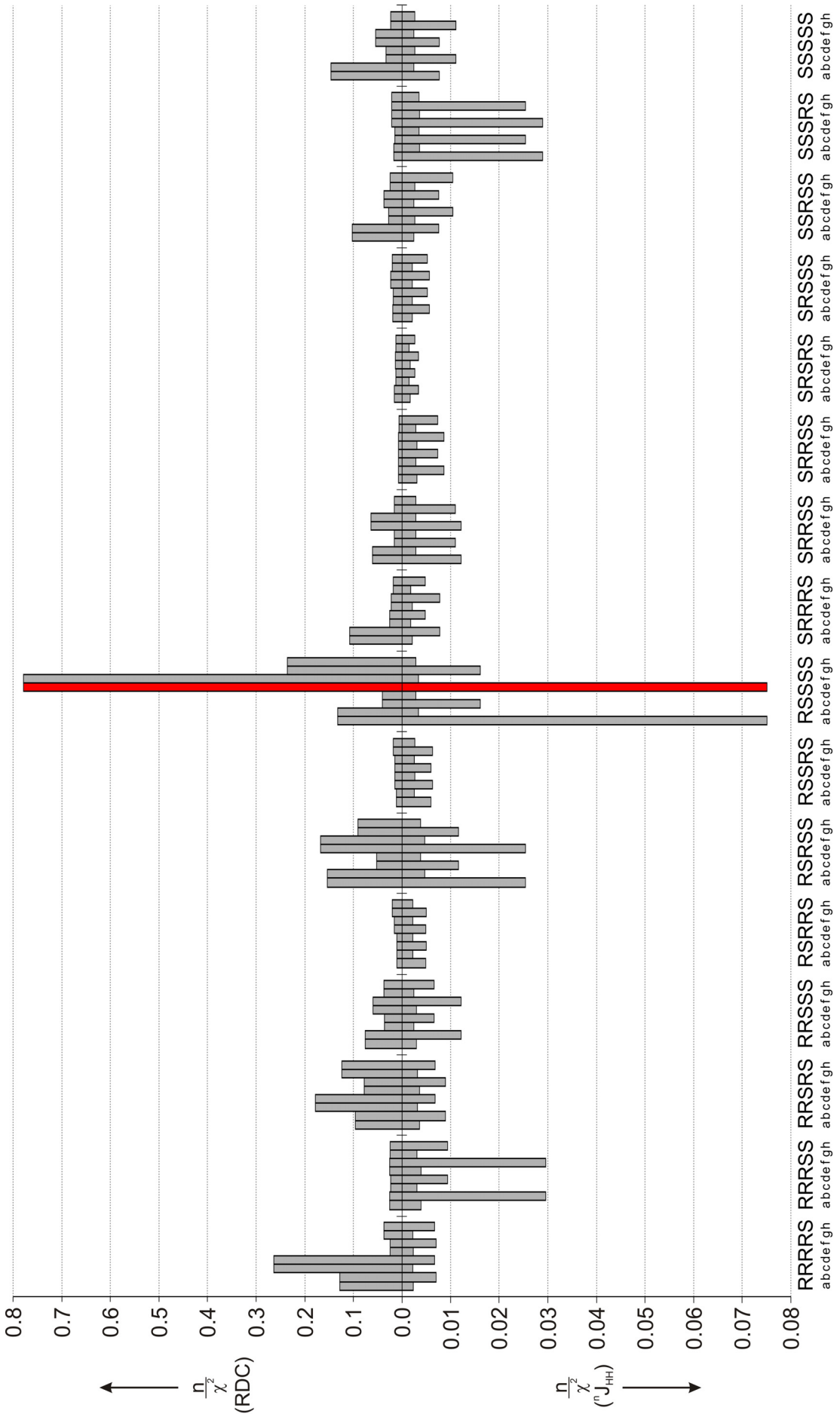
RRRRS RRRSS RRSRS RRSSS RSRRS RSRSS RSSRS RSSSS SRRRS SRRSS SRSRS SRSSS SSRRS SSRSS SSSRS SSSSS
abcdefgh abcdefgh abcdefgh abcdefgh abcdefgh abcdefgh abcdefgh abcdefgh abcdefgh abcdefgh abcdefgh abcdefgh abcdefgh abcdefgh abcdefgh abcdefgh
0.8 0.7 0.6 0.5 0.4 0.3 0.2 0.1 0.0 0.01 0.02 0.03 0.04 0.05 0.06 0.07 0.08
n/χ² (RDC)
n/χ² (nJHH)

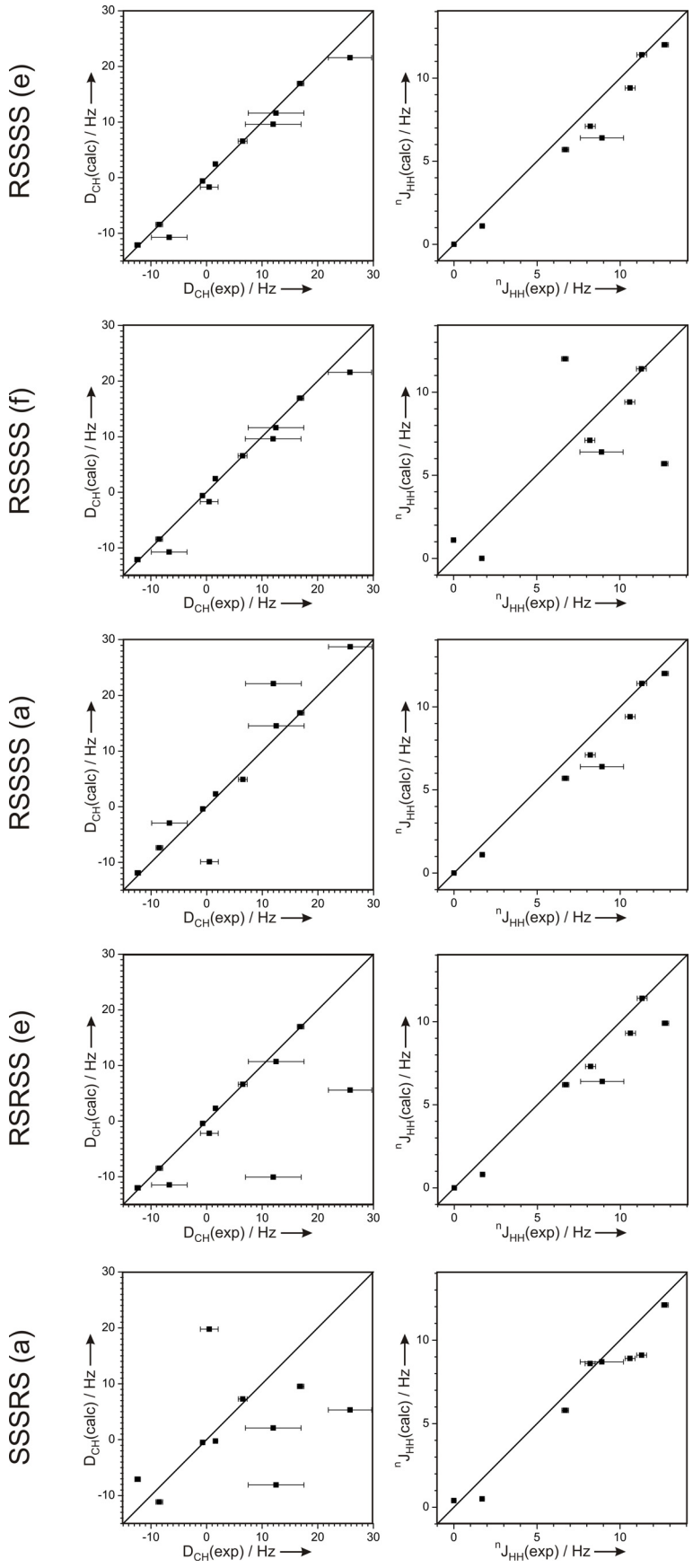

Figure 5.6.: Plots of back-calculated vs. measured RDCs (left) and J_{HH}-couplings (right) for selected diastereomers of tricyclocohumol.

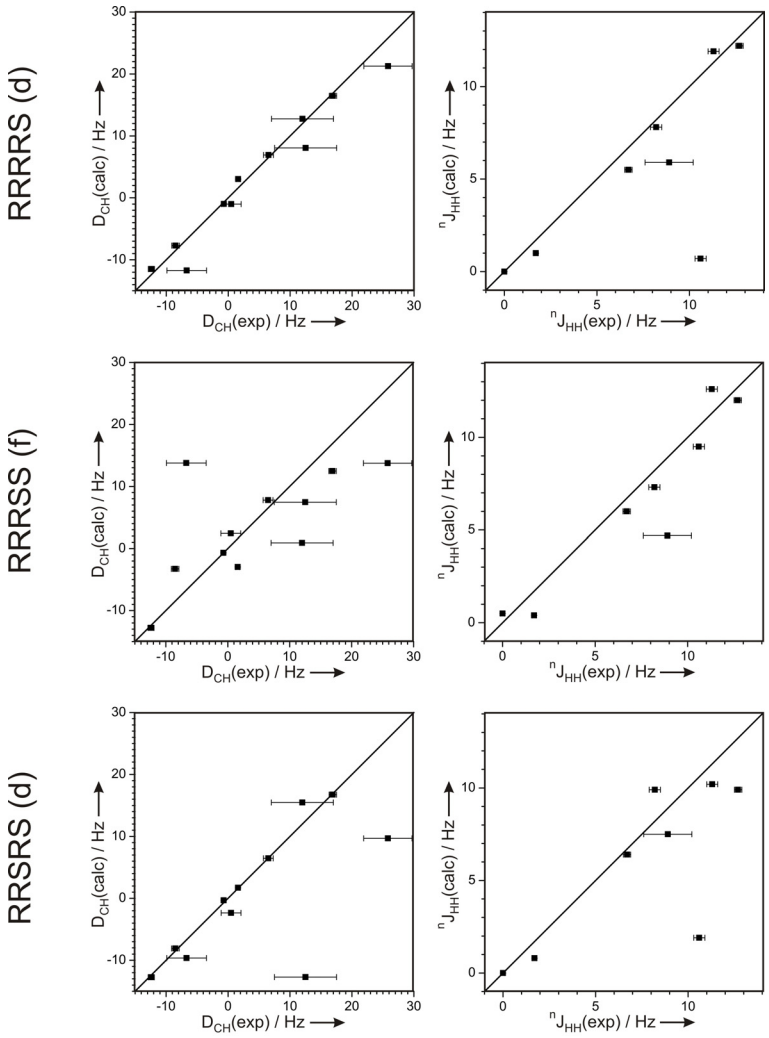

Figure 5.6. (continued): Plots of back-calculated vs. measured RDCs (left) and J_{HH}-couplings (right) for selected diastereomers of tricyclocohumol.

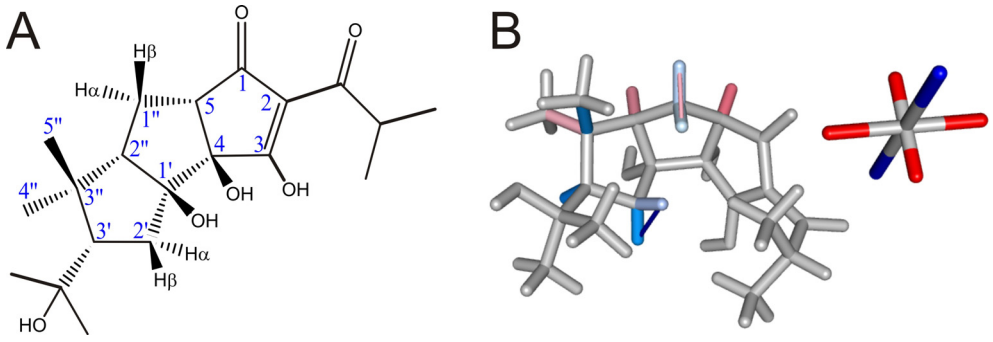

Figure 5.7.: The RSSSS diastereomer of tricyclocohumol with the correct prochiral assignment (A) and the molecule with color-coded bonds representing negative (red) and positive (blue) RDCs with axes of the corresponding alignment tensor drawn next to it (B).

5.1.6 Conclusion

For the previously unknown major degradation product of the beer's bitter principle, the tricyclic hydrocarbon named tricyclocohumol, a full analysis of the stereochemical configuration and the assignment of all prochiral groups has been performed with the combined analysis of RDCs and J_{HH}-couplings. Clearly only one of the 128 possible structural models is consistent with the experimental data and can therefore be regarded as the correctly assigned diastereomer.

In this case, the combination of the two methods leads to the unambiguous assignment. RDCs only as well as J_{HH}-couplings only would not have been conclusive enough. The RDC analysis would clearly have favored the correct diastereomer, but would have failed with the prochiral assignment of one of the CH_2-groups, as both CH-vectors of this methylene group coincidental showed almost identical RDC values. On the other hand, the J_{HH}-coupling analysis alone would be not reliable enough, as the chain of $^3J_{HH}$-couplings is interrupted between the different rings of the molecule by quaternary carbon atoms. The only connection between the two spin-systems is a very weak $^4J_{HH}$-coupling on which therefore the J_{HH}-coupling analysis depends. However, in combination with the RDC analysis the stereochemical problem could be solved.

This project was done in cooperation with Dipl. Chem. Daniel Intelmann and other coworkers of Prof. Dr. Thomas Hofmann (TUM, Munich), who isolated the compound from aged beer samples and model experiments, did all the constitutional analysis of tricyclocohumol, and extracted experimental $^nJ_{HH}$-couplings from 1D spectra and calculated $^nJ_{HH}$-couplings from the proposed structures by MestreNova.

Results presented in this chapter have been published:

Daniel Intelmann; Grit Kummerlöwe; Gesa Haseleu; Nina Desmer; Kerstin Schulze; Roland Fröhlich; Oliver Frank; Burkhard Luy; Thomas Hofmann: '*Structures of Storage-Induced Transformation Products of the Beer's Bitter Principle, Revealed by Sophisticated NMR and LC/MS Techniques*' in *Chemistry - A European Journal* **2009**, *15*, 13047-13058.

5.2 Configurational and Conformational Analysis of Staurosporine

5.2.1 Introduction and Motivation

Staurosporine (see Figure 5.8.) is a natural product first isolated from *Streptomyces staurosporeus*[206] and known as a potent inhibitor of several protein kinases,[207] notably protein kinase C (PKC), where it appears to bind strongly to the catalytic subunit.[208] A series of inhibitors of PKC has been designed from the staurosporine structural lead[209] and more potent drugs based on this natural product can be expected.

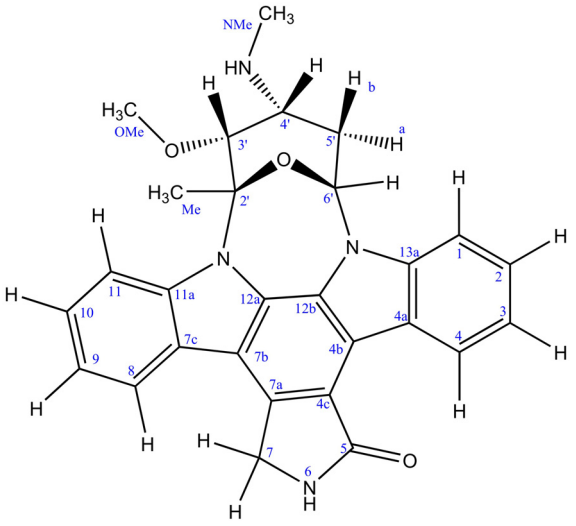

Figure 5.8.: Molecular structure of the SRRR diastereomer of staurosporine with the numbering used within this chapter.

Considering its potential application, the structure of staurosporine is of high interest. The absolute configuration is most likely the SRRR diastereomer, like Funato et al. determined by X-ray crystallography of the methyl methiodide derivate of staurosporine.[210] For the conformation of this derivate in the crystal they found a chair-like structure of the tetrahydropyran ring. For the conformation in solution, however, the chair as well as the boat conformation is discussed, depending on the degree of protonation of the NHMe-group of staurosporine.[211]

The aim of this project was to use staurosporine as a test molecule for the measurement of RDCs in the newly developed alignment medium dPS/$CDCl_3$ (see

chapter 3.2) and to use these RDCs for the configurational und conformational analysis of staurosporine in chloroform.

5.2.2 Possible Conformations and Configurations of Staurosporine

The natural product staurosporine consists of an extensive aromatic ring system and a six-membered tetrahydropyran ring attached via two nitrogen atoms (see Figure 5.8.). The tetrahydropyran ring in principle contains 4 stereogenic centers (C2′, C3′, C4′, and C6′) but cyclization reduces the degree of freedom to 3, resulting in $2^3 = 8$ possible configurations. These are the four diastereomers SRRR, SRSR, SSRR, SSSR, and their enantiomers RSSS, RSRS, RRSS, RRRS. Since the NMR experiments were carried out in an achiral environment, enantiomers show identical spectra and only the four diastereomers have to be considered.

Finally, in addition to the different configurations, chair or boat conformations can be assumed for the six-membered ring, resulting in a total of 8 distinguishable structures. These eight structural models of staurosporine were created and energy-minimized using the program Sybyl.[204]

5.2.3 RDCs Measured on Staurosporine

Residual dipolar couplings of staurosporine have been measured by the acquisition of corresponding CLIP-HSQC spectra[107] for a solution sample and a sample of ≈ 4 mM staurosporine diffused in a stretched dPS/$CDCl_3$ gel. The aromatic region of the CLIP-HSQC spectrum acquired in this almost signal free alignment medium, has already been shown in Figure 3.11. in chapter 3.2.5.

Out of the acquired spectra, 13 one-bond $^1H,^{13}C$-RDCs could be extracted (see Table 5.2.) and used for the structural analysis.

Table 5.2.: One-bond couplings of staurosporine obtained from CLIP-HSQC[107] spectra: $^1J_{CH}$ coupling constants measured in $CDCl_3$, $^1J_{CH} + D_{CH}$ couplings measured in the dPS/$CDCl_3$ gel and calculated D_{CH} couplings.

Group	$^1J_{CH}$ [Hz]	$^1J_{CH} + D_{CH}$ [Hz]	D_{CH} [Hz]
3'	140.3 ± 0.5	120.5 ± 5.0	-19.8 ± 5.0
4'	135.2 ± 0.3	131.5 ± 1.0	-3.7 ± 1.0
5'a	131.7 ± 1.0	139.2 ± 3.0	7.5 ± 3.2
5'b	126.4 ± 1.0	-[a]	-
6'	159.3 ± 0.5	165.1 ± 1.0	5.8 ± 1.1
Me	129.2 ± 0.2	126.0 ± 1.0	-3.2 ± 1.0[b]
1	158.0 ± 1.5	130.8 ± 2.0	-27.2 ± 2.5
2	158.1 ± 3.0	147.0 ± 7.0	-11.1 ± 7.6
3	160.6 ± 3.0	162.3 ± 3.0	1.7 ± 4.2
4	165.0 ± 0.3	137.9 ± 1.0	-27.1 ± 1.0
8	158.1 ± 0.3	132.8 ± 1.0	-25.3 ± 1.0
9	160.9 ± 2.0	148.0 ± 5.0	-12.9 ± 5.4
10	159.6 ± 2.0	162.2 ± 3.0	2.6 ± 3.6
11	162.5 ± 0.5	137.1 ± 1.0	-25.4 ± 1.1

[a] Because of signal overlap with the NMe signal no coupling could be extracted.
[b] For the fits with PALES[128, 129] the D_{CH} coupling of the methyl group was converted[125] to the corresponding D_{CC} coupling (0.9 Hz).

5.2.4 Fitting Results

The 8 potential structural models for staurosporine have been fitted against the measured RDCs with the program PALES[128, 129] using the "-bestFit" option (SVD-fit). A comparison of the plots of back-calculated vs. experimental RDCs (see Figure 5.9.) clearly supports the SRRR configuration in the chair conformation which was also previously reported for the free base of staurosporine.[211, 212]

In Figure 5.10. A the squares of the corresponding correlation factors, R^2, for the fits are shown in comparison. The best correlation ($R^2 = 0.996$) clearly results for the SRRR configuration in the chair conformation. In Figure 5.10. B this structure is shown with the representation of its alignment tensor as calculated during the SVD-fit.

The results obtained with the SVD-fitting are also corroborated by RDC-restrained molecular dynamics simulations where the best match of measured and back calculated RDCs is obtained for the same structure.[26]

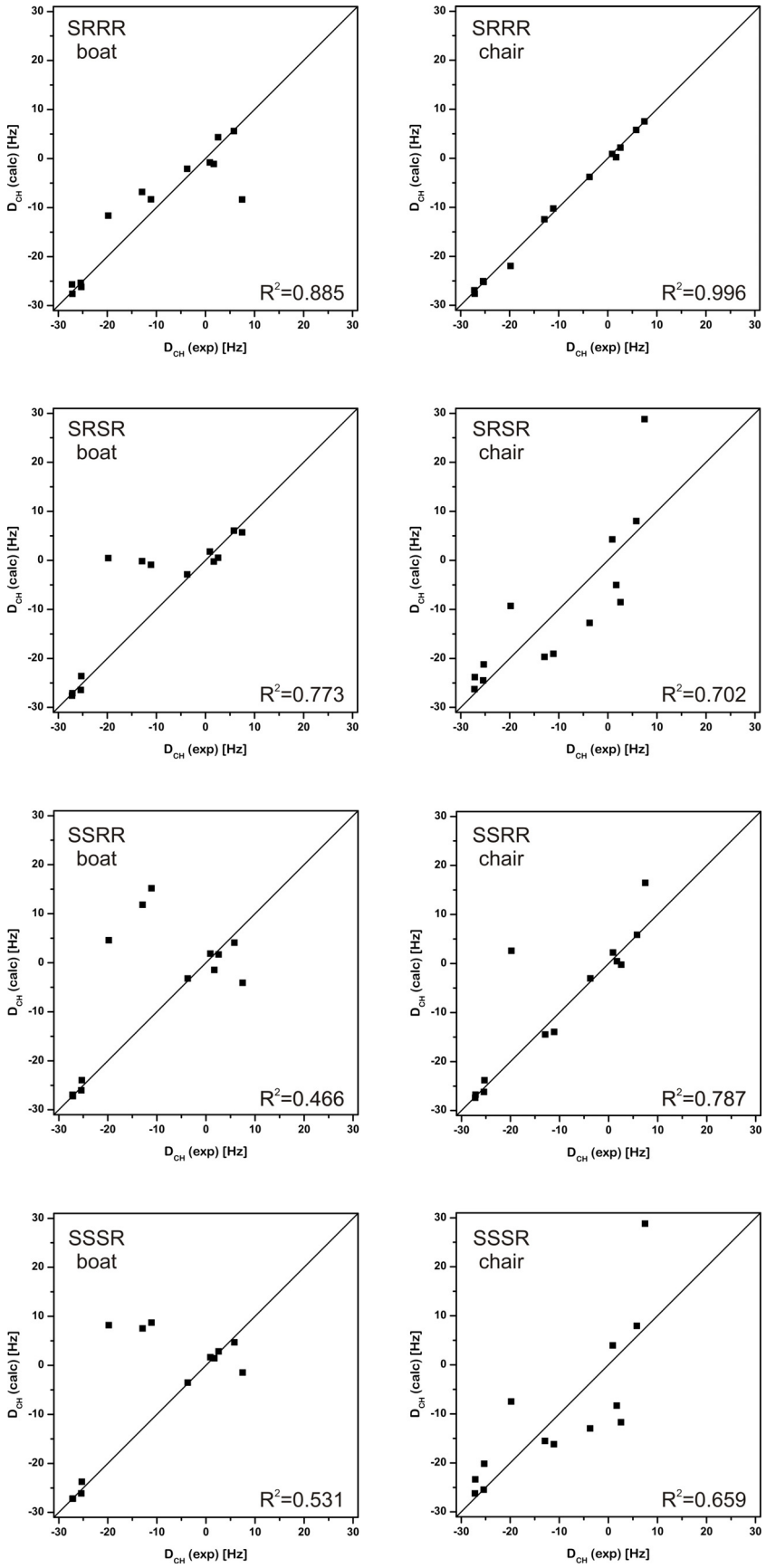

Figure 5.9.: Comparison of measured RDCs (D_{CH}(exp)) of staurosporine and RDCs back-calculated with PALES[128, 129] (D_{CH}(calc)) for the different possible configurations and conformations. Clearly, only the SRRR diastereomer in its chair conformation is in consistence with the experimental data.

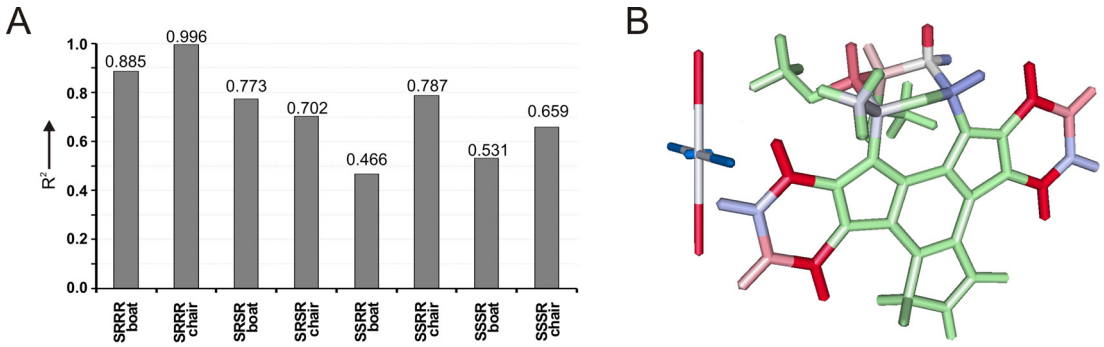

Figure 5.10.: Correlation between measured RDCs and potential staurosporine structures. The square of the correlation factor R^2 from the SVD-fits for the different configurations and conformations (A) supports the SRRR chair structure shown in (B). The structure is depicted with color-coded bonds representing negative (red) and positive (blue) $^{1}H,^{13}C$-RDCs and the axes of the corresponding alignment tensor next to it.

5.2.5 Conclusion

In summary, the configuration and conformation of the natural product staurosporine as present in chloroform solution has been proven by the analysis of one-bond proton carbon RDCs measured in a stretched deuterated polystyrene gel. Therefore all potential structures in terms of different diastereomers and different conformers of the six-membered ring have been fitted against the experimental data.

Only the SRRR diasteromer in its chair-like conformation supports the measured RDCs. The results presented in this chapter therefore not only verify the proposed structure of staurosporine but demonstrate also the potential of RDC analysis for the determination of configuration and conformation of small organic molecules.

This project was done in cooperation with Dr. Sebastian Knör (TUM, Munich), who synthesized the cross-linked deuterated polystyrene and Dr. Andreas O. Frank (TUM, Munich), who at the same time analyzed the measured RDCs with his new approach of RDC driven MD simulations (results not presented here).

Results presented in this chapter have been published:

Grit Kummerlöwe; Sebastian Knör; Andreas O. Frank; Thomas Paululat; Horst Kessler; Burkhard Luy: *'Deuterated Polymer Gels for Measuring Anisotropic NMR Parameters with Strongly Reduced Artefacts.'* in *Chemical Communications* **2008**, 5722-5724.

5.3 Solving the Constitution of an Unknown Reaction Product

5.3.1 Introduction and Motivation

As has been shown on a multitude of examples, RDCs are a useful tool to determine the configuration and/or the conformation of a molecule. However, their use to determine a molecules constitution was not reported so far. In this chapter the probably first example for the determination of the constitution of an unknown substance by the analysis of experimental RDCs is described.

The molecule under investigation is an unexpected reaction product synthesized by Manuel Kretschmer and Benedikt Crone from the group of Dr. Stefan F. Kirsch from "Chair of Organic Chemistry" at the Technische Universität München. They were conducting the reaction shown in Figure 5.11. but did not receive any expected product. Unfortunately, the structure elucidation for the major reaction product turned out to be impossible by standard techniques, as will be shown in the beginning of this chapter. After all standard techniques failed, the idea was born to solve this problem with the help of RDCs.

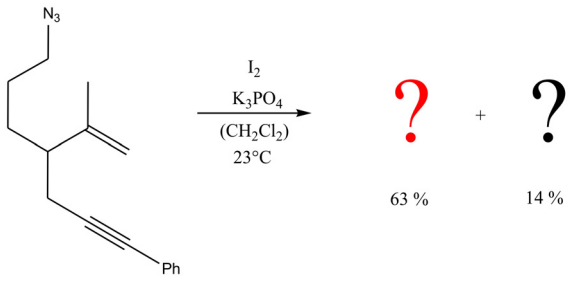

Figure 5.11.: Reaction scheme for the formation of the unknown compound.

5.3.2 Analyzing the Unknown Compound by Classical Methods

Initial characterization of the unknown reaction product included mass spectrometry (MS), infrared spectroscopy (IR) and the acquisition of 1D NMR spectra. The first revealed the chemical composition to be $C_{16}H_{18}IN$ ($m/z = 351$ $[M^+]$), the second suggested no NH- or NH_2-group as corresponding absorption bands were missing in the spectrum. 1D NMR spectra supported this findings: in the proton spectrum the 5 protons of a phenyl group, a singlet with

integral 3 around 1.2 ppm for a methyl group and 10 aliphatic protons with resonances between 1.8 and 3.5 ppm could be observed; in the carbon spectrum 8 signals between 10 and 60 ppm, one signal around 95 ppm and 5 signals between 125 and 150 ppm (therefore one more than the expected 4 signals for the phenyl group) are present. (For spectra see Appendix.)

Figure 5.12. A shows the aliphatic region of a standard HSQC recorded on the substance. Clearly the 10 aliphatic protons belong to 5 methylene groups and except for the phenyl-ring (signals not shown) there is no CH-group in the molecule. This was of special interest from the chemical point of view, as in contrast the educt possesses a CH-group, which therefore must be involved in the reaction.

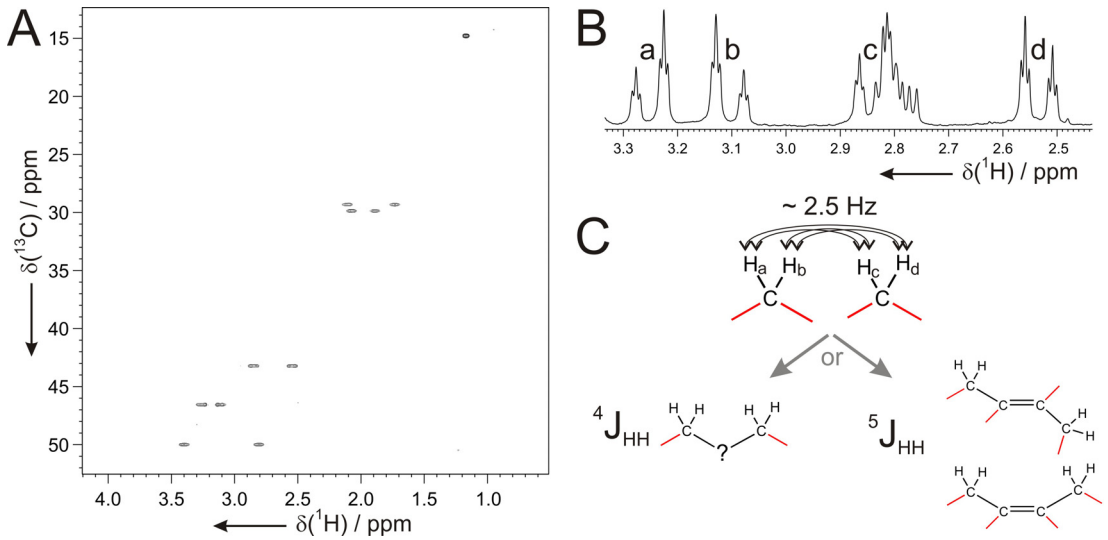

Figure 5.12.: Selected NMR spectra for the unknown major reaction product. In the aliphatic region of a standard HSQC spectrum (A) the methyl group and five methylene groups can be identified. The aromatic region showing three signals for a phenyl-ring is not shown. In the enlargement of the ^{1}H-1D-spectrum (B) the 4 signals for aliphatic protons a, b, c, and d show all pseudo-triplets with a coupling of ≈ 2.5 Hz (and doublets with the large geminal coupling). Hence each of the 4 protons has not only the $^{2}J_{HH}$-coupling to the proton within the same methylene group, but also two small J_{HH}-couplings to *both* protons of the other methylene group (C). Those might be $^{4}J_{HH}$-couplings or $^{5}J_{HH}$-couplings in an olefinic system.

In a COSY spectrum, three of the five methylene groups could be correlated to build an enclosed spin system and therefore a chain of subsequent CH_2-groups. Between the two remaining methylene groups very weak cross peaks could be observed in the COSY. This is due to small proton-proton couplings of about 2.5 Hz between each of the 4 protons with the two protons of the other methylene group, respectively. This can best be seen in the enlargement of the ^{1}H-1D-spectrum as

shown in Figure 5.12. B. As both couplings to the protons of the other CH_2-group are that small, they can not be $^3J_{HH}$-couplings between neighboring groups. Therefore they must be either $^4J_{HH}$-couplings, and hence the two methylene groups are connected via one unknown hetero atom, or $^5J_{HH}$-couplings in an olefinic system[213] (see Figure 5.12. C).

Figure 5.13. A sums up the analysis as described so far, by showing the molecule's fragments as known out of 1D proton, 1D carbon, COSY, and HSQC spectra. Note that there are five quaternary carbon atoms.

A standard NMR analysis would also include the acquisition of an HMBC spectrum and in this case a $^1H,^{13}C$-HMBC as well as a $^1H,^{15}N$-HMBC have been acquired. However, the analysis of these experiments was not at all conclusive. In the $^1H,^{13}C$-HMBC altogether 58 signals have been detected, among them 21 signals within the fragments as shown in Figure 5.13. A and 37 signals correlating different fragments. In the $^1H,^{15}N$-HMBC 8 signals have been detected, leaving only one of the methylene groups without a correlation to the nitrogen atom (this being the one in the middle of the $-CH_2-CH_2-CH_2-$ chain). Thus, both HMBC spectra are correlating almost every known fragment with every other one and no conclusion about the connection of the fragments can be drawn. In addition one should keep in mind, that a missing cross peak in an HMBC spectrum does not necessarily indicate that the corresponding spins are far apart, but only that their coupling is small.

In order to connect the known fragments, a 2D 1,1-ADEQUATE spectrum[214] was acquired. This experiment uses magnetization transfer via $^1J_{CC}$ and $^1J_{CH}$ couplings and thus correlating neighboring carbon atoms. Five additional carbon-carbon bonds (see Figure 5.13. B) could be detected, reducing the number of fragments. However, as a 1,1-ADEQUATE spectrum is proton detected, no correlations between two quaternary carbons can be made. As the molecule possesses five quaternary carbons this leaves a lot of possible bonds undefined. An additional problem are the two methylene groups for which still one connection is missing (see Figure 5.13. B), as it is not clear whether these signals are simply missing in the 1,1-ADEQUATE spectrum due to a bad transfer via not well matching coupling constants, or whether these methylene groups are connected with the nitrogen atom. Altogether there are still too many possible structures to solve the constitution of the molecule.

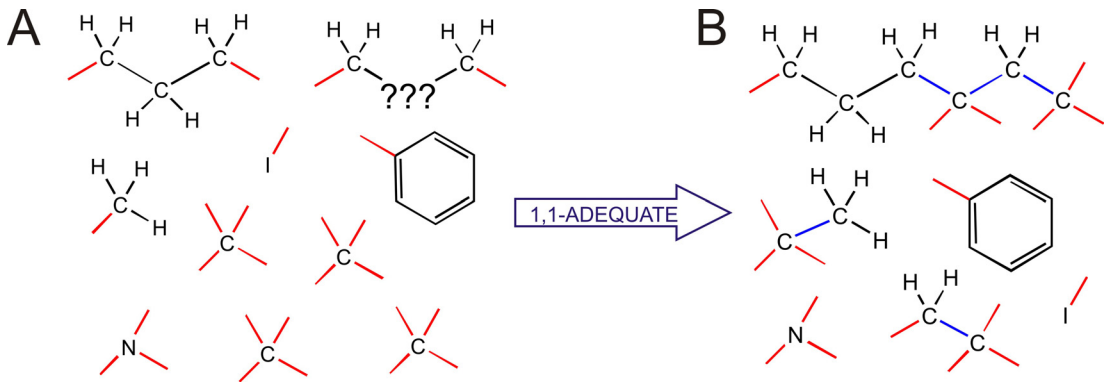

Figure 5.13.: Fragments of the unknown reaction product as analyzed by NMR spectroscopy. The information drawn out of 1D proton, 1D carbon, COSY, and HSQC spectra lead to the 10 fragments shown in (A). By the acquisition of a 1,1-ADEQUATE spectrum, those 10 fragments can be reduced to 6 fragments, as five carbon-carbon-correlations (shown in blue) have been detected (B). Red bonds indicate an unknown connection to another fragment.

Attempts have been made to connect the known fragments by the signals detected with the HMBC spectra under the assumption that every cross peak is due to a $^{2}J_{XH}$, $^{3}J_{XH}$, or $^{4}J_{XH}$ coupling, independent of the intensity of the cross peak. However, no structure could be obtained which made sense in terms of any imaginable reaction mechanism or in terms of carbon chemical shifts to be expected.

In summary, the structural analysis with classical methods failed. Main problems are the high number of quaternary carbons which could not be correlated and the high number of HMBC correlations which indicate that the product has a bridged cyclic structure.

5.3.3 New Approach for the Determination of a Molecule's Constitution

After classical NMR analysis failed, the idea came up to solve the constitution of the molecule with the help of RDCs. As discussed in chapter 2.6.2, RDCs are a suitable tool to verify a proposed structural model. In chapters 5.1 and 5.2 two examples for this have been shown, in which the tested structural models have been different diastereomers or structural conformers of the same molecule. The principle of excluding all wrong structural models and verifying only one of the proposed structures should also work if the tested structures are different molecules in terms of different constitutions.

There are two conditions which must be fulfilled for successfully applying this method. On one hand, the experimental data must be sufficient enough to exclude all wrong structures, and on the other hand, the correct structure must be among all tested. These conditions must be fulfilled in every case, and the first is simply achieved by the acquisition of many different RDCs. The latter one is usually no problem in the analysis of configurations, as simply all possible diastereomers are used as input-structures, like it has been done in chapters 5.1 and 5.2. However, for different constitutions, the probability to miss one potential structures is far higher, as by hand it is hardly manageable to create all possible structures in a systematic way. Therefore, for the analysis of the constitution of a molecule, special attention must be paid when creating the set of input structures. Obviously the method is going to fail, if the correct structure is not among all tested.

5.3.4 RDCs Measured for the Unknown Compound

For the measurement of residual dipolar couplings, the compound has been aligned in a stretched polystyrene/chloroform gel. The corresponding scalar couplings have been measured in a chloroform solution sample.

In order to measure one-bond CH-RDCs, CLIP-HSQC spectra[107] have been acquired for the isotropic and anisotropic sample. Two-bond HH-RDCs between the geminal protons of methylene groups have been obtained from corresponding P.E.HSQC spectra.[114] (For all couplings and chemical shifts measured on the substance see Appendix.)

Altogether 17 RDCs have been obtained for the structural analysis: 10 one-bond CH-RDCs in the 5 CH_2-goups, 1 one-bond CH-RDC for the *para*-CH-group in the phenyl-ring, 5 two-bond HH-RDCs within the 5 CH_2-goups, and 1 one-bond RDC for the methyl group. For the latter one, the corresponding CH-coupling has been converted[125] to either a CC or a CN coupling, depending whether the methyl group is attached to a carbon or a nitrogen atom in the corresponding structural model.

5.3.5 Structural Models Used for RDC Analysis

To build the group of tested input-structures for the SVD-fittings, Dr. Stefan Kirsch was asked to create all structures he can think of, which fulfill the following criteria: The molecular formula $C_{16}H_{18}IN$ must be satisfied, the molecule must

contain a chain of three methylene groups and two isolated methylene groups as well as a phenyl-ring and an isolated methyl-group, four more quaternary carbons and a tertiary nitrogen. These conditions are basically those drawn out of the analysis of 1D, COSY and HSQC spectra (see Figure 5.13. A). Furthermore the molecule should be somehow reasonable in terms of the educt of the reaction. Dr. Kirsch came up with the molecules depicted in Figure 5.14., which therefore served as tested structures.

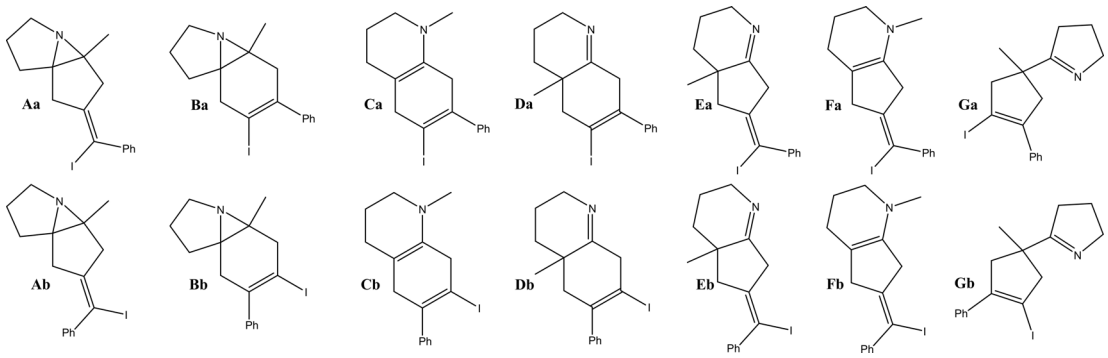

Figure 5.14.: Potential reaction products suggested for the reaction shown in Figure 5.11. and composed out of the fragments shown in Figure 5.13. A. Structures have been named using a two-letter-code which will be used in the following to identify the different molecules. The phenyl-ring is abbreviated by Ph.

For none of the 14 suggested reaction products, there is the possibility for a diastereomer, which would enlarge the number of structures to be tested. The 14 input-structures for the unknown compound were created and energy-minimized using the program Sybyl.[204] The structural models were then used as input for the program PALES[128, 129] for fitting experimental RDC data. Within the fitting process, all prochiral assignments for the five methylene groups have been permutated, leading to $2^5 = 32$ fits for each of the 14 structures. Furthermore the assignment of the two isolated methylene groups was varied as this assignment would not been known on the basis of the 1D, COSY and HSQC spectra only. (With the 1,1-ADEQUATE spectrum in hand, it is defined which of the two isolated CH_2-groups is which one in the suggested structures. However it should be demonstrated, that the acquisition of the 1,1-ADEQUATE spectrum would not have been necessary for solving the structure by RDCs.) The number of fits therefore increases to 64 for each suggested molecule, leading to a total number of $64 \bullet 14 = 896$ fits.

5.3.6 Fitting Results

To compare this incredible amount of fitting-data, the quality factor n/χ^2 has been calculated for each fit. Then the highest n/χ^2 value for each structure has been selected among the 64 fits with permutated assignment. In Figure 5.15. the results are summarized by showing n/χ^2 for the best permutation of each of the 14 structures.

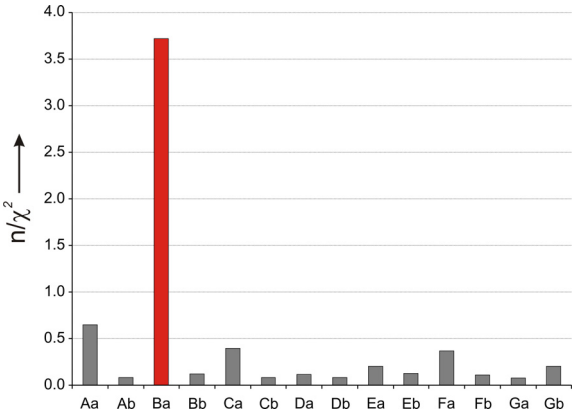

Figure 5.15.: Comparison of quality factors n/χ^2 for the SVD-fits done with PALES.[128, 129] For each of the 14 structures altogether 64 different permutations of the assignment have been fitted and only the one with the best n/χ^2 value is shown here. Structure **Ba** is the only one with an n/χ^2 value larger than 1.

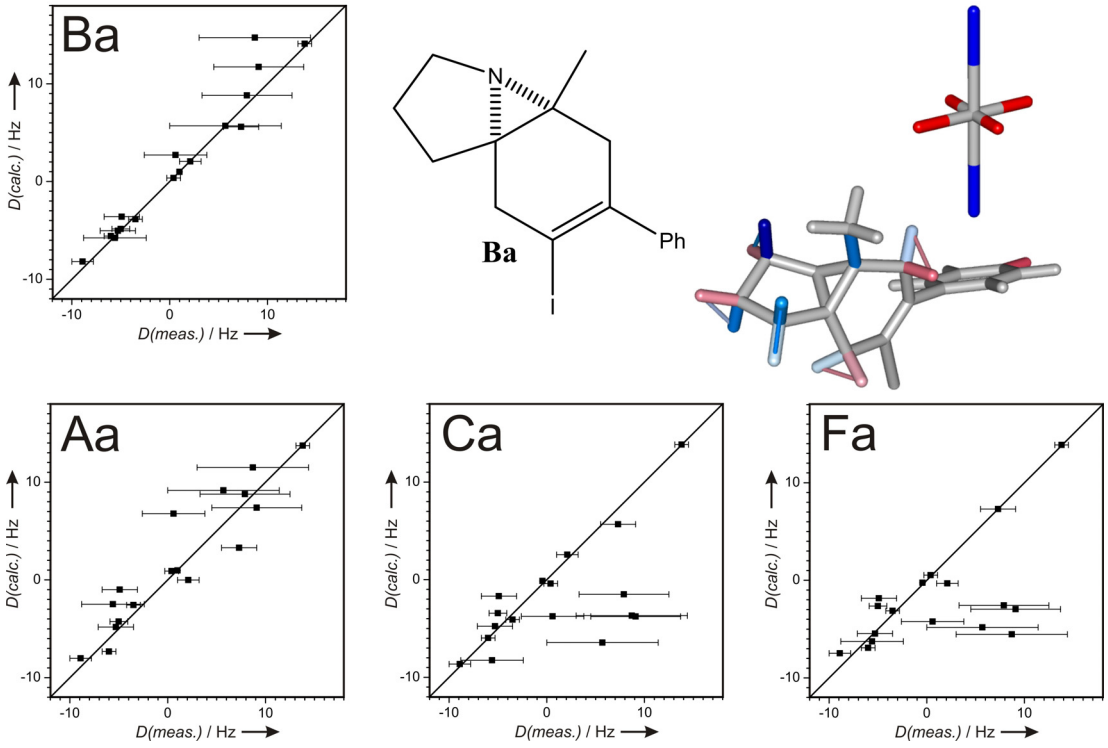

Figure 5.16.: Comparison of back-calculated and experimental RDCs for the fits with best n/χ^2 value. The structure **Ba** (top, middle) has not only the best n/χ^2 value, but shows also a reasonable good correlation between measured and calculated couplings (top, left), while the data do not correlate for the structures **Aa**, **Ca** and **Fa** (bottom). The structural model of **Ba** is depicted with color-coded bonds (red: negative; blue: positive RDCs) and the axis of the corresponding alignment tensor next to it (top, right).

Clearly only structure **Ba** has a reasonable high n/χ^2 value which is far higher than for all other structures. If one compares back-calculated and experimental RDCs for the four structures (and the corresponding permutation of assignment) with the best n/χ^2 value, it becomes evident too, that only for structure **Ba** a good correlation is existent (see Figure 5.16.). Therefore all structures other than **Ba** can be excluded, and **Ba** can be considered as the correct structural model for the unknown reaction product.

5.3.7 Discussion of Previous Data and Verification of the Constitution

In retrospective, it is interesting why the classical analysis failed. As described in chapter 5.3.2, it was tried to find possible structures on the basis of the fragments obtained from 1D, COSY, HSQC, and ADEQUATE spectra (see Figure 5.13. B) and the data from the HMBC spectra. For this, all cross peaks in the $^{1}H,^{13}C$-HMBC spectrum have been assumed to originate from $^{2}J_{CH}$, $^{3}J_{CH}$, or $^{4}J_{CH}$ couplings, but the obtained structures made no sense in terms of reaction mechanism or chemical shifts to be expected. Also the identified structure **Ba**, was not among them and the reason for excluding it were two pronounced HMBC signals between both protons of a methylene group and a carbon atom of the phenyl-ring. In retrospective, these cross peaks originate from $^{5}J_{CH}$-couplings (see Figure 5.17. A). The signals are especially unexpected, as the phenyl-ring is rotating, which can be concluded from the identical chemical shifts of both *ortho*- and *para*-carbons as well as hydrogens.

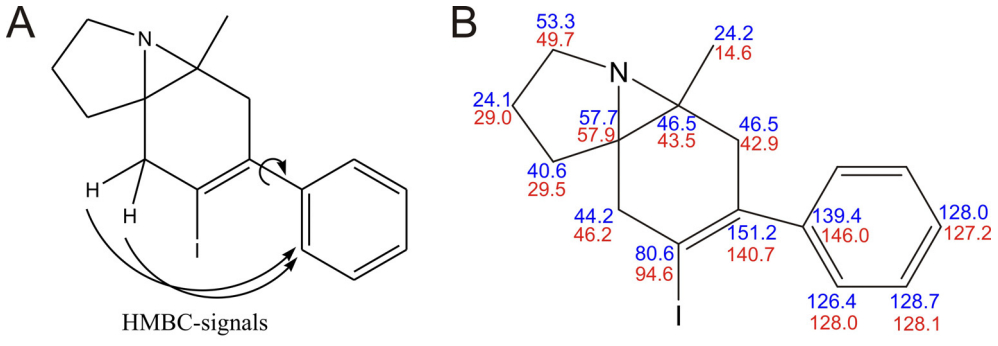

Figure 5.17.: Reasons for the failure of classical NMR analysis. The HMBC signals between two protons of a methylene group to the *ortho*-carbons of the phenyl-ring were not expected, especially as the phenyl-ring probably rotates fast around its carbon-carbon bond (A). The carbon chemical shifts predicted by ChemDraw[215] (blue), are partly far apart from the experimental values (red) measured for the unknown reaction product (B). Chemical shifts are given in ppm.

However, if it would not have been the HMBC signals, the structure **Ba** would probably have been excluded in a classical analysis due to the chemical shifts. Carbon chemical shifts measured for the compound differ up to 14 ppm from shifts predicted by the NMR-prediction of ChemDraw.[215] Altogether 4 of 16 carbon chemical shifts differ about 10 ppm or more from predicted values (see Figure 5.17. B), which shows how unreliable such chemical shift prediction is for bridged cycles, as the spatial arrangement of the atoms is not considered.

As this was the first example for the determination of a molecules constitution with the help of RDC analysis, efforts were made to verify the obtained result with alternative methods. Therefore a 2D INADEQUATE spectrum[216-218] was acquired for the substance. This was only possible after the students of Dr. Stefan Kirsch synthesized the incredible amount of almost 100 mg of the substance. Out of this experiment, which cost 3 days of spectrometer time, three additional carbon-carbon connections could be identified, which are all in agreement with the determined structure (see Figure 5.18. A). Additional evidence could be obtained by labeling the educt of the reaction with ^{15}N-azide and taking a ^{13}C-1D spectrum of the resulting ^{15}N-labled product. In this spectrum all carbon resonances coupled to the ^{15}N are split to a doublet and therefore indicate that the corresponding carbon atoms are only one or two bonds apart from the nitrogen. Observed carbon-nitrogen couplings are shown in Figure 5.18. B and all of the five correlations are in agreement with the structure determined by RDCs.

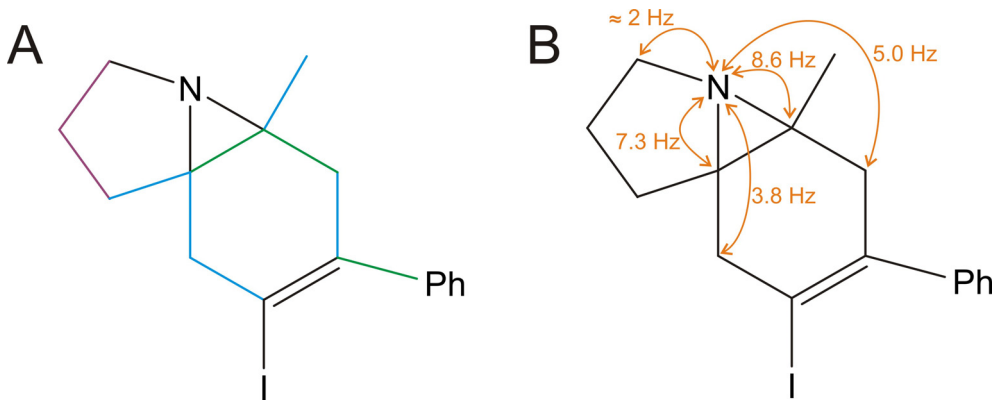

Figure 5.18.: Additional evidence for the correct determination of the constitution. (A) The INADEQUATE spectrum could reveal three carbon-carbon bonds (shown in green) additional to those known from the analysis of COSY (purple) and ADEQUATE spectra (blue). (B) The ^{15}N-isotope labeling of the molecule enabled the identification of five nitrogen-carbon coupling constants, which are all in agreement with the determined structure.

5.3.8 Conclusion

For the unknown reaction product investigated in this chapter, it was shown for the first time, that RDCs might be a helpful tool to determine the constitution of a molecule. Initial structural analysis by mass spectrometry, infrared spectroscopy and classical NMR experiments like 1D, COSY, HSQC, HMBC, and ADEQUATE spectra led to no conclusion for the constitution of the compound. In contrast, the fit of 17 experimental RDCs against a set of potential structures selected only one to be consistent with the measured values. The determined constitution was supported by additional data obtained by ^{15}N-labeling of the substance and the acquisition of a 2D INADEQUATE spectrum.

As discussed in detail, two conditions must be fulfilled for the successful application of this method: enough experimental data must be available to exclude all wrong structures and the correct structure must be among all tested. For the first condition, further improvements in the technique of partial alignment and further development for the measurement of RDCs will help to make more experimental data available. Especially the reliable extraction of long-range RDCs will be necessary for the successful application of the technique to molecules with less one-bond RDCs in reach, e.g. molecules with less protons. For the second condition, it would be helpful to use programs which automatically generate possible structures e.g. on the basis of known fragments, the molecular formula or even experimental data. Therefore the further development of programs like COCON[219, 220] would be highly desirable. With the help of such programs the probability of missing the correct structure when building the set of proposed structures could be reduced.

To make the method widely applicable, it would also be necessary to automatize the generation of the input files, especially the generation and energy minimization of the structures, as well as the fitting procedure itself, especially the permutation of potentially ambiguous assignments. Furthermore the evaluation of fits in terms of calculating and comparing quality factors, should be simplified. If these practical aspects are further improved, this very general technique might be widely used.

This project was done in cooperation with the group of Dr. Stefan F. Kirsch (TUM, Munich): Dipl. Chem. Manuel Kretschmer did the first synthesis for the compound and Dipl. Chem. Benedikt Crone resynthesized the substance in a larger scale and with ^{15}N-labeling.

Results presented in this chapter have not yet been published.

5.4 Cross-Fitting of RDCs

5.4.1 Introduction and Motivation

As outlined already, the five independent components of the alignment tensor can be derived by mathematical methods like the singular value decomposition (SVD) if a set of at least 5 independent RDCs is available and if the molecule can be considered as rigid. As long as considerably more then 5 independent RDCs are given, this method can be used for the assignment of prochiral groups and/or for the configurational or conformational analysis of rigid molecules. Problems arise when the number of RDCs for fitting is not sufficient to unambiguously differentiate between different structural models. The situation gets significantly worse if flexible parts of a molecule must be taken into account.

Therefore alternative approaches, which work for a smaller set of RDCs, are desirable. In this project, the method of cross-fitting anisotropic parameters, this means the transfer of structural information between molecules with similar alignment properties, was investigated. The general idea of cross-fitting will be lined out and tested for the configurational analysis of steroids as model structures. Its potentials and limitations as well as its advantages over other approaches will be discussed in detail.

5.4.2 The General Idea of Cross-Fitting RDCs

Probably the most elegant and effective solution to the problem of a limited set of RDCs would be the prediction of alignment from first principles. This would theoretically allow distinguishing different structural models, e.g. diastereomers, by a single measured, decisive RDC.

Many attempts have been made to predict the alignment of a molecule by considering steric[128] and electrostatic[163] interactions between the solute and the alignment medium, as it is for example done in PALES ("-stPales" option).[129] Other methods consider inherent properties of the solute molecule like its tensor of gyration.[164, 165] The prediction of alignment works well for large biomacromolecules like proteins or DNA. However, for small molecules it often fails because the effects of the fine-structure of the alignment medium and corresponding dynamics play a much more important role.

A different approach is the use of RDCs of a molecule of known, very similar structure for a cross-fit with the RDCs from the molecule of interest. This idea was first used by Ziani et al. for the identification of absolute configuration using RQCs measured for a similar molecule of known stereochemistry.[166] As the alignment and therefore RDCs are strongly influenced by steric and electrostatic interactions of the solute with the polymer of the alignment medium, the molecule used for cross-fitting should possess very similar overall shape and charge distribution and the dynamic behavior of the molecules should also match. If such a molecule is available, cross-fitting of RDCs should allow the differentiation of diastereomers even in the case of otherwise insufficient RDC data.

The cross-fitting approach can in principle be implemented in two ways: RDCs of the cross-fitting molecule can either be used to calculate an alignment tensor which is then applied to the solute of interest, or the couplings can be compared directly. This means, if only the conservation of a specific part of the molecule shall be tested, a direct comparison of RDCs of this specific part should lead straightforwardly to the desired result without complicated fittings to an orientational model.

In the following it should be tested in how far the hypothesis of cross-fitting is applicable to real molecules.

5.4.3 Two Steroids as Model Compounds

Steroids have been selected as test molecules for the cross-fitting approach for several reasons. Firstly, steroids in general play a very important role in chemistry, biology, and medicine, where many drugs are based on the steroid scaffold.[221-223] Secondly, they build a large group of molecules which differ in both configuration and substituents while they conserve the overall molecular shape determined by the four fused rings. The ring system contains also highly rigid parts as well as a relatively flexible five-membered ring. This makes steroids an ideal system to study the principle of cross-fitting.

As representative steroids the commercially available cholesterol and 5-α-cholestan-3-one have been chosen. The structure of 5-α-cholestan-3-one is mainly determined by the keto-group and the fully saturated ring system (see Figure 5.19.). In contrast, cholesterol contains a double bond in ring B which bends the ring system and leads to a distinct variation in structure. Otherwise the two

molecules have identical substituents and their overall shape can be considered to be quite similar.

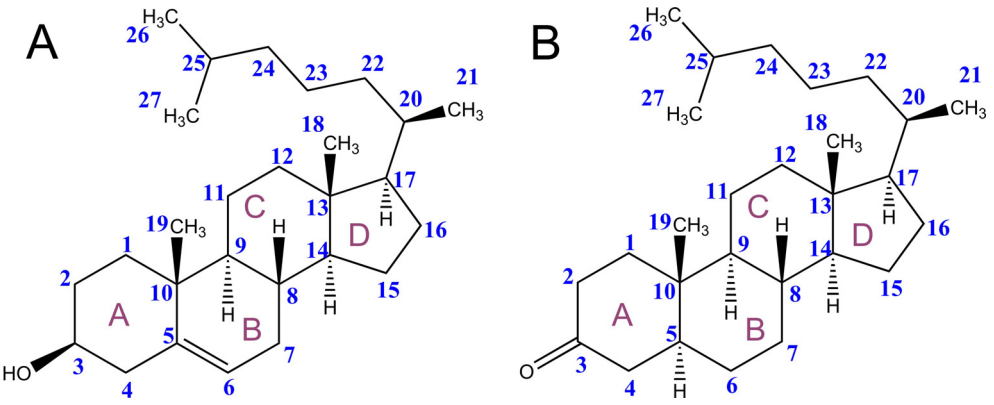

Figure 5.19.: Structure and numbering of cholesterol (A) and 5-α-cholestan-3-one (B).

Furthermore, in steroids the problematic lack of sufficient RDC-data might arise due to the small range in chemical shifts. Most NMR signals appear in the region between 15 ppm and 40 ppm in ^{13}C dimension and between 0.5 ppm and 2.0 ppm in ^{1}H dimension, respectively (see Figure 5.20.). This does not only lead to signal overlap but might also cause immense strong coupling artifacts which prevent a reliable extraction of coupling constants. In addition, the chair-like structure of six-membered rings in steroids reduces the number of independent RDCs as all axial CH-bonds are practically parallel. Therefore it might well happen that RDC-data measured on steroids are not sufficient for a desired configurational analysis. As will be shown in the following, cross-fitting of RDCs can overcome this problem.

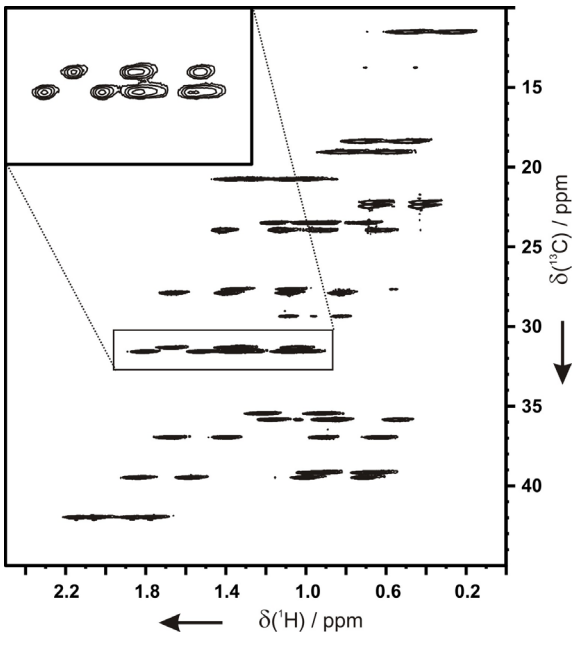

Figure 5.20.: Aliphatic region of the CLIP-HSQC spectrum[107] acquired on cholesterol in a stretched PDMS/$CDCl_3$ gel. Almost all steroid signals appear in a very narrow spectral range causing signal overlap and strong coupling artifacts. As an example of signal overlap the inset shows five doublets: C2-H2α, C2-H2β, C7-H7α, C7-H7β, and C8H8.

5.4.4 RDC Measurements

The assignment of all NMR resonances (see Appendix) has been achieved by standard COSY, HSQC and ADEQUATE spectra performed on ≈ 31 mM samples of both steroids in $CDCl_3$. The isotropic samples were also used to measure scalar couplings. Anisotropic samples were prepared in the new stretching apparatus introduced in chapter 4.2: PDMS sticks[67] were swollen inside the Kalrez® 8002UP tube with a solution of 150 µl $CDCl_3$ and 16 mg of the corresponding steroid. The elastomer tube of the device was then stretched accordingly for obtaining equivalent alignment strength for both samples. The alignment strength was measured by the quadrupolar splitting of the deuterated solvent $CDCl_3$ and was adjusted to be 30.2 Hz for the cholesterol sample and 30.8 Hz for the 5-α-cholestan-3-one sample, respectively.

$^1H,^{13}C$ one-bond couplings and homonuclear $^1H,^1H$ couplings between geminal protons in CH_2-goups were measured, as they contain the most easily accessible RDCs. For the measurement of $^1J_{CH}$ and $^1T_{CH} = {}^1J_{CH}+D_{CH}$ the CLIP-HSQC and CLAP-HSQC pulse sequences[107] have been used. The coupling constants were extracted by selecting a slice of the CLIP-HSQC at the appropriate carbon frequency and manually shifting a copy of the slice until the corresponding multiplet components were centered with respect to each other (see chapter 2.5.3 Figure 2.13.). For overlapping signals of a CH_2-group the IPAP-approach was used as described by Enthart et al.[107]

$^2T_{HH}$ couplings were measured using the P.E.-HSQC pulse sequence.[114] The coupling constants were extracted from resulting spectra by selecting two slices at the appropriate carbon frequencies of one signal and manually shifting them until the corresponding multiplet components were centered with respect to each other. The sign of the $^2T_{HH}$ is given by the tilt of the multiplet (see chapter 2.5.3 Figure 2.12.).

RDCs were then calculated from the difference of couplings measured in the anisotropic sample and couplings measured in the isotropic sample (see Appendix for all couplings and Table 5.3. for RDCs of both steroids). In the case of cholesterol 16 $^1D_{CH}$ and 7 $^2D_{HH}$ couplings and for 5-α-cholestan-3-one 21 $^1D_{CH}$ and 8 $^2D_{HH}$ couplings could be extracted within the four rings. Additional 9 $^1D_{CH}$ couplings for the flexible side chain of each steroid were extracted. Missing couplings could not reliably be extracted due to signal overlap or strong coupling artifacts.

Table 5.3.: Comparison of $^{1}H,^{13}C$ one-bond RDCs measured on cholesterol and 5-α-cholestan-3-one in similarly stretched PDMS/$CDCl_3$ gels.

Group[a]	$^{1}D_{CH}$ (exp) cholesterol	$^{1}D_{CH}$ (exp) 5-α-cholestan-3-one
C19-H19	-6.6 ± 0.6	-7.2 ± 0.8
C18-H18	-7.0 ± 0.6	-7.2 ± 0.5
C16-H16a	0.3 ± 5.8	-1.9 ± 5.8
C16-H16b	5.1 ± 5.8	8.5 ± 5.4
C15-H15a	-[b]	11.6 ± 5.1
C15-H15b	14.0 ± 5.8	14.0 ± 5.1
C7-H7β	14.2 ± 5.8	4.1 ± 5.0
C7-H7α	-[b]	25.9 ± 1.5
C8-H8	20.7 ± 8.5	27.2 ± 1.0
C2-H2α	11.3 ± 3.9	6.9 ± 3.2
C2-H2β	16.1 ± 3.9	21.1 ± 3.2
C1-H1β	9.0 ± 1.4	7.3 ± 1.2
C1-H1α	18.2 ± 1.4	20.7 ± 1.7
C12-H12α	22.4 ± 1.4	27.4 ± 1.6
C12-H12β	5.1 ± 1.4	4.3 ± 1.1
C9-H9	23.6 ± 4.0	23.7 ± 1.1
C21-H21	-4.9 ± 0.6	-5.0 ± 0.7
C25-H25	10.8 ± 0.9	11.4 ± 0.8
C20-H20	23.3 ± 1.1	23.3 ± 1.0
C27-H27	-0.2 ± 0.4	-0.5 ± 0.4
C26-H26	0.2 ± 0.4	0.2 ± 0.4
C23-H23a	18.1 ± 5.1	20.5 ± 8.2
C23-H23b	5.2 ± 2.7	8.5 ± 8.5
C22-H22a	25.6 ± 6.4	26.7 ± 5.8
C22-H22b	8.7 ± 10.4	8.7 ± 5.1

[a] Methylene protons marked with a, b indicate that prochiral assignment is not available. Protons marked with α or β are assigned following standard steroid nomenclature.
[b] Couplings not extracted due to signal overlap or strong coupling artifacts.

5.4.5 Calculation and Comparison of Alignment Tensors

For the cross-fitting of RDCs between different molecules the assumption that both molecules possess the same alignment tensor must be fulfilled in a good approximation. Therefore, first the alignment tensors of both steroids under investigation have been calculated for comparison. For this the "-bestFit" option of PALES[128, 129] (SVD-fit) was applied to fit measured RDCs to structural models of cholesterol and 5-α-cholestan-3-one that were created and energy-minimized using the program Sybyl.[204]

RDCs measured in the five-membered rings (D-ring) did not fit to back-calculated RDCs, which was expected as the flexible rings most likely experience a different orientational averaging and therefore a different average alignment compared to the rigid part of the steroids. As a result, the number of RDCs used for SVD calculations was reduced to 18 for cholesterol and 23 for 5-α-cholestan-3-one, respectively.

Since the prochiral assignment of methylene groups were not known a priori, a permutation of all prochiral protons was performed, resulting in 16 and 64 structural models for cholesterol and 5-α-cholestan-3-one, respectively. The best fit, as measured by the correlation factor n/χ^2, leads to the prochiral assignment for the entire molecule.

As expected, for both molecules corresponding alignment tensors could be calculated with high precision and measured RDCs of the rigid parts fit well with the back-calculated values. (see Appendix for back-calculated couplings and alignment tensor parameters). A comparison of both calculated alignment tensors shows that they are very similar, as can also be seen in Figure 5.21. Hence, this essential condition for the applicability of the cross-fitting approach is fulfilled.

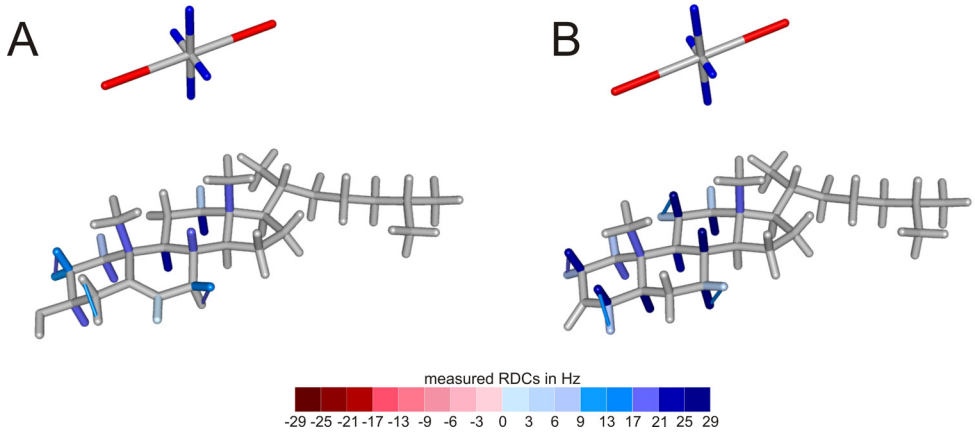

Figure 5.21.: Structures of cholesterol (A) and 5-α-cholestan-3-one (B) with color-coded bonds representing negative (red) and positive (blue) RDCs. The axes of the corresponding alignment tensors are drawn next to the structural models. Apparently the alignment tensors of both steroids are very similar but not fully identical.

5.4.6 Cross-Fitting RDCs via the Alignment Tensor

As the alignment tensors of both steroids in the stretched PDMS/$CDCl_3$ gels are almost identical, a fit of measured RDCs for one of the molecules using the alignment tensor of the other molecule should also lead to a good agreement between measured

and back-calculated RDC data. To test this both steroids have been cross-fitted to the alignment tensor derived for the other steroid using the PALES option for a user supplied order matrix ("-saupe" option).[128, 129]

As expected, the quality factors of the corresponding fits drop compared to the direct fit with the PALES "-bestFit" option (from $n/\chi^2 = 5.42$ to 0.59 for cholesterol and from $n/\chi^2 = 1.13$ to 0.26 for 5-α-cholestan-3-one). However, measured and back-calculated RDCs are still in very good agreement and deviations are small. For cholesterol fitted against the alignment tensor of 5-α-cholestan-3-one this can be seen in Figure 5.22. C with the comparison of the corresponding direct SVD-fit in Figure 5.22. A. Detailed results on the fittings and analog Figures for 5-α-cholestan-3-one fitted against the alignment tensor of cholesterol can be found in the Appendix.

Generally, this result can be seen as direct proof of principle for the cross-fitting approach based on the alignment tensor as the orientational model for rigid parts of molecules.

5.4.7 Differentiation of Diastereomers by Cross-Fitting RDCs

After this proof of principle, it was tested in how far the cross-fitting approach would be applicable to identify the correct relative configuration of an unknown molecule. Therefore measured RDCs were cross-fitted against a potential diastereomer of one steroid using the alignment tensor of the other steroid to see if fitting results would be able to differentiate the correct diastereomer from a false one.

10-α-cholesterol has been chosen as a diastereomer of cholesterol, which has an inverted chiral center at carbon atom C10. A structural model of 10-α-cholesterol has again been created and energy-minimized with the program Sybyl.[204] For comparison, experimental RDCs measured on cholesterol have been directly fitted against the structure of 10-α-cholesterol with the "-bestFit" option and cross-fitted with the fixed orientation of the alignment tensor derived for 5-α-cholestan-3-one using the "-saupe" option of PALES. Again the protons of all prochiral methylene groups were permutated as their assignment was considered to be unknown and the best permutation was selected for comparison.

Plots of RDCs measured on cholesterol and back-calculated for 10-α-cholesterol with the two methods can be seen in Figure 5.22 B and D along with the deviation of

the RDCs mapped to the structural model. Comparing the results with those for the cholesterol structure (Figure 5.22 A and C), one can clearly differentiate the correct diastereomer cholesterol from the wrong diastereomer 10-α-cholesterol.

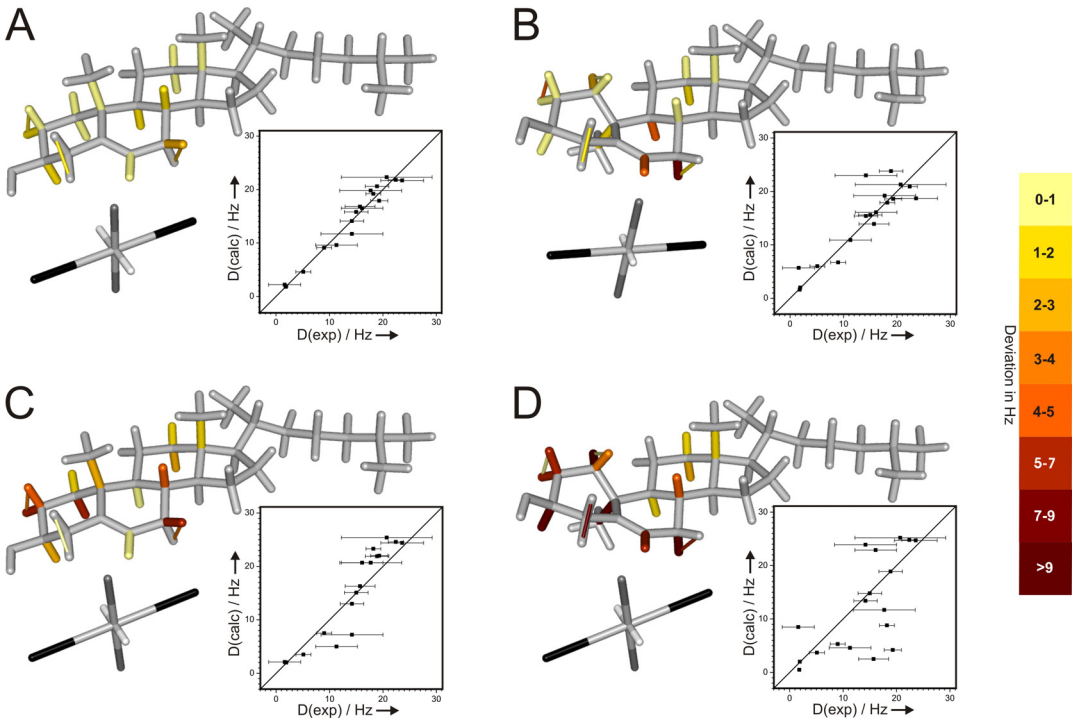

Figure 5.22.: Comparison of SVD-fits (top) and cross-fitting results (bottom) for cholesterol (left) and its potential diastereomer 10-α-cholesterol (right). For each fit a plot of calculated vs. experimental RDCs and the corresponding structure with color-coded bonds denoting the deviation between measured and back-calculated RDCs are shown. The corresponding alignment tensors are visualized with their principal axis systems (black: A_{zz}; gray: A_{yy}; white: A_{xx}). Experimental RDCs measured on cholesterol have been SVD-fitted against the structural models of cholesterol (A) and 10-α-cholesterol (B) using the "-bestFit" option of PALES. For cross-fitting the alignment tensor derived from 5-α-cholestan-3-one was used as orientation to calculate RDCs for the structures of cholesterol (C) and 10-α-cholesterol (D).

In an analog way RDCs measured on 5-α-cholestan-3-one have been fitted against the structure of its potential diastereomer 5-β-cholestan-3-one with both methods. Results for this fits can be seen in analogous Figures in the Appendix. Also in this case the correct diastereomer could clearly be distinguished from the wrong one.

However, it should be mentioned that differentiation of diastereomers for the two steroids works with both methods: cross-fitting and conventional RDC-based configurational analysis for which RDCs are directly fitted to the structural models of

the diastereomers. It therefore can be concluded that if there is a sufficient number of RDCs for fitting available, a reliable differentiation between diastereomers is generally possible with either approach.

5.4.8 Differentiation of Diastereomers with Reduced RDC Data

If the number of available RDCs is reduced, the situation can change significantly as the reliability of the alignment tensor of a direct SVD fit might be strongly decreased.

For the simulation of this effect the number of RDCs used for fitting have been successively reduced. Out of the 18 measured RDCs of cholesterol, various subsets of 15, 12, 9, 8, 7 and 6 RDCs were generated by random selection of RDC-combinations. As with a decreasing number of RDCs within a subset the influence of the actual composition of the subset increases, it was decided to create the more subsets the less RDCs are contained within the subsets. The hope was to get an overall trend for what happens to the fitting quality with a decreasing number of RDCs (See Appendix for the actual combinations of RDCs in the used subsets).

Altogether 54 subsets of RDCs measured for cholesterol have been built and fitted to the structures of cholesterol and 10-α-cholesterol in order to differentiate the correct diastereomer. For comparison both methods have been used: SVD-fitting and the cross-fitting with the alignment tensor given by 5-α-cholestan-3-one. For each subset and structure again all possible permutations for prochiral methylene groups were performed and the one with the best fitting result in terms of highest n/χ^2 value was chosen.

A summary of the results is shown in Figure 5.23. which compares n/χ^2 values for the direct SVD-fits (top) and the cross-fitting against the alignment tensor of 5-α-cholestan-3-one (bottom) for both diastereomers and different RDC-subsets.

One can clearly see the breakdown of the SVD approach with a decreasing number of RDCs: although n/χ^2 rises from an initial value on the order of 1 for all 18 RDCs to over 1000 if only 6 RDCs are used for the fitting routine (actually indicating a better fit to the structure), this rise is artificial since the lower number of restraints more easily allows a good fit to the five degrees of freedom of the alignment tensor. In fact less RDCs are more easily fitted to a structure but this does not mean that the

fit reflects the real orientational behavior of the molecule. Considering that a fit with only 5 RDCs always gives a perfect match and therefore an infinitely high quality factor, it is no surprise that the quality factors increase with a decreasing number of RDCs. However, it becomes also obvious that one can not trust a fit with only few RDCs.

In this regard it is not surprising that also the differentiation of the two diastereomers fails with decreasing number of RDCs. For the randomly chosen subsets used in this study, the wrong diastereomer was favored for several combinations of 8, 7 and 6 RDCs. For one of the subsets with 9 RDCs and several combinations of 8, 7 and 6 RDCs a wrong permutation of the prochiral assignment for cholesterol was favored (marked in Figure 5.23. with an * for each wrongly assigned prochiral center).

The cross-fitting approach, instead, leads to a completely different behavior for a decreasing number of RDCs. First of all, the quality of the fit does not depend on the number of RDCs and n/χ^2 values are generally on the same order close to 1 and vary only slightly due to the actual composition of the subset. While the average molecular orientation is allowed to vary freely in the SVD approach, the alignment tensor is fixed by the full set of 21 RDCs of 5-α-cholestan-3-one in the cross-fitting case and the reliability of the alignment tensor is independent of the available number of RDCs of cholesterol.

As a consequence the full information content of the measured RDCs can be used for the differentiation of diastereomers and the correct diastereomer is favored for *all* randomly chosen subsets used for Figure 5.23. In addition it should be noted, that for each subset the correct prochiral assignment of cholesterol is reflected in the fits.

The cross-fitting approach, in principle, will allow distinguishing the diastereomers even with less than 5 RDCs. However, its comparison with the SVD-fit makes only sense for more than 5 RDCs. It is also evident that with a decreasing number of RDCs the actual composition of the subset of RDCs becomes more and more important. As can be easily derived from Figure 5.22. D by looking at the coupling deviations of individual RDCs, almost any RDC measured in the A-ring will be sufficient to differentiate the correct from the wrong diastereomer, while the whole set of RDCs of the C-ring will not lead to conclusive results.

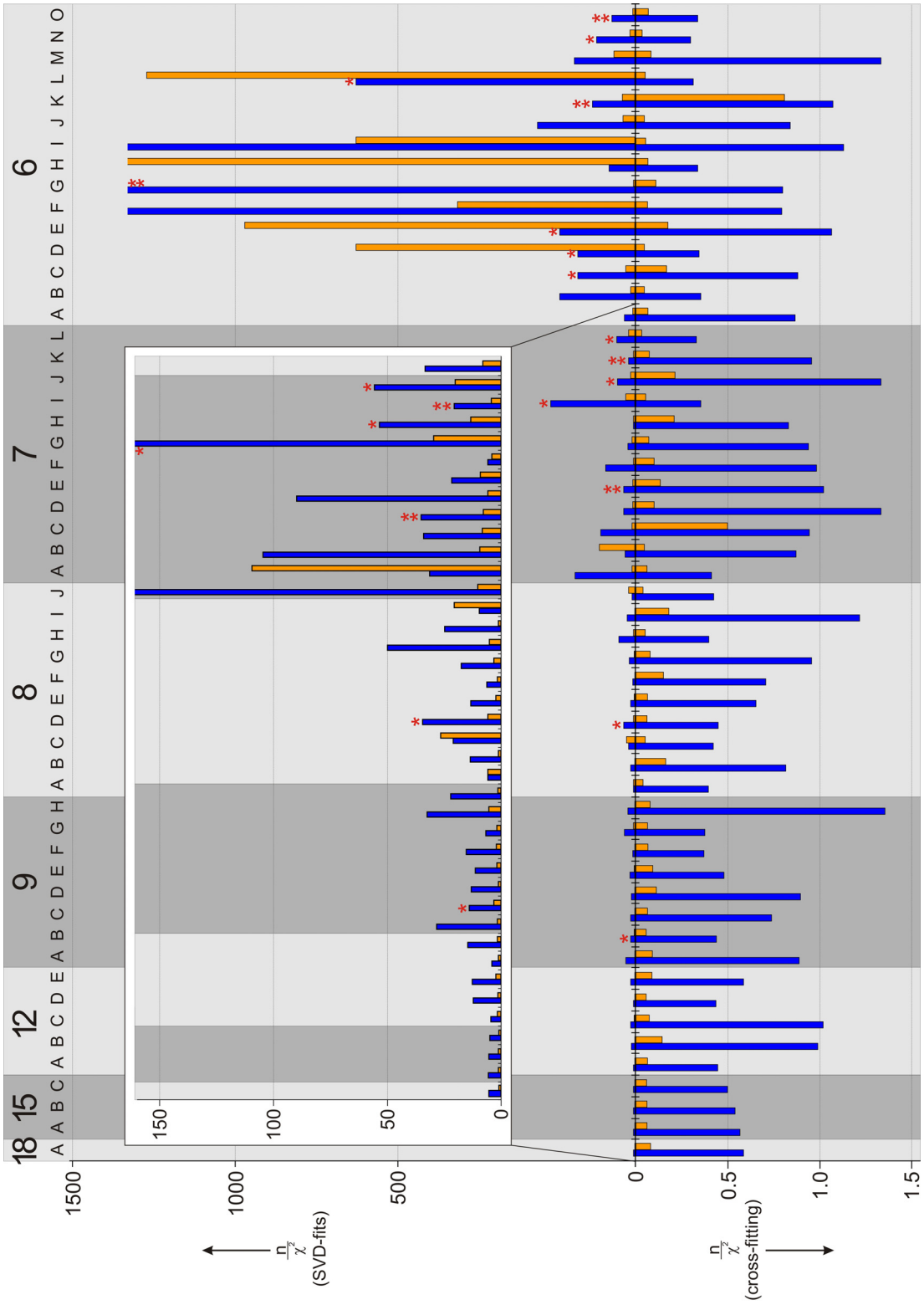
18 15 12 9 8 7 6
A B C D E F G H I J K L M N O
1500
1000
500
0
150
100
50
0
0
0.5
1.0
1.5
$\frac{n}{\chi^2}$ (SVD-fits)
$\frac{n}{\chi^2}$ (cross-fitting)

Figure 5.23. (previous page): Differentiation of diastereomers with reduced sets of RDCs. Compared are quality factors n/χ^2 obtained for the direct SVD-fitting method (top) and the cross-fitting approach (bottom) using subsets of RDCs measured on cholesterol for fitting against the structures of cholesterol (blue) and 10-α-cholesterol (orange). RDC-data was reduced by building various subsets of the 18 measured RDCs with 15, 12, 9, 8, 7 and 6 RDCs. The individual subsets are marked with letters (15A-C, 12A-E, 9A-H, 8A-J, 7A-L, 6A-O) for which the corresponding RDC combinations can be found in the Appendix. For each fit the prochiral assignment of CH_2-groups was permutated and only the fit with the best result is shown here. For each asterisk (*) one methylene group was obtained with incorrect prochiral assignment for the best permutation. Fewer RDCs for the SVD-fitting lead to highly unreliable results and strongly increased n/χ^2 values, while the cross-fitting approach maintains the correct differentiation of diastereomers and prochiral assignments even for sparse data.

5.4.9 Comparison with Other Methods

As mentioned before, RDC prediction would be the most elegant way of deriving the alignment tensor of a given molecule. However, established methods only work for large proteins but often fail for small molecules. In addition, the prediction of alignment is highly susceptible to flexible parts, whose influence on the induced orientation is generally overestimated by static approaches.

The two steroids investigated here do not contain any charged groups and their orientation is most certainly dominated by the relatively rigid ring systems. They therefore represent almost ideal candidates for predicting the alignment tensor by the prediction routine of PALES[128] ("-stPales" option).

However, RDCs predicted by PALES for the whole steroid structure fit only reasonably to the measured RDCs. The situation improves, when the steroid structure is shortened at the flexible side chain attached to C17, as was found out by stepwise shortening and subsequent prediction of alignment (for details see Appendix). For cholesterol best prediction results were achieved with the cholesterol fragment C1-C24 (cholesterol shortened by C25, C26 and C27 and adjacent protons) with a very good n/χ^2 value of 3.29. For 5-α-cholestan-3-one prediction was best for the fragments C1-C23 (shortened by C24, C25, C26 and C27 and adjacent protons) and C1-C20 (shortened by the whole side chain) with n/χ^2 values of 0.92 and 0.87, respectively. Obviously the influence of the flexible side-chain is overestimated and better results are therefore achieved after shortening the side chain. However, the optimal length of the flexible side chain for the PALES prediction differs even in this

case of two very similar molecules, showing how unreliable and unpredictable the method is.

More problems with the PALES prediction arise when the interaction between solute and alignment medium is not purely steric but charges need to be considered. The PALES prediction performed for sodium cholate, for example, does not at all reflect RDCs measured for sodium cholate in PAA/D_2O[148] (see Appendix). Considering how difficult and unreliable an accurate RDC-prediction with currently available methods is, cross-fitting appears to be the superior approach whenever applicable.

5.4.10 Direct Cross-Fitting of RDCs in Flexible Parts

The cross-fitting via an alignment tensor allows the indirect comparison of RDCs measured even in differing parts of two similar molecules. However, quite often it is only necessary to transfer e.g. the assignment of prochiral groups. Furthermore, it might be desirable to identify signals in a flexible part for which the alignment tensor approach is not applicable. As has been shown previously for residual quadrupolar couplings by Ziani et al.,[166] the anisotropic couplings can in this case directly be transferred between two molecules with very similar orientational behavior without the detour over an orientational model.

A comparison between RDCs measured on cholesterol and 5-α-cholestan-3-one (see Table 5.3.) leads to a unique assignment for practically all prochiral protons with the exception of C7-H7 close to the structural difference in ring B. Furthermore, a comparison of the RDCs measured within the flexible side chain (carbon atoms C20 to C27) reveals a striking match of RDCs measured for the two molecules.

For more or less identical parts of two molecules that fulfill the conditions for cross-fitting, the direct comparison of anisotropic NMR parameters like RDCs therefore must be considered as a highly effective tool to obtain an assignment or to independently verify a given assignment. Especially for molecules like the presented steroids with many signals within narrow chemical shift ranges this can be very useful as the potentially slightly better resolution for closely related compounds can be directly used by transferring corresponding RDCs.

5.4.11 Limitations and Potentials

In contrast to methods for prediction of alignment from first principles, the cross-fitting approach does not need to consider structural details or charges of the alignment medium, as the orientational information is taken from experimental data. However, a number of conditions must be fulfilled: both the molecule of interest and the molecule used for cross-fitting RDCs must be rather similar in their overall shape and charge distribution, and RDCs must be measured for both molecules in the same alignment medium. Otherwise the cross-fitting of RDCs will fail.

The influence of the alignment medium and/or the influence of the molecule's charge distribution might be seen when comparing experimental data measured on sodium cholate in PAA/D_2O[148] with the data acquired on cholesterol and 5-α-cholestan-3-one in PDMS/$CDCl_3$. Sodium cholate is another molecule with steroid scaffold, but in contrast to the other steroids it is charged. In Figure 5.24. the three steroids are shown with the axes of their alignment tensors as derived by the SVD-fit of the corresponding experimental RDCs. The alignment of cholesterol and 5-α-cholestan-3-one in PDMS/$CDCl_3$ is fairly different compared to that of sodium cholate in PAA/D_2O and therefore the cross-fitting approach in this case would not work. Notably the prediction of alignment with PALES does also not work for the charged sodium cholate (see chapter 5.4.9 and Appendix).

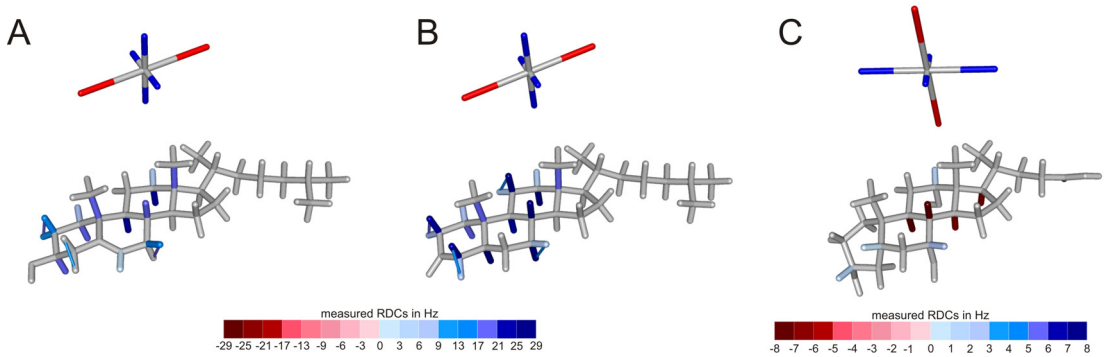

Figure 5.24.: Comparison of alignment tensors for steroids in different alignment media. RDCs have been measured for cholesterol (A) and 5-α-cholestan-3-one (B) in stretched PDMS/$CDCl_3$ gels and for sodium cholate (C) in a compressed PAA/D_2O gel. The structures are shown with color-coded bonds representing negative (red) and positive (blue) RDCs and the axes of the corresponding alignment tensors next to it. The alignment is considerably different due to the influence of the alignment medium and/or the influence of the molecule's charge distribution.

It should be mentioned, that cross-fitting based on an alignment tensor requires rigid or at least partly rigid molecules, as only for those an alignment tensor is well-defined. The method, however, should be extendable to flexible molecules by the use of more general mean-field descriptions of orientational properties.

By directly comparing RDCs from a reference molecule with the molecule of interest, flexibility has no influence on the results as long as the molecules show similar dynamic behavior. The success of the method therefore is not limited by the cross-fitting approach in general, but by finding a reference molecule of known structure with sufficient similarity to the molecule of interest.

5.4.12 Conclusion

In this chapter, the cross-fitting approach as a general tool was discussed in detail. It was shown that structural information obtained from anisotropic parameters can be transferred between similar molecules, using the example of 5-α-cholestan-3-one and cholesterol. It was demonstrated, that the alignment of the two steroids cholesterol and 5-α-cholestan-3-one in stretched PDMS/$CDCl_3$ gels is rather similar and that it is therefore possible to use the alignment tensor derived for one of the molecules to fit the RDCs of the other one. As has been shown in detail, cross-fitted RDCs can be used to unambiguously distinguish diastereomers of the two measured compounds even in the case of massively reduced RDC datasets.

The approach of cross-fitting RDCs can also be applied without the detour of fitting an alignment tensor but by directly comparing RDCs of a known reference molecule with RDCs from the solute of interest. In this case no restriction in terms of rigidity of the molecules applies and molecules can be compared even when no overall alignment tensor can be defined.

General limitation of the approach is the necessity of a known reference molecule with sufficiently similar structure and dynamic behavior.

This project was done in cooperation with B.Sc. Sebastian Schmitt (TUM, Munich) who helped throughout the whole project, especially by writing some useful scripts for fitting and illustration of fitting results.

Results presented in this chapter have been published:

Grit Kummerlöwe; Sebastian Schmitt; Burkhard Luy: '*Cross-Fitting of Residual Dipolar Couplings*' in *The Open Spectroscopy Journal* **2010**, *4*, 16-27.

6 Summary

NMR spectroscopy is an indispensible technique to determine the structure of organic molecules. However, classical NMR methods often fail, as only short-ranged structural information can be gained. The investigation of anisotropic NMR parameters can, in many cases, help to overcome these problems, as those parameters contain angular information relative to an external reference.

Within the scope of this work the large field of NMR in anisotropic environments was covered in terms of developing new techniques for the measurement of anisotropic parameters and applying them to the structural analysis of organic molecules. In this respect, fundamental research merged with actual questions of the chemist's everyday life. This thesis is dealing with the following important aspects of anisotropic parameters for structural analysis:

1. development of new alignment media for small organic molecules
2. development of tools to adjust and vary defined alignment strengths
3. improvement of the analysis for the case of scarce experimental data

The adaptability of the newly developed methods has been audited with several examples of structural analysis for molecules of different origin. The discussion of these examples has been used to reveal crucial interrelationships between experimental parameters, data evaluation, and problems to be solved.

A crucial point for the measurement of anisotropic parameters is the availability of adequate alignment media to partially align the molecule of interest. Within this thesis a number of novel, gel-based alignment media were developed closing several gaps in the variety of already existing media. All the developed alignment media belong to the class of stretched polymer gels, which have several advantages over other classes of alignment media like e.g. liquid crystals.

One of the gaps was related to the most important solvent in pharmaceutical NMR, dimethylsulfoxide (DMSO). Only few alignment media for DMSO existed and all of them suffered from major disadvantages. In chapter 3.1 of this thesis, stretched gels of cross-linked poly(acrylonitrile) (PAN) were introduced as a new medium to partially align DMSO soluble compounds. The commercially available linear polymer was cross-linked by irradiation with accelerated electrons. The resulting cross-linked PAN has excellent swelling properties in DMSO, and the gels show only a few broad

NMR signals. As the developed alignment medium is uncharged and compatible with peptides, natural products and other molecules, it is widely applicable and meanwhile has become the favored alignment medium for small to medium-sized molecules soluble in DMSO.

One common problem for most of the existing alignment media is their contribution to acquired ^{1}H-spectra as they generally introduce undesired NMR-signals which can result in severe overlap with signals of the molecule of interest. Especially at low solute concentrations the intense proton signals of the alignment medium cause problems, as the sensitivity of the spectrometer has to be adjusted to the most intense signal. Perdeuterated alignment media can be considered as a general approach to circumvent this problem. Hence, one scope of the present thesis was to examine the potential of cross-linked deuterated polymers as alignment media. Two examples, cross-linked deuterated polystyrene (dPS) and cross-linked deuterated poly(acrylonitrile) (dPAN) have been introduced. The two gels have been synthesized, characterized, and successfully applied as alignment media for several molecules, as described in chapter 3.2 and chapter 3.3 of this thesis. While dPS is suitable for apolar organic solvents like chloroform, dichloromethane, benzene, dioxane, or tetrahydrofurane, dPAN is compatible with polar organic solvents like DMSO or DMF, and thus the two deuterated polymers already cover the most important solvents for the analysis of small organic molecules.

The fourth alignment medium developed within this thesis is of special interest, because it is able to distinguish enantiomers. Although many of the existing alignment media possess stereogenic centers, only media with a chiral super structure are referred to as chiral alignment media since only those are capable of distinguishing enantiomers. A variety of chiral alignment media for organic solvents is known. In water, the triple helical gelatin forms a chiral hydrogel which is especially interesting because of its unbeatable low price. However, there was no chiral alignment medium known suitable for pure DMSO as the solvent. Within this thesis, this gap could be successfully closed by the covalent cross-linking of gelatin which was achieved by irradiation of gelatin with accelerated electrons. This so-called e^{-}-gelatin is not only suitable for pure DMSO as the solvent, but also enlarges the applicable temperature range of conventional gelatin/water gels, as the latter are solely formed by hydrogen bonds and hence melt for temperatures above about 35°C. In chapter 3.4 it has been shown, that e^{-}-gelatin/water and

e^--gelatin/DMSO gels are able to distinguish chiral and prochiral centers and therefore can be used for the estimation of enantiomeric excess.

Furthermore cross-linked poly(ethylene oxide) (PEO) was developed as alignment medium which covers a very broad range of solvents, ranging from water over polar organic solvents (including DMSO, methanol, acetonitrile) to apolar organic solvents (including dioxane, THF, DCM, chloroform, benzene). The first results for PEO presented in chapter 3.5 are very promising, however, preparation of the cross-linked gels is difficult and has yet to be improved. Moreover, some additional work in terms of characterization of the alignment medium has to be done, before PEO gels will probably be the most widely applicable alignment media.

In order to get spectra with the best possible resolution while being able to precisely measure RDCs, it is crucial to have the optimal alignment strength: if the partial alignment of the molecule of interest is too strong this will result in broad lines and hence extraction of RDCs will be difficult. If, on the other hand, the partial alignment is too weak, RDCs will be averaged to very small values and hence might not be sufficiently larger than the experimental error. It is therefore necessary to carefully adjust the alignment strength. With the newly developed gel based alignment media, it is usually possible to achieve different degrees of alignment by varying the chain length of the polymer, the amount of cross-linking or other parameters. However, this always requires the preparation of a new sample, which is material and time consuming or might even be impossible. Therefore it is desirable to change the strength of alignment in a single sample.

In chapter 4.1 it was described how this is achieved in a stretching device based on a flexible silicone tube which works as an expandable container for the aligning gel that gets automatically stretched, when the silicone tube is expanded. It has been shown that this apparatus can be used to stretch different gels based on water or DMSO as the solvent. For different examples it was demonstrated, that due to the linear scaling of the measurable anisotropic parameters with the extension of the gel, RDCs can be measured with a higher accuracy.

Furthermore the stretching device has been significantly improved by replacing the silicone tube with a flexible tube of the perfluoroelastomer Kalrez® 8002, which extends the approach to the full range of gel based alignment media because of its general resistance to basically all solvents. In addition, the specially produced

Kalrez® 8002UP tube by DuPont Elastomers is gas-tight and does not contribute to NMR spectra because it does not contain any protons. The application of this important technique has been described in chapter 4.2.

Several examples for the application of RDCs for structural analysis have been given, which demonstrate that the newly developed alignment media and stretching devices significantly improve the possibilities of RDC measurements.

Configurational analysis has been carried out in chapter 5.1 for the formerly unknown, main degradation product of the key bitter compound in hop products. This compound named tricyclocohumol has been isolated from aged beer samples and the constitution of the tricyclic compound was identified by MS and NMR. However classical NMR parameters like $^{3}J_{HH}$ couplings and NOE/ROE data failed in the determination of the correct (relative) configuration of all 5 stereogenic centers. Main problems were the ambiguous prochiral assignment of the methylene protons and the quaternary carbons which interrupt the chain of short-ranged information. Only with the analysis of RDCs measured in a dPAN/DMSO gel the relative configuration of tricyclocohumol could be solved. For this analysis, the structures of all possible diasteromers of tricyclocohumol including all possible prochiral assignments have been fitted against the experimental RDC values. Only one model was found to be consistent with experimental values and hence the configuration along with the correct prochiral assignment has been unambiguously determined.

Furthermore, configurational and conformational analysis was done for the natural product staurosporine as described in chapter 5.2. The four different possible diastereomers, each in its chair and boat conformation, have been fitted against the RDCs measured on staurosporine in a stretched gel of cross-linked deuterated polystyrene. Clearly the structure also found for a crystallized derivate of staurosporine was favored in the RDC analysis and can therefore be considered as the correct structure in chloroform solution.

The first application for the determination of a molecule's constitution, was described in chapter 5.3. For the unknown reaction product of a novel reaction, classical analysis by MS, IR and NMR spectra like ^{1}H and ^{13}C 1D, COSY, NOESY, ROESY, HSQC and HMBC spectra, did not help to solve the constitution. Main problems were the five quaternary carbons and the tertiary nitrogen, which could not be correlated unambiguously and the overwhelming number of HMBC cross-peaks,

correlating every heteronucleus with almost every proton and therefore giving no conclusive connection of the molecule's atoms. Even an 1,1-ADEQUATE experiment could not solve the problem because of the high number of quaternary carbons. The analysis of 17 RDCs measured in a stretched polystyrene/chloroform gel could solve these structural problems. Therefore, experimental RDCs have been fitted against structures proposed on the basis of the reaction, the molecular formula and simple NMR spectra. As expected for a sufficient set of RDCs only one of the suggested structural models gave a good correlation between experimental and back-calculated couplings and thus, can be considered as the correct structure. The determined constitution of the unknown reaction product has later on been confirmed by the acquisition of an INADEQUATE experiment and the ^{15}N-isotope-labeling of the substance.

The general approach of cross-fitting RDCs between structurally similar molecules has been explored in the last chapter of the thesis. For two steroids it has been demonstrated, that their alignment induced by the same alignment medium is similar enough to use the alignment tensor calculated for one of the molecules to back-calculated RDCs for the other one with a good agreement to experimental values. This approach of cross-fitting RDCs could be used to distinguish potential diastereomers of the steroids. The differentiation between correct and wrong stereochemistry turned out to be even possible, when the set of experimental data was significantly reduced. In contrast, other methods, like the conventional SVD-fitting or the prediction of alignment from first principles, are not suited for the problem of insufficient RDC data. Therefore the cross-fitting approach, as demonstrated in detail, overcomes several limitations of classical RDC analysis.

7 Appendix

7.1 List of Abbreviations and Symbols

1D, 2D, 3D	one- / two- / three-dimensional
A	alignment tensor
Å	Ångström, 10^{-10} m
ACN	acetonitrile
ADEQUATE	adequate sensitivity double-quantum spectroscopy
AIBN	azobisisobutyronitrile
B_0	static magnetic field (strength)
c	*cyclo*-
C	carbon atom
$C_{12}E_5$	pentaethylene glycol monododecyl ether
calc	calculated
CLIP-HSQC	clean-inphase-HSQC
COSY	correlated spectroscopy
CPMG	Carr-Purcell-Meiboom-Gill (relaxation filter)
CS	chemical shift
CSA	chemical shift anisotropy
D	dipolar coupling or dipolar splitting
DBP	dibenzoylperoxide
DCM	dichloromethane
DEPT	distorsion-less enhancement by polarization transfer (spectroscopy)
DMF	*N,N*-dimethylformamide
DMSO	dimethylsulfoxide
DNA	desoxyribonucleic acid
dPAN	deuterated PAN
dPS	deuterated PS
DVB	divinylbenzene
e^-	electron

exp	experimental
F1 / F2	indirect / direct NMR dimension
FID	free induction decay
h	hour(s)
H	hydrogen atom
HMBC	heteronuclear multiple bond correlation
HMQC	heteronuclear multiple quantum coherence
HPLC	high performance liquid chromatography
HSQC	heteronuclear single quantum coherence
Hz	Hertz
INADEQUATE	incredible natural abundance double quantum transfer experiment
IR	infrared (spectroscopy)
IUPAC	International Union of Pure and Applied Chemistry
J	scalar coupling constant
K	degree Kelvin
kGy	kilogray
LC	liquid crystalline (phase)
LC-MS	liquid chromatography mass spectrometry
M	molar
MD	molecular dynamics (simulation)
Me	methyl-
meas	measured
MeOH	methanol
MHz	megahertz
min	minutes
Mio	million
mL	milliliter
MM	molecular mechanics (calculations)
mM	millimolar
mm	millimeter
mmol	millimol
MS	mass spectrometry

MW	molecular weight
N	nitrogen atom
n/χ^2	quality factor
NMR	nuclear magnetic resonance (spectroscopy)
NOE	nuclear Overhauser effect
NOESY	nuclear Overhauser enhancement spectroscopy
O	oxygen atom
P	probability tensor
P.E.HSQC	primitive exclusive HSQC
PAA	poly(acrylamide)
PAN	poly(acrylonitrile)
PBLG	poly-γ-benzyl-L-glutamate
PCBLL	poly-ε-carbobenzyloxy-L-lysin
PCBP	4-*n*-pentyl-4'-cyanobiphenyl
PCS	pseudo contact shift
PDB	protein data bank
PDMS	poly(dimetylsiloxane)
PELG	poly-γ-ethyl-L-glutamate
PEO	poly(ethylene oxide)
Ph	phenyl-
PH-PDMAA	"Peter Haberz" dimethylacrylamide co-polymers
PMMA	poly(methyl methacrylate)
ppm	parts per million
PS	polystyrene
PU	polyurethan
PVAc	poly(vinyl acetate)
Q	quality factor by Cornilescu et al.
QM	quantum-mechanical (calculation)
R	correlation coefficient
RCSA	residual chemical shift anisotropy
RDC	residual dipolar coupling
RMS	root mean square
RMSD	root mean square deviation

ROE	rotating-frame Overhauser effect (peak volume)
ROESY	rotating-frame Overhauser effect spectroscopy
RQC	residual quadrupolar coupling
RT	room temperature
S	Saupe matrix
SAG	strain induced alignment in a gel
SVD	singular value decomposition
T	Tesla
T1 / T2	longitudinal / transversal relaxation times
TFE	trifluoroethanol
THF	tetrahydrofurane
TMS	trimethylsilyl- / trimethylsilane
TOCSY	total correlation spectroscopy
UV / VIS	ultraviolet / visible (spectroscopy)
vdW	van der Waals
°C	degree Celsius
δ	chemical shift
$\Delta\nu_Q$	quadrupolar splitting
µL	microliter
µM	micromolar
ν	frequency
Ξ	extension factor

7.2 Supplemental Material for Chapter 3.1

PAN-sticks and PAN/DMSO-d_6 solutions were irradiated with 10 MeV electrons generated by an industrial electron accelerator (*Beta-Gamma-Systems* in Saal an der Donau, Germany). Sticks and tubes were placed perpendicular to the electron beam during irradiation. The samples were irradiated by single irradiation doses of 40 kGy which took several seconds each. The time interval between two subsequent irradiation steps was approximately 10-15 min. Total irradiation doses of 120-480 kGy were applied.

For the preparation of PAN gels of the second generation, standard 5 mm NMR tubes and sylilated NMR tubes were used. Tubes were silylated by treatment with a 1:1 mixture of $ClSi(CH_3)_3$ and $Cl_2Si(CH_3)_2$ for 24 h at room temperature, and washed 3 times with dichloromethane before drying them at 50°C.

The following samples were used:

PAN gel for Figure 3.3.: PAN gel of the second generation. PAN with MW = 150000 g/mol was irradiated as 280 g/L DMSO-d_6 solution in a silylated NMR tube with a total irradiation dose of 320 kGy. After irradiation, additional DMSO-d_6 was added for swelling.

PAN gels for Figure 3.4.: PAN gels of the second generation. PAN with MW = 150000 g/mol was irradiated as ≈ 250 g/L DMSO-d_6 solution in silylated or not silylated NMR tubes with total irradiation doses of 280 kGy, 360 kGy, 400 kGy, or 480 kGy. After irradiation, additional DMSO-d_6 was added for swelling.

PAN gel for Figures 3.5., A2.3. and Tables A2.3., A2.4., A2.5.: PAN gel of the second generation. PAN with MW = 231000 g/mol was irradiated as 280 g/L DMSO-d_6 solution in a silylated NMR tube with a total irradiation dose of 240 kGy. After irradiation, additional DMSO-d_6 was added for swelling. 8 mg of the peptide *cyclo*(-D-Ala-Ala-Ala-(*N*Me)Ala-Ala-) were added after 21 days of swelling.

PAN gel for Figure 3.6.: PAN gel of the second generation. PAN with MW = 150000 g/mol was irradiated as 280 g/L DMSO-d_6 solution in a silylated NMR tube with a total irradiation dose of 480 kGy. After irradiation, additional DMSO-d_6 was added for swelling. 6.2 mg norcamphor were added after 165 days of swelling.

PAN gels for Figure 3.7. A: PAN gels of the second generation. PAN with MW = 150000 g/mol or MW = 231000 g/mol was irradiated as 280 g/L DMSO-d_6 solution in silylated NMR tubes with total irradiation doses between 120 kGy and 480 kGy. After irradiation, additional DMSO-d_6 was added for swelling.

PAN gels for Figure 3.7. B: PAN gels of the second generation. PAN with MW = 150000 g/mol was irradiated as 140 g/L, 210 g/L, or 280 g/L DMSO-d_6 solutions in silylated NMR tubes with total irradiation doses of 240 kGy, 400 kGy, or 480 kGy. After irradiation, additional DMSO-d_6 was added for swelling.

PAN gel for Figure 3.8. and Table A2.1.: PAN gel of the second generation. PAN with MW = 150000 g/mol was irradiated as ≈ 250 g/L DMSO-d_6 solution in a silylated NMR tube with a total irradiation dose of 400 kGy. After irradiation, additional DMSO-d_6 was added for swelling. 200 µL of a 1M norcamphor DMSO-d_6 solution were added after 20 days of swelling.

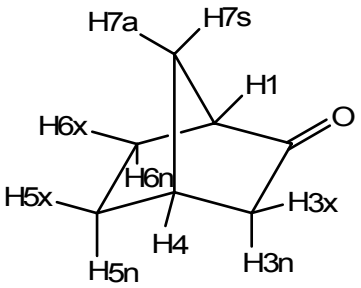

Figure A2.1.: Structure of norcamphor with nomenclature used in Table A2.1.

Table A2.1.: Assignment and measured one-bond couplings for norcamphor in isotropic DMSO solution and diffused into a PAN/DMSO gel with a quadrupolar splitting $\Delta\nu_Q$ of 21.1 Hz.[96]

Signal	$\delta(^{13}C)$ [ppm]	$\delta(^{1}H)$ [ppm]	$^{1}J_{CH}$ [Hz]	$^{1}J_{CH} + D_{CH}$ [Hz]	D_{CH} [Hz]
C1-H1	49.0	2.45	148.8 ± 0.2	145.4 ± 0.3	-3.4 ± 0.36
C3-H3x	44.4	2.01	128.1 ± 0.2	119.9 ± 0.5	-8.2 ± 0.54
C3-H3n		1.73	134.5 ± 0.3	128.6 ± 0.5	-5.9 ± 0.58
C7-H7s	36.8	1.67	133.5 ± 0.5	127.3 ± 0.5	-6.2 ± 0.71
C7-H7a		1.48	136.7 ± 0.5	143.6 ± 0.5	6.9 ± 0.71
C4-H4	36.8	2.57	144.8 ± 0.2	151.8 ± 0.3	7.0 ± 0.36
C5-H5x	34.6	1.71	131.9 ± 0.3	145.2 ± 1.0	13.3 ± 1.04
C5-H5n		1.48	133.2 ± 0.5	126.8 ± 0.3	-6.4 ± 0.58
C6-H6x	23.5	1.76	135.6 ± 0.3	130.7 ± 1.0	-4.9 ± 1.04
C6-H6n		1.35	134.1 ± 0.3	140.4 ± 0.7	6.3 ± 0.76

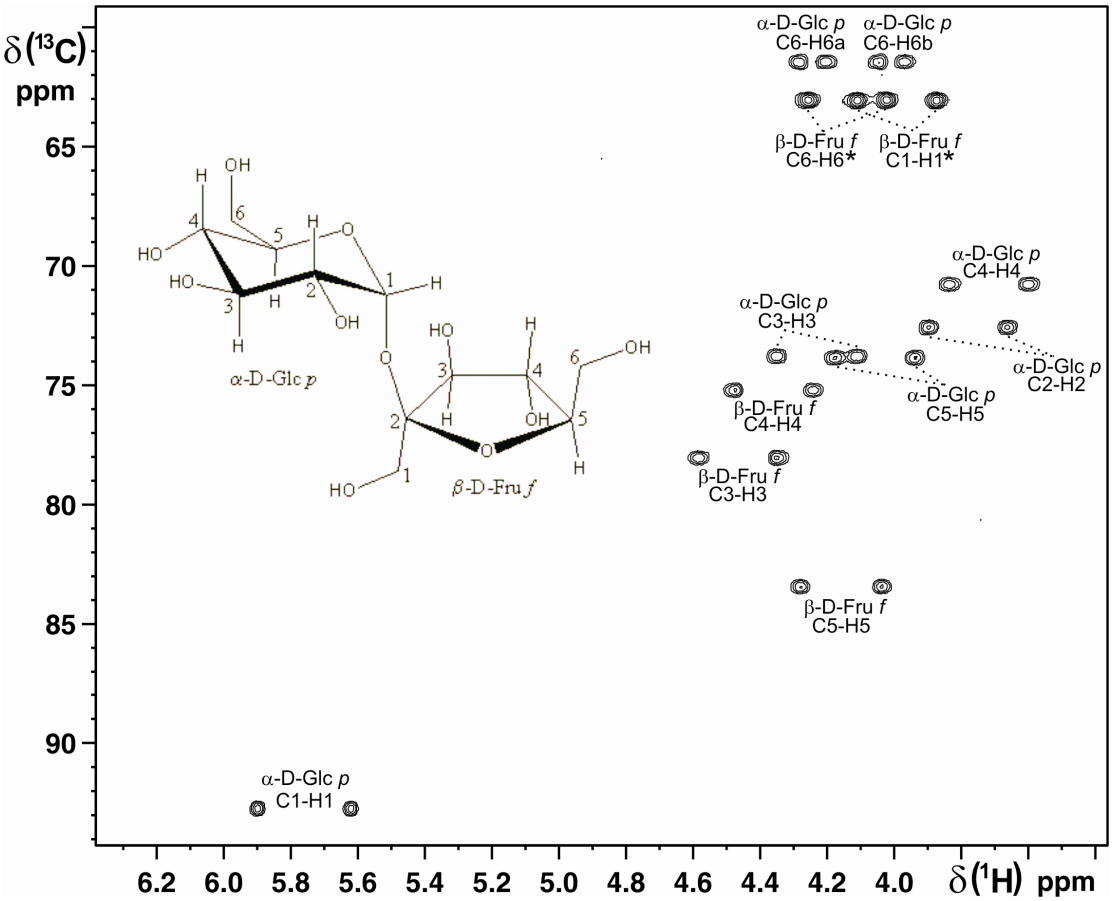

Figure A2.2.: $^{1}H,^{13}C$-CLIP-HSQC[107] of sucrose acquired inside a stretched PAN/DMSO gel with a quadrupolar splitting $\Delta\nu_Q$ of DMSO-d_6 of 40.4 Hz. The structure of sucrose with corresponding numbering of the carbon atoms is shown as inlet.

Table A2.2.: Measured one-bond couplings of sucrose in isotropic DMSO solution and diffused into a PAN/DMSO gel with a quadrupolar DMSO-d_6 deuterium splitting $\Delta\nu_Q$ of 40.4 Hz.

Signal		$^1J_{CH}$	$^1J_{CH}+D_{CH}$	D_{CH}
α-D-Glc*p*	C6-H6a	141.1 ± 0.5 Hz	133.3 ± 0.8 Hz	-7.8 ± 0.9 Hz
α-D-Glc*p*	C6-H6b	139.4 ± 0.5 Hz	151.5 ± 0.8 Hz	12.1 ± 0.9 Hz
(β-D-Fru*f*	C6-H6*[a]	140.7 ± 1.0 Hz	135.5 ± 0.6 Hz	-5.2 ± 1.2 Hz)
(β-D-Fru*f*	C1-H1*[a]	141.9 ± 0.3 Hz	144.9 ± 0.6 Hz	3.0 ± 0.7 Hz)
α-D-Glc*p*	C4-H4	141.7 ± 0.4 Hz	146.1 ± 0.5 Hz	4.4 ± 0.6 Hz
α-D-Glc*p*	C2-H2	141.1 ± 0.6 Hz	148.2 ± 0.3 Hz	7.1 ± 0.7 Hz
α-D-Glc*p*	C3-H3	143.5 ± 0.7 Hz	150.0 ± 0.8 Hz	6.5 ± 1.1 Hz
α-D-Glc*p*	C5-H5	143.3 ± 0.7 Hz	150.0 ± 0.8 Hz	6.7 ± 1.1 Hz
β-D-Fru*f*	C4-H4	144.2 ± 1.0 Hz	128.8 ± 0.5 Hz	-15.4 ± 1.1 Hz
β-D-Fru*f*	C3-H3	144.9 ± 1.0 Hz	126.2 ± 0.5 Hz	-18.7 ± 1.1 Hz
β-D-Fru*f*	C5-H5	146.2 ± 0.6 Hz	128.4 ± 0.5 Hz	-17.8 ± 0.8 Hz
α-D-Glc*p*	C1-H1	167.2 ± 0.4 Hz	182.5 ± 0.4 Hz	15.3 ± 0.6 Hz

[a] individual protons have not been resolved and measured RDCs can not be used for structural input

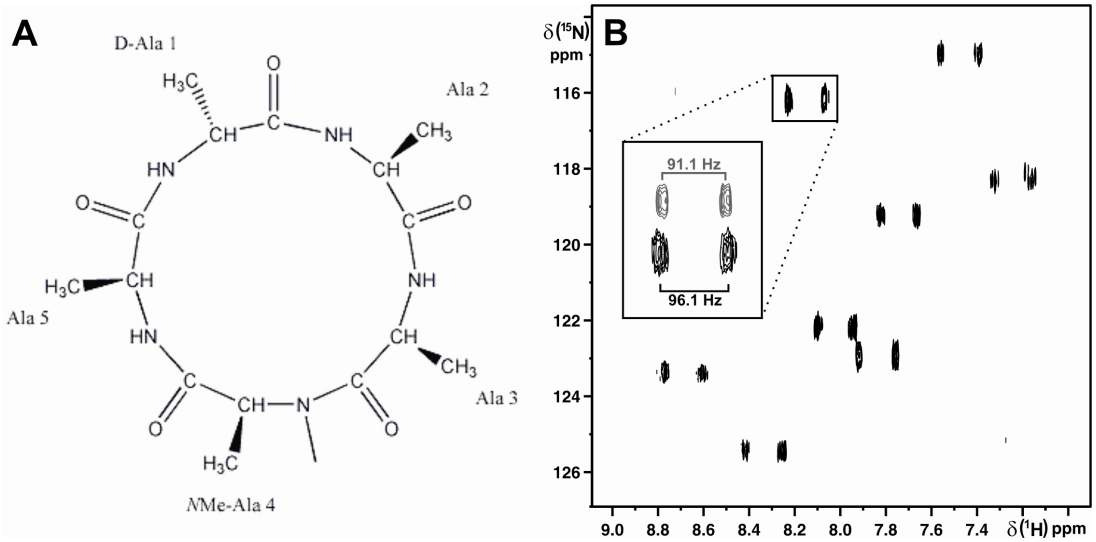

Figure A2.3.: Structure (A) and coupled $^{1}H,^{15}N$-CLIP-HSQC[107] (B) of the cyclic pentapeptide *cyclo*(-D-Ala-Ala-Ala-(NMe)Ala-Ala-) inside the PAN/DMSO gel with $\Delta\nu_Q$ = 21.2 Hz. The inlet compares the amide group of Ala 3 of conformer 1 with the cross peak in isotropic DMSO-d_6 solution (in gray).

Table A2.3.: ^{1}H, ^{15}N and ^{13}C assignment for the two conformations of *cyclo*(-D-Ala-Ala-Ala-(NMe)Ala-Ala-). Isotropic chemical shift values are given in ppm.

	Hα	Hβ	$H_{N\text{-}Me}$	HN	N	Cα	Cβ	CO
Conformer 1								
D-Ala 1	4.33	1.13	-	8.05	122.2	47.0	16.2	170.4
Ala 2	4.26	1.19	-	7.23	118.3	50.4	18.9	171.0
Ala 3	4.41	1.19	-	8.15	116.2	45.2	16.7	169.9
*N*Me-Ala 4	4.48	1.29	2.59	-	-	55.4	14.1	168.5
Ala 5	4.37	1.18	-	7.81	122.9	47.1	16.5	170.1
Conformer 2								
D-Ala 1	4.10	1.16	-	8.38	125.5	49.2	16.4	172.5
Ala 2	3.93	1.27	-	8.68	123.4	49.6	16.6	171.1
Ala 3	4.61	1.09	-	7.48	115.0	45.1	17.7	171.5
*N*Me-Ala 4	3.52	1.54	2.85	-	-	64.6	14.8	171.6
Ala 5	4.45	1.17	-	7.74	119.1	47.1	16.0	169.9

Table A2.4.: One-bond couplings measured for conformer 1 of the pentapeptide *cyclo*(-D-Ala-Ala-Ala-(NMe)Ala-Ala-) in isotropic DMSO-d_6 solution and inside the PAN/DMSO-d_6 gel with $\Delta\nu_Q$ = 21.2 Hz.

Signal		$^1J_{XH}$ [Hz]	$^1J_{XH}+D_{XH}$ [Hz]	D_{XH} [Hz]
D-Ala 1	Cβ-Hβ	128.3 ± 0.1	128.7 ± 0.3	0.4 ± 0.3
D-Ala 1	Cα-Hα	136.6 ± 0.3	142.3 ± 2.0	5.7 ± 2.0
D-Ala 1	N-NH	91.2 ± 0.3	94.6 ± 2.5	3.4 ± 2.5
Ala 2	Cβ-Hβ	128.5 ± 0.1	127.8 ± 0.5	-0.8 ± 0.5
Ala 2	Cα-Hα	143.3 ± 0.2	157.8 ± 2.5	14.5 ± 2.5
Ala 2	N-NH	91.0 ± 0.7	95.8 ± 1.5	4.8 ± 1.7
Ala 3	Cβ-Hβ	128.7 ± 0.2	130.7 ± 0.6	2.0 ± 0.6
Ala 3	Cα-Hα	138.2 ± 0.3	150.6 ± 2.0	12.4 ± 2.0
Ala 3	N-NH	91.1 ± 0.2	96.1 ± 1.5	5.0 ± 1.5
*N*Me-Ala 4	Cβ-Hβ	128.5 ± 0.2	130.3 ± 0.6	1.8 ± 0.6
*N*Me-Ala 4	Cα-Hα	134.9 ± 0.4	142.3 ± 2.0	7.4 ± 2.0
*N*Me-Ala 4	Cm-Hm	138.8 ± 0.1	136.0 ± 0.8	-2.8 ± 0.8
Ala 5	Cβ-Hβ	128.1 ± 0.1	123.6 ± 0.5	-4.5 ± 0.5
Ala 5	Cα-Hα	136.5 ± 0.5	142.5 ± 3.5	6.0 ± 3.5
Ala 5	N-NH	91.5 ± 0.2	95.1 ± 1.5	3.6 ± 1.5

Table A2.5.: One-bond couplings measured for conformer 2 of the pentapeptide *cyclo*(-D-Ala-Ala-Ala-(NMe)Ala-Ala-) in isotropic DMSO-d_6 solution and inside the PAN/DMSO-d_6 gel with $\Delta\nu_Q$ = 21.2 Hz.

Signal		$^1J_{XH}$ [Hz]	$^1J_{XH}+D_{XH}$ [Hz]	D_{XH} [Hz]
D-Ala 1	Cβ-Hβ	128.3 ± 0.1	122.8 ± 2.0	-5.5 ± 2.0
D-Ala 1	Cα-Hα	142.8 ± 0.4	165.6 ± 1.0	22.8 ± 1.1
D-Ala 1	N-NH	92.8 ± 0.3	98.2 ± 1.5	5.4 ± 1.5
Ala 2	Cβ-Hβ	129.1 ± 0.1	136.4 ± 1.3	7.3 ± 1.3
Ala 2	Cα-Hα	143.5 ± 0.3	171.3 ± 3.0	27.8 ± 3.0
Ala 2	N-NH	92.4 ± 8.0	104.5 ± 5.0	12.1 ± 9.4
Ala 3	Cβ-Hβ	128.5 ± 0.2	128.4 ± 0.6	-0.1 ± 0.6
Ala 3	Cα-Hα	139.3 ± 0.3	175.7 ± 1.5	36.4 ± 1.5
Ala 3	N-NH	91.6 ± 0.3	102.2 ± 5.0	10.6 ± 5.0
*N*Me-Ala 4	Cβ-Hβ	129.0 ± 0.1	123.6 ± 0.5	-5.4 ± 0.5
*N*Me-Ala 4	Cα-Hα	139.8 ± 0.8	159.3 ± 4.0	19.5 ± 4.1
*N*Me-Ala 4	Cm-Hm	138.8 ± 0.1	131.3 ± 1.0	-7.5 ± 1.0
Ala 5	Cβ-Hβ	128.7 ± 0.1	130.3 ± 1.0	1.6 ± 1.0
Ala 5	Cα-Hα	141.4 ± 0.5	158.4 ± 5.0	17.0 ± 5.0
Ala 5	N-NH	89.7 ± 0.5	94.04 ± 3.0	4.3 ± 3.0

7.3 Supplemental Material for Chapter 3.2

For the preparation of dPS/$CDCl_3$ and PS/$CDCl_3$ gels, sticks of cross-linked dPS and PS were placed in NMR-tubes and $CDCl_3$ was added. The swollen gels were allowed to equilibrate for approximately 3 weeks before NMR experiments were carried out.

The following samples were used:

PS for Figure 3.9. A: Polymer stick with 3.4 mm diameter, polymerized with 0.75% DVB and 0.1% AIBN, swollen in NMR tube with 5.0 mm outer and 4.2 mm inner diameter. Quadrupolar splitting of the solvent $CDCl_3$: 147 Hz. No solute was added.

***dPS for Figure 3.9. A*:** Polymer stick with 3.4 mm diameter, polymerized with 0.5% DVB and 0.1% AIBN, swollen in NMR tube with 5.0 mm outer and 4.2 mm inner diameter. Quadrupolar splitting of the solvent $CDCl_3$: 135 Hz. No solute was added.

***PS for Figure 3.9. B*:** Polymer stick with 3.4 mm diameter, polymerized with 0.5% DVB and 0.1% AIBN, swollen in NMR tube with 5.0 mm outer and 4.2 mm inner diameter. Quadrupolar splitting of the solvent $CDCl_3$: 128 Hz. 8 mg of strychnine was added and allowed to diffuse for about 3 days.

dPS for Figures 3.9. B, 3.12. B, 3.13.: Polymer stick with 3.4 mm diameter, polymerized with 0.5% DVB and 0.1% AIBN, swollen in NMR tube with 5.0 mm outer and 4.2 mm inner diameter. Quadrupolar splitting of the solvent $CDCl_3$: 121 Hz. 8 mg of strychnine was added and allowed to diffuse for 3-4 days.

PS for Figure 3.11. A: Polymer stick with 3.4 mm diameter, polymerized with 0.2% DVB and 0.05% AIBN, swollen in NMR tube with 5.0 mm outer and 4.2 mm inner diameter. Quadrupolar splitting of the solvent $CDCl_3$: 36 Hz. 2.5 mg of staurosporine was added and allowed to diffuse for 10 days.

dPS for Figures 3.10., 3.11. B: Polymer stick with 1.6 mm diameter, polymerized with 0.2% DVB and 0.1% AIBN, swollen in NMR tube with 3.0 mm outer and 2.4 mm inner diameter. Quadrupolar splitting of the solvent $CDCl_3$: 26.8 Hz. 2 mg of staurosporine was added and allowed to diffuse for about 1 week.

PS for Figure 3.12. A: Polymer stick with 3.4 mm diameter, polymerized with 1.0% DVB and 0.01% AIBN, swollen in NMR tube with 5.0 mm outer and 4.2 mm inner diameter. Quadrupolar splitting of the solvent $CDCl_3$: 38 Hz. 8 mg of strychnine was added and allowed to diffuse for about 20 days.

7.4 Supplemental Material for Chapter 3.3

Deuterated acrylonitrile (≥ 98% deuterated, Cambridge Isotope Laboratories, Andover, USA) was purified by distillation under argon. 2.78 g (500 eq.) purified monomer was dissolved in 25 mL degassed water. 2.7 ml of a 1% (w/v) aqueous solution of $K_2S_2O_8$ (1 eq.) and 2.2 mL of a 1% aqueous solution of $K_2S_2O_5$ (1 eq.) were added and the reaction mixture was stirred for 15 h at room temperature. During polymerization the building polymer precipitates and after filtering and washing it was dried by lyophilization.

A dPAN/DMSO-d_6-solution with a concentration of 220 g/L was filled in glass and Teflon® tubes of 2.4, 3.0, and 3.4 mm inner diameter. Polymer solutions were irradiated with 10 MeV electrons generated by an industrial electron accelerator (Beta-Gamma-Systems, Saal an der Donau, Germany). During irradiation, tubes were placed perpendicular to the electron beam. The samples were irradiated by single irradiation doses of 40 kGy which took several seconds each. The time interval between two subsequent irradiation steps was approximately 10-15 min. Total irradiation doses of 120-480 kGy were applied.

The following samples were used:

PAN gel for Figure 3.15.: PAN gel of the third generation. PAN with MW = 150000 g/mol was irradiated as 150 g/L DMSO solution in a 3.4 mm Teflon® tube with a total irradiation dose of 480 kGy. After irradiation, the polymer was precipitated and re-swollen with DMSO-d_6 in a standard 5 mm NMR tube.

dPAN gel for Figure 3.15.: Synthesized dPAN was irradiated as 220 g/L DMSO solution in a 3.4 mm Teflon® tube with a total irradiation dose of 480 kGy. After irradiation, the polymer was precipitated and re-swollen with DMSO-d_6 in a standard 5 mm NMR tube.

PAN gel for Figure 3.16.: PAN gel of the third generation. PAN with MW = 150000 g/mol was irradiated as 200 g/L DMSO solution in a 2.4 mm Teflon® tube with a total irradiation dose of 480 kGy. After irradiation, the polymer was precipitated and re-swollen with a solution of 12.5 mg of the 11-mer peptide in 100 µL DMSO-d_6 within a stretching device equipped with a Kalrez® 8002UP tube.

dPAN gel for Figures 3.16., A4.2. and Table A4.1.: Synthesized dPAN was irradiated as 220 g/L DMSO solution in a 3.4 mm Teflon® tube with a total irradiation dose of 480 kGy. After irradiation, the polymer was precipitated and re-swollen with a solution of 12.5 mg of the 11-mer peptide in 100 µL DMSO-d_6 within a stretching device equipped with a Kalrez® 8002UP tube.

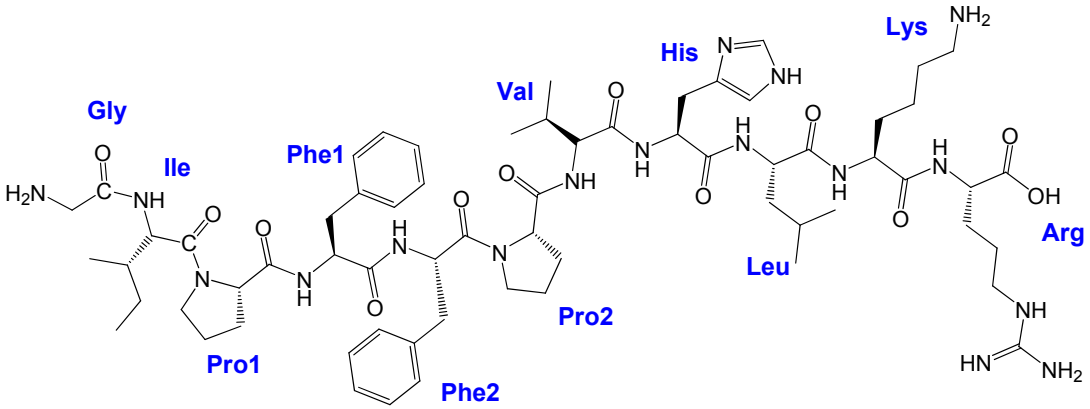

Figure A4.1.: Linear 11-mer peptide derived from SPC(I) used for demonstration of dPAN/DMSO-d_6 gels as alignment medium.

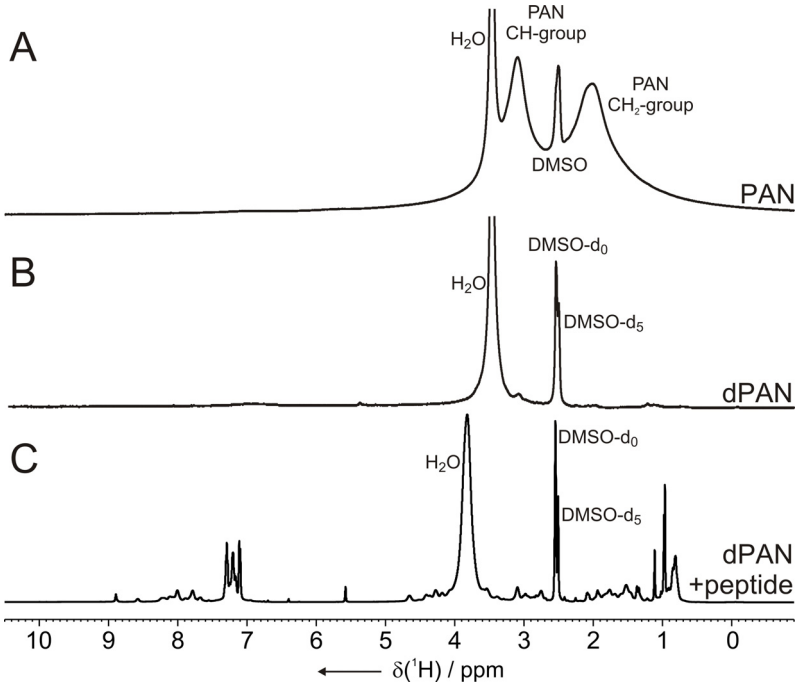

Figure A4.2.: ^{1}H-1D-spectra of a conventional PAN/DMSO-d_6 gel (A), a perdeuterated dPAN/DMSO-d_6 gel (B) and a dPAN/DMSO-d_6 gel with approximately 30 mM SPC(I)-derived 11-mer peptide diffused into it (C).

Table A4.1.: One-bond proton carbon couplings measured for the linear 11-mer peptide shown in Figure A4.1. Residual dipolar couplings (D_{CH}) are calculated from the difference of couplings measured in a stretched dPAN/DMSO gel with $\Delta\nu_Q$ = 8.6 Hz ($^1J_{CH} + D_{CH}$) and in DMSO solution ($^1J_{CH}$).

Signal	$^1J_{CH}$ [Hz]	$^1J_{CH} + D_{CH}$ [Hz]	D_{CH} [Hz]
Ile Cδ - Hδ	124.9 ± 0.1	123.3 ± 0.2	-1.6 ± 0.2
Ile Cγ' - Hγ'	125.9 ± 0.1	127.4 ± 0.2	1.5 ± 0.2
Leu Cδ2 - Hδ2	125.6 ± 0.2	125.6 ± 0.4	0.0 ± 0.4
Leu Cδ1 - Hδ1	125.9 ± 0.1	128.8 ± 0.3	2.9 ± 0.3
His Cβ - Hβ1	132.8 ± 0.4	140.0 ± 2.0	7.2 ± 2.0
His Cβ - Hβ2	131.4 ± 0.4	127.3 ± 3.0	-4.1 ± 3.0
Val Cβ - Hβ	130.1 ± 0.3	130.0 ± 0.4	-0.1 ± 0.5
Arg Cβ- Hβ1	127.4 ± 0.5	136.3 ± 0.5	8.9 ± 0.7
Arg Cβ - Hβ2	129.9 ± 0.5	124.3 ± 0.5	-5.6 ± 0.7
Ile Cβ - Hβ	129.3 ± 0.3	135.3 ± 0.5	6.0 ± 0.6
Pro2 Cδ - Hδ1	144.4 ± 0.3	159.1 ± 2.0	14.7 ± 2.0
Pro2 Cδ - Hδ2	145.0 ± 0.3	130.9 ± 3.0	-14.1 ± 3.0
Pro1 Cδ - Hδ1	145.2 ± 0.3	150.8 ± 2.0	5.6 ± 2.0
Pro1 Cδ - Hδ2	142.8 ± 0.3	128.7 ± 3.0	-14.1 ± 3.0
Lys Cα - Hα	140.6 ± 0.2	153.5 ± 0.4	12.9 ± 0.4
Phe2 Cα - Hα	140.5 ± 0.3	155.7 ± 0.8	15.2 ± 0.9
Arg Cα - Hα	139.8 ± 0.2	157.4 ± 0.5	17.6 ± 0.5
Phe1 Cα - Hα	141.7 ± 0.2	156.3 ± 0.8	14.6 ± 0.8
Ile Cα - Hα	138.7 ± 0.2	147.6 ± 0.6	8.9 ± 0.6
Val Cα - Hα	140.3 ± 0.2	154.8 ± 0.8	14.5 ± 0.8
Pro1 Cα - Hα	146.7 ± 0.3	156.5 ± 0.6	9.8 ± 0.7
Pro2 Cα - Hα	146.5 ± 0.3	159.3 ± 1.5	12.8 ± 1.5

7.5 Supplemental Material for Chapter 3.4

For all experiments porcine gelatin (Naumann Gelatine und Leim GmbH, Memmingen, Germany) with an approximate Bloomgrade of 250 was used.

Gelatin sticks and hydrogels were irradiated with 10 MeV electrons generated by an industrial electron accelerator (Beta-Gamma-Systems, Saal an der Donau, Germany). Sticks and Teflon® tubes were placed perpendicular to the electron beam and kept cool by an ice/water bath during irradiation. The samples were irradiated by single irradiation doses of 10 kGy or 40 kGy which took several seconds each. The time interval between two subsequent irradiation steps was approximately 10-15 min. Total irradiation doses of 10-480 kGy were applied.

All NMR measurements were carried out in the stretching apparatus equipped with silicone tubes purchased from J. Lindemann GmbH (Helmstedt, Germany) with 4.0 mm outer and 3.0 mm inner diameter (tube type I) or silicone tubes purchased from VWR International GmbH (Darmstadt, Germany) with 4.2 mm outer and 2.4 mm inner diameter (tube type II). Sticks of covalently cross-linked gelatin were placed in the silicone tube of the stretching apparatus and solvent (D_2O, DMSO-d_6, D_2O/DMSO-d_6 mixtures) or solution (e.g. alanine in D_2O) was added. To all samples a small amount of NaN_3 was added to prevent bacteria growth. Prepared samples were allowed to swell and equilibrate for about 3 days at room temperature before NMR experiments were carried out.

The following samples were used:

Figure 3.18.: Sticks prepared according to preparation scheme A (a, b, e: no irradiation; c, d, f: irradiation with 80 kGy). Sticks b and c were kept in water, e and f in DMSO at 50°C for about 3 days.

***Figure 3.19. A (●)*:** Sample with conventional (not irradiated) gelatin. A warm 30% (w/v) solution of gelatin in D_2O was filled in the stretching apparatus (tube type I) and cooled in a refridgerator for gelation prior to measurement.

***Figure 3.19. A (■)**:* Stick prepared according to preparation scheme B (30%, 3.0 mm, 320 kGy) swollen in D_2O within a tube of type I.

Figure 3.19. A (▲): Stick prepared according to preparation scheme B (30%, 3.0 mm, 80 kGy) swollen in D_2O within a tube of type I.

Figures 3.19. B, 3.20., 3.23. and Tables A5.1., A5.2.: Stick prepared according to preparation scheme B (40%, 3.0 mm, 60 kGy) swollen in 220 µL D_2O + 16.5 mg D-Ala + 33 mg L-Ala within a tube of type I.

Figures 3.21., 3.22.: Stick prepared according to preparation scheme B (30%, 3.0 mm, 280 kGy) swollen in 200 µL D_2O + 10 mg D-Ala + 20 mg L-Ala within a tube of type I.

Figures 3.25. A and C: Stick prepared according to preparation scheme B (40%, 3.0 mm, 140 kGy) swollen in pure DMSO-d_6 within a tube of type II.

Figure 3.25. B: Stick prepared according to preparation scheme B (40%, 3.0 mm, 90 kGy) swollen in DMSO-d_6/D_2O (4:1) within a tube of type II.

Figure 3.24. and Tables A5.3., A5.4.: Stick prepared according to preparation scheme B (40%, 3.0 mm, 140 kGy) swollen in 200 µL D_2O + 34 mg sucrose within a tube of type I.

For Figure 3.23. one-bond CH-RDCs (see Table A5.1.) of the CαHα and CβHβ groups of D-Ala and L-Ala have been extracted out of 1D traces along the J-dimension from $^{1}H,^{13}C$-J-BIRD^{d,X}-HSQCs[52] at various temperatures. The series of spectra was recorded on a single e^{-}-gelatin/D_2O gel with constant extension factor $\Xi = 0.6$ starting with 15°C (row 1 in Table A5.1.) and subsequent heating, cooling, and reheating as described in Figures 3.19. B and 3.20. Obtained RDCs have then be normalized by the quadrupolar splitting of the solvent (see Table A5.2.).

Table A5.1.: $^{1}T_{CH}$ ($^{1}T_{CH} = {}^{1}J_{CH} + D_{CH}$) couplings for alanine in covalently cross-linked gelatin and the quadrupolar splitting ($\Delta\nu_Q$) of D_2O at different temperatures.

T / °C	$\Delta\nu_Q$ / Hz	3* $^{1}T_{C\beta H\beta}$ / Hz		$^{1}T_{C\alpha H\alpha}$ / Hz	
		L-Ala	D-Ala	L-Ala	D-Ala
15	266.5 ± 6.5	371.4 ± 0.1	384.8 ± 0.1	168.9 ± 0.5	185.8 ± 1.5
20	242.0 ± 2.0	371.8 ± 0.1	384.2 ± 0.1	168.2 ± 0.3	-
25	209.0 ± 0.2	372.8 ± 0.2	384.0 ± 0.1	166.2 ± 0.3	179.0 ± 1.5
30	162.5 ± 3.5	375.6 ± 0.1	384.5 ± 0.1	162.7 ± 0.3	172.4 ± 1.0
35	105.5 ± 6.5	379.7 ± 0.2	385.6 ± 0.2	157.2 ± 0.3	163.6 ± 1.0
40	54.0 ± 3.0	383.6 ± 0.1	386.6 ± 0.2	152.3 ± 0.3	155.4 ± 1.0
45	30.5 ± 1.5	385.3 ± 0.1	386.9 ± 0.2	150.1 ± 0.3	151.0 ± 1.0
50	17.0 ± 1.0	386.1 ± 0.2	386.9 ± 0.4	149.0 ± 1.0	149.0 ± 1.0
55	10.5 ± 0.5	386.8 ± 0.5	386.8 ± 0.5	148.5 ± 0.5	148.5 ± 1.0
50	12.5 ± 0.5	386.8 ± 0.5	386.8 ± 0.5	148.5 ± 0.5	148.5 ± 1.0
40	26.5 ± 0.5	386.0 ± 0.2	387.0 ± 0.5	149.2 ± 0.3	150.3 ± 0.5
30	62.5 ± 3.5	384.1 ± 0.2	387.2 ± 0.2	151.5 ± 0.2	155.1 ± 0.4
20	106.0 ± 3.0	382.0 ± 0.2	387.4 ± 0.1	154.4 ± 0.2	160.5 ± 0.7
30	68.5 ± 1.5	383.6 ± 0.1	387.2 ± 0.1	152.0 ± 0.4	156.0 ± 1.0
40	29.0 ± 0.2	385.8 ± 0.2	387.0 ± 0.5	149.3 ± 0.3	150.6 ± 0.7
50	13.0 ± 0.2	386.7 ± 0.5	386.9 ± 0.5	148.5 ± 0.5	148.5 ± 0.7
20	89.5 ± 3.5	383.1 ± 0.2	387.7 ± 0.2	152.7 ± 0.2	158.0 ± 1.5
20	isotropic	389.1 ± 0.1	389.1 ± 0.1	144.8 ± 0.1	144.8 ± 0.1

Table A5.2.: Measured $^1D_{CH}$ RDCs (as derived from Table A5.1.) normalized by the quadrupolar deuterium splitting of the solvent D_2O to obtain potential information about changes in the alignment properties of e^--gelatin (see Figure 3.23.).

T / °C	$(3*\,{}^1D_{C\beta H\beta} / \Delta\nu_Q)$		$({}^1D_{C\alpha H\alpha} / \Delta\nu_Q)$	
	L-Ala	D-Ala	L-Ala	D-Ala
15	-0.066 ± 0.002	-0.016 ± 0.001	0.090 ± 0.003	0.154 ± 0.007
20	-0.071 ± 0.001	-0.020 ± 0.000	0.097 ± 0.001	-
25	-0.078 ± 0.001	-0.024 ± 0.000	0.102 ± 0.001	0.164 ± 0.007
30	-0.083 ± 0.002	-0.028 ± 0.001	0.110 ± 0.003	0.170 ± 0.007
35	-0.089 ± 0.006	-0.033 ± 0.003	0.118 ± 0.008	0.178 ± 0.015
40	-0.102 ± 0.006	-0.046 ± 0.005	0.139 ± 0.010	0.196 ± 0.021
45	-0.125 ± 0.007	-0.072 ± 0.007	0.174 ± 0.013	0.203 ± 0.034
50	-0.176 ± 0.016	-0.129 ± 0.025	0.247 ± 0.061	0.247 ± 0.061
55	-0.219 ± 0.049	-0.219 ± 0.049	0.352 ± 0.050	0.352 ± 0.097
50	-0.184 ± 0.041	-0.184 ± 0.041	0.296 ± 0.042	0.296 ± 0.081
40	-0.117 ± 0.008	-0.079 ± 0.019	0.166 ± 0.012	0.208 ± 0.019
30	-0.080 ± 0.006	-0.030 ± 0.004	0.107 ± 0.007	0.165 ± 0.011
20	-0.067 ± 0.003	-0.016 ± 0.001	0.091 ± 0.003	0.148 ± 0.008
30	-0.080 ± 0.002	-0.028 ± 0.002	0.105 ± 0.006	0.164 ± 0.015
40	-0.114 ± 0.007	-0.072 ± 0.017	0.155 ± 0.010	0.200 ± 0.024
50	-0.185 ± 0.039	-0.169 ± 0.039	0.285 ± 0.039	0.285 ± 0.054
20	-0.067 ± 0.003	-0.016 ± 0.002	0.088 ± 0.004	0.147 ± 0.018

To investigate whether the alignment tensors of a solute in conventional gelatin gels and e^--gelatin gels differ, sucrose was chosen as a test molecule, because RDC data were already available for sucrose in conventional gelatin (see chapter 4.1.). $^1T_{CH}$ ($^1T_{CH} = {}^1J_{CH} + D_{CH}$) couplings of sucrose have been measured using the CLIP-HSQC pulse sequence[107] for different extensions of the e^--gelatin/D_2O gel. The temperature was chosen to be identical to measurements in conventional gelatin (293 K / 20°C). Measured couplings are given in Table A5.3. Linear regressions of $^1T_{CH}$ couplings with respect to the quadrupolar splittings $\Delta\nu_Q$ were done with the Linear Fit option of Origin.[224] Fit parameters A and B of the regression equation $Y = A + B \bullet X$, with Y being the measured $^1T_{CH}$ couplings and X being the corresponding $\Delta\nu_Q$ values, are given in Table A5.4. for all CH-couplings of sucrose in the e^--gelatin/D_2O gel and conventional gelatin (see chapter 4.1.) for comparison. See also Figure 3.24.

Table A5.3.: $^1T_{CH}$ ($^1T_{CH} = {}^1J_{CH} + D_{CH}$) couplings for sucrose in covalently cross-linked gelatin and the quadrupolar splitting ($\Delta\nu_Q$) of D_2O at different extensions.

$\Delta\nu_Q$ / Hz	$^1T_{CH}$ / Hz						
	C4'H4'	C2'H2'	C3'H3'	C5'H5'	C3H3	C5H5	C1'H1'
-5.5 ± 0.5	144.0 ± 0.3	143.7 ± 0.5	143.5 ± 0.5	144.5 ± 0.5	145.0 ± 2.0	149.0 ± 2.0	168.7 ± 0.4
61.0 ± 0.7	145.5 ± 0.5	147.5 ± 0.5	146.4 ± 0.5	147.9 ± 0.5	140.0 ± 3.0	136.0 ± 2.0	179.6 ± 0.5
99.9 ± 0.5	146.2 ± 0.5	150.4 ± 0.5	148.1 ± 0.5	150.5 ± 0.5	137.0 ± 3.0	128.0 ± 2.0	185.8 ± 0.5
136.1 ± 1.0	147.5 ± 0.5	152.0 ± 0.7	149.5 ± 0.7	152.8 ± 0.7	135.0 ± 2.0	120.0 ± 1.5	191.1 ± 0.5
153.0 ± 0.8	147.7 ± 0.7	154.0 ± 0.7	150.6 ± 0.7	153.7 ± 1.0	131.0 ± 2.0	116.0 ± 1.5	194.1 ± 0.5
155.2 ± 0.8	147.8 ± 0.7	154.0 ± 0.7	150.2 ± 0.7	153.5 ± 1.0	132.0 ± 2.0	116.0 ± 1.5	194.4 ± 0.5
solution	144.0 ± 0.2	144.5 ± 0.2	144.2 ± 0.2	145.3 ± 0.2	144.8 ± 1.5	148.5 ± 1.0	169.4 ± 0.2

Table A5.4.: Fit parameters for the slopes of $^1T_{CH}$ couplings of sucrose measured in conventional and covalently cross-linked gelatin.

	conventional gelatin / D_2O		e^--gelatin / D_2O	
	A [Hz]	B	A [Hz]	B
C1'H1'	169.17 ± 0.18	0.147 ± 0.001	168.96 ± 0.43	0.165 ± 0.004
C2'H2'	145.33 ± 0.19	0.042 ± 0.001	143.80 ± 0.33	0.064 ± 0.003
C3'H3'	145.03 ± 0.36	0.043 ± 0.002	143.75 ± 0.22	0.043 ± 0.002
C4'H4'	145.86 ± 0.49	0.022 ± 0.003	143.90 ± 0.09	0.025 ± 0.001
C5'H5'	145.60 ± 0.38	0.050 ± 0.002	144.67 ± 0.27	0.058 ± 0.002
C3H3	144.92 ± 0.15	-0.059 ± 0.001	145.23 ± 0.56	-0.085 ± 0.005
C5H5	148.87 ± 0.36	-0.189 ± 0.002	149.32 ± 0.37	-0.216 ± 0.003

7.6 Supplemental Material for Chapter 3.5

Solubility of linear PEO (purchased from FLUKA Chemie GmbH, Buchs, Germany) with MW = 35000 g/mol was roughly estimated by the following procedure: a certain amount of PEO (between 200 mg and 3 g) was weighed in a vial and solvent was added stepwise (in steps of 0.2 ml to 0.05 ml). After every step of adding solvent, the vial was closed and heated to 55°C for one day before cooling down to room temperature again. If the polymer was not completely dissolved, more solvent was added. When the polymer was dissolved completely, the amount of solvent was added up and the concentration was calculated. For each solvent at least three different batches have been dissolved and results have been averaged to reduce the error of this solubility estimation.

Solvent	**Estimated Solubility [g/mL]**
acetonitrile	0.96 ± 0.1
dichloromethane	1.95 ± 0.1
dioxane	0.23 ± 0.2
DMF	0.13 ± 0.1
DMSO	< 0.07
water	1.47 ± 0.2
methanol	0.14 ± 0.05
TFE	1.70 ± 0.2
THF	< 0.05
chloroform	1.90 ± 0.1

7.7 Supplemental Material for Chapter 4.1

All NMR measurements were carried out in the stretching apparatus equipped with silicone tubes purchased from J. Lindemann GmbH (Helmstedt, Germany) with 4.0 mm outer and 3.0 mm inner diameter (tube type I) or silicone tubes purchased from VWR International GmbH (Darmstadt, Germany) with 4.2 mm outer and 2.4 mm inner diameter (tube type II). Sticks of covalently cross-linked polymer were placed in the silicone tube of the stretching apparatus and solvent or solution was added before samples were allowed to swell and equilibrate for about 5 days at room temperature. Gelatin samples were prepared by filling hot (50°C) gelatin/water solutions in the tube and cool it down (5°C) for gelation.

The following samples were used:

Figure 4.3. A: Stick of e^--gelatin prepared according to preparation scheme B (30%, 3.0 mm, 280 kGy) swollen in D_2O within a tube of type I.

Figure 4.3. B: Stick of e^--gelatin prepared according to preparation scheme B (40%, 3.0 mm, 140 kGy) swollen in pure DMSO-d_6 within a tube of type II.

Figures 4.5., 4.6. A and Table A7.1.: Sample of conventional (not irradiated) gelatin. A warm 40% (w/v) solution of gelatin in D_2O with approximately 500 mM sucrose was filled in the stretching apparatus (tube type I) and cooled in a refrigerator for gelation prior to measurements.

Figure 4.6. B and Table A7.2.: PAA was prepared from an aqueous solution of 8.55% (w/v) acrylamide and 0.45% (w/v) N,N‘-methylene bis(acrylamide) with 0.1% (w/v) ammonium persulfate and 0.1% (v/v) N,N,N‘,N‘-tetramethyl ethylen diamin for cross-linking.[29] Radical polymerization was allowed for 1 h within a glass tube of 2.4 mm inner diameter. The obtained gel was washed three times with water to remove free acrylamide before it was dried at room temperature. The stick was re-swollen with a solution of 500 mM sucrose in D_2O within a tube of type I.

Figure 4.6. C and Table A7.3.: PAN gel of the third generation. PAN with MW = 150000 g/mol was irradiated as 280 g/L DMSO solution in a 2.4 mm Teflon® tube with a total irradiation dose of 320 kGy. After irradiation, the polymer was precipitated and re-swollen with a solution of 200 mM sucrose in DMSO-d_6 within a tube of type I.

Figure 4.7.: PAN gel of the third generation. PAN with MW = 150000 g/mol was irradiated as 280 g/L DMSO solution in a 2.4 mm Teflon® tube with a total irradiation dose of 480 kGy. After irradiation, the polymer was precipitated and re-swollen with a solution of 50 mM of the cyclic peptide in DMSO-d_6 within a tube of type I.

Linear regressions of $^1T_{CH}$ couplings with respect to the quadrupolar splittings $\Delta\nu_Q$ as shown in Figure 4.6. were done with the Linear Fit option of Origin.[224] Fit parameters A and B of the regression equation Y = A + B • X, with Y being measured $^1T_{CH}$ couplings and X being the corresponding $\Delta\nu_Q$ values, are given in Tables A7.1., A7.2., and A7.3. for all CH-couplings of sucrose in the different alignment media used. Furthermore, maximum deviations of the measured $^1T_{CH}$ couplings from the linear fit (max. Δ^1T_{CH}) and root mean square deviations (σ ($^1T_{CH}$)) of all the measured couplings are given.

Table A7.1.: Fit parameters for $^1T_{CH}$ couplings of sucrose measured in gelatin/D_2O.

Signal	A [Hz]	B	max. Δ^1T_{CH} [Hz]	σ ($^1T_{CH}$) [Hz]
1'	169.17± 0.18	0.147± 0.001	1.6 /-1.0	0.53
2'	145.33± 0.19	0.042± 0.001	1.1 /-1.0	0.63
3'	145.03± 0.36	0.043± 0.002	1.7 /-2.6	1.13
4'	145.86± 0.49	0.022± 0.003	1.9 /-2.6	1.54
5'	145.60± 0.38	0.050± 0.002	2.1 /-1.9	1.16
3	144.92± 0.15	-0.059± 0.001	0.6 /-1.1	0.49
4	146.76± 0.31	-0.010± 0.002	2.3 /-1.9	1.14
5	148.87± 0.36	-0.189± 0.002	2.1 /-2.0	1.11

Table A7.2.: Fit parameters for $^1T_{CH}$ couplings of sucrose measured in PAA/D_2O.

Signal	A [Hz]	B	max. Δ^1T_{CH} [Hz]	σ ($^1T_{CH}$) [Hz]
1'	144.15± 0.02	0.115± 0.010	0.1 /-0.5	0.3
3'	145.42± 0.43	0.217± 0.014	0.6 /-0.6	0.4
4'	143.23± 0.79	0.180± 0.027	0.3 /-1.3	0.6
5'	147.53± 0.33	-0.318± 0.014	0.3 /-0.4	0.6
3	145.84± 0.25	-0.333± 0.010	0.6 /-0.4	0.4
4	149.81± 0.40	-0.443± 0.015	0.6 /-1.6	0.8
5	169.97± 0.13	0.220± 0.005	0.2 /-0.1	0.1

Table A7.3.: Fit parameters for $^{1}T_{CH}$ couplings of sucrose measured in PAN/DMSO.

Signal	A [Hz]	B	max. $\Delta^{1}T_{CH}$ [Hz]	σ ($^{1}T_{CH}$) [Hz]
1'	167.42± 0.10	0.372± 0.006	0.4 /-0.5	0.26
2'	141.00± 0.10	0.182± 0.006	0.5 /-0.4	0.25
3'	143.12± 0.23	0.184± 0.014	0.9 /-0.8	0.59
4'	141.76± 0.18	0.089± 0.011	1.0 /-0.8	0.46
5'	143.22± 0.34	0.168± 0.022	2.4 /-2.0	0.89
3	141.47± 0.22	-0.392± 0.014	0.9 /-1.2	0.57
4	141.54± 0.27	-0.320± 0.018	1.3 /-1.1	0.72
5	145.99± 0.19	-0.426± 0.012	1.2 /-0.8	0.50

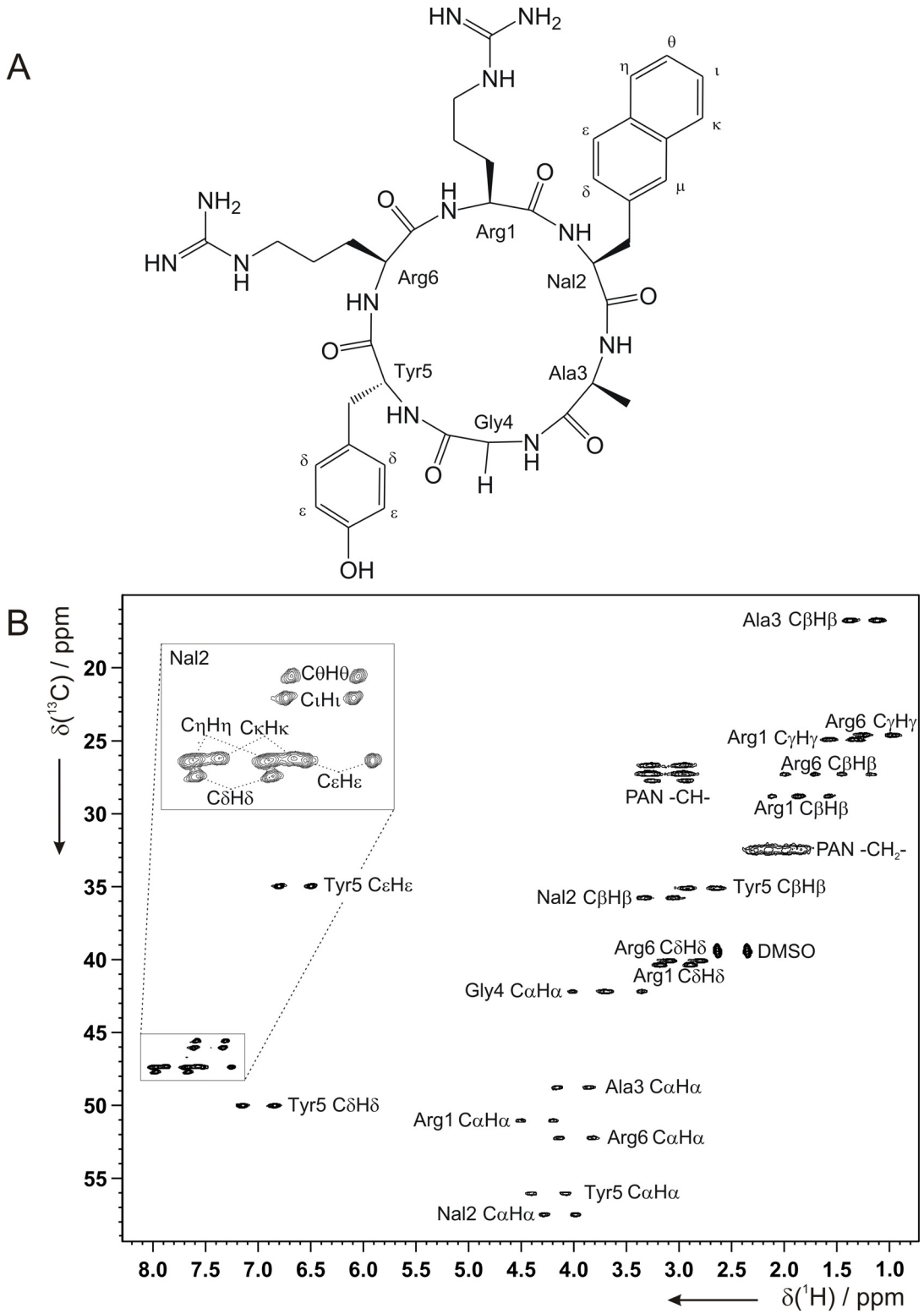

Figure A7.1.: Structure (A) and CLIP-HSQC spectrum[107] (B) of the cyclic hexapeptide *cyclo*(Arg–Nal–Ala–Gly–D-Tyr–Arg) in the unstretched PAN/DMSO gel.

7.8 Supplemental Material for Chapter 4.2

All measurements were carried out in the described stretching apparatus equipped with Kalrez® 8002UP tubes of 4.2 mm outer and 3.2 mm inner diameter or silicone tubes of 4.0 mm outer and 3.0 mm inner diameter. Sticks of covalently cross-linked polymer were placed in the elastomer tube of the stretching apparatus and solvent or solution was added before samples were allowed to swell and equilibrate for about 5 days at room temperature before NMR experiments were carried out. Gelatin samples were prepared by filling hot (50°C) gelatin/water solutions in the tube and cool it down (5°C) for gelation.

The following samples were used:

Figure 4.13. and Table A8.1.: Stick of cross-linked PDMS (2.4 mm diameter, 480 kGy) swollen in 150 µL $CDCl_3$ + 25 mg hydroquinidine within a Kalrez® 8002UP tube.

Figure 4.11. A: A hot solution of 125 mg porcine gelatin + 14.8 mg D-Ala + 7.4 mg L-Ala in 250 µL D_2O was filled in a silicone tube and cooled down for gelation. A small amount of NaN_3 was added to prevent bacteria growth. The gel was stretched with an extension factor $\Xi = 0.56$ resulting in a quadrupolar splitting $\Delta\nu_Q(D_2O) = 390.3$ Hz.

Figures 4.11. B, 4.14. D: A hot solution of 125 mg porcine gelatin + 14.8 mg D-Ala + 7.4 mg L-Ala in 250 µL D_2O was filled in a Kalrez® 8002UP tube and cooled down for gelation. A small amount of NaN_3 was added to prevent bacteria growth. The gel was stretched with an extension factor $\Xi = 0.58$ resulting in a quadrupolar splitting $\Delta\nu_Q(D_2O) = 417.6$ Hz.

Figure 4.14. A: A hot solution of 125 mg porcine gelatin + 22.2 mg D-Ala in 250 µL D_2O was filled in a Kalrez® 8002UP tube and cooled down for gelation. A small amount of NaN_3 was added to prevent bacteria growth. The gel was stretched with an extension factor $\Xi = 0.57$ resulting in a quadrupolar splitting $\Delta\nu_Q(D_2O) = 395.0$ Hz.

Figure 4.14. B: A hot solution of 125 mg porcine gelatin + 22.2 mg L-Ala in 250 µL D_2O was filled in a Kalrez® 8002UP tube and cooled down for gelation. A small amount of NaN_3 was added to prevent bacteria growth. The gel was stretched with an extension factor $\Xi = 0.57$ resulting in a quadrupolar splitting $\Delta\nu_Q(D_2O) = 407.2$ Hz.

Figures 4.15., A8.2. and Table A8.2. (isotropic sample): Solution of 7.2 mg parthenolide in 500 µL DMSO-d_6 in a standard 5 mm NMR tube.

Figures 4.15., A8.2. and Table A8.2. (gel sample): Stick of cross-linked PAN of the third generation (irradiated as 180 g/L PAN/DMSO solution in a 2.4 mm PTFE tube with 480 kGy and precipitated in water/DMSO) swollen in 200 µL DMSO-d_6 + 2.9 mg parthenolide within a Kalrez® 8002UP tube. The gel was stretched with an extension factor $\Xi = 0.23$ resulting in a quadrupolar splitting $\Delta\nu_Q(DMSO) = 4.5$ Hz.

Table A8.1.; Chemical shifts and measured one-bond couplings taken from CLIP-HSQC spectra[107] for hydroquinidine in a PDMS/$CDCl_3$ gel at various stages of stretching.

Assignment	$\delta\,^{13}C$ [ppm]	$\delta\,^{1}H$ [ppm]	$^{1}T_{CH}$ [Hz]						
			Ξ A)	0.07	0.21	0.38	0.61	0.77	1.07
			$\Delta\nu_Q$ [Hz] B)	10.5	31.8	73.4	104.0	132.0	181.9
C10-H10	12.0	0.87		124.8 ± 0.2	125.8 ± 0.3	126.5 ± 0.2	127.0 ± 0.3	127.5 ± 0.3	127.6 ± 0.5
C3-H3 a	20.8	1.97		130.5 ± 0.5	131.0 ± 0.4	132.0 ± 0.3	133.3 ± 0.3	135.2 ± 0.6	137.4 ± 0.5
C3-H3 b	20.8	1.03		130.7 ± 0.5	126.9 ± 0.8	121.2 ± 0.7	117.2 ± 0.4	113.5 ± 1.0	106.9 ± 0.6
C9-H9 a/b	25.3	1.46		- C)	- C)	- C)	- C)	- C)	- C)
C4-H4	26.3	1.66		137.0 ± 0.4	139.7 ± 0.1	143.4 ± 0.2	146.3 ± 0.2	147.2 ± 0.4	152.5 ± 0.8
C8-H8 a/b	27.2	1.44		- C)	- C)	- C)	- C)	- C)	- C)
C5-H5 E)	37.5	1.38		122.5 ± 2.0	122.8 ± 3.0	121.0 ± 2.5	119.0 ± 2.5	119.0 ± 2.5	113.0 ± 2.0
C7-H7 a E)	50.3	2.82		58.8 ± 0.5	58.5 ± 1.0	- D)	- D)	- D)	- D)
C7-H7 b E)	50.3	2.70		54.0 ± 0.7	50.0 ± 1.0	- D)	- D)	- D)	- D)
C6-H6 a	51.3	3.11		- D)	- D)	- D)	- D)	- D)	- D)
C6-H6 b	51.3	2.86		- D)	- D)	- D)	- D)	- D)	- D)
C10'-H10'	55.6	3.83		145.3 ± 0.2	146.7 ± 0.1	149.9 ± 0.3	152.9 ± 0.3	155.1 ± 0.2	158.2 ± 0.2
C2-H2	60.0	2.97		134.5 ± 0.3	134.3 ± 0.2	134.5 ± 0.1	134.5 ± 0.5	134.0 ± 0.5	132.6 ± 0.5
C1''-H1''	71.7	5.57		143.0 ± 0.2	146.2 ± 0.3	150.6 ± 0.4	154.2 ± 0.3	157.3 ± 0.5	164.5 ± 0.5
C5'-H5'	101.3	7.16		154.9 ± 0.3	147.6 ± 0.3	133.8 ± 0.5	122.9 ± 0.5	113.3 ± 0.3	97.2 ± 0.8
C3'-H3'	118.5	7.49		163.7 ± 0.2	164.9 ± 0.2	165.1 ± 0.2	167.3 ± 0.2	167.1 ± 0.5	171.5 ± 0.5
C7'-H7'	121.3	7.23		162.3 ± 0.2	162.4 ± 0.7	163.1 ± 0.5	163.9 ± 0.4	165.2 ± 0.2	164.7 ± 0.5
C8'-H8'	131.2	7.87		159.3 ± 0.3	153.4 ± 0.5	138.5 ± 0.4	128.3 ± 0.5	117.9 ± 0.4	103.4 ± 0.3
C2'-H2' E)	147.3	8.45		177.1 ± 2.8	178.4 ± 2.3	174.6 ± 2.8	170.5 ± 3.0	170.6 ± 3.3	180.0 ± 3.0

A) Extension factor Ξ = [(length of stretched gel) / (length of unstretched gel) - 1]. B) Quadrupolar splitting of the solvent $CDCl_3$ at the corresponding stretching state. C) No couplings measured because of unresolved methylene group. D) No coupling extraction possible due to signal overlap. E) Signal not plotted in Figure 4.13. because of large experimental error or overlapping signals.

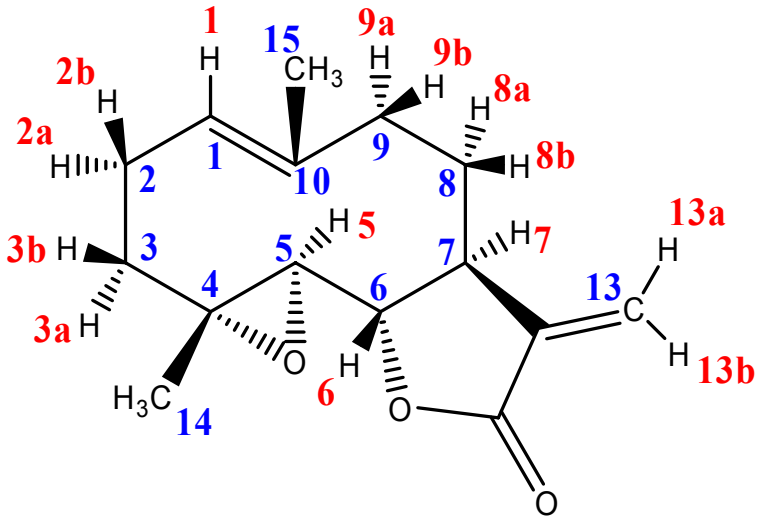

Figure A8.1.: Molecular structure of parthenolide with the numbering used in Table A8.2.

Table A8.2.: Chemical shifts in DMSO and measured one-bond couplings taken from CLIP-HSQC spectra[107] of parthenolide in isotropic DMSO solution ($^1J_{CH}$) and diffused into a PAN/DMSO gel ($^1J_{CH}$ + $^1D_{CH}$) and the resulting residual dipolar couplings ($^1D_{CH}$).

Group	δ (^{13}C) [Hz]	δ (^{1}H) [Hz]	$^1J_{CH}$ [Hz]	$^1J_{CH}$ + $^1D_{CH}$ [Hz]	$^1D_{CH}$ [Hz]
C15-H15	17.1	1.67	125.4 ± 0.1	124.7 ± 0.2	-0.7 ± 0.2 A)
C14-H14	17.3	1.22	126.5 ± 0.2	125.8 ± 0.3	-0.7 ± 0.4 A)
C2-H2a	24.2	2.08	129.5 ± 0.7	127.5 ± 1.0	-2.0 ± 1.2
C2-H2b	24.2	2.38	127.1 ± 0.5	128.8 ± 0.8	1.7 ± 0.9
C8-H8b	30.1	1.75	128.1 ± 0.3	131.1 ± 0.6	3.0 ± 0.7
C8-H8a	30.1	2.12	127.8 ± 0.4	122.0 ± 0.6	-5.8 ± 0.7
C3-H3a	36.5	1.13	129.1 ± 0.8	133.0 ± 1.2	3.9 ± 1.4
C3-H3b	36.5	2.05	129.3 ± 0.4	122.9 ± 0.6	-6.4 ± 0.7
C9-H9a	41.1	2.14	127.5 ± 0.8	129.9 ± 1.2	2.4 ± 1.4
C9-H9b	41.1	2.23	126.0 ± 1.5	132.6 ± 1.8	6.6 ± 2.3
C7-H7	46.9	2.97	130.1 ± 0.3	132.1 ± 0.5	2.0 ± 0.6
C5-H5	65.7	2.92	176.3 ± 0.3	178.6 ± 0.5	2.3 ± 0.6
C6-H6	82.7	4.06	155.6 ± 0.4	158.6 ± 0.6	3.0 ± 0.7
C13-H13a	121.2	5.80	161.7 ± 0.4	169.1 ± 0.6	7.4 ± 0.7
C13-H13b	121.2	6.14	161.5 ± 0.3	157.5 ± 0.5	-4.0 ± 0.6
C1-H1	125.0	5.26	150.4 ± 0.4	151.4 ± 0.6	1.0 ± 0.7

A) D_{CH}-couplings of methyl-groups have been converted to the corresponding D_{CC}-couplings[125] (D_{CC}(C15-C10) = 0.2 ± 0.06 Hz; D_{CC}(C14-C4) = 0.2 ± 0.1 Hz).

Technical Information

Kalrez® perfluoroelastomer parts
From DuPont Performance Elastomers

Kalrez® 8002

Product Description

Kalrez® 8002 is a clear, transparent product for ashing/stripping and "select" etching and deposition process applications, e.g., SACVD, etc. This unfilled product offers ultra-low particle generation in oxygen and fluorine-based plasmas versus mineral-filled products. Kalrez® 8002 exhibits excellent resistance to "dry" process chemistry, has good mechanical strength and is well suited for static, low stress/low sealing force and "select" bonded door seal applications. A maximum continuous service temperature of 275°C (527°F) is suggested. Ultrapure post-cleaning and packaging is standard for all Kalrez® 8002 parts.

Typical Physical Properties[1]	
Color	Clear
Maximum Application Temperature[2], °C (°F)	275 (527)
Maximum Application Pressure[2], MPa (psi)	3.45 (500)
Durometer, Shore A[3]	69
Durometer, Shore M (o-ring)	76
100% Modulus[4], MPa (psi)	2.88 (418)
Elongation at break[4], %	246
Tensile at break[4], MPa (psi)	15.95 (2313)
Compression set[5], % (70 hours at 204°C (400°F))	
Pellet	
Size 214 O-Ring	15
Specific Gravity, g/cc	

[1]Not to be used for specification
[2]DuPont Performance Elastomers proprietary test method – maximum application temperature and Pressure may vary with seal design and application specifics
[3]ASTM D2240 (pellet test specimen)
[4]ASTM D412, 500mm/min
[5]ASTM D395B

Additional Physical Properties[1]	
Tg[2], °C (°F)	
TR-10[3], °C (°F)	1 (33)
Brittle Point[4], °C (°F)	
Abrasion Resistance[5], (volume loss, cubic mm)	131.3
Coefficient of friction[6] (to steel) Static Dynamic	
Volume resistivity[7], ohms/square	
Surface resistivity[7], Ohm-cm	
Dielectric Constant[8] at 150°C and 1 MHz	
Dissipation Factor[8] at 150°C and 1MHz	

[1]Not to be used for specification
[2]DuPont Performance Elastomers proprietary test method – maximum application temperature and Pressure may vary with seal design and application specifics
[3]ASTM D1329
[4]ASTM D746
[5]Din 53 516
[6]ASTM 1894
[7]ASTM D 257
[8]ASTM D150

For further information please contact one of the offices below, or visit our website at www.dupontelastomers.com/kalrez

Global Headquarters – Wilmington, DE USA
Tel. +1-800-853-5515
+1-302-792-4000
Fax +1-302-792-4450

European Headquarters - Geneva
Tel. +41-22-717-4000
Fax +41-22-717-4001

South & Central America Headquarters - Brazil
Tel. +55-11-4166-8978
Fax +55-11-4166-8989

Asia Pacific Headquarters - Singapore
Tel. +65-6275-9383
Fax +65-6275-9395

Japan Headquarters – Tokyo
Tel. +81-3-6402-6300
Fax. +81-3-6402-6301

Technical Information

Preliminary Product Datasheet

Kalrez® perfluoroelastomer parts
From DuPont Performance Elastomers

Kalrez® 8002UP for NMR Tubing

Kalrez® 8002UP perfluoroealstomer parts for NMR (nuclear magnetic resonance) tubing is a clear, transparent flexible product designed specifically for NMR sample tubes in standard and superior research applications of RDC NMR (residual dipolar coupling nuclear magnetic resonance). Kalrez® 8002UP for tubing has been shown in third party testing[1] to provide for more reliable and precise results. Because Kalrez® 8002UP for tubing is an elastomeric part, it can be stretched to disperses the sample in a uniform and highly controllable manner to provide superior RDC data sets. Kalrez® 8002UP perfluoroelastomer parts are especially useful as they contribute no proton background, are transparent, and are resistant to common NMR solvents in addition to their highly controllable stretch properties.

Performance Features/Benefits

- Flexibility for controlled sample orientation
- Quick recovery properties
- Clear and transparent enabling easy evaluation of the sample condition
- Strength, with a high resistance to breakage when stretched in the presence of common NMR solvents allowing thin, highly homogeneous tubes
- Excellent UV and thermal stability
- Excellent resistance to aggressive chemicals
- Tubes can be placed in a vacuum, frozen (>-10°C) and thawed for easy degassing
- High-temperature stability (up to 275°C) for excellent variable temperature (VT) capability

Specifications

Kalrez® 8002UP for NMR tubing is available in one size and is individually bar-coded and packaged for traceability. Ultrapure post-cleaning and packaging is standard for all parts made from Kalrez® 8002UP.

Part #	Outer Diameter (mm)	Thickness (mm)	Length (mm)
K665107	4.2	0.5	178

7.9 Supplemental Material for Chapter 5.1

Table A9.1.: NMR data[a, b] of compounds **3a**, **4a**, **5a**, and **6a**[c] as determined by Daniel Intelmann.

No.[d]	*trans*-Isocohumulone **(3a)**		Tricyclocohumol **(4a)**		Tricyclocohumene **(5a)**		Isotricyclocohumene **(6a)**	
	δ_H, m, *J* in Hz [e]	δ_C, m [f]	δ_H, m, *J* in Hz [e]	δ_C, m [f]	δ_H, m, *J* in Hz [e]	δ_C, m [f]	δ_H, m, *J* in Hz [e]	δ_C, m [f]
1		203.6 [C]		204.1 [C]		203.8 [C]		204.4 [C]
2		111.4 [C]		112.4 [C]		n.a. [g]		n.a. [g]
3		198.3 [C]		201.1 [C]		n.a. [g]		n.a. [g]
4		90.4 [C]		85.4 [C]		84.3 [C]		85.7 [C]
5	2.96, dd, 9.6, 5.3	57.1 [CH]	2.98, dd, 10.6, 8.2	55.6 [CH]	3.01, dd, 10.7, 7.5	56.2 [CH]	2.84, dd, 10.5, 8.0	55.2 [CH]
1'		210.0 [C]		86.7 [C]		87.9 [C]		86.6 [C]
2'α	3.43, dd, 20.2, 6.8	39.9 [CH_2]	1.62, dd, 13.2, 12.7	39.0 [CH_2]	1.62, d, 9.6	40.5 [CH_2]	2.29, m, 16.7	43.2 [CH_2]
2'β	3.46, dd, 20.2, 6.9		1.74, ddd, 13.2, 6.7, 1.8				2.44, m, 16.7	
3'	5.24, dd, 6.9, 6.8	116.5 [CH]	2.17, dd, 12.7, 6.7	59.9 [CH]	2.78, dd, 9.6, 9.6	56.8 [CH]		141.4 [C]
4'		136.2 [C]		73.0 [C]		146.1 [C]		125.7 [C]
5'	1.59, s	18.2 [CH_3]	1.27, s	29.8 [CH_3]	1.70, s	24.2 [CH_3]	1.71, s	20.6 [CH_3]
6'α	1.73, s	25.9 [CH_3]	1.13, s	31.2 [CH_3]	4.54, s	111.3 [CH_2]	1.50, s	23.6 [CH_3]
6'β					4.81, s			
1"α	2.26, ddd, 15.4, 9.6, 9.6	24.9 [CH_2]	1.59, ddd, 13.8, 11.3, 8.2	27.8 [CH_2]	1.50, ddd, 14.1, 10.5, 7.5	27.4 [CH_2]	1.27, m	28.8 [CH_2]
1"β	2.49, m, 15.4, 5.3, 5.1		2.11, ddd, 13.8, 10.6, 8.9		2.13, ddd, 14.1, 10.7, 7.5		2.16, m	
2"	5.17, m, 9.6, 5.1	122.3 [CH]	2.31, ddd, 11.3, 8.9, 1.8	66.6 [CH]	2.39, dd, 10.5, 7.5	65.8 [CH]	2.24, m	66.4 [CH]
3"		134.9 [C]		43.3 [C]		42.4 [C]		45.5 [C]
4"	1.51, s	18.1 [CH_3]	1.15, s	23.6 [CH_3]	0.77, s	22.3 [CH_3]	1.21, s	26.5 [CH_3]
5"	1.67, s	25.9 [CH_3]	1.26, s	36.3 [CH_3]	1.25, s	34.4 [CH_3]	1.35, s	28.8 [CH_3]
1'"		204.3 [C]		206.6 [C]		205.4 [C]		205.1 [C]
2'"	3.53, m, 6.8	36.3 [CH]	3.56, m, 6.8	37.3 [CH]	3.58, m, 6.8	36.3 [CH]	3.65, m, 6.8	37.2 [CH]
3'"	1.14, d, 6.8	18.3 [CH_3]	1.12, d, 6.8	18.0 [CH_3]	1.10, d, 6.8	18.1 [CH_3]	1.07, d, 6.8	18.5 [CH_3]
4'"	1.09, d, 6.8	18.4 [CH_3]	1.12, d, 6.8	18.5 [CH_3]	1.10, d, 6.8	18.1 [CH_3]	1.07, d, 6.8	18.9 [CH_3]

[a] Bruker DMX 400 NMR spectrometer, CD_3OD as NMR solvent, ^1H and ^{13}C chemical shifts are given in ppm referenced to the solvent signal (δ_H = 3.31 ppm, δ_C = 49.05 ppm). [b] Assignment made by 2D NMR experiments (COSY, HMQC, HMBC). [c] Compound numbering is referring to Figures 5.1. and 5.2. [d] Arbitrary numbering of atoms according to structures **3a**, **4a**, **5a**, and **6a** in Figures 5.1. and 5.2. [e] Coupling constants of multiplet signals are obtained by means of *J*-simulation with MestreNova.[Mestre] [f] Multiplicity determined by either DEPT 135 for **3a** or 2D NMR experiments (COSY, HMQC, HMBC) for **4a**-**6a**. [g] not assigned.

7.10 Supplemental Material for Chapter 5.2

The following samples were used:

Staurosporine solution sample: 4.2 mg staurosporine were dissolved in 450 µL $CDCl_3$ in a standard 5 mm NMR tube.

dPS sample for RDC measurements: Polymer stick with 1.6 mm diameter, polymerized with 0.2% DVB and 0.1% AIBN, swollen in NMR tube with 3.0 mm outer and 2.4 mm inner diameter. Quadrupolar splitting of the solvent $CDCl_3$: 26.8 Hz. 2 mg of staurosporine was added and allowed to diffuse for about 1 week.

Table A10.1.: Proton and carbon chemical shifts of staurosporine in $CDCl_3$ and in the corresponding dPS/$CDCl_3$ gel.

Group	chemical shifts in $CDCl_3$		chemical shifts in dPS gel	
	^{1}H[ppm]	^{13}C[ppm]	^{1}H[ppm]	^{13}C[ppm]
2'	-	91.2	-	*
3'	3.90	84.1	3.87	84.0
4'	3.37	50.5	3.33	50.5
5'a	2.75	30.3	2.70	30.1
5'b	2.42	30.3	2.37	30.1
6'	6.57	80.4	6.52	80.2
Me	2.38	30.0	2.32	30.0
N Me	1.60	33.3	1.56	33.2
O Me	3.42	57.5	3.31	57.4
1	7.30	106.8	7.23	107.0
2	7.49	125.0	7.43	125.2
3	7.38	119.8	7.32	119.9
4	9.43	126.5	9.40	126.7
5	-	173.7	-	*
7	5.03	46.0	4.99	45.9
8	7.90	120.6	7.83	120.8
9	7.34	120.0	7.28	120.1
10	7.43	124.2	7.38	124.3
11	7.95	115.1	7.88	115.2
11a	-	139.8	-	*
12a	-	120.0	-	*
12b	-	127.2	-	*
13a	-	136.8	-	*
4a	-	123.7	-	*
4b	-	115.4	-	*
4c	-	132.3	-	*
7a	-	118.4	-	*
7b	-	114.1	-	*
7c	-	124.7	-	*

* shifts of quaternary carbons were not assigned in the gel sample.

Table A10.2. (next page): Alignment tensor parameters for the different possible structures of staurosporine as calculated with PALES[128, 129] using the RDCs given in Table 5.2. The accuracy of the fits is described by R^2 and χ^2. Axial and rhombic components (D_a, D_r) and principal axes of the alignment tensor (A_{xx}, A_{yy}, A_{zz}) with their corresponding eigenvectors (EV) are given. The Euler angles (α, β, γ) define the orientation in the gel. Only one of the four possible Euler angle combinations is given.

	SRRR boat	SRRR chair	SRSR boat	SRSR chair	SSRR boat	SSRR chair	SSSR boat	SSSR chair
R^2	0.8885	0.996	0.773	0.702	0.466	0.787	0.531	0.659
χ^2	33.903	0.780	29.301	179.973	70.172	32.497	61.143	200.014
D_a	4.3583×10^{-4}	-3.1395×10^{-4}	-3.4827×10^{-4}	6.6798×10^{-4}	-3.4988×10^{-4}	-3.7753×10^{-4}	-3.3605×10^{-4}	6.0918×10^{-4}
D_r	1.2668×10^{-4}	-1.5978×10^{-4}	-1.1055×10^{-4}	2.5079×10^{-4}	-1.7095×10^{-4}	-2.4164×10^{-4}	-7.1647×10^{-5}	2.3794×10^{-4}
A_{xx}	-2.4581×10^{-4}	7.4279×10^{-5}	1.8245×10^{-4}	-2.9180×10^{-4}	9.3453×10^{-5}	1.5072×10^{-5}	2.2858×10^{-4}	-2.5227×10^{-4}
A_{yy}	-6.2585×10^{-4}	5.5362×10^{-4}	5.1409×10^{-4}	-1.0442×10^{-3}	6.0631×10^{-4}	7.3998×10^{-4}	4.4352×10^{-4}	-9.6610×10^{-4}
A_{zz}	8.7166×10^{-4}	-6.2790×10^{-4}	-6.9654×10^{-4}	1.3360×10^{-3}	-6.9976×10^{-4}	-7.5505×10^{-4}	-6.7210×10^{-4}	1.2184×10^{-3}
EV A_{xx}	0.37, 0.66, -0.66	-0.87, -0.17, 0.46	0.53, 0.84, -0.11	0.30, 0.95, 0.11	-0.15, 0.78, 0.61	0.58, 0.81, 0.07	0.04, 0.79, 0.61	0.25, 0.97, 0.04
EV A_{yy}	0.83, -0.55, -0.09	0.45, -0.64, 0.62	-0.34, 0.33, 0.88	0.90, -0.32, 0.30	-0.39, -0.61, 0.69	-0.22, 0.07, 0.97	-0.56, -0.49, 0.67	0.92, -0.25, 0.28
EV A_{zz}	0.42, 0.51, 0.75	0.19, 0.75, 0.63	0.78, -0.42, 0.46	-0.32, 0.01, 0.95	0.91, -0.14, 0.40	0.78, -0.58, 0.21	0.83, -0.37, 0.43	-0.29, 0.03, 0.96
α	172.11°	233.30°	277.27°	290.49°	228.41°	265.76°	227.75°	261.64°
β	41.57°	50.67°	62.61°	18.63°	66.57°	77.61°	64.71°	163.27°
γ	129.66°	104.25°	208.61°	358.21°	188.66°	216.49°	203.89°	186.61°

7.11 Supplemental Material for Chapter 5.3

The following samples were used:

Solution sample I (used for 1D, COSY, HSQC, HMBC, ADEQUATE spectra and CLIP-HSQC, PE.HSQC spectra): unknown amount of the compound (estimated ≈ 10 mg) dissolved in 450 µL $CDCl_3$ in a standard 5 mm NMR tube.

PS gel sample (used for CLIP-HSQC, P.E.HSQC spectra): Polymer stick with 3.4 mm diameter, polymerized with 0.5% DVB and 0.075% AIBN, swollen in NMR tube with 5.0 mm outer and 4.2 mm inner diameter. Quadrupolar splitting of the solvent $CDCl_3$: 103 Hz. ≈ 30 mg of the compound was added and allowed to diffuse for 8 days.

Solution sample II (used for INADEQUATE spectrum): ≈ 80 mg of the compound dissolved in 250 µL $CDCl_3$ in a 5 mm Shigemi tube (matched for $CDCl_3$).

Solution sample III (used for ^{15}N,^{13}C couplings): ≈ 5 mg of the ^{15}N-isotope labeled compound dissolved in 250 µL $CDCl_3$ in a 5 mm Shigemi tube (matched for $CDCl_3$).

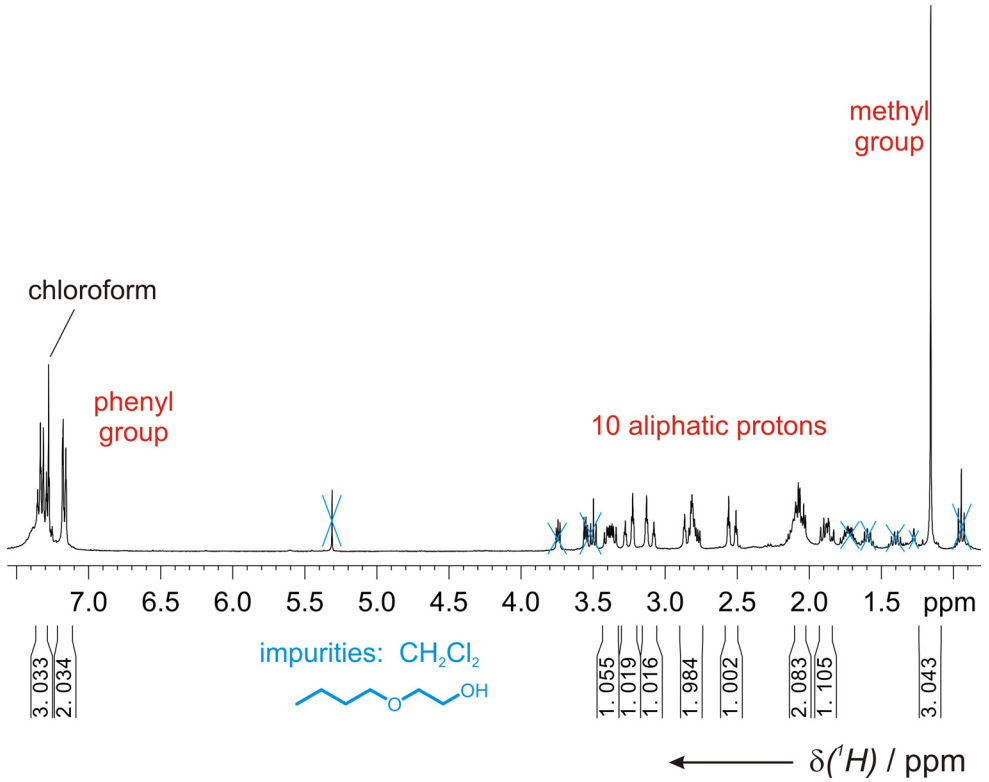

Figure A11.1.: Proton 1D spectrum of the unknown compound. Dichloromethane and 2-butoxyethanol could be identified as impurities (blue). A singlet for an isolated methyl group, the signals of a phenyl group, and 10 aliphatic protons can be observed.

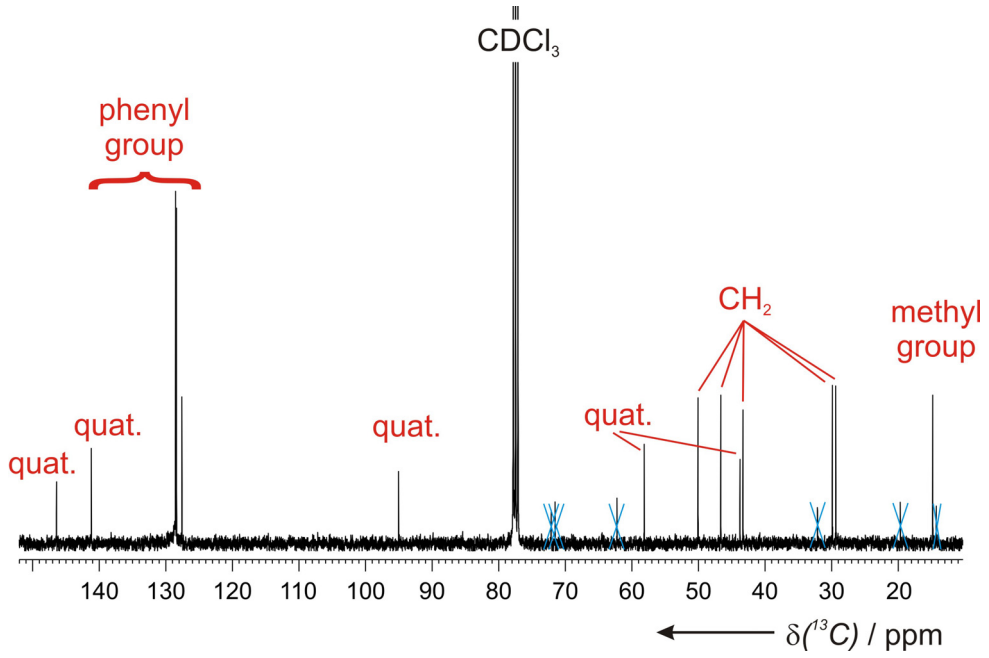

Figure A11.2.: Carbon 1D spectrum of the unknown compound. Signals of the compound are labeled according to their assignment as taken from 2D spectra (e.g. HSQC). Signals of the impurities dichloromethane and 2-butoxyethanol are crossed out (blue).

Table A11.1.: Carbon and proton chemical shifts for the unknown reaction product as taken from 1D and COSY spectra. Hydrogen atoms are assigned to their neighboring carbon atoms according to cross peaks of the HSQC spectrum. Shifts are referenced to the solvent signal (δ ($^{13}CDCl_3$) = 77.0 ppm; δ ($CHCl_3$) = 7.26 ppm).

^{13}C atom	δ (^{13}C) [ppm]	adjacent ^{1}H atom	δ (^{1}H) [ppm]
A	146.0	-	-
B	140.7	-	-
C	128.1	Ph3	7.35
D	128.0	Ph1	7.18
E	127.2	Ph2	7.28
F	94.6	-	-
J	57.9	-	-
K	49.7	7	2.81
		11	3.39
L	46.2	9	3.12
		10	3.26
M	43.5	-	-
N	42.9	6	2.54
		8	2.86
P	29.5	3	1.89
		4	2.07
Q	29.0	2	1.74
		5	2.12
S	14.6	1	1.17

Table A11.2.: Measured one-bond proton-carbon and two-bond proton-proton couplings taken from CLIP-HSQC[107] and PE.HSQC spectra[97] of the compound in isotropic $CDCl_3$ solution ($^1J_{CH}$ and $^2J_{HH}$) and diffused into a PS/$CDCl_3$ gel ($^1J_{CH} + D_{CH}$ and $^2J_{HH} + D_{HH}$) and the resulting residual dipolar couplings (D_{CH} and D_{HH}).

Group[a]	**$^1J_{CH}$ [Hz]**	**$^1J_{CH} + D_{CH}$ [Hz]**	**D_{CH} [Hz]**
S - 1	126.3 ± 0.2	122.7 ± 0.1	-3.6 ± 0.2[b]
Q - 2	129.9 ± 3.0	139.0 ± 3.5	9.1 ± 4.6
Q - 5	130.0 ± 2.0	124.4 ± 2.5	-5.6 ± 3.2
P - 3	128.3 ± 3.0	136.2 ± 3.5	7.9 ± 4.6
P - 4	129.0 ± 2.0	129.6 ± 2.5	0.6 ± 3.2
N - 6	126.0 ± 0.5	120.0 ± 0.5	-6.0 ± 0.7
N - 8	130.0 ± 1.0	132.1 ± 0.5	2.1 ± 1.1
L - 9	128.7 ± 0.5	125.2 ± 0.5	-3.5 ± 0.7
L - 10	131.6 ± 0.5	132.0 ± 0.5	0.4 ± 0.7
K - 7	136.8 ± 0.5	150.6 ± 0.5	13.8 ± 0.7
K - 11	141.4 ± 0.5	136.4 ± 0.8	-5.0 ± 0.9
E - Ph2	160.5 ± 0.5	151.6 ± 1.0	-8.9 ± 1.1
Group	**$^2J_{HH}$ [Hz]**	**$^2J_{HH} + D_{HH}$ [Hz]**	**D_{HH} [Hz]**
2 - 5	-9.9 ± 4.0	-4.2 ± 4.0	5.7 ± 5.7
3 - 4	-13.2 ± 4.0	-4.5 ± 4.0	8.7 ± 5.7
6 - 8	-18.5 ± 1.0	-23.4 ± 1.5	-4.9 ± 1.8
9 - 10	-18.6 ± 1.0	-23.9 ± 1.5	-5.3 ± 1.8
7 - 11	-12.2 ± 1.0	-4.9 ± 1.5	7.3 ± 1.8

[a] Numbering according to assignment given in Table A11.1.

[b] For the RDC analysis with PALES[128, 129] the D_{CH}-coupling of the methyl group has been converted[125] to the corresponding D_{CC}-coupling (D_{CC} = 1.0 ± 0.1 Hz) or D_{CN}-coupling (D_{CN} = -0.44 ± 0.1 Hz).

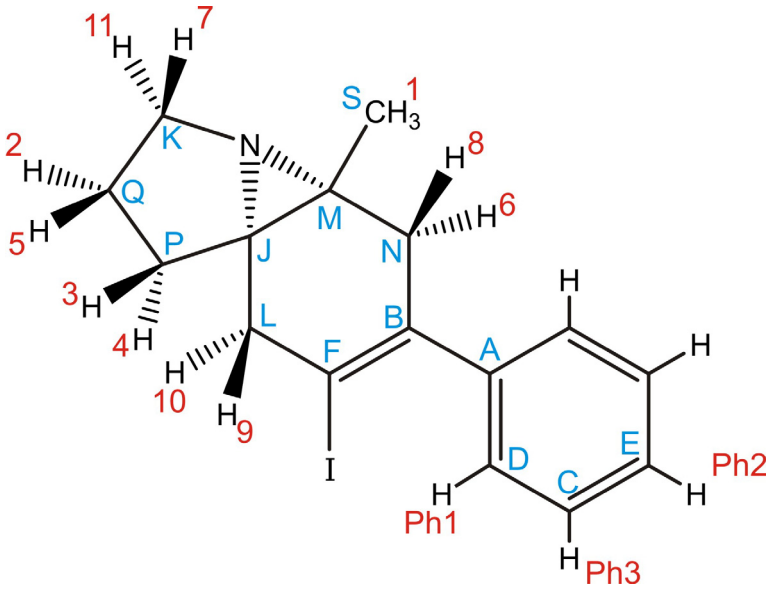

Figure A11.3.: Structure of the identified reaction product with resonance assignment including the assignment of prochiral groups. Carbons (blue letters) and hydrogens (red numbers) are labeled according to the assignment used in Tables A11.1. and A11.2.

7.12 Supplemental Material for Chapter 5.4

Table A12.1: Chemical shifts[(a)] of cholesterol and 5-α-cholestan-3-one in $CDCl_3$.

Group	cholesterol			5-α-cholestan-3-one		
	$\delta\ ^{13}C$ [ppm]	$\delta\ ^{1}H_a$[(b)] [ppm]	$\delta\ ^{1}H_b$[(b)] [ppm]	$\delta\ ^{13}C$ [ppm]	$\delta\ ^{1}H_a$[(b)] [ppm]	$\delta\ ^{1}H_b$[(b)] [ppm]
C1	37.3	1.1 (α)	1.9 (β)	38.6	1.3 (α)	2.0 (β)
C2	31.6	1.5 (β)	1.8 (α)	38.1	2.3 (α)	2.4 (β)
C3	71.7	3.5	-	212.1	-	-
C4	42.3	2.2	2.3	44.7	2.1 (α)	2.2 (β)
C5	141.2	-	-	46.7	1.5	-
C6	121.6	5.4	-	29.0	1.3	1.3
C7	31.9	1.5 (α)	2.0 (β)	31.7	0.9 (α)	1.7 (β)
C8	31.9	1.5	-	35.4	1.4	-
C9	50.2	0.9	-	53.9	0.7	-
C10	36.9	-	-	36.0	-	-
C11	21.1	1.5	1.5	21.5	1.4 (β)	1.5 (α)
C12	39.8	1.2 (α)	2.0 (β)	39.9	1.1 (α)	2.0 (β)
C13	42.7	-	-	43.0	-	-
C14	56.8	1.0	-	56.3	1.0	-
C15	24.3	1.1	1.6	24.2	1.1	1.6
C16	28.3	1.3	1.8	28.3	1.2	1.8
C17	56.2	1.1	-	56.3	1.1	-
C18	11.9	0.7	-	12.1	0.7	-
C19	19.4	1.0	-	11.4	1.0	-
C20	35.8	1.4	-	35.8	1.4	-
C21	18.8	0.9	-	18.7	0.9	-
C22	36.2	1.0	1.4	36.2	1.0	1.3
C23	23.9	1.2	1.4	23.8	1.1	1.3
C24	39.6	1.1	1.2	39.5	1.1	1.1
C25	28.0	1.5	-	28.0	1.5	-
C26	22.7	0.9	-	22.8	0.9	-
C27	22.9	0.9	-	22.6	0.8	-

(a) Chemical shifts are referenced to the solvent signals: $\delta\ ^{1}H$ ($CHCl_3$) = 7.26 ppm and $\delta\ ^{13}C$ ($CDCl_3$) = 77.2 ppm.
(b) The prochiral assignment for Hα and Hβ protons was done with the help of measured RDCs (see Tables A12.2. and A12.3.). Protons a and b have not been assigned to position α and β wherever no or inconclusive RDCs were measured. α and β refers to the standard steroid nomenclature.

Table A12.2.: Couplings of cholesterol measured in solution ($^1J_{CH}$) and in the stretched PDMS gel ($^1T_{CH}$), corresponding RDCs ($^1D_{CH}$) and RDCs back calculated with the "-bestFit" option of PALES[128, 129] (SVD-fit). All couplings are given in Hz.

Group [a]	$^1J_{CH}$	$^1T_{CH} = {}^1J_{CH} + {}^1D_{CH}$	$^1D_{CH}$ (exp)	$^1D_{CH}$ (calc) (SVD-fit)
C18-H18	124.3 ± 0.3	117.3 ± 0.5	-7.0 ± 0.6[b]	(1.9)[b]
C19-H19	125.6 ± 0.3	119.0 ± 0.5	-6.6 ± 0.6[b]	(1.8)[b]
C16-H16a	125.3 ± 3.0	125.6 ± 5.0	0.3 ± 5.8	-[c]
C16-H16b	129.7 ± 3.0	134.8 ± 5.0	5.1 ± 5.8	-[c]
C15-H15b	130.0 ± 3.0	144.0 ± 5.0	14.0 ± 5.8	-[c]
C2-H2α	129.3 ± 2.5	140.6 ± 3.0	11.3 ± 3.9	9.6
C2-H2β	125.2 ± 2.5	141.3 ± 3.0	16.1 ± 3.9	16.5
C8-H8	122.0 ± 3.0	142.7 ± 8.0	20.7 ± 8.5	22.3
C7-H7β	126.5 ± 3.0	140.7 ± 5.0	14.2 ± 5.8	11.7
C1-H1β	128.4 ± 1.0	137.4 ± 1.0	9.0 ± 1.4	9.1
C1-H1α	124.3 ± 0.8	142.5 ± 1.2	18.2 ± 1.4	19.2
C12-H12α	123.2 ± 1.0	145.6 ± 1.0	22.4 ± 1.4	21.8
C12-H12β	127.0 ± 1.0	132.1 ± 1.0	5.1 ± 1.4	4.6
C6-H6	152.7 ± 0.3	154.3 ± 3.0	1.6 ± 3.0	2.2
C9-H9	122.4 ± 0.5	146.0 ± 4.0	23.6 ± 4.0	21.7
C3-H3	142.1 ± 0.5	161.4 ± 1.5	19.3 ± 1.6	17.9
C21-H21	124.1 ± 0.3	119.2 ± 0.5	-4.9 ± 0.6	-[d]
C25-H25	124.8 ± 0.5	135.6 ± 0.8	10.8 ± 0.9	-[d]
C20-H20	123.6 ± 0.5	146.9 ± 1.0	23.3 ± 1.1	-[d]
C27-H27	124.1 ± 0.3	124.3 ± 0.3	-0.2 ± 0.4	-[d]
C26-H26	124.1 ± 0.3	123.9 ± 0.3	0.2 ± 0.4	-[d]
C23-H23a	124.1 ± 1.0	142.2 ± 5.0	18.1 ± 5.1	-[d]
C23-H23b	124.3 ± 1.0	129.5 ± 2.5	5.2 ± 2.7	-[d]
C22-H22a	123.0 ± 5.0	148.6 ± 4.0	25.6 ± 6.4	-[d]
C22-H22b	126.0 ± 10.0	134.7 ± 3.0	8.7 ± 10.4	-[d]
Group	$^2J_{HH}$	$^2T_{HH} = {}^2J_{HH} + {}^2D_{HH}$	$^2D_{HH}$ (exp)	$^2D_{HH}$ (calc) (SVD-fit)
H16α-H16β	-12.0 ± 2.0	5.7 ± 3.0	17.7 ± 3.6	-[c]
H15α-H15β	-11.0 ± 3.0	3.0 ± 3.0	14.0 ± 4.2	-[c]
H2α-H2β	-12.2 ± 1.0	6.7 ± 2.0	18.9 ± 2.2	20.6
H7α-H7β	-16.0 ± 3.0	1.7 ± 5.0	17.7 ± 5.8	19.8
H1α-H1β	-13.0 ± 1.0	2.0 ± 2.0	15.0 ± 2.2	15.8
H12α-H12β	-12.2 ± 1.0	2.0 ± 2.0	14.2 ± 2.2	14.1
H4α-H4β	-12.7 ± 2.0	3.0 ± 2.0	15.7 ± 2.8	16.8

(a) The prochiral assignment for all Hα and Hβ protons was determined by fitting all possible permutations with the "-bestFit" option of PALES[128, 129] and selecting the one with the best fitting result (in terms of highest n/χ^2 value).

(b) D_{CH}-couplings of methyl groups have been converted[125] to the corresponding D_{CC}-couplings: (D_{CC}(C18-C13) = 1.9 ± 0.2 Hz; D_{CC}(C19-C10) = 1.8 ± 0.2 Hz).

(c) As couplings in the D-ring did not fit in the initial fittings (see main text) they were not used in the further fittings.

(d) Couplings measured in the flexible side chain, were not used for PALES fits.

Table A12.3.: Couplings of 5-α-cholestan-3-one measured in solution ($^1J_{CH}$) and in the stretched PDMS gel ($^1T_{CH}$), corresponding RDCs ($^1D_{CH}$) and RDCs back calculated with the "-bestFit" option of PALES[128, 129] (SVD-fit). All couplings are given in Hz.

Group [a]	$^1J_{CH}$	$^1T_{CH} = {}^1J_{CH} + {}^1D_{CH}$	$^1D_{CH}$ (exp)	$^1D_{CH}$ (calc) (SVD-fit)
C19-H19	124.4 ± 0.2	117.2 ± 0.8	-7.2 ± 0.8[b]	(2.1)[b]
C18-H18	124.1 ± 0.2	116.9 ± 0.5	-7.2 ± 0.5[b]	(2.0)[b]
C16-H16a	125.6 ± 3.0	123.7 ± 5.0	-1.9 ± 5.8	-[c]
C16-H16b	129.9 ± 2.0	138.4 ± 3.0	8.5 ± 5.4	-[c]
C15-H15a	126.6 ± 1.0	138.2 ± 5.0	11.6 ± 5.1	-[c]
C15-H15b	130.1 ± 1.0	144.1 ± 5.0	14.0 ± 5.1	-[c]
C11-H11β	122.1 ± 0.2	148.8 ± 3.0	26.7 ± 3.0	24.4
C11-H11α	125.5 ± 0.2	131.0 ± 3.0	5.5 ± 3.0	3.9
C7-H7β	127.9 ± 0.2	132.0 ± 5.0	4.1 ± 5.0	2.5
C7-H7α	122.8 ± 0.3	148.7 ± 1.5	25.9 ± 1.5	24.6
C8-H8	122.5 ± 0.3	149.7 ± 1.0	27.2 ± 1.0	25.2
C2-H2α	134.1 ± 1.0	141.0 ± 3.0	6.9 ± 3.2	6.4
C2-H2β	122.4 ± 1.0	143.5 ± 3.0	21.1 ± 3.2	20.5
C1-H1β	129.6 ± 0.7	136.9 ± 1.0	7.3 ± 1.2	7.6
C1-H1α	125.8 ± 0.7	146.5 ± 1.5	20.7 ± 1.7	23.5
C12-H12α	123.1 ± 0.5	150.5 ± 1.5	27.4 ± 1.6	24.8
C12-H12β	127.0 ± 0.5	131.3 ± 1.0	4.3 ± 1.1	3.8
C4-H4α	132.6 ± 0.7	139.3 ± 0.8	6.7 ± 1.1	6.9
C4-H4β	122.3 ± 0.7	145.0 ± 1.5	22.7 ± 1.7	23.1
C5-H5	123.3 ± 2.0	151.1 ± 3.0	27.8 ± 3.6	24.3
C9-H9	121.3 ± 0.5	145.0 ± 1.0	23.7 ± 1.1	24.7
C21-H21	124.1 ± 0.2	119.1 ± 0.7	-5.0 ± 0.7	-[d]
C25-H25	124.8 ± 0.2	136.2 ± 0.8	11.4 ± 0.8	-[d]
C20-H20	124.0 ± 0.2	147.3 ± 1.0	23.3 ± 1.0	-[d]
C27-H27	124.2 ± 0.2	123.7 ± 0.3	-0.5 ± 0.4	-[d]
C26-H26	124.0 ± 0.2	124.2 ± 0.3	0.2 ± 0.4	-[d]
C23-H23a	124.0 ± 1.8	144.5 ± 8.0	20.5 ± 8.2	-[d]
C23-H23b	123.5 ± 3.0	132.0 ± 8.0	8.5 ± 8.5	-[d]
C22-H22a	123.0 ± 3.0	149.7 ± 5.0	26.7 ± 5.8	-[d]
C22-H22b	125.8 ± 1.0	134.5 ± 5.0	8.7 ± 5.1	-[d]
Group	$^2J_{HH}$	$^2T_{HH} = {}^2J_{HH} + {}^2D_{HH}$	$^2D_{HH}$ (exp)	$^2D_{HH}$ (calc) (SVD-fit)
H16α-H16β	-10.1 ± 2.0	7.1 ± 3.0	17.2 ± 3.6	-[c]
H15α-H15β	-9.9 ± 2.0	5.8 ± 3.0	15.7 ± 3.6	-[c]
H11α-H11β	-13.2 ± 1.0	0.0 ± 3.0	13.2 ± 3.2	17.6
H7α-H7β	-11.8 ± 1.0	3.0 ± 3.0	14.8 ± 3.2	17.4
H2α-H2 β	-15.2 ± 1.5	3.0 ± 3.0	18.2 ± 3.4	22.6
H1α-H1 β	-12.8 ± 1.0	4.2 ± 3.0	17.0 ± 3.2	16.9
H12α-H12β	-11.8 ± 1.5	1.5 ± 3.0	13.3 ± 3.4	13.8
H4α-H4β	-14.6 ± 1.5	2.4 ± 3.0	17.0 ± 3.4	18.9

(a) The prochiral assignment for all Hα and Hβ protons was determined by fitting all possible permutations with the -bestFit option of PALES[128, 129] and selecting the one with the best fitting result (in term of highest n/χ^2 value).

(b) D_{CH}-couplings of methyl-groups have been converted[125] to the corresponding D_{CC}-couplings: (D_{CC}(C19-C10) = 1.9 ± 0.2 Hz; D_{CC}(C18-C13) = 1.9 ± 0.1 Hz)

(c) As couplings in the D-ring did not fit in the initial fittings (see main text) they were not used in the further fittings.

(d) Couplings measured in the flexible side chain, were not used for PALES fits.

Group	D (exp)	D (calc) (SVD-fit)		D (calc) (cross-fitting)		D (calc) (predicted C1-C27)	
		Cholesterol	10αCholesterol	Cholesterol	10αCholesterol	Cholesterol	10αCholesterol
C18-C13	1.9 ± 0.2	1.9	2.0	2.0	2.0	1.8	2.0
C19-C10	1.8 ± 0.2	1.8	1.6	2.0	0.5	1.7	1.2
C2-H2α	11.3 ± 3.9	9.6	10.9	5.0	4.6	4.9	7.8
C2-H2β	16.1 ± 3.9	16.5	16.1	20.7	22.9	15.0	18.2
C8-H8	20.7 ± 8.5	22.3	21.3	25.4	25.2	21.7	20.6
C7-H7β	14.2 ± 5.8	11.7	23.0[(a)]	7.2	23.9[(a)]	6.5	22.4[(a)]
C1-H1β	9.0 ± 1.4	9.1	6.7[(a)]	7.5	5.3	11.2	11.5[(a)]
C1-H1α	18.2 ± 1.4	19.2	17.9[(a)]	23.3	8.8	18.2	12.8[(a)]
C12-H12α	22.4 ± 1.4	21.8	20.9	24.6	24.8	21.3	20.7
C12-H12β	5.1 ± 1.4	4.6	6.0	3.5	3.7	8.7	12.5
C6-H6	1.6 ± 3.0	2.2	5.7	2.1	8.5	7.1	9.5
C9-H9	23.6 ± 4.0	21.7	18.7	24.4	24.7	21.2	19.0
C3-H3	19.3 ± 1.6	17.9	18.6	22.0	4.2	16.7	14.9
H2α-H2β	18.9 ± 2.2	20.6	23.8	21.9	18.9	19.6	20.7
H7α-H7β	17.7 ± 5.8	19.8	19.2	20.7	11.7	18.4	15.3
H1α-H1β	15.0 ± 2.2	15.8	15.6	15.1	14.8	15.3	14.8
H12α-H12β	14.2 ± 2.2	14.1	15.4	13.0	13.4	15.5	19.8
H4α-H4β	15.7 ± 2.8	16.8	13.9	16.3	2.5	15.9	14.7
	D_a	-3.94E-04	-3.56E-04	-3.97E-04		-3.72E-04	-4.06E-04
	D_r	-6.44E-05	-1.31E-04	-1.10E-04		-7.02E-05	-6.97E-05
	A_{xx}	2.98E-04	1.59E-04	2.32E-04		2.67E-04	3.02E-04
	A_{yy}	4.91E-04	5.53E-04	5.62E-04		4.77E-04	5.11E-04
	A_{zz}	-7.89E-04	-7.12E-04	-7.94E-04		-7.44E-04	-8.12E-04
	EV A_{xx}	-0.48; 0.85; -0.22	-0.36; 0.93; -0.09	-0.45; 0.87; -0.19		-0.34; 0.92; -	-0.24; 0.92; -
	EV A_{yy}	-0.58; -0.12; 0.80	-0.43; -0.08; 0.90	-0.65; -0.17; 0.74		-0.61; -0.08;	-0.55; 0.13; 0.83
	EV A_{zz}	0.65; 0.52; 0.55	0.83; 0.36; 0.43	0.62; 0.45; 0.64		0.71; 0.38; 0.59	0.80; 0.37; 0.47
	n	18	18	18	18	18	18
	χ^2	3.32	16.96	30.71	225.07	21.17	82.82
	n/χ^2	5.42	1.06	0.59	0.08	0.85	0.22
	R	0.984	0.911	0.940	0.679	0.900	0.800
	Q	0.082	0.195	0.214	0.435	0.198	0.275

(a) Hα and Hβ proton assignment was permutated compared to the assignment of cholesterol. (Of all possible permutations of the prochiral methylene groups only the fit with the best result is shown.)

Table A12.4. (previous page): RDCs measured on cholesterol and RDCs back calculated for cholesterol and 10-α-cholesterol for the SVD-fit, the fit with fixed orientation given by the alignment tensor of 5-α-cholestan-3-one (cross-fitting), and the fit with orientation predicted by PALES. All couplings are given in Hz. Additionally, alignment tensor parameters and quality factors for the different fits are given: Axial and rhombic components (D_a, D_r) and principal axes of the alignment tensor (A_{xx}, A_{yy}, A_{zz}) with their corresponding eigenvectors (EV), number of RDCs used for fitting (n) and quality factors χ^2, n/χ^2, correlation factor (R) and quality factor by Cornilescu et al. (Q).

Table A12.5. (next page): RDCs measured on 5-α-cholestan-3-one and RDCs back calculated for 5-α-cholestan-3-one and 5-β-cholestan-3-one a for the SVD-fit, the fit with fixed orientation given by the alignment tensor of 5-α-cholestan-3-one (cross-fitting), and the fit with orientation predicted by PALES. All couplings are given in Hz. Additionally, alignment tensor parameters and quality factors for the different fits are given: Axial and rhombic components (D_a, D_r) and principal axes of the alignment tensor (A_{xx}, A_{yy}, A_{zz}) with their corresponding eigenvectors (EV), number of RDCs used for fitting (n) and quality factors χ^2, n/χ^2, correlation factor (R) and quality factor by Cornilescu et al. (Q).

Group	D (exp)	D (calc) (SVD-fit)		D (calc) (cross-fitting)		D (calc) (predicted C1-C27)	
	5αCholestan3one	5αCholestan3one	5βCholestan3one	5αCholestan3one	5βCholestan3one	5αCholestan3one	5βCholestan3one
C19-C10	1.9 ± 0.2	2.1	2.2	1.8	1.7	1.9	1.8
C18-C13	1.9 ± 0.1	2.0	1.7	1.9	1.9	2.0	1.9
C11-H11β	26.7 ± 3.0	24.4	22.8	21.5	21.7	23.0	22.0
C11-H11α	5.5 ± 3.0	3.9	-9.1	9.0	7.9	1.4	-0.7
C7-H7β	4.1 ± 5.0	2.5	-11.2	7.8	6.5	-0.2	-2.6
C7-H7α	25.9 ± 1.5	24.5	24.7	21.1	21.8	22.5	22.2
C8-H8	27.2 ± 1.0	25.2	25.5	22.4	22.2	23.9	22.6
C2-H2α	6.9 ± 3.2	6.4	-4.9	10.8	1.4[(a)]	4.7	2.8
C2-H2β	21.1 ± 3.2	20.5	26.6	15.7	10.4[(a)]	16.0	6.1
C1-H1β	7.3 ± 1.2	7.6	5.5	9.4	7.5[(a)]	13.0	11.5[(a)]
C1-H1α	20.7 ± 1.7	23.5	30.0	18.6	14.7[(a)]	20.0	14.5([(a)]
C12-H12α	27.4 ± 1.6	24.8	24.4	21.8	21.9	23.3	22.2
C12-H12β	4.3 ± 1.1	3.8	4.0	5.0	5.0	10.6	11.7
C4-H4α	6.7 ± 1.1	6.9	5.3[(a)]	8.6	5.1[(a)]	13.0	-10.4
C4-H4β	22.7 ± 1.7	23.1	11.0[(a)]	17.2	-15.4[(a)]	19.1	11.8
C5-H5	27.8 ± 3.6	24.3	-0.5	20.0	-23.1	21.5	-19.3
C9-H9	23.7 ± 1.1	24.7	25.3	21.5	21.5	23.0	22.0
H11α-H11β	13.2 ± 3.2	17.5	10.4	18.2	17.6	17.1	14.5
H7α-H7β	14.8 ± 3.2	17.4	9.5	18.1	16.9	16.8	13.3
H2α-H2 β	18.2 ± 3.4	22.6	26.8	20.9	17.9	21.5	19.6
H1α-H1 β	17.0 ± 3.2	16.9	16.7	16.9	13.7	17.9	12.4
H12α-H12β	13.3 ± 3.4	13.7	6.3	14.7	14.5	17.6	16.4
H4α-H4β	17.0 ± 3.4	18.8	7.7	18.2	-12.7	19.4	-2.6
D_a		-3.97E-04	-4.29E-04	-3.94E-04		-4.32E-04	-4.04E-04
D_r		-1.10E-04	-2.08E-04	-6.44E-05		-6.63E-05	-7.87E-05
A_{xx}		2.32E-04	1.17E-04	2.98E-04		3.33E-04	2.86E-04
A_{yy}		5.62E-04	7.41E-04	4.91E-04		5.32E-04	5.22E-04
A_{zz}		-7.94E-04	-8.58E-04	-7.89E-04		-8.64E-04	-8.08E-04
EV A_{xx}		-0.45; 0.87; -0.19	0.54; -0.84; -0.99	-0.48; 0.85; -0.22		-0.31; 0.94; -0.16	-0.36; 0.93; -0.08
EV A_{yy}		-0.65; -0.17; 0.74	0.65; 0.49; -0.59	-0.58; -0.12; 0.80		-0.62; -0.07; 0.78	-0.62; -0.18; 0.77
EV A_{zz}		0.62; 0.45; 0.64	0.54; 0.25; 0.80	0.65; 0.52; 0.55		0.72; 0.34; 0.61	0.70; 0.33; 0.64
n		23	23	23	23	23	23
χ^2		20.21	231.92	87.04	865.19	133.31	634.70
n/χ^2		1.13	0.10	0.26	0.03	0.17	0.04
R		0.974	0.741	0.929	0.203	0.902	0.429
Q		0.114	0.514	0.212	0.849	0.216	0.700

(a) Hα and Hβ proton assignment was permutated compared to the assignment of 5-α-cholestan-3-one. (Of all possible permutations of the prochiral methylene groups only the fit with the best result is shown.)

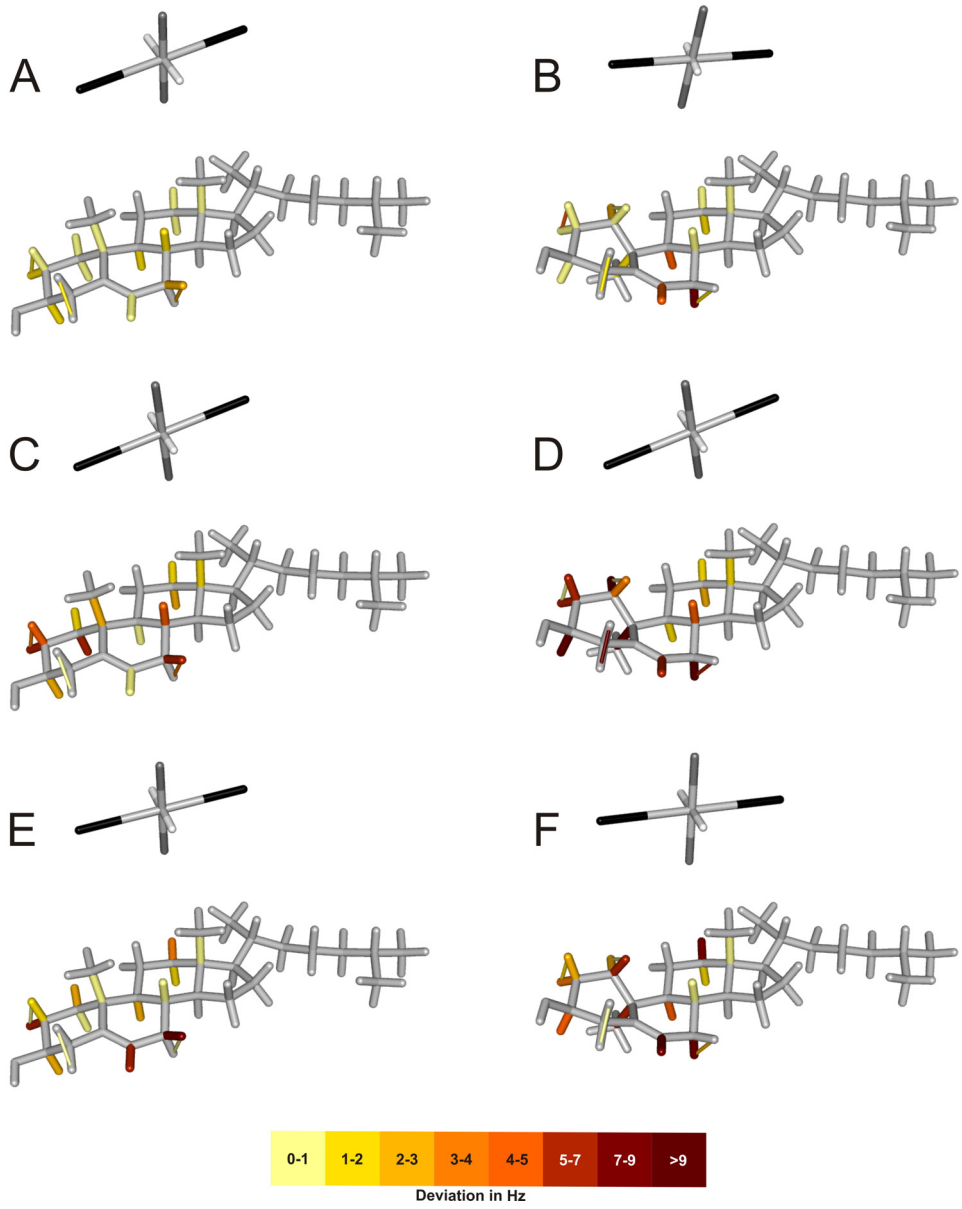

Figure A12.1.: Comparison of RDCs measured on cholesterol and back-calculated for the structures of cholesterol (left: A, C, E) and 10-α-cholesterol (right: B, D, F) using the "-bestFit" option (SVD-fit) of PALES[128, 129] (top: A, B), the cross-fitting approach with the alignment tensor determined for 5-α-cholestan-3-one in PDMS/$CDCl_3$ (middle: C, D) and the prediction by PALES[128, 129] (bottom: E, F). The structures are shown with color-coded bonds denoting the deviation between measured and back-calculated RDCs for the different fits. The corresponding alignment tensors are visualized with their principal axis systems (black: A_{zz}; gray: A_{yy}; white: A_{xx}).
For all three methods the cholesterol structure (left) gives clearly the better fit. The direct SVD-fit for 10-α-cholesterol (B) results in an alignment tensor which differs most significantly from the alignment tensors for all other fits, since it tries to match RDCs measured on cholesterol to the wrong structural model. It therefore has the least ability to distinguish the diastereomers. In contrast the fit with the fixed orientation given by the alignment tensor of 5-α-cholestan-3-one (D) shows small deviations (yellow) in regions similar to cholesterol (C-ring) and strong deviations (red) for those different to cholesterol (A- and B-ring).

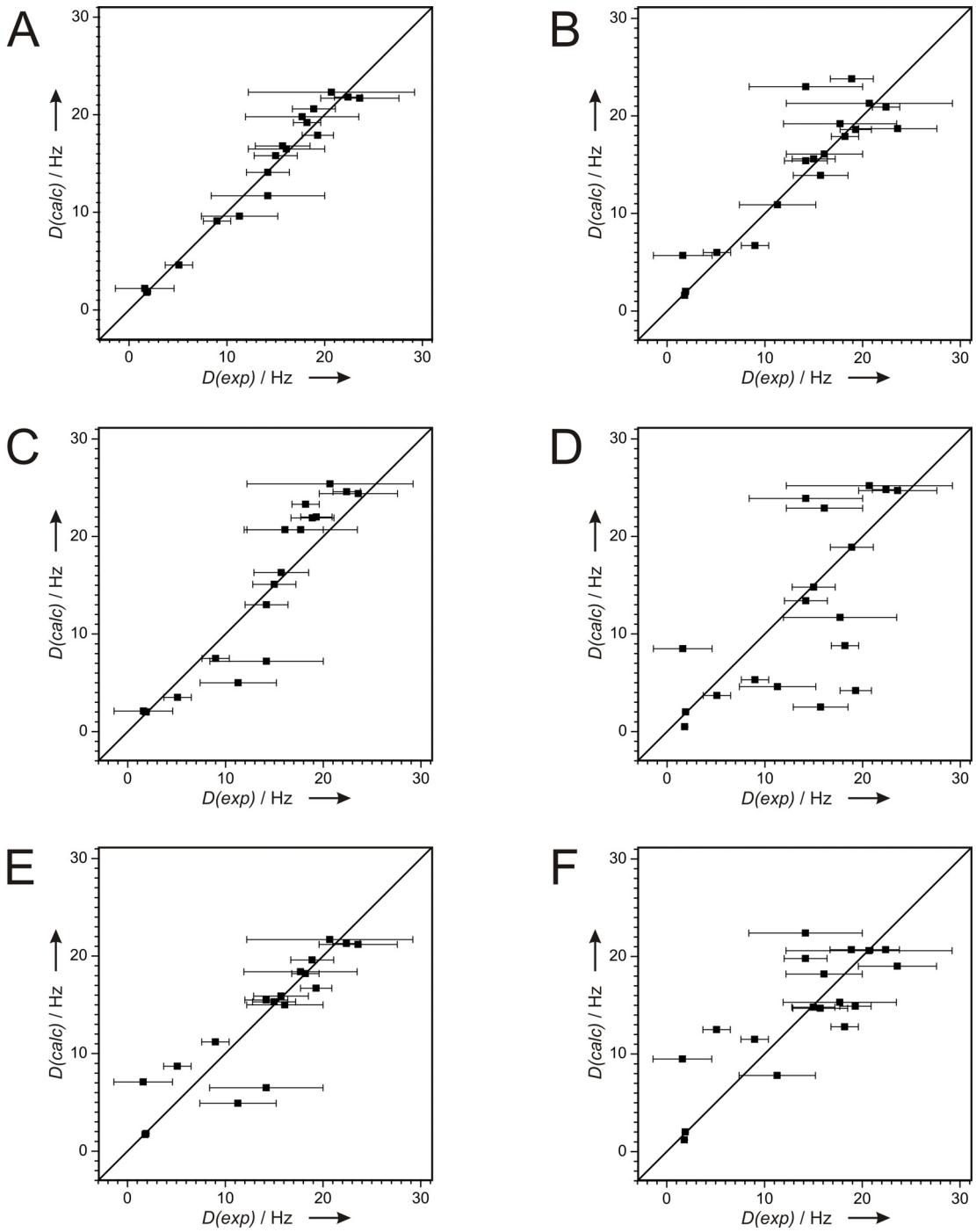

Figure A12.2.: Comparison of RDCs measured on cholesterol and back-calculated for the structures of cholesterol (left: A, C, E) and 10-α-cholesterol (right: B, D, F) using the "-bestFit" option (SVD-fit) of PALES[128, 129] (top: A, B), the cross-fitting approach (middle: C, D) and the prediction by PALES[128, 129] (bottom: E, F). The plots show the back-calculated RDCs, D(calc), as a function of the measured RDCs, D(exp). Clearly the correct diastereomer cholesterol (left) is favored in all three methods.

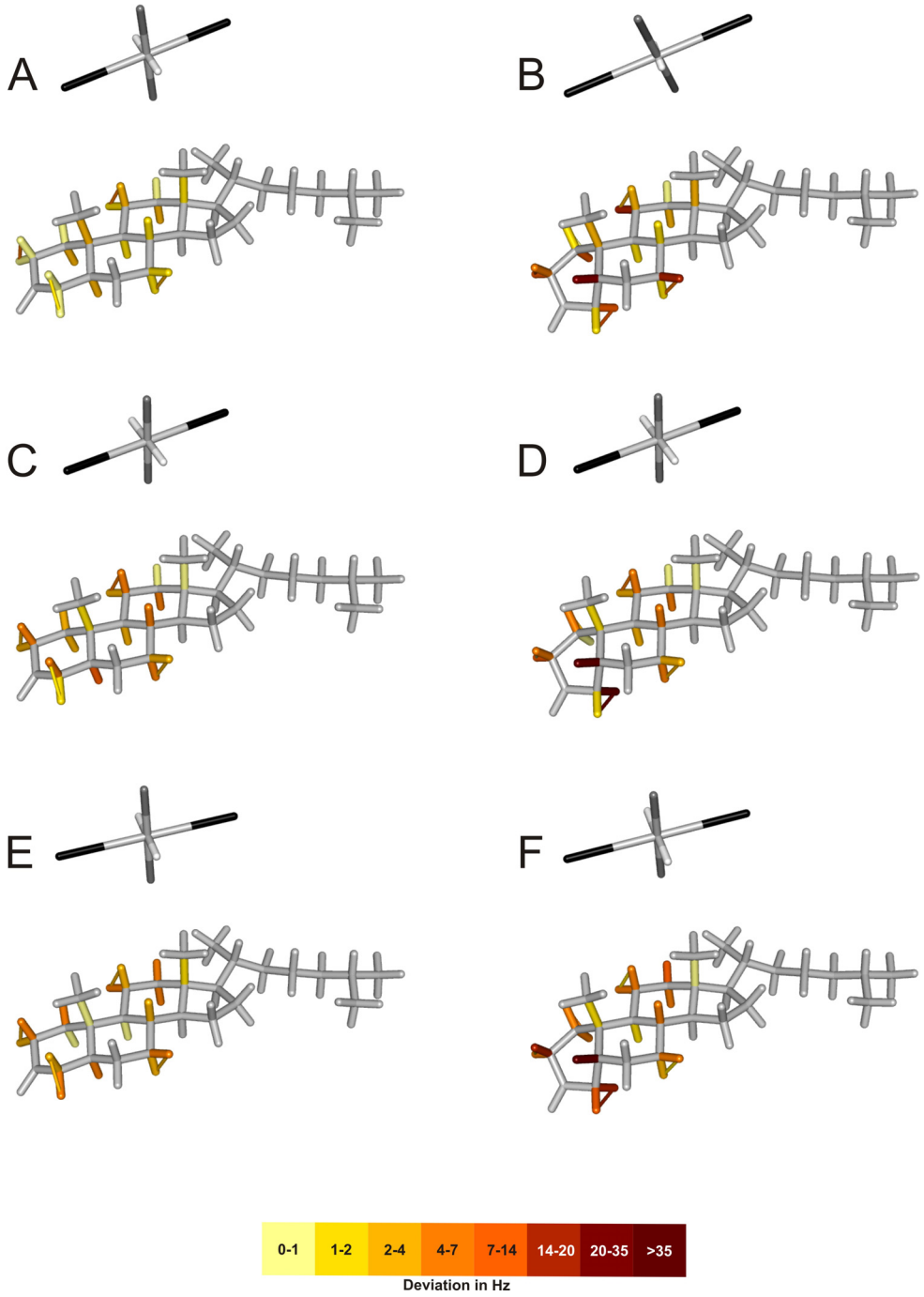

Figure A12.3.: Comparison of RDCs measured on 5-α-cholestan-3-one and back-calculated for the structures of 5-α-cholestan-3-one (left: A, C, E) and 5-β-cholestan-3-one (right: B, D, F) using the "-bestFit" option (SVD-fit) of PALES[128, 129] (top: A, B), the cross-fitting approach with the alignment tensor determined for cholesterol in PDMS/$CDCl_3$ (middle: C, D) and the prediction by PALES[128, 129] (bottom: E, F). The structures are shown with color-coded bonds denoting the deviation between measured and back-calculated RDCs for the different fits. The corresponding alignment tensors are visualized with their principal axis systems (black: A_{zz}; gray: A_{yy}; white: A_{xx}). For all three methods the 5-α-cholestan-3-one structure (left) gives clearly the better fit.

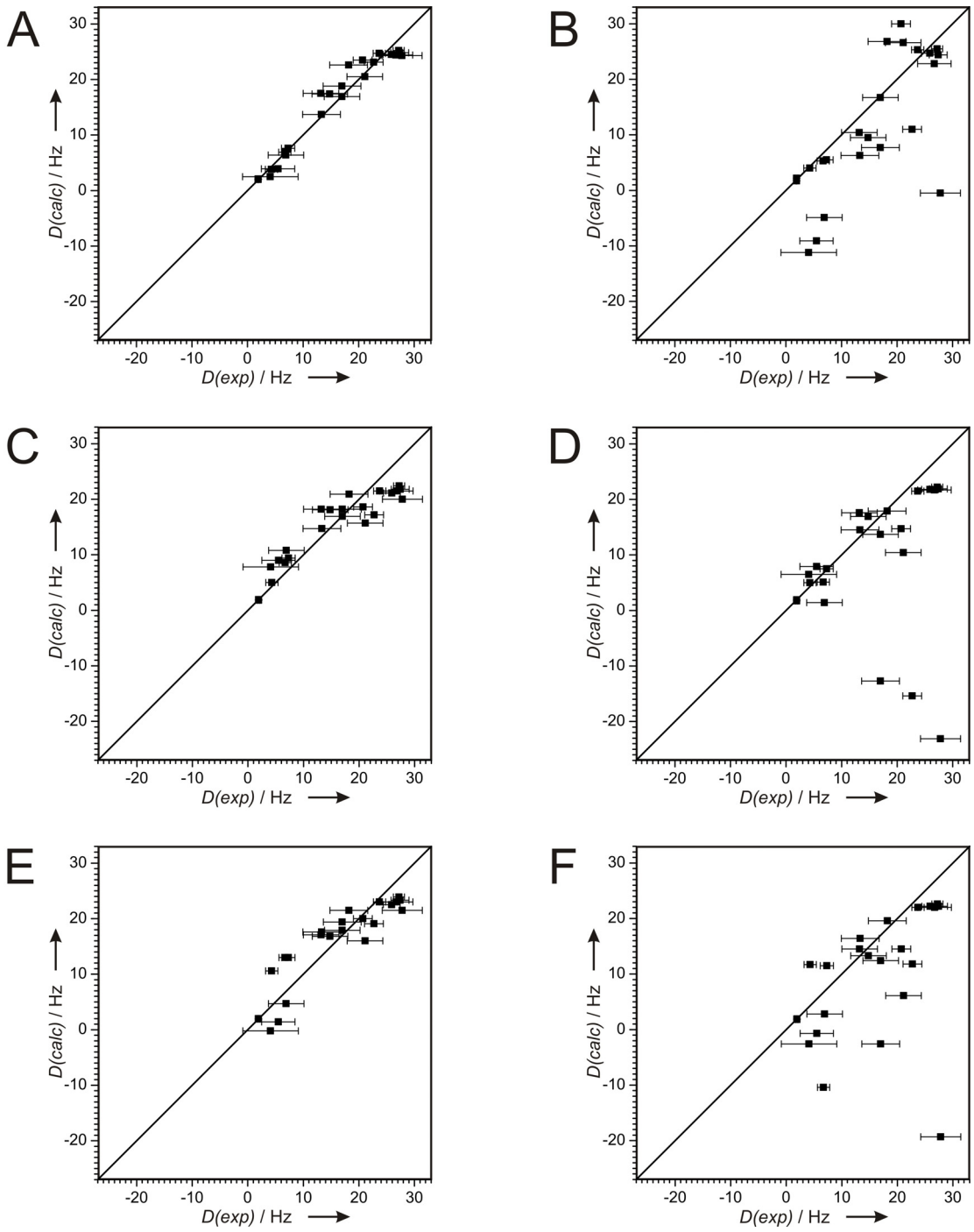

Figure A12.4.: Comparison of RDCs measured on 5-α-cholestan-3-one and back-calculated for the structures of 5-α-cholestan-3-one (left: A, C, E) and 5-β-cholestan-3-one (right: B, D, F) using the "-bestFit" option (SVD-fit) of PALES[128, 129] (top: A, B), the cross-fitting approach (middle: C, D) and the prediction by PALES[128, 129] (bottom: E, F).The plots show the back-calculated RDCs, D(calc), as a function of the measured RDCs, D(exp). Clearly the correct diastereomer 5-α-cholestan-3-one (left) is favored in all three methods.

Out of the 18 measured RDCs of cholesterol, various subsets of 15, 12, 9, 8, 7 and 6 RDCs were generated by random selection of RDC-combinations. As with a decreasing number of RDCs within a subset the influence of the actual composition of the subset increases, the more subsets have been created, the less RDCs are contained within the subsets.

Table A12.6.: Composition of RDCs used in each subset with 18, 15, 12, 9 or 8 RDCs.

Group	D [Hz]	Name of subset																											
		18A	15A	15B	15C	12A	12B	12C	12D	12E	9A	9B	9C	9D	9E	9F	9G	9H	8A	8B	8C	8D	8E	8F	8G	8H	8I	8J
C18-C13	1.9±0.2	x	/	x	x	/	x	x	/	x	x	/	x	/	x	/	x	/	x	/	/	x	/	/	/	x	/	x
C19-C10	1.8±0.2	x	x	x	x	/	x	x	/	x	/	x	x	x	/	x	x	/	/	x	x	x	/	x	/	x	x	/
C2-H2α	11.3±3.9	x	x	/	x	x	x	x	x	/	x	/	/	x	x	x	x	/	x	/	x	/	x	x	/	x	/	/
C2-H2β	16.1±3.9	x	x	x	x	x	x	x	x	/	/	x	/	/	x	x	x	/	/	x	/	/	x	x	x	/	/	x
C8-H8	20.7±8.5	x	x	x	/	/	x	x	/	x	x	/	x	/	/	/	x	/	/	/	x	x	/	/	x	/	x	/
C7-H7β	14.2±5.8	x	/	x	x	x	x	x	x	/	/	x	x	x	/	/	x	/	x	/	/	/	x	/	x	/	/	/
C1-H1β	9.0±1.4	x	x	x	x	x	x	x	/	x	x	/	/	x	x	/	x	/	/	x	/	/	/	/	x	/	x	/
C1-H1α	18.2±1.4	x	x	x	x	x	/	/	x	x	/	x	/	/	x	x	x	/	x	/	x	x	/	/	/	x	/	x
C12-H12α	22.4±1.4	x	/	x	x	x	/	/	x	x	x	/	x	/	/	x	x	/	/	x	/	x	x	x	/	x	/	/
C12-H12β	5.1±1.4	x	x	x	x	/	x	/	x	x	/	x	x	x	/	x	/	x	/	x	x	/	x	x	x	/	x	x
C6-H6	1.6±3.0	x	x	/	x	x	x	/	/	x	x	/	/	x	x	/	/	x	x	/	x	/	/	/	x	/	/	x
C9-H9	23.6±4.0	x	x	x	/	x	/	x	x	x	/	x	/	/	x	/	/	x	/	x	/	x	/	/	x	/	x	/
C3-H3	19.3±1.6	x	x	x	x	x	/	x	x	/	x	/	x	/	/	/	/	x	x	/	/	/	x	/	x	/	/	x
H2α-H2β	18.9±2.2	x	x	x	x	x	x	/	x	/	/	x	x	x	/	x	/	x	/	x	/	/	/	x	/	/	x	/
H7α-H7β	17.7±5.8	x	x	/	x	x	/	x	x	x	x	/	/	x	x	x	/	x	/	/	x	x	/	x	/	/	x	/
H1α-H1β	15.0±2.2	x	x	x	x	x	/	x	/	x	/	x	/	/	x	x	/	x	x	/	/	x	/	x	/	x	/	x
H12α-H12β	14.2±2.2	x	x	x	/	/	x	/	x	x	x	/	x	/	/	/	/	x	/	x	/	/	x	/	/	x	x	/
H4α-H4β	15.7±2.8	x	x	x	x	/	x	x	x	/	/	x	/	x	/	/	/	x	x	/	x	/	x	/	/	x	/	x

x = RDC used in this subset, / = RDC not used in this subset.

Table A12.7.: Composition of RDCs used in each subset with 7 or 6 RDCs.

Group	D [Hz]	Name of subset																											
		7A	7B	7C	7D	7E	7F	7G	7H	7I	7J	7K	7L	6A	6B	6C	6D	6E	6F	6G	6H	6I	6J	6K	6L	6M	6N	6O
C18-C13	1.9±0.2	x	/	x	/	/	x	/	/	/	/	x	/	x	/	/	x	/	/	x	/	/	/	x	/	/	x	/
C19-C10	1.8±0.2	/	x	/	x	x	x	/	/	x	/	/	x	/	x	/	x	/	/	x	/	/	x	/	/	x	/	/
C2-H2α	11.3±3.9	/	/	x	/	x	x	x	/	x	/	/	/	/	/	x	/	x	/	x	/	/	/	/	x	/	x	/
C2-H2β	16.1±3.9	x	x	/	/	/	/	x	/	/	x	/	x	x	/	/	/	x	/	x	/	/	/	x	/	/	/	x
C8-H8	20.7±8.5	x	/	/	x	/	/	x	/	x	x	/	x	/	x	/	/	/	x	x	/	/	x	/	/	x	/	/
C7-H7β	14.2±5.8	/	/	x	/	x	/	/	x	/	/	x	/	/	/	x	/	/	x	x	/	/	/	/	x	/	x	/
C1-H1β	9.0±1.4	/	x	/	/	x	/	/	x	/	/	/	/	x	/	/	/	/	x	/	x	/	x	x	/	/	/	/
C1-H1α	18.2±1.4	x	/	/	/	/	/	/	/	x	/	/	x	/	x	/	x	/	/	/	x	/	/	/	x	/	x	x
C12-H12α	22.4±1.4	/	/	x	/	/	x	/	x	x	/	x	x	/	/	x	x	/	/	/	x	/	/	x	/	x	/	/
C12-H12β	5.1±1.4	/	x	/	x	/	/	/	x	/	x	/	/	x	/	/	/	x	/	/	x	/	x	/	/	/	/	x
C6-H6	1.6±3.0	x	/	/	x	/	/	x	/	/	x	/	/	/	x	/	/	x	/	/	x	/	/	/	/	x	/	/
C9-H9	23.6±4.0	/	/	x	/	x	/	x	/	x	/	x	/	/	/	x	/	/	x	/	x	/	/	x	/	/	/	x
C3-H3	19.3±1.6	/	x	/	/	/	/	x	/	/	/	x	x	x	/	/	/	/	x	/	/	x	x	/	/	/	x	/
H2α-H2β	18.9±2.2	x	/	/	x	/	/	/	x	/	x	/	/	/	x	/	/	/	x	/	/	x	/	/	x	/	/	x
H7α-H7β	17.7±5.8	/	/	x	/	x	/	/	x	/	x	/	/	/	/	x	x	/	/	/	/	x	/	x	/	x	/	/
H1α-H1β	15.0±2.2	/	x	/	/	x	x	/	/	x	/	x	x	x	/	/	x	/	/	/	/	x	/	/	/	/	x	/
H12α-H12β	14.2±2.2	/	/	x	x	/	x	x	/	/	/	x	/	/	x	/	/	x	/	/	/	x	x	/	x	/	/	x
H4α-H4β	15.7±2.8	x	x	/	x	/	x	/	x	/	x	/	/	/	/	x	/	x	/	/	/	x	/	/	x	x	/	/

x = RDC used in this subset, / = RDC not used in this subset.

To investigate the influence of the flexible side chain on the orientation predicted by PALES[128, 129] several pdb-files of both steroids with decreasing length of the side-chain have been created. The alkyl chain has been shortened stepwise and the resulting fragments are named after the containing carbon atoms (e.g. C1-C24 is the fragment with carbon atoms 1 to 24 and all adjacent oxygen and hydrogen atoms. Accordingly C1-C27 is the whole steroid molecule). With all steroid fragments prediction of alignment and back-calculation of the measured RDCs were performed with PALES (-stPales mode) assuming a rod-shaped alignment medium (-pf1 flag) and including all hydrogen atoms (-H flag).[128, 129] The concentration of the alignment medium (-wv flag)[128, 129] which only scales the resulting RDCs linearly, was varied in steps of 0.001 to give the best result (best n/χ^2 value).

next pages:

Table A12.8.: RDCs measured on cholesterol and RDCs back calculated for various cholesterol fragments as result of the orientation predicted by PALES.[128, 129] All couplings are given in Hz. Alignment tensor parameters and quality factors for the different fits are given: Axial and rhombic components (D_a, D_r) and principal axes of the alignment tensor (A_{xx}, A_{yy}, A_{zz}) with their corresponding eigenvectors (EV), number of RDCs used for fitting (n) and quality factors χ^2, n/χ^2, correlation factor (R) and quality factor by Cornilescu et al. (Q). Additionally the concentration (-wv) used for the best prediction is given.

Table A12.9.: RDCs measured on 5-α-cholestan-3-one and RDCs back calculated for various 5-α-cholestan-3-one fragments as result of the orientation predicted by PALES.[128, 129] All couplings are given in Hz. Alignment tensor parameters and quality factors for the different fits are given: Axial and rhombic components (D_a, D_r) and principal axes of the alignment tensor (A_{xx}, A_{yy}, A_{zz}) with their corresponding eigenvectors (EV), number of RDCs used for fitting (n) and quality factors χ^2, n/χ^2, correlation factor (R) and quality factor by Cornilescu et al. (Q). Additionally the concentration (-wv) used for the best prediction is given.

Group	D (exp)	D (calc) according to prediction by PALES for the fragment of cholesterol						
		C1-C27	C1-C26	C1-C25	C1-C24	C1-C23	C1-C22	C1-C21	C1-C20
C18-C13	1.9 ± 0.2	1.8	1.8	1.8	1.9	1.8	1.8	1.8	1.7
C19-C10	1.8 ± 0.2	1.7	1.7	1.8	1.8	1.8	1.8	1.8	1.8
C2-H2α	11.3 ± 3.9	4.9	5.7	4.5	10.5	7.1	10.9	8.6	6.2
C2-H2β	16.1 ± 3.9	15.0	14.5	16.7	15.8	18.4	17.8	19.2	18.8
C8-H8	20.7 ± 8.5	21.7	21.2	21.1	22.3	21.8	22.0	21.6	22.3
C7-H7β	14.2 ± 5.8	6.5	7.9	7.2	12.8	9.4	12.7	10.0	9.4
C1-H1β	9.0 ± 1.4	11.2	12.8	11.5	10.4	7.3	5.4	2.2	8.0
C1-H1α	18.2 ± 1.4	18.2	17.7	19.1	18.7	20.3	19.9	20.7	20.7
C12-H12α	22.4 ± 1.4	21.3	20.8	20.8	21.7	21.5	21.7	21.3	21.4
C12-H12β	5.1 ± 1.4	8.7	9.8	7.9	5.7	2.8	0.2	-2.7	3.1
C6-H6	1.6 ± 3.0	7.1	8.2	6.1	3.4	0.4	-2.7	-5.3	1.8
C9-H9	23.6 ± 4.0	21.2	20.7	20.8	21.6	21.5	21.6	21.2	21.3
C3-H3	19.3 ± 1.6	16.7	16.2	17.9	17.3	19.4	18.9	19.9	19.7
H2α-H2β	18.9 ± 2.2	19.6	19.5	18.4	21.0	19.0	20.1	18.9	19.4
H7α-H7β	17.7 ± 5.8	18.4	18.6	17.3	20.4	17.9	19.2	17.6	19.0
H1α-H1β	15.0 ± 2.2	15.3	15.9	16.5	16.1	15.8	15.2	13.5	14.1
H12α-H12β	14.2 ± 2.2	15.5	15.6	14.9	14.5	13.1	12.4	10.4	10.9
H4α-H4β	15.7 ± 2.8	15.9	16.4	17.3	16.9	17.0	16.5	15.1	15.4
	D_a	-3.72E-04	-3.89E-04	-3.81E-04	-4.10E-04	-3.73E-04	-3.84E-04	-3.48E-04	-3.88E-04
	D_r	-7.02E-05	-5.27E-05	-5.41E-05	-5.74E-05	-7.02E-05	-6.62E-05	-8.58E-05	-7.29E-05
	A_{xx}	2.67E-04	3.10E-04	2.99E-04	3.24E-04	2.68E-04	2.85E-04	2.19E-04	2.78E-04
	A_{yy}	4.77E-04	4.68E-04	4.62E-04	4.96E-04	4.78E-04	4.83E-04	4.76E-04	4.97E-04
	A_{zz}	-7.44E-04	-7.79E-04	-7.61E-04	-8.20E-04	-7.46E-04	-7.68E-04	-6.95E-04	-7.76E-04
	EV A_{xx}	-0.34; 0.92; -0.17	-0.39; 0.91; -0.14	-0.34; 0.90; -0.28	-0.52; 0.84; -0.15	0.40; -0.84; -0.37	0.50; -0.80; 0.34	0.47; -0.78; 0.43	-0.52; 0.83; -0.18
	EV A_{yy}	-0.61; -0.08; 0.79	-0.59; -0.12; 0.80	-0.67; -0.02; 0.74	-0.53; -0.19; 0.82	-0.69; -0.01; 0.73	-0.63; -0.06; 0.78	0.70; 0.03; -0.71	-0.62; -0.23; 0.75
	EV A_{zz}	0.71; 0.38; 0.59	0.71; 0.39; 0.59	0.66; 0.43; 0.61	0.67; 0.51; 0.55	0.61; 0.54; 0.58	0.60; 0.60; 0.53	0.54; 0.63; 0.55	0.58; 0.50; 0.64
	n	18	18	18	18	18	18	18	18
	χ^2	21.17	33.57	18.26	5.48	10.35	24.45	69.94	12.57
	n/χ^2	0.85	0.54	0.99	3.29	1.74	0.74	0.26	1.43
	R	0.900	0.890	0.911	0.981	0.970	0.976	0.952	0.959
	Q	0.198	0.205	0.187	0.09	0.128	0.135	0.228	0.145
	-wv	0.049	0.050	0.057	0.064	0.068	0.073	0.074	0.088

Group	D exp	D (calc) according to prediction by PALES for the fragment of 5-α-cholestan-3-one							
		C1-C27	C1-C26	C1-C25	C1-C24	C1-C23	C1-C22	C1-C21	C1-C20
C19-C10	1.9 ± 0.2	1.9	1.8	2.0	1.9	2.1	2.1	2.2	2.2
C18-C13	1.9 ± 0.1	2.0	2.0	2.0	2.1	2.0	2.1	2.0	1.9
C11-H11β	26.7 ± 3.0	23.0	22.3	23.6	23.5	24.8	24.9	24.9	24.3
C11-H11α	5.5 ± 3.0	1.4	2.7	2.0	8.4	4.6	8.7	6.2	3.0
C7-H7β	4.1 ± 5.0	-0.2	1.2	0.6	7.0	3.4	7.6	5.2	1.6
C7-H7α	25.9 ± 1.5	22.5	21.8	23.2	23.0	24.6	24.6	24.9	24.9
C8-H8	27.2 ± 1.0	23.9	23.1	23.7	24.5	24.8	25.3	24.8	24.8
C2-H2α	6.9 ± 3.2	4.7	5.5	4.1	10.6	6.4	10.5	7.8	4.7
C2-H2β	21.1 ± 3.2	16.0	15.4	18.5	16.9	21.1	20.4	22.6	22.3
C1-H1β	7.3 ± 1.2	13.0	14.5	13.5	12.0	8.7	6.7	3.2	8.9
C1-H1α	20.7 ± 1.7	20.0	19.2	21.3	20.4	23.2	22.6	24.1	24.8
C12-H12α	27.4 ± 1.6	23.3	22.5	23.4	23.8	24.6	24.8	24.6	24.6
C12-H12β	4.3 ± 1.1	10.6	11.7	10.0	7.6	4.1	1.3	-2.1	4.7
C4-H4α	6.7 ± 1.1	13.0	14.0	12.9	11.1	8.2	6.1	2.8	7.4
C4-H4β	22.7 ± 1.7	19.1	18.3	20.3	19.1	21.9	21.1	22.8	24.7
C5-H5	27.8 ± 3.6	21.5	20.7	22.4	21.9	24.0	23.7	24.6	25.1
C9-H9	23.7 ± 1.1	23.0	22.2	23.3	23.5	24.6	24.7	24.8	24.7
H11α-H11β	13.2 ± 3.2	17.1	16.9	15.4	19.6	16.5	18.9	16.7	15.7
H7α-H7β	14.8 ± 3.2	16.8	16.7	15.3	19.4	16.3	18.6	16.4	15.9
H2α-H2 β	18.2 ± 3.4	21.5	21.0	20.4	22.8	21.2	22.4	21.1	21.9
H1α-H1 β	17.0 ± 3.2	17.9	18.1	19.5	18.8	19.3	18.8	17.6	17.2
H12α-H12β	13.3 ± 3.4	17.6	17.6	17.5	16.7	15.6	15.0	12.8	12.8
H4α-H4β	17.0 ± 3.4	19.4	19.3	20.7	20.1	20.9	20.6	19.7	18.9
	D_a	-4.04E-04	-3.89E-04	-4.18E-04	-4.18E-04	-4.39E-04	-4.04E-04	-4.12E-04	-3.79E-04
	D_r	-7.87E-05	-5.27E-05	-5.84E-05	-6.78E-05	-6.61E-05	-9.59E-05	-9.29E-05	-1.16E-04
	A_{xx}	2.86E-04	3.10E-04	3.30E-04	3.16E-04	3.40E-04	2.60E-04	2.73E-04	2.05E-04
	A_{yy}	5.22E-04	4.68E-04	5.06E-04	5.19E-04	5.38E-04	5.47E-04	5.51E-04	5.53E-04
	A_{zz}	-8.08E-04	-7.79E-04	-8.36E-04	-8.35E-04	-8.77E-04	-8.07E-04	-8.24E-04	-7.58E-04
	EV A_{xx}	-0.31; 0.94; -0.16	-0.33; 0.93; -0.15	-0.28; 0.92; -0.28	-0.46; 0.87; -0.19	0.35; -0.87; -0.36	0.44; -0.82; 0.37	0.41; -0.80; 0.44	-0.47; 0.87; -0.17
	EV A_{yy}	-0.62; -0.07; 0.78	-0.62; -0.09; 0.78	-0.69; 0.01; 0.72	-0.58; -0.14; 0.80	0.71; 0.00; -0.70	0.67; 0.03; -0.74	0.74; 0.01; -0.68	-0.67; -0.23; 0.71
	EV A_{zz}	0.72; 0.34; 0.61	0.71; 0.36; 0.60	0.66; 0.40; 0.64	0.67; 0.48; 0.57	0.61; 0.50; 0.62	0.60; 0.57; 0.56	0.54; 0.60; 0.59	0.58; 0.45; 0.69
	n	23	23	23	23	23	23	23	23
	χ^2	133.31	183.64	121.17	81.52	24.91	35.16	78.96	26.57
	n/χ^2	0.17	0.13	0.19	0.28	0.92	0.65	0.29	0.87
	R	0.902	0.882	0.920	0.931	0.974	0.956	0.962	0.974
	Q	0.216	0.238	0.195	0.201	0.114	0.152	0.143	0.115
	-wv	0.056	0.057	0.067	0.075	0.081	0.088	0.093	0.109

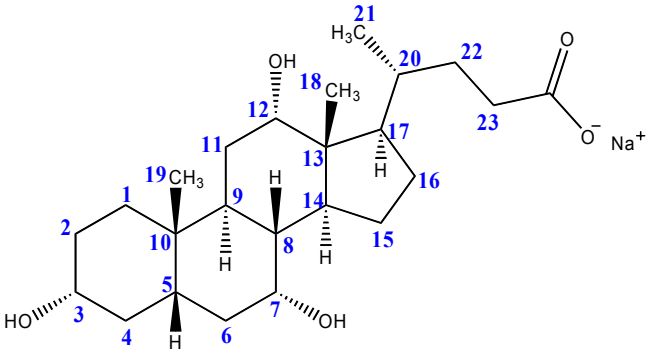

Figure A12.5.: Structure and nomenclature of sodium cholate.

Table A12.10.: RDCs measured on sodium cholate and RDCs back calculated for sodium cholate with the SVD method, the fit with fixed orientation given by the alignment tensor of 5-α-cholestan-3-one (cross-fitting) and fit with orientation predicted by PALES.[128, 129] All couplings are given in Hz. Additionally, alignment tensor parameters and quality factors for the different fits are given: Axial and rhombic components (D_a, D_r) and principal axes of the alignment tensor (A_{xx}, A_{yy}, A_{zz}) with their corresponding eigenvectors (EV), number of RDCs used for fitting (n) and quality factors χ^2, n/χ^2, correlation factor (R) and quality factor by Cornilescu et al. (Q).

Group	$^1D_{CH}$ (exp) [(a)]	$^1D_{CH}$ (calc) (SVD-fit)	$^1D_{CH}$ (calc) (cross-fitting)	$^1D_{CH}$ (calc) (predicted)
C3-H3	1.5 ± 1.0	1.9	-22.7	0.0553
C5-H5	0.9 ± 1.0	0.5	-16.8	0.0530
C7-H7	2.5 ± 1.0	2.7	1.3	-0.0024
C8-H8	-7.8 ± 1.0	-7.2	25.3	-0.0570
C9-H9	-7.5 ± 1.0	-7.0	24.8	-0.0560
C12-H12	1.6 ± 1.0	1.4	3.7	-0.0307
C14-H14	-6.6 ± 1.0	-6.9	24.2	-0.0546
C17-H17	-6.0 ± 1.0	-6.8	23.8	-0.0533
	D_a	-8.047E-05	-3.97E-04	1.16E-06
	D_r	-3.11E-05	-1.10E-04	8.66E-08
	A_{xx}	3.38E-05	2.32E-04	-1.03E-06
	A_{yy}	1.27E-04	5.62E-04	-1.29E-06
	A_{zz}	-1.61E-04	-7.94E-04	2.31E-06
	EV A_{xx}	-0.08; 0.98; 0.16	-0.45; 0.87; -0.19	-0.54; 0.84; 0.04
	EV A_{yy}	0.74; -0.05; 0.68	-0.65; -0.17; 0.74	-0.53; -0.38; 0.76
	EV A_{zz}	-0.67; -0.17; 0.72	0.62; 0.45; 0.64	0.65; 0.39; 0.65
	n	8	8	8
	χ^2	4.35	4881.82	205.30
	n/χ^2	5.42	0.002	0.04
	R	0.994	-0.867	0.782
	Q	0.094	4.839	0.992

(a) Experimental data was taken from Mangoni et al.[148] As no experimental errors are given by Mangoni et al.[148] they were set to 1Hz for the fitting with PALES.

8 References

[1] K. Wüthrich: *'NMR of Proteins and Nucleic Acids'*, 1st ed., Wiley-VCH, Weinheim, **1986**.

[2] S. Berger; D. Sicker: *'Classics in NMR spectroscopy: Isolation and structure elucidation of natural products'*, Wiley-VCH, Weinheim, **2009**.

[3] J. W. Emsley; J. C. Lindon: *'NMR Spectroscopy using liquid crystal solvents'*, Pergamon Press, Oxford, **1975**.

[4] R. Y. Dong: *'Nuclear Magnetic Resonance of Liquid Crystals'*, 2nd ed., Springer, New York, **1997**.

[5] G. Kummerlöwe; B. Luy: *'Residual dipolar couplings for the configurational and conformational analysis of organic molecules'* in *Annu. Rep. NMR Spectrosc.* **2009**, *68*, 193-232.

[6] F. Kramer; M. V. Deshmukh; H. Kessler; S. J. Glaser: *'Residual dipolar coupling constants: An elementary derivation of key equations'* in *Concepts in Magnetic Resonance Part A* **2004**, *21A*, 10-21.

[7] A. Saupe; G. Englert: *'High-Resolution Nuclear Magnetic Resonance Spectra of Oriented Molecules'* in *Phys. Rev. Lett.* **1963**, *11*, 462-464.

[8] A. Saupe: *'Kernresonanz in kristallinen Flüssigkeiten und in kristallin-flüssigen Lösungen, Teil 1'* in *Zeitschrift für Naturforschung* **1964**, *19a*, 161.

[9] E. E. Burnell; C. A. De Lange: *'On the Average Orientation of Molecules Undergoing Large-Amplitude Conformational-Changes in Anisotropic Liquids'* in *Chem. Phys. Lett.* **1980**, *76*, 268-272.

[10] E. E. Burnell: *'Effects of Interaction between Molecular Internal Motion and Reorientation on NMR of Anisotropic Liquids'* in *J. Magn. Reson.* **1980**, *39*, 461-480.

[11] N. J. D. Lucas: *'The influence of vibrations on molecular structure determinations from N.M.R. in liquid crystals - I. Application to methyl fluoride'* in *Mol. Phys.* **1971**, *22*, 147 - 154.

[12] N. J. D. Lucas: *'The influence of vibrations on molecular structure determinations from N.M.R. in liquid crystals - II. Cyclopropane'* in *Mol. Phys.* **1971**, *22*, 233 - 239.

[13] N. J. D. Lucas: *'On the vibrationally averaged structure and vibrational expectation values'* in *Mol. Phys.* **1972**, *23*, 825 - 826.

[14] J. W. Emsley: *'Liquid-crystalline Materials'* in: *'Solid-State NMR Spectroscopy'* (Ed.: M. J. Duer), Blackwell Science, Oxford, **2002**, pp. 512-562.

[15] L. C. Snyder; S. Meiboom: *'NMR of Tetrahedral Molecules in Nematic Solvent'* in *J. Chem. Phys.* **1966**, *44*, 4057-4058.

[16] J. G. Snijders; C. A. Delange; E. E. Burnell: *'Vibration-Rotation Coupling in Anisotropic Environments - NMR of Methanes in Liquid-Crystals'* in *J. Chem. Phys.* **1982**, *77*, 5386-5395.

[17] J. G. Snijders; C. A. Delange; E. E. Burnell: *'Vibration-Rotation Coupling in Anisotropic Environments: 2. Quadrupolar Couplings of Methanes in Liquid-Crystals'* in *J. Chem. Phys.* **1983**, *79*, 2964-2969.

[18] D. J. Photinos; E. T. Samulski; H. Toriumi: *'Alkyl Chains in a Nematic Field. 1. A Treatment of Conformer Shape'* in *J. Phys. Chem.* **1990**, *94*, 4688-4694.

[19] J. W. Emsley; G. R. Luckhurst; C. P. Stockley: *'A Theory of Orientational Ordering in Uniaxial Liquid-Crystals Composed of Molecules with Alkyl Chains'* in *Proc. R. Soc. London, A* **1982**, *381*, 117-138.

[20] D. Catalano; L. Dibari; C. A. Veracini; G. N. Shilstone; C. Zannoni: *'A Maximum-Entropy Analysis of the Problem of the Rotameric Distribution for Substituted Biphenyls Studied by ^{1}H Nuclear-Magnetic-Resonance Spectroscopy in Nematic Liquid-Crystals'* in *J. Chem. Phys.* **1991**, *94*, 3928-3935.

[21] B. Stevensson; C. Landersjö; G. Widmalm; A. Maliniak: *'Conformational distribution function of a disaccharide in a liquid crystalline phase determined using NMR spectroscopy'* in *J. Am. Chem. Soc.* **2002**, *124*, 5946-5947.

[22] B. Stevensson; D. Sandström; A. Maliniak: *'Conformational distribution functions extracted from residual dipolar couplings: A hybrid model based on maximum entropy and molecular field theory'* in *J. Chem. Phys.* **2003**, *119*, 2738-2746.

[23] C. M. Thiele; A. Marx; R. Berger; J. Fischer; M. Biel; A. Giannis: *'Determination of the relative configuration of a five-membered lactone from residual dipolar couplings'* in *Angew. Chem., Int. Ed.* **2006**, *45*, 4455-4460.

[24] A. Schuetz; J. Junker; A. Leonov; O. F. Lange; T. F. Molinski; C. Griesinger: *'Stereochemistry of Sagittamide A from Residual Dipolar Coupling Enhanced NMR'* in *J. Am. Chem. Soc.* **2007**, *129*, 15114-15115.

[25] A. Schuetz; T. Murakami; N. Takada; J. Junker; M. Hashimoto; C. Griesinger: *'RDC-Enhanced NMR Spectroscopy in Structure Elucidation of Sucro-Neolambertellin'* in *Angew. Chem., Int. Ed.* **2008**, *47*, 2032-2034.

[26] A. O. Frank: Dissertation *'About the Interplay of NMR Spectroscopy and Molecular Modeling within Bioorganic and Medicinal Chemistry'*, Technische Universität München (Munich), **2009**.

[27] R. D. Spence; H. A. Moses; P. L. Jain: *'The Proton Magnetic Resonance Line in Liquid Crystals'* in *J. Chem. Phys.* **1953**, *21*, 380-380.

[28] B. Deloche; E. T. Samulski: *'Short-Range Nematic-like Orientational Order in Strained Elastomers: A Deuterium Magnetic Resonance Study'* in *Macromolecules* **1981**, *14*, 575-581.

[29] R. Tycko; F. J. Blanco; Y. Ishii: *'Alignment of biopolymers in strained gels: A new way to create detectable dipole-dipole couplings in high-resolution bio-molecular NMR'* in *J. Am. Chem. Soc.* **2000**, *122*, 9340-9341.

[30] H. J. Sass; G. Musco; S. J. Stahl; P. T. Wingfield; S. Grzesiek: *'Solution NMR of proteins within polyacrylamide gels: Diffusional properties and residual alignment by mechanical stress or embedding of oriented purple membranes'* in *J. Biomol. NMR* **2000**, *18*, 303-309.

[31] N. Tjandra; A. Bax: *'Direct measurement of distances and angles in biomolecules by NMR in a dilute liquid crystalline medium'* in *Science* **1997**, *278*, 1111.

[32] M. Ottiger; A. Bax: *'Characterization of magnetically oriented phospholipid micelles for measurement of dipolar couplings in macromolecules'* in *J. Biomol. NMR* **1998**, *12*, 361-372.

[33] M. Ottiger; F. Delaglio; A. Bax: *'Measurement of J and dipolar couplings from simplified two-dimensional NMR spectra'* in *J. Magn. Reson.* **1998**, *131*, 373.

[34] J. A. Losonczi; J. H. Prestegard: *'Improved dilute bicelle solutions for high-resolution NMR of biological macromolecules'* in *J. Biomol. NMR* **1998**, *12*, 447-451.

[35] M. Rückert; G. Otting: *'Alignment of Biological Macromolecules in Novel Nonionic Liquid Crystalline Media for NMR Experiments'* in *J. Am. Chem. Soc.* **2000**, *122*, 7793-7797.

[36] G. M. Clore; M. R. Starich; A. M. Gronenborn: *'Measurement of residual dipolar couplings of macromolecules aligned in the nematic phase of a colloidal suspension of rod-shaped viruses'* in *J. Am. Chem. Soc.* **1998**, *120*, 10571-10572.

[37] M. R. Hansen; L. Mueller; A. Pardi: *'Tunable alignment of macromolecules by filamentous phage yields dipolar coupling interactions'* in *Nat. Struct. Biol.* **1998**, *5*, 1065-1074.

[38] M. R. Hansen; P. Hanson; A. Pardi: *'Pf1 filamentous phage as an alignment tool for generating local and global structural information in nucleic acids'* in *J. Biomol. Struct. Dyn.* **2000**, 365-369.

[39] K. Fleming; D. Gray; S. Prasannan; S. Matthews: *'Cellulose crystallites: A new and robust liquid crystalline medium for the measurement of residual dipolar couplings'* in *J. Am. Chem. Soc.* **2000**, *122*, 5224-5225.

[40] R. S. Prosser; J. A. Losonczi; I. V. Shiyanovskaya: *'Use of a novel aqueous liquid crystalline medium for high-resolution NMR of macromolecules in solution'* in *J. Am. Chem. Soc.* **1998**, *120*, 11010-11011.

[41] L. G. Barrientos; C. Dolan; A. M. Gronenborn: *'Characterization of surfactant liquid crystal phases suitable for molecular alignment and measurement of dipolar couplings'* in *J. Biomol. NMR* **2000**, *16*, 329-337.

[42] L. G. Barrientos; K. Gawrisch; N. Cheng; A. C. Steven; A. M. Gronenborn: *'Structural Characterization of the Dilute Aqueous Surfactant Solution of Cetylpyridinium Bromide/Hexanol/Sodium Bromide'* in *Langmuir* **2002**, *18*, 3773-3779.

[43] H. J. Sass; F. Cordier; A. Hoffmann; M. Rogowski; a. Cousin; J. G. Omichinski; H. Lowen; S. Grzesiek: *'Purple Membrane Induced Alignment of Biological Macromolecules in the Magnetic Field'* in *J. Am. Chem. Soc.* **1999**, *121*, 2047-2005.

[44] B. W. Koenig; D. C. Mitchell; S. König; S. Grzesiek; B. J. Litman; A. Bax: *'Measurement of dipolar couplings in a transducin peptide fragment weakly bound to oriented photo-activated rhodopsin'* in *J. Biomol. NMR* **2000**, *16*, 121-125.

[45] H. Desvaux; J.-C. P. Gabriel; P. Berthault; F. Camerel: *'First Use of a Mineral Liquid Crystal for Measurement of Residual Dipolar Couplings of a Non-labeled Biomolecule'* in *Angew. Chem., Int. Ed.* **2001**, *40*, 373-376.

[46] J.-C. P. Gabriel; F. Camerel; B. J. Lemaire; H. Desvaux; P. Davidson; P. Batail: *'Swollen liquid-crystalline lamellar phase based on extended solid-like sheets'* in *Nature* **2001**, *413*, 504-508.

[47] S. M. Douglas; J. J. Chou; W. M. Shih: *'DNA-nanotube-induced alignment of membrane proteins for NMR structure determination'* in *Proc. Natl. Acad. Sci. U. S. A.* **2007**, *104*, 6644-6648.

[48] J. Lorieau; L. S. Yao; A. Bax: *'Liquid crystalline phase of G-tetrad DNA for NMR study of detergent-solubilized proteins'* in *J. Am. Chem. Soc.* **2008**, *130*, 7536-7537.

[49] Y. Ishii; M. A. Markus; R. Tycko: *'Controlling residual dipolar couplings in high-resolution NMR of proteins by strain induced alignment in a gel'* in *J. Biomol. NMR* **2001**, *21*, 141-151.

[50] S. Meier; D. Häussinger; S. Grzesiek: *'Charged acrylamide copolymer gels as media for weak alignment'* in *J. Biomol. NMR* **2002**, *24*, 351-356.

[51] T. Cierpicki; J. H. Bushweller: *'Charged gels as orienting media for measurement of residual dipolar couplings in soluble and integral membrane proteins'* in *J. Am. Chem. Soc.* **2004**, *126*, 16259-16266.

[52] K. Kobzar; H. Kessler; B. Luy: *'Stretched Gelatin Gels as Chiral Alignment Media for the Discrimination of Enantiomers by NMR Spectroscopy'* in *Angew. Chem., Int. Ed.* **2005**, *44*, 3145-3147;

Corrigendum: *Angew. Chem., Int. Ed.* **2005**, *44*, 3509.

[53] U. Eliav; G. Navon: *'Collagen Fibers as a Chiral Agent: A Demonstration of Stereochemistry Effects'* in *J. Am. Chem. Soc.* **2006**, *128*, 15956-15957.

[54] J. H. Ma; G. I. Goldberg; N. Tjandra: *'Weak Alignment of Biomacromolecules in Collagen Gels: An Alternative Way to Yield Residual Dipolar Couplings for NMR Measurements'* in *J. Am. Chem. Soc.* **2008**, *130*, 16148-16149.

[55] S. A. Riley; J. R. Giuliani; M. P. Augustine: *'Capture and manipulation of magnetically aligned Pf1 with an aqueous polymer gel'* in *J. Magn. Reson.* **2002**, *159*, 82-86.

[56] J. F. Trempe; F. G. Morin; Z. C. Xia; R. H. Marchessault; K. Gehring: *'Characterization of polyacrylamide-stabilized Pf1 phage liquid crystals for protein NMR spectroscopy'* in *J. Biomol. NMR* **2002**, *22*, 83-87.

[57] K. Ruan; J. R. Tolman: *'Composite Alignment Media for the Measurement of Independent Sets of NMR Residual Dipolar Couplings'* in *J. Am. Chem. Soc.* **2005**, *127*, 15032-15033.

[58] P. Doty; A. M. Holtzer; J. H. Bradbury; E. R. Blout: *'The Configuration of Polymers of γ-Benzyl-*L*-Glutamate in Solution'* in *J. Am. Chem. Soc.* **1954**, *76*, 4493-4494.

[59] M. Panar; W. D. Phillips: *'Magnetic Ordering of Poly-γ-Benzyl-L-Glutamate Solutions'* in *J. Am. Chem. Soc.* **1968**, *90*, 3880-3881.

[60] J. P. Bayle; J. Courtieu; E. Gabetty; A. Loewenstein; J. M. Pechine: *'Enantiomeric Analysis in a Polypeptide Lyotropic Liquid-Crystal through Proton Decoupled Deuterium NMR'* in *New J. Chem.* **1992**, *16*, 837-838.

[61] C. M. Thiele: *'Simultaneous Assignment of All Diastereotopic Protons in Strychnine Using RDCs: PELG as Alignment Medium for Organic Molecules'* in *J. Org. Chem.* **2004**, *69*, 7403-7413.

[62] C. Aroulanda; M. Sarfati; J. Courtieu; P. Lesot: *'Investigation of the enantioselectivity of three polypeptide liquid-crystalline solvents using NMR spectroscopy'* in *Enantiomer* **2001**, *6*, 281-287.

[63] B. Bendiak: *'Sensitive through-space dipolar correlations between nuclei of small organic molecules by partial alignment in a deuterated liquid solvent'* in *J. Am. Chem. Soc.* **2002**, *124*, 14862-14863.

[64] B. Luy; K. Kobzar; H. Kessler: *'An easy and scalable method for the partial alignment of organic molecules for measuring residual dipolar couplings'* in *Angew. Chem., Int. Ed.* **2004**, *43*, 1092-1094.

[65] B. Luy; K. Kobzar; S. Knör; J. Furrer; D. Heckmann; H. Kessler: *'Orientational Properties of Stretched Polystyrene Gels in Organic Solvents and the Suppression of Their Residual ^{1}H NMR Signals'* in *J. Am. Chem. Soc.* **2005**, *127*, 6459-6465.

[66] J. C. Freudenberger; S. Knör; K. Kobzar; D. Heckmann; T. Paululat; H. Kessler; B. Luy: *'Stretched Polyvinylacetate-Gels as NMR-Alignment Media for the Measurement of Residual Dipolar Couplings in Polar Organic Solvents'* in *Angew. Chem., Int. Ed.* **2005**, *44*, 423-426.

[67] J. C. Freudenberger; P. Spiteller; R. Bauer; H. Kessler; B. Luy: *'Stretched Poly(dimethylsiloxane) Gels as NMR Alignment Media for Apolar and Weakly Polar Organic Solvents: An Ideal Tool for Measuring RDCs at Low Molecular Concentrations'* in *J. Am. Chem. Soc.* **2004**, *126*, 14690-14691.

[68] R. R. Gil; C. Gayathri; N. V. Tsarevsky; K. Matyjaszewski: *'Stretched Poly(methyl methacrylate) Gel Aligns Small Organic Molecules in Chloroform. Stereochemical Analysis and Diastereotopic Proton NMR Assignment in Ludartin Using Residual Dipolar Couplings and ^{3}J Coupling Constant Analysis'* in *J. Org. Chem.* **2008**, *73*, 840-848.

[69] P. Kaden: Dissertation *'Neue Methoden zur Bestimmung anisotroper Parameter in der NMR-Spektroskopie und Strukturaufklärung eines hMC1R-Agonisten'*, Technische Universität München (Munich), **2009**.

[70] P. Doty; J. H. Bradbury; A. M. Holtzer: *'Polypeptides .4. The Molecular Weight, Configuration and Association of Poly-γ-Benzyl-L-Glutamate in Various Solvents'* in *J. Am. Chem. Soc.* **1956**, *78*, 947-954.

[71] V. V. Klochkov; B. I. Khairutdinov; A. V. Klochkov; M. S. Tagirov; C. M. Thiele; S. Berger; I. S. Vershinina; Stoikova, II; I. S. Antipin; A. I. Konovalov: *'The use of a lyotropic liquid-crystalline medium and residual dipolar coupling constants for determination of the spatial structure of thiacalix 4 arenes in solutions'* in *Russ. Chem. Bull.* **2004**, *53*, 1466-1470.

[72] V. V. Klochkov; A. V. Klochkov; C. M. Thiele; S. Berger: *'A novel liquid crystalline system for partial alignment of polar organic molecules'* in *J. Magn. Reson.* **2006**, *179*, 58-63.

[73] P. Haberz; J. Farjon; C. Griesinger: *'A DMSO-Compatible Orienting Medium: Towards the Investigation of the Stereochemistry of Natural Products'* in *Angew. Chem., Int. Ed.* **2005**, *44*, 427-429.

[74] J. M. Péchiné; A. Meddour; J. Courtieu: *'Monitoring the differential ordering of enantiomers included into cyclodextrins through deuterium NMR in lyotropic liquid crystals'* in *Chem. Commun.* **2002**, 1734-1735.

[75] A. Solgadi; A. Meddour; J. Courtieu: *'Enantiomeric discrimination of water soluble compounds using deuterium NMR in a glucopon/buffered water/n-hexanol chiral lyotropic liquid crystal'* in *Tetrahedron - Asymmetry* **2004**, *15*, 1315-1318.

[76] C. Naumann; P. W. Kuchel: *'Prochiral and Chiral Resolution in ^2H NMR Spectra: Solutes in Stretched and Compressed Gelatin Gels'* in *J. Phys. Chem. A* **2008**, *112*, 8659-8664.

[77] C. Naumann; P. W. Kuchel: *'NMR (Pro)chiral Discrimination Using Polysaccharide Gels'* in *Chem. Eur. J.* **2009**, *15*, 12189-12191.

[78] C. M. Thiele: *'Residual Dipolar Couplings (RDCs) in Organic Structure Determination'* in *Eur. J. Org. Chem.* **2008**, 5673-5685.

[79] J. J. Chou; S. Gaemers; B. Howder; J. M. Louis; A. Bax: *'A simple apparatus for generating stretched polyacrylamide gels, yielding uniform alignment of proteins and detergent micelles'* in *J. Biomol. NMR* **2001**, *21*, 377-382.

[80] B. Luy; H. Kessler: *'Partial Alignment for Structure Determination of Organic Molecules'* in: *'Modern Magnetic Resonance', Vol. 2* (Ed.: G. A. Webb), Springer, **2006**, pp. 1261-1267.

[81] A. Marx; C. Thiele: *'Orientational Properties of Poly-γ-benzyl-L-glutamate: Influence of Molecular Weight and Solvent on Order Parameters of the Solute'* in *Chem. Eur. J.* **2009**, *15*, 254-260.

[82] F. M. Leslie; G. R. Luckhurst; H. J. Smith: *'Magnetohydrodynamic Effects in Nematic Mesophase'* in *Chem. Phys. Lett.* **1972**, *13*, 368-371.

[83] J. Courtieu; D. W. Alderman; D. M. Grant; J. P. Bayles: *'Director Dynamics and NMR Applications of Nematic Liquid-Crystals Spinning at Various Angles from the Magnetic-Field'* in *J. Chem. Phys.* **1982**, *77*, 723-730.

[84] R. M. Hornreich: *'Instability Threshold of a Nematic Liquid-Crystal in a Biased Rotating Magnetic-Field'* in *Phys. Rev. A* **1977**, *15*, 1767-1772.

[85] J. Courtieu; D. W. Alderman; D. M. Grant: *'Spinning near the Magic Angle - a Means of Obtaining 1st-Order Dipolar NMR-Spectra of Molecules Dissolved in Nematic Liquid-Crystals'* in *J. Am. Chem. Soc.* **1981**, *103*, 6783-6784.

[86] J. Courtieu; J. P. Bayle; B. M. Fung: *'Variable-Angle Sample-Spinning NMR in Liquid-Crystals'* in *Progress in Nuclear Magnetic Resonance Spectroscopy* **1994**, *26*, 141-169.

[87] C. M. Thiele: *'Scaling the Alignment of Small Organic Molecules in Substituted Polyglutamates by Variable-Angle Sample Spinning'* in *Angew. Chem., Int. Ed.* **2005**, *44*, 2787-2790.

[88] T. Väänänen; J. Jokisaari; M. Seläntaus: *'Variable-Angle Spinning ^{1}H-NMR Spectra of Molecules in Liquid-Crystalline Phases with Positive and Negative Diamagnetic Anisotropy'* in *Chem. Phys. Lett.* **1986**, *129*, 399-402.

[89] N. T. Lai; J. P. Bayle; J. M. Ouvrard; J. Courtieu: *'Two-Dimensional NMR in Liquid-Crystal Solvents Spinning at Various Angles from the Magnetic-Field'* in *Liq. Cryst.* **1988**, *3*, 745-751.

[90] F. Tian; J. A. Losonczi; M. W. F. Fischer; J. H. Prestegard: *'Sign determination of dipolar couplings in field-oriented bicelles by variable angle sample spinning (VASS)'* in *J. Biomol. NMR* **1999**, *15*, 145-150.

[91] T. H. Chen; J. Z. Wang; H. X. Li; K. X. Wang; F. Deng; Y. R. Du; D. T. Ding: *'Sodium-Cation Locations in Zeolite-Omega Studied by ^{23}Na VASS NMR'* in *Chem. Phys. Lett.* **1995**, *238*, 82-87.

[92] P. T. F. Williamson; G. Zandomeneghi; B. Bonev; F. J. Barrantes; A. Watts; B. H. Meier: *'Structural characterization of the M4-TMD of the nicotinic acetylcholine receptor by VASS NMR of ordered liquid crystalline phases'* in *Biophys. J.* **2001**, *80*, 699.

[93] A. I. Kishore; J. H. Prestegard: *'Molecular orientation and conformation of phosphatidylinositides in membrane mimetics using variable angle sample spinning (VASS) NMR'* in *Biophys. J.* **2003**, *85*, 3848-3857.

[94] N. Lancelot; K. Elbayed; M. Piotto: *'Applications of variable-angle sample spinning experiments to the measurement of scaled residual dipolar couplings and ^{15}N CSA in soluble proteins'* in *J. Biomol. NMR* **2005**, *33*, 153-161.

[95] L. Beguin; J. Courtieu; L. Ziani; D. Merlet: *'Simplification of the ^{1}H NMR spectra of enantiomers dissolved in chiral liquid crystals, combining variable angle sample spinning and selective refocusing experiments'* in *Magn. Reson. Chem.* **2006**, *44*, 1096-1101.

[96] G. Kummerlöwe: Master's Thesis *'Partielle Orientierung und die Messung von residualer chemischer Verschiebungsanisotropie'*, Technische Universität München (Garching), **2006**.

[97] P. Tzvetkova; S. Simova; B. Luy: *'Sign-Sensitive Measurement of Residual Quadrupolar Couplings'* poster presentation at *28th Annual Discussion Meeting of the GDCh Magnetic Resonance Division* (Tübingen, Germany), **2006**.

[98] G. Kummerlöwe; S. Grage; C. M. Thiele; B. Luy: *'Variable Angle NMR-Spectroscopy in Stretched Gels: Scaling of Anisotropic Parameters and Measurement of Residual Chemical Shift Anisotropy (RCSA)'* poster presentation at *47th ENC Conference* (Asilomar, CA, USA), **2006**.

[99] P. W. Kuchel; B. E. Chapman; N. Müller; W. A. Bubb; D. J. Philp; A. M. Torres: *'Apparatus for rapid adjustment of the degree of alignment of NMR samples in aqueous media: Verification with residual quadrupolar splittings in ^{23}Na and ^{133}Cs spectra'* in *J. Magn. Reson.* **2006**, *180*, 256-265.

[100] C. Naumann; W. A. Bubb; B. E. Chapman; P. W. Kuchel: *'Tunable-Alignment Chiral System Based on Gelatin for NMR Spectroscopy'* in *J. Am. Chem. Soc.* **2007**, *129*, 5340-5341.

[101] S. Lee; M. F. Mesleh; S. J. Opella: *'Structure and dynamics of a membrane protein in micelles from three solution NMR experiments'* in *J. Biomol. NMR* **2003**, *26*, 327-334.

[102] Z. Wu; N. Tjandra; A. Bax: *'^{31}P Chemical Shift Anisotropy as an Aid in Determining Nucleic Acid Structure in Liquid Crystals'* in *J. Am. Chem. Soc.* **2001**, *123*, 3617-3618.

[103] A. Meddour; I. Canet; A. Loewenstein; J. M. Pechine; J. Courtieu: *'Observation of Enantiomers, Chiral by Virtue of Isotopic-Substitution, through Deuterium NMR in a Polypeptide Liquid-Crystal'* in *Journal of the American Chemical Society* **1994**, *116*, 9652-9656.

[104] I. Canet; J. Courtieu; A. Loewenstein; A. Meddour; J. M. Pechine: *'Enantiomeric Analysis in a Polypeptide Lyotropic Liquid-Crystal by Deuterium NMR'* in *J. Am. Chem. Soc.* **1995**, *117*, 6520-6526.

[105] M. Sarfati; P. Lesot; D. Merlet; J. Courtieu: *'Theoretical and experimental aspects of enantiomeric differentiation using natural abundance multinuclear NMR spectroscopy in chiral polypeptide liquid crystals'* in *Chem. Commun.* **2000**, 2069-2081.

[106] C. Aroulanda; P. Lesot; D. Merlet; J. Courtieu: *'Structural Ambiguities Revisited in Two Bridged Ring Systems Exhibiting Enantiotopic Elements, Using Natural Abundance Deuterium NMR in Chiral Liquid Crystals'* in *J. Phys. Chem.* **2003**, *107*, 10911-10918.

[107] A. Enthart; J. C. Freudenberger; J. Furrer; H. Kessler; B. Luy: *'The CLIP/CLAP-HSQC: Pure Absorptive Spectra for the Measurement of One-Bond Couplings'* in *Journal of Magnetic Resonance* **2008**, *192*, 314-322.

[108] J. Yan; A. D. Kline; H. Mo; M. J. Shapiro; E. R. Zartler: *'A Novel Method for the Determination of Stereochemistry in Six-Membered Chairlike Rings Using Residual Dipolar Couplings'* in *J. Org. Chem.* **2003**, *68*, 1786-1795.

[109] T. E. Skinner; T. O. Reiss; B. Luy; N. Khaneja; S. J. Glaser: *'Application of optimal control theory to the design of broadband excitation pulses for high-resolution NMR'* in *J. Magn. Reson.* **2003**, *163*, 8-15.

[110] T. E. Skinner; T. O. Reiss; B. Luy; N. Khaneja; S. J. Glaser: *'Reducing the duration of broadband excitation pulses using optimal control with limited RF amplitude'* in *J. Magn. Reson.* **2004**, *167*, 68-74.

[111] K. Kobzar; T. E. Skinner; N. Khaneja; S. J. Glaser; B. Luy: *'Exploring the Limits of Broadband Excitation and Inversion Pulses'* in *J. Magn. Reson.* **2004**, *170*, 236.

[112] B. Luy; K. Kobzar; T. E. Skinner; N. Khaneja; S. J. Glaser: *'Construction of universal rotations from point-to-point transformations'* in *J. Magn. Reson.* **2005**, *176*, 179-186.

[113] P. Nolis; J. F. Espinosa; T. Parella: *'Optimum spin-state selection for all multiplicities in the acquisition dimension of the HSQC experiment.'* in *J. Magn. Reson.* **2006**, *180*, 39-50.

[114] P. Tzvetkova; S. Simova; B. Luy: *'P.E.HSQC: A simple experiment for simultaneous and sign-sensitive measurement of ($^1J_{CH}$+D_{CH}) and ($^2J_{HH}$+D_{HH}) couplings'* in *J. Magn. Reson.* **2007**, *186*, 193-200.

[115] M. J. Thrippleton; J. Keeler: *'Elimination of Zero-Quantum Interference in Two-Dimensional NMR Spectra'* in *Angew. Chem., Int. Ed.* **2003**, *42*, 3938-3941.

[116] J. R. Garbow; D. P. Weitekamp; A. Pines: *'Bilinear Rotation Decoupling of Homonuclear Scalar Interactions'* in *Chem. Phys. Lett.* **1982**, *93*, 504-509.

[117] D. Uhrín; T. Liptaj; K. E. Kövér: *'Modified Bird Pulses and Design of Heteronuclear Pulse Sequences'* in *J. Magn. Reson., Ser. A* **1993**, *101*, 41-46.

[118] K. Feher; S. Berger; K. E. Kövér: *'Accurate determination of small one-bond heteronuclear residual dipolar couplings by F1 coupled HSQC modified with a G-BIRD(r) module'* in *J. Magn. Reson.* **2003**, *163*, 340-346.

[119] L. Ziani; J. Courtieu; D. Merlet: *'Visualisation of enantiomers via insertion of a BIRD module in X-H correlation experiments in chiral liquid crystal solvent'* in *J. Magn. Reson.* **2006**, *183*, 60-67.

[120] J. Furrer; M. John; H. Kessler; B. Luy: *'J-Spectroscopy in the Presence of Residual Dipolar Couplings: Determination of One-Bond Coupling Constants and Scalable Resolution'* in *J. Biomol. NMR* **2007**, *37*, 231-243.

[121] T. Carlomagno; W. Peti; C. Griesinger: *'A new method for the simultaneous measurement of magnitude and sign of $^1D_{CH}$ and $^1D_{HH}$ dipolar couplings in methylene groups'* in *J. Biomol. NMR* **2000**, *17*, 99-109.

[122] E. Miclet; D. C. Williams; G. M. Clore; D. L. Bryce; J. Boisbouvier; A. Bax: *'Relaxation-optimized NMR spectroscopy of methylene groups in proteins and nucleic acids'* in *J. Am. Chem. Soc.* **2004**, *126*, 10560-10570.

[123] B. L. Marquez; W. H. Gerwick; R. T. Williamson: *'Survey of NMR experiments for the determination of $^nJ_{CH}$ heteronuclear coupling constants in small molecules'* in *Magn. Reson. Chem.* **2001**, *39*, 499-530.

[124] K. Kobzar; B. Luy: *'Analyses, extensions and comparison of three experimental schemes for measuring ($^nJ_{CH}$+D_{CH})-couplings at natural abundance'* in *J. Magn. Reson.* **2007**, *186*, 131-141.

[125] L. Verdier; P. Sakhaii; M. Zweckstetter; C. Griesinger: *'Measurement of long range H,C couplings in natural products in orienting media: a tool for structure elucidation of natural products'* in *J. Magn. Reson.* **2003**, *163*, 353-359.

[126] L. Jin; D. Uhrín: *'^{13}C-detected IPAP-INADEQUATE for simultaneous measurement of one-bond and long-range scalar or residual dipolar coupling constants'* in *Magn. Reson. Chem.* **2007**, *45*, 628-633.

[127] J. A. Losonczi; M. Andrec; M. W. F. Fischer; J. H. Prestegard: *'Order matrix analysis of residual dipolar couplings using singular value decomposition'* in *J. Magn. Reson.* **1999**, *138*, 334-342.

[128] M. Zweckstetter; A. Bax: *'Prediction of sterically induced alignment in a dilute liquid crystalline phase: Aid to protein structure determination by NMR'* in *J. Am. Chem. Soc.* **2000**, *122*, 3791-3792.

[129] M. Zweckstetter: *'NMR: prediction of molecular alignment from structure using the PALES software'* in *Nat. Protoc.* **2008**, *3*, 679-690.

[130] M. Martín-Pastor; C. A. Bush: *'Refined structure of a flexible heptasaccharide using ^{1}H-^{13}C and ^{1}H-^{1}H NMR residual dipolar couplings in concert with NOE and long range scalar coupling constants'* in *J. Biomol. NMR* **2001**, *19*, 125-139.

[131] H. F. Azurmendi; C. A. Bush: *'Conformational studies of blood group A and blood group B oligosaccharides using NMR residual dipolar couplings'* in *Carbohydr. Res.* **2002**, *337*, 905-915.

[132] H. F. Azurmendi; M. Martín-Pastor; C. A. Bush: *'Conformational studies of Lewis X and Lewis A trisaccharides using NMR residual dipolar couplings'* in *Biopolymers* **2002**, *63*, 89-98.

[133] D. I. Freedberg: *'An alternative method for pucker determination in carbohydrates from residual dipolar couplings: A solution NMR study of the fructofuranosyl ring of sucrose'* in *J. Am. Chem. Soc.* **2002**, *124*, 2358-2362.

[134] T. N. Pham; S. L. Hinchley; D. W. H. Rankin; T. Liptaj; D. Uhrín: *'Determination of Sugar Structures in Solution from Residual Dipolar Coupling Constants: Methodology and Application to Methyl α-*D*-Xylo-pyranoside'* in *J. Am. Chem. Soc.* **2004**, *126*, 13100-13110.

[135] J. Klages; C. Neubauer; M. Coles; H. Kessler; B. Luy: *'Structure Refinement of Cyclosporin A in Chloroform by Using RDCs Measured in a Stretched PDMS-Gel'* in *ChemBioChem* **2005**, *6*, 1672–1678.

[136] M. Martín-Pastor; A. Canales; F. Corzana; J. L. Asensio; J. Jiménez-Barbero: *'Limited flexibility of lactose detected from residual dipolar couplings using molecular dynamics simulations and steric alignment methods'* in *J. Am. Chem. Soc.* **2005**, *127*, 3589-3595.

[137] A. V. Klochkov; B. I. Khairutdinov; M. S. Tagirov; V. V. Klochkov: *'Determination of the spatial structure of glutathione by residual dipolar coupling analysis'* in *Magn. Reson. Chem.* **2005**, *43*, 948-951.

[138] C. Landersjö; J. L. M. Jansson; A. Maliniak; G. Widmalm: *'Conformational analysis of a tetrasaccharide based on NMR spectroscopy and molecular dynamics simulations'* in *J. Phys. Chem. B* **2005**, *109*, 17320-17326.

[139] C. Landersjö; B. Stevensson; R. Eklund; J. Östervall; P. Söderman; G. Widmalm; A. Maliniak: *'Molecular conformations of a disaccharide investigated using NMR spectroscopy'* in *J. Biomol. NMR* **2006**, *35*, 89-101.

[140] U. M. Reinscheid; J. Farjon; M. Radzom; P. Haberz; A. Zeeck; M. Blackledge; C. Griesinger: *'Effect of the solvent on the conformation of a depsipeptide: NMR-derived solution structure of hormaomycin in DMSO from residual dipolar couplings in a novel DMSO-compatible alignment medium'* in *ChemBioChem* **2006**, *7*, 287-296.

[141] M. B. Schmid; M. Fleischmann; V. D'Elia; O. Reiser; W. Gronwald; R. M. Gschwind: *'Residual Dipolar Couplings in Short Peptidic Foldamers: Combined Analyses of Backbone and Side-Chain Conformations and Evaluation of Structure Coordinates of Rigid Unnatural Amino Acids'* in *ChemBioChem* **2009**, *10*, 440-444.

[142] V. V. Klochkov; R. F. Baikeev; V. D. Skirda; A. V. Klochkov; F. R. Muhamadiev; I. Baskyr; S. Berger: *'Spatial structure of peptides determined by residual dipolar couplings analysis'* in *Magn. Reson. Chem.* **2009**, *47*, 57-62.

[143] R. S. Stoll; M. V. Peters; A. Kuhn; S. Heiles; R. Goddard; M. Buhl; C. M. Thiele; S. Hecht: *'Photoswitchable Catalysts: Correlating Structure and Conformational Dynamics with Reactivity by a Combined Experimental and Computational Approach'* in *J. Am. Chem. Soc.* **2009**, *131*, 357-367.

[144] V. M. Sánchez-Pedregal; R. Santamaría-Fernández; A. Navarro-Vázquez: *'Residual Dipolar Couplings of Freely Rotating Groups in Small Molecules. Stereochemical Assignment and Side-Chain Conformation of 8-Phenylmenthol'* in *Org. Lett.* **2009**, *11*, 1471-1474.

[145] C. Farès; J. Hassfeld; D. Menche; T. Carlomagno: *'Simultaneous Determination of the Conformation and Relative Configuration of Archazolide A by Using Nuclear Overhauser Effects, J Couplings, and Residual Dipolar Couplings'* in *Angew. Chem., Int. Ed.* **2008**, *47*, 3722-3726.

[146] N. Cramer; S. Helbig; A. Baro; S. Laschat; R. Diestel; F. Sasse; D. Mathieu; C. Richter; G. Kummerlöwe; B. Luy; H. Schwalbe: *'Synthesis and Biological Properties of Cylindramide Derivatives: Evidence for Calcium-Dependent Cytotoxicity of Tetramic Acid Lactams'* in *ChemBioChem* **2008**, *9*, 2474-2486.

[147] C. Aroulanda; V. Boucard; F. Guibé; J. Courtieu; D. Merlet: *'Weakly oriented liquid-crystal NMR solvents as a general tool to determine relative configurations'* in *Chem. Eur. J.* **2003**, *9*, 4536-4539.

[148] A. Mangoni; V. Esposito; A. Randazzo: *'Configuration assignment in small organic molecules via residual dipolar couplings'* in *Chem. Commun.* **2003**, 154-155.

[149] J. L. Yan; F. Delaglio; A. Kaerner; A. D. Kline; H. P. Mo; M. J. Shapiro; T. A. Smitka; G. A. Stephenson; E. R. Zartler: *'Complete relative stereochemistry of multiple stereocenters using only residual dipolar couplings'* in *J. Am. Chem. Soc.* **2004**, *126*, 5008-5017.

[150] J. L. Yan; A. D. Kline; H. P. Mo; M. J. Shapiro; E. R. Zartler: *'The absolute sign of J coupling constants determined using the order matrix calculation'* in *Magn. Reson. Chem.* **2004**, *42*, 962-967.

[151] J. D. Swarbrick; T. D. Ashton: *'NMR Studies of Dextromethorphan in Both Isotropic and Anisotropic States'* in *Chirality* **2010**, *22*, 42-49.

[152] C. M. Thiele; S. Berger: *'Probing the diastereotopicity of methylene protons in strychnine using residual dipolar couplings'* in *Org. Lett.* **2003**, *5*, 705-708.

[153] G. Cornilescu; J. L. Marquardt; M. Ottiger; A. Bax: *'Validation of protein structure from anisotropic carbonyl chemical shifts in a dilute liquid crystalline phase'* in *J. Am. Chem. Soc.* **1998**, *120*, 6836-6837.

[154] M. Blackledge: *'Recent progress in the study of biomolecular structure and dynamics in solution from residual dipolar couplings'* in *Prog. Nucl. Magn. Reson. Spectrosc.* **2005**, *46*, 23-61.

[155] M. Martín-Pastor; C. A. Bush: *'Conformational studies of human milk oligosaccharides using ^{1}H-^{13}C one-bond NMR residual dipolar couplings'* in *Biochemistry* **2000**, *39*, 4674-4683.

[156] A. T. Brunger; P. D. Adams; G. M. Clore; W. L. DeLano; P. Gros; R. W. Grosse-Kunstleve; J. S. Jiang; J. Kuszewski; M. Nilges; N. S. Pannu; R. J. Read; L. M. Rice; T. Simonson; G. L. Warren: *'Crystallography & NMR system: A new software suite for macromolecular structure determination'* in *Acta Crystallogr., Sect. D: Biol. Crystallogr.* **1998**, *54*, 905-921.

[157] C. D. Schwieters; J. J. Kuszewski; N. Tjandra; G. M. Clore: *'The Xplor-NIH NMR molecular structure determination package'* in *J. Magn. Reson.* **2003**, *160*, 65-73.

[158] P. Güntert; C. Mumenthaler; K. Wüthrich: *'Torsion angle dynamics for NMR structure calculation with the new program DYANA'* in *J. Mol. Biol.* **1997**, *273*, 283-298.

[159] V. Tsui; L. M. Zhu; T. H. Huang; P. E. Wright; D. A. Case: *'Assessment of zinc finger orientations by residual dipolar coupling constants'* in *J. Biomol. NMR* **2000**, *16*, 9-21.

[160] D. A. Pearlman; D. A. Case; J. W. Caldwell; W. S. Ross; T. E. Cheatham; S. Debolt; D. Ferguson; G. Seibel; P. Kollman: *'Amber, a Package of Computer-Programs for Applying Molecular Mechanics, Normal-Mode Analysis, Molecular-Dynamics and Free-Energy Calculations to Simulate the Structural and Energetic Properties of Molecules'* in *Comput. Phys. Commun.* **1995**, *91*, 1-41.

[161] J. Farjon; D. Merlet; P. Lesot; J. Courtieu: *'Enantiomeric excess measurements in weakly oriented chiral liquid crystal solvents through 2D ^{1}H selective refocusing experiments'* in *J. Magn. Reson.* **2002**, *158*, 169-172.

[162] V. M. Marathias; G. J. Tawa; I. Goljer; A. C. Bach II: *'Stereochemical identification of (R)- and (S)-ibuprofen using residual dipolar couplings, NMR, and modeling'* in *Chirality* **2007**, *19*, 741-750.

[163] M. Zweckstetter; A. Bax: *'Characterization of molecular alignment in aqueous suspensions of Pf1 bacteriophage'* in *J. Biomol. NMR* **2001**, *20*, 365-377.

[164] H. F. Azurmendi; C. A. Bush: *'Tracking alignment from the moment of inertia tensor (TRAMITE) of biomolecules in neutral dilute liquid crystal solutions'* in *J. Am. Chem. Soc.* **2002**, *124*, 2426-2427.

[165] B. Wu; M. Petersen; F. Girard; M. Tessari; S. S. Wijmenga: *'Prediction of molecular alignment of nucleic acids in aligned media'* in *J. Biomol. NMR* **2006**, *35*, 103-115.

[166] L. Ziani; P. Lesot; A. Meddour; J. Courtieu: *'Empirical determination of the absolute configuration of small chiral molecules using natural abundance ^{2}H NMR in chiral liquid crystals'* in *Chem. Commun.* **2007**, 4737-4739.

[167] A. Charlesby: *'Crosslinking and Degradation of Polymers'* in *Radiat. Phys. Chem.* **1981**, *18*, 59-66.

[168] G. N. Patel; A. Keller: *'Crystallinity and Effect of Ionizing-Radiation in Polyethylene: 2. Crosslinking in Chain-Folded Single-Crystals'* in *J. Polym. Sci., Part B: Polym. Phys.* **1975**, *13*, 323-331.

[169] G. N. Patel; A. Keller: *'Crystallinity and Effect of Ionizing-Radiation in Polyethylene: 3. Experiment on Irradiation-Induced Crosslinking in N-Hexatriacontane'* in *J. Polym. Sci., Part B: Polym. Phys.* **1975**, *13*, 333-338.

[170] G. N. Patel: *'Irradiation of a Single Crystalline and Highly Amorphous Polydiacetylene'* in *Radiat. Phys. Chem.* **1980**, *15*, 637-641.

[171] *'Polymer Handbook', Vol. 1*, 4th ed., Wiley-Interscience, Hoboken, **1999**.

[172] J. Chatterjee; D. Mierke; H. Kessler: *'N-Methylated Cyclic Pentaalanine Peptides as Template Structures'* in *J. Am. Chem. Soc.* **2006**, *128*, 15164-15172.

[173] H. Y. Carr; E. M. Purcell: *'Effects of Diffusion on Free Precession in Nuclear Magnetic Resonance Experiments'* in *Phys. Rev.* **1954**, *94*, 630-638.

[174] P. Haberz: Dissertation *'Development and Application of NMR-methods for Structural Investigations of Small Molecules and Proteins'*, Georg-August-Universität (Göttingen), **2007**.

[175] S. Knör: Dissertation *'Design and Synthesis of FVIII- and uPAR-Selective Ligands and Cross-Linked Polymers as Media for NMR-Spectroscopy'*, Technische Universität München (Munich), **2007**.

[176] J. Klages; H. Kessler; S. J. Glaser; B. Luy: *'J-ONLY-TOCSY: Efficient suppression of RDC-induced transfer in homonuclear TOCSY experiments using JESTER-1-derived multiple pulse sequences'* in *J. Magn. Reson.* **2007**, *189*, 217–227.

[177] F. Kramer; S. J. Glaser: *'Efficiency of homonuclear Hartmann-Hahn and COSY-type mixing sequences in the presence of scalar and residual dipolar couplings'* in *J. Magn. Reson.* **2002**, *155*, 83-91.

[178] B. Luy; S. J. Glaser: *'Analytical polarization and coherence transfer functions for three dipolar coupled spins 1/2'* in *J. Magn. Reson.* **2000**, *142*, 280-287.

[179] M. R. Hansen; M. Rance; A. Pardi: *'Observation of long-range ^{1}H-^{1}H distances in solution by dipolar coupling interactions'* in *J. Am. Chem. Soc.* **1998**, *120*, 11210-11211.

[180] F. Kramer; W. Peti; C. Griesinger; S. J. Glaser: *'Optimized homonuclear Carr-Purcell-type dipolar mixing sequences'* in *J. Magn. Reson.* **2001**, *149*, 58.

[181] E. Sackmann; S. Meiboom; L. C. Snyder: *'Nuclear Magnetic Resonance Spectra of Enantiomers in Optically Active Liquid Crystals'* in *J. Am. Chem. Soc.* **1968**, *90*, 2183-2184.

[182] N. Giraud; M. Joos; J. Courtieu; D. Merlet: *'Application of a ^{1}H delta-resolved 2D NMR experiment to the visualization of enantiomers in chiral environment, using sample spatial encoding and selective echoes'* in *Magn. Reson. Chem.* **2009**, *47*, 300-306.

[183] P. Lesot; M. Sarfati; J. Courtieu: *'Natural abundance deuterium NMR spectroscopy in polypeptide liquid crystals as a new and incisive means for the enantiodifferentiation of chiral hydrocarbons'* in *Chem. Eur. J.* **2003**, *9*, 1724-1745.

[184] M. Tavasli; J. Courtieu; R. J. M. Goss; A. Meddour; D. O'Hagan: *'Extreme enantiomeric discrimination of fluoroalkanes using deuterium NMR in chiral liquid crystalline media'* in *Chem. Commun.* **2002**, 844-845.

[185] D. Merlet; J. W. Emsley; P. Lesot; J. Courtieu: *'The relationship between molecular symmetry and second-rank orientational order parameters for molecules in chiral liquid crystalline solvents'* in *J. Chem. Phys.* **1999**, *111*, 6890-6896.

[186] E. Lafontaine; J. P. Bayle; J. Courtieu: *'High-Resolution NMR in Cholesteric Medium - Visualization of Enantiomers'* in *J. Am. Chem. Soc.* **1989**, *111*, 8294-8296.

[187] B. E. Weiss-López; M. Azocar; R. Montecinos; B. K. Cassels; R. Araya-Maturana: *'Differential incorporation of* L- *and* D-*N-acyl-1-phenyl-d_5-2-aminopropane in a cesium N-dodecanoyl-*L-*alaninate cholesteric nematic lyomesophase'* in *Langmuir* **2001**, *17*, 6910-6914.

[188] G. Kummerlöwe; M. U. Kiran; B. Luy: *'Covalently Cross-Linked Gelatin Allows Chiral Distinction at Elevated Temperatures and in DMSO'* in *Chem. Eur. J.* **2009**, *15*, 12192-12195.

[189] E. W. Merrill; K. A. Dennison; C. Sung: *'Partitioning and Diffusion of Solutes in Hydrogels of Poly(Ethylene Oxide)'* in *Biomaterials* **1993**, *14*, 1117-1126.

[190] J. L. Stringer; N. A. Peppas: *'Diffusion of small molecular weight drugs in radiation-crosslinked poly(ethylene oxide) hydrogels'* in *J. Controlled Release* **1996**, *42*, 195-202.

[191] M. Aumailley; M. Gurrath; G. Muller; J. Calvete; R. Timpl; H. Kessler: *'Arg-Gly-Asp Constrained within Cyclic Pentapeptides - Strong and Selective Inhibitors of Cell-Adhesion to Vitronectin and Laminin Fragment-P1'* in *FEBS Lett.* **1991**, *291*, 50-54.

[192] M. A. Dechantsreiter; E. Planker; B. Mathä; E. Lohof; G. Hölzemann; A. Jonczyk; S. L. Goodman; H. Kessler: *'N-Methylated Cyclic RGD Peptides as Highly Active and Selective $\alpha_v\beta_3$ Integrin Antagonists'* in *J. Med. Chem.* **1999**, *42*, 3033-3040.

[193] F. Halbach: Master's Thesis *'A Novel Approach to Structural Characterization of Symmetric Homodimers Using Resdiual Dipolar Couplings'*, Technische Universität München (Munich), **2007**.

[194] A. S. Bawdekar; G. R. Kelkar; S. C. Bhattach: *'Terpenoids 89: Absolute Configuration of Parthenolide'* in *Tetrahedron Lett.* **1966**, 1225-1226.

[195] A. Quick; D. Rogers: *'Crystal and Molecular-Structure of Parthenolide [4,5-Epoxygermacra-1(10),11(13)-Dien-12,6-Olactone]'* in *J. Chem. Soc., Perkin Trans. 2* **1976**, 465-469.

[196] H. Neukirch; N. C. Kaneider; C. J. Wiedermann; A. Guerriero; M. D'Ambrosio: *'Parthenolide and its photochemically synthesized 1(10)Z isomer: Chemical reactivity and structure-activity relationship studies in human leucocyte chemotaxis'* in *Bioorg. Med. Chem.* **2003**, *11*, 1503-1510.

[197] D. De Keukeleire; M. Verzele: *'Absolute Configuration of Isohumulones and Humulinic Acids'* in *Tetrahedron* **1971**, *27*, 4939-4945.

[198] B. M. King; C. A. A. Duineveld: *'Changes in bitterness as beer ages naturally'* in *Food Qual. Pref.* **1999**, *10*, 315-324.

[199] S. Araki; M. Takashio; K. Shinotsuka: *'A new parameter for determination of the extent of staling in beer'* in *J. Am. Soc. Brew. Chem.* **2002**, *60*, 26-30.

[200] D. Intelmann; G. Haseleu; T. Hofmann: *'LC-MS/MS Quantitation of Hop-Derived Bitter Compounds in Beer Using the ECHO Technique'* in *J. Agric. Food Chem.* **2009**, *57*, 1172-1182.

[201] D. Intelmann; G. Kummerlöwe; G. Haseleu; N. Desmer; K. Schulze; R. Fröhlich; O. Frank; B. Luy; T. Hofmann: *'Structures of Storage-induced Transformation Products of the Beer's Bitter Principle, Revealed by Sophisticated NMR and LC/MS Techniques'* in *Chem. Eur. J.* **2009**, *15*, 13047-13058.

[202] G. Haseleu; D. Intelmann; T. Hofmann: *'Structure determination and sensory evaluation of novel bitter compounds formed from β-acids of hop (Humulus lupulus L.) upon wort boiling'* in *Food Chem.* **2009**, *116*, 71-81.

[203] D. Intelmann; O. Demmer; N. Desmer; T. Hofmann: *'^{18}O Stable Isotope Labeling, Quantitative Model Experiments, and Molecular Dynamics Simulation Studies on the Trans-Specific Degradation of the Bitter Tasting Iso-α-acids of Beer'* in *J. Agric. Food Chem.* **2009**, *57*, 11014-11023.

[204] *Sybyl® program* by Tripos L.P., vers.: 7.2, (St. Louis, Missouri). http://tripos.com/

[205] *MestreNova® program* by Mestrelab Research S.L., vers.: (LA CORUNA, Spain). www.mestrec.com

[206] S. Omura; Y. Iwai; A. Hirano; A. Nakagawa; J. Awaya; H. Tsuchiya; Y. Takahashi; R. Masuma: *'New Alkaloid Am-2282 of Streptomyces Origin Taxonomy, Fermentation, Isolation and Preliminary Characterization'* in *J. Antibiot.* **1977**, *30*, 275-282.

[207] T. Tamaoki; H. Nomoto; I. Takahashi; Y. Kato; M. Morimoto; F. Tomita: *'Staurosporine, a Potent Inhibitor of Phospholipid/Ca^{2+} Dependent Protein-Kinase'* in *Biochem. Biophys. Res. Commun.* **1986**, *135*, 397-402.

[208] G. D. Spacey; R. W. Bonser; R. W. Randall; L. G. Garland: *'Selectivity of Protein-Kinase Inhibitors in Human Intact Platelets'* in *Cellular Signalling* **1990**, *2*, 329-338.

[209] R. A. Bit; P. D. Davis; L. H. Elliott; W. Harris; C. H. Hill; E. Keech; H. Kumar; G. Lawton; A. Maw; J. S. Nixon; D. R. Vesey; J. Wadsworth; S. E. Wilkinson: *'Inhibitors of Protein-Kinase-C: 3. Potent and Highly Selective Bisindolylmaleimides by Conformational Restriction'* in *J. Med. Chem.* **1993**, *36*, 21-29.

[210] N. Funato; H. Takayanagi; Y. Konda; Y. Toda; Y. Harigaya; Y. Iwai; S. Omura: *'Absolute-Configuration of Staurosporine by X-Ray-Analysis'* in *Tetrahedron Lett.* **1994**, *35*, 1251-1254.

[211] P. D. Davis; C. H. Hill; W. A. Thomas; I. W. A. Whitcombe: *'The Design of Inhibitors of Protein Kinase C; The Solution Conformation of Staurosporine'* in *J. Chem. Soc., Chem. Commun.* **1991**, 182-184.

[212] I. Takahashi; Y. Saitoh; M. Yoshida; H. Sano; H. Nakano; M. Morimoto; T. Tamaoki: *'UCN-01 and UCN-02, new Selective Inhibitors of Protein Kinase C: II. Purification, Physico-Chemical Properties, Structural Determination and Biological Activities'* in *J. Antibiot.* **1989**, *42*, 571-577.

[213] M. Hesse; H. Meier; B. Zeeh: *'Spektroskopische Methoden in der organischen Chemie'*, 6th ed., Thieme, Stuttgart, **2002**.

[214] B. Reif; M. Kock; R. Kerssebaum; H. Kang; W. Fenical; C. Griesinger: *'ADEQUATE, a new set of experiments to determine the constitution of small molecules at natural abundance'* in *J. Magn. Reson., Ser. A* **1996**, *118*, 282-285.

[215] *ChemDraw® Ultra program* by CambridgeSoft Corporation, vers.: 8, (Cambridge, MA).

[216] A. Bax; R. Freeman; S. P. Kempsell: *'Natural Abundance ^{13}C-^{13}C Coupling Observed Via Double-Quantum Coherence'* in *J. Am. Chem. Soc.* **1980**, *102*, 4849-4851.

[217] A. Bax; R. Freeman; T. A. Frenkiel; M. H. Levitt: *'Assignment of ^{13}C NMR Spectra via Double-Quantum Coherence'* in *J. Magn. Reson.* **1981**, *43*, 478-483.

[218] J. Buddrus; J. Lambert: *'Connectivities in molecules by INADEQUATE: recent developments'* in *Magn. Reson. Chem.* **2002**, *40*, 3-23.

[219] T. Lindel; J. Junker; M. Kock: *'COCON: From NMR correlation data to molecular constitutions'* in *Journal of Molecular Modeling* **1997**, *3*, 364-368.

[220] T. Lindel; J. Junker; M. Kock: *'2D-NMR-guided constitutional analysis of organic compounds employing the computer program COCON'* in *Eur. J. Org. Chem.* **1999**, 573-577.

[221] B. Schönecker; C. Lange: *'Steroids as chiral model compounds for selective reactions with metals'* in *J. Organomet. Chem.* **2006**, *691*, 2107-2124.

[222] J. R. Hanson: *'Steroids: partial synthesis in medicinal chemistry'* in *Nat. Prod. Rep.* **2007**, *24*, 1342-1349.

[223] C. F. Nising; S. Bräse: *'Highlights in Steroid Chemistry: Total Synthesis versus Semisynthesis'* in *Angew. Chem., Int. Ed.* **2008**, *47*, 9389-9391.

[224] *OriginPro® program* by OriginLab Cooperation, vers.: 7.5G SR2.1, **2003** (Northhampton, MA, USA).

Danksagung

Diese Arbeit wäre nicht was sie ist, ohne die direkte oder indirekte Hilfe einer ganzen Reihe von Leuten. An dieser Stelle möchte ich mich dafür bedanken, dass sie auf ihre Art und Weise zu diesem Werk beigetragen haben.

Mein tiefster Dank gebührt ***PD Dr. Burkhard Luy*** für die Aufnahme in seinen Arbeitskreis, für den nicht-enden-wollenden Fluss von interessanten und fruchtbaren Ideen und Projekten, für alles was ich lernen durfte, für die Freiheit in wissenschaftlichen Dingen, sowie auch für die Akzeptanz meiner außeruniversitären Spielereien und für die mal mehr, mal weniger vorhandene Geduld mit und stete Toleranz gegenüber meinem Dickkopf!

Dem gesamten **AK BuLu** mit all seinen aktuellen und ehemaligen Mitgliedern danke ich für die gute Atmosphäre. Besonderer Dank gilt:

- ***M.Sc. Pavleta Tzvetkova*** für geduldige Erklärungen und jede Menge Tipps.
- ***Dr. Kyryl Kobzar*** für so manch Hilfe in Spektrometer-Not.
- ***M.Sc. Felix Halbach*** und ***M.Sc. Marelli Udaya Kiran*** für die Zusammenarbeit an den gemeinsamen Projekten.

Besonderer Dank geht auch an ***Prof. Dr. Horst Kessler*** und den gesamten **AK Kessler** für die einzigartige Infrastruktur die ich mitbenutzen durfte: das waren Jahre wie im Forscher-Schlaraffenland! Auch für das freundliche und produktive Klima im gesamten Arbeitskreis ist allen zu danken, spezieller Dank geht an:

- ***Dr. Burkhardt Laufer*** für so manch geliehenes Laborgerät, die gute Gesellschaft in meinem „Ausweichquartier“, die vielen Heimfahrten, die unzähligen Antworten auf meine dummen Fragen, die noch häufigeren Fragen - mal nervig, mal höchst interessant - die an mich gingen und vor allem dafür, mich überhaupt in diesen Arbeitskreis gebracht zu haben.
- ***Dr. Andreas O. Frank*** für unglaublich geduldige Hilfe bei blöden Fragen zu noch blöderen Programmen und viele interessante wissenschaftliche und nicht-wissenschaftliche Diskussionen.
- ***Dipl. Chem. Elke Otto*** und ***Dr. Sebastian Knör*** für eine sehr angenehme Atmosphäre im Labor.
- ***Dr. Rainer Haessner*** dafür, den gesamten Arbeitskreis am Laufen zu halten, für seine Hilfe bei unzähligen Computerproblemen und seine Gelassenheit, wenn ich schon wieder ein Spektrometer kaputt gekriegt hatte… und natürlich für die vielen Freitage!
- ***Dr. Jochen J. Klages*** und ***Dr. Andreas Enthardt*** für ihre Tipps und Tricks in diversen NMR-Fragen.
- ***Dr. Peter Kaden*** für die freundliche und kompetente Hilfe in Computerfragen, beim Posterdruck und bei Mangel an Lösungsmittel.
- ***Dr. Murry Coles*** für seine Hilfe mit Xplor.

Ein herzliches Dankeschön auch an den **AK Glaser** für die gute Stimmung auf unserem Gang, zahlreiche Schweine-Mahlzeiten und die anschließenden Verdauungs-Kicker.

Diese Arbeit wäre nicht was sie ist ohne die Kooperationspartner, die an den einzelnen Projekten mehr oder minder intensiv beteiligt waren:

- Für die Synthese diverser Peptide oder die Bereitstellung anderer Testsubstanzen danke ich ***Dr. Burkhardt Laufer***, ***Dr. Jörg Auernheimer***, ***Dr. Jayanta Chatterjee***, ***Thomas Paululat*** und ***Prof. Stefan Bräse***.
- Der Gruppe um ***Prof. Dr. Andreas Lendlein*** von der **GKSS** in Teltow, insbesondere ***Dr. Aleksandra Volkmann***, ***Dr. Steffen Kelch*** und ***Dr. Marc Behl***, danke ich für nützliche Tipps zur Synthese von PAN sowie für die Polymere, die sie für uns polymerisiert und charakterisiert haben.
- ***Dr. Sebastian Knör*** danke ich für die Polymerisation des deuterierten und nicht deuterierten Polystyrols.
- ***M.Sc. Marelli Udaya Kiran*** sei für die Hilfe beim e^--Gelatine-Projekt und ***Prof. Bharatam Jagadeesh*** für das Nebenprojekt seiner β-Peptide gedankt.
- Der Dank dafür, fast beinahe das PEO-Projekt von meinen Schultern genommen zu haben, geht an ***M.Sc. Felix Halbach***, auch wenn er es dann doch nicht getan hat…
- Für die Hilfe bei der Bestrahlung mit γ-Stahlen an ihrer Cobalt-Quelle danke ich ***Wolfgang Stöwer*** and ***Dr. Christoph Lierse von Gostomski***.
- Zu Dank bin ich auch **DuPont Performance Elastomers** verpflichtet, insbesondere ***Dr. Elizabeth F. McCord***, ***Dr. Steve F. Cheatham***, ***Steve Niss*** and ***Russell W. Schnell***, für ihre Ideen zur Steckapparatur, so manche Telefonkonferenz und die Produktion der Kalrez® 8002UP-tubes.
- Dem Team der **Mechanik-Werkstatt** der TUM, insbesondere ***Otto Strasser***, sei für die vielen gefertigten Kleinteile und Schrauben und vor allem für ihre Einfälle zu deren Verbesserung gedankt.
- Besonderer Dank geht auch an ***Dipl. Chem. Daniel Intelmann*** sowie ***Prof. Dr. Thomas Hofmann*** für das interessante Projekt zum bitteren Bier. Es lebe ein frisches Pils!
- ***Dr. Andreas O. Frank*** danke ich nicht nur für „sein" Cilengitide, sondern auch für seine Berechnungen zu „meinem" Staurosporin, ohne die wir wohl nie die Fehler des Knechtes entdeckt hätten…
- Für die knifflige Aufgabe das unbekannte Reaktionsprodukt analysieren zu dürfen danke ich ***Dr. Stefan F. Kirsch***. Seinen Mitarbeitern ***Dipl. Chem. Benedikt Crone*** und ***Dipl. Chem. Manuel Kretschmer*** sei für ihre Synthesen gedankt.
- Meinem „HiWi" ***Sebastian Schmitt*** danke ich für all seine Hilfe mit den Steroiden, insbesondere für die nützlichen Programme, die er geschrieben hat, ohne die es viele hübsche Abbildungen in dieser Arbeit wohl nicht gäbe.
- Der Firma **BetaGammaSystems (BGS)** in Saal an der Donau sei für sämtliche Bestrahlungen mit beschleunigten Elektronen zu danken.

- ***Dr. Stephan Grage*** sei für die Aufenthalte in Karlsruhe, die gemeinsamen RCSA-Messungen und die netten Abende gedankt.
- Allen Mitgliedern der **DFG Forschergruppe FOR 934** danke ich für die interessanten Meetings, den inspirierenden Wissensaustausch und die nächtlichen Diskussionen bei jeder Menge Bier und Wein.
- Auch ***Dr. Senta Üzgün*** und ***Johannes Geiger*** vom Kinderklinikum sei dafür gedankt, dass sie mich immer wieder mal mit Routinemessungen vom Arbeiten abgehalten haben und all ihre „Entschädigungen" hierfür.
- Und schließlich all denen, die meinem schlechten Gedächtnis und dem momentanen Stress zum Opfer gefallen sind.

Eine ganze Reihe von Studenten hat mich immer wieder viel Zeit für noch mehr Erklärungen gekostet, aber auch immer wieder interessante Projekte angestoßen und fortgeführt. Für ihre Bemühungen, ihre Ideen und so manch hilfreiche Tipps danke ich meinen ehemaligen „Knechten": ***Björn Schröder***, ***Amy Schönegge***, ***Katharina Wussow***, ***Michael Hell***, ***Johannes Schmid***, ***Thomas Neubauer*** und ***Sebastian Schmitt***.

Besonders danken möchte ich auch denjenigen, die sich um das Korrekturlesen dieser Arbeit verdient gemacht haben: ***Dr. Burkhardt Laufer***, ***Prof. Dr. Claudia Kummerlöwe*** und ***PD Dr. Burkhard Luy*** für das Auffinden so mancher „false friends" und Tippfehler, sowie ***Dipl.-Ing. (FH) Rico Oehme*** für die Korrektur der finalen Version.

Schließlich möchte ich auch noch denjenigen danken, die mich während der Zeit, in der diese Arbeit entstand, begleitet haben, all denen, die auf ihre Weise für den nötigen Ausgleich gesorgt und damit dazu beigetragen haben, dass ich immer ausreichen Kraft, Ausdauer und Motivation für meine Arbeit hatte:

- ***Burki*** danke ich für die vielen gemeinsam durchlebten Jahre des Studiums und der Promotion, für ganz viel Antrieb, auch wenn ich es dann jetzt doch nicht rechtzeitig schaffe; für all die Ehrlichkeit und Kritik, für die vielen angeregten und anregenden Diskussionen, sowie für manch schönen Abend bei Skat, Billard, Prager Bier oder Kaminfeuer. Kurzum, für diese einzigartige Freundschaft!
  Der Dank für viele erholsame Ausflüge und Abende geht nicht nur an ihn, sondern genauso an seine Frau ***Juliane***.
- ***Helen*** danke ich für die lange Freundschaft, für ihre Geduld mit mir, für ihre stets offenen Ohren und ganz viel Neutralität, sowie für jede Menge Entspannung bei Sport, Spiel oder Feierabendbier.
  Ihr und ihrem Mann ***Matthias*** sei außerdem für all die vielen gemeinsamen Unternehmungen gedankt.

- Meiner „persönlichen Therapeutin“ ***Bele*** danke ich für ihr Verständnis, ihre guten Ratschläge - auch die vielen unbefolgten - und für ganz viel Aufmunterung. (Hoffentlich müssen wir nie wieder so viele Gespräche über böse Männer führen!) Außerdem sei Bele noch für ihre erfrischend verrückten Ideen und so manch entspannenden Sauna-Besuch gedankt.
- ***Elke*** danke ich für so manch aufbauendes Gespräch, für einige sehr gelungene Bastelprojekte, ihre Spiele-Kompetenz und ihr und ihrem Mann ***Martin*** für viele nette Abende mit Geistern, Enten oder Nobelpreisen.
- Meinen Freundinnen ***Nici*** und ***Barbara*** würde ich niemals im gleichen Satz danken! Deswegen: ein großer Dank an Barbara für gute Unterhaltung bei Rommee, Film oder Cocktail. Und: ein großer Dank an Nici für Tikal-Abende, Museen und ganz viel Einblick in die Assyriologie.
  Danke für die Freundschaft!
- Den Jungs und Mädels der Badminton-Gruppe des **FTM-Süd** danke ich für die donnerstägliche Abwechslung und all die Siege und Niederlagen.
- Außerdem danke ich noch ***Andi***+***Sarah***, ***Bulu***+***Manu***, ***Christian***, ***Chrissi***+***Susi***, ***Christoph***, ***Flocki***+***Katrin***, ***Julia***+***Dominik***, ***GMM***+***TM***, ***Maxi***+***Tilla***, ***Olli***+***Andrea***, ***Pavleta***, ***Romy***, ***Rudi***, ***Thom***+***Julia***, ***Thomas***, ***Tobi***+***Alma*** für die schönen Momente bei was auch immer.

Allen Potsdamer „T(h)ieren“ danke ich für die Abwechslung und die Entspannung fernab vom Stress. Ganz besonders danke ich ***Claude*** und ***Lucy***, dafür dass sie ihre Tante so stolz und glücklich machen.

Bei meinen ***Eltern*** möchte ich mich aufs Herzlichste für all die Unterstützung bedanken, die ich während meines gesamten Studiums und der Promotion von ihnen erhalten habe. Und für die Gewissheit, dass sie dies auch weiterhin tun werden.

Schließlich möchte ich mich noch für all die mentale Unterstützung auf der Zielgeraden bedanken. Für all die Geduld mit mir diss-schreibendem Nervenbündel, für die wohltuende Ablenkung durch zahlreiche Unternehmung und zahllose schöne Momente, für ganz viel Rückhalt, Zuneigung und unbegreiflich viel Glück. ***Rico***, ich liebe dich!